

<https://doi.org/10.15388/vu.thesis.874>
<https://orcid.org/0009-0003-8436-3940>

VILNIUS UNIVERSITY
STATE RESEARCH INSTITUTE
CENTER FOR PHYSICAL SCIENCES AND TECHNOLOGY

Neringa Bakutė

Biomaterials Research in the Field of Biocompatibility, Cell Adhesion, and Applications in Microfluidic Systems

DOCTORAL DISSERTATION

Natural Sciences,
Chemistry (N 003)

VILNIUS 2025

The dissertation was prepared between 2020 and 2025 at the State Research Institute Center for Physical Sciences and Technology.

Academic supervisor – Dr. Arūnas Stirė

(State Research Institute Center for Physical Science and Technology, Natural Sciences, Chemistry, N 003).

This doctoral dissertation will be defended in a public meeting of the Dissertation Defence Panel:

Chairman – Prof. Dr. Evaldas Naujalis (State Research Institute Center for Physical Science and Technology, Natural Sciences, Chemistry, N 003).

Members:

Assoc. Prof. Dr. Brigita Abakeviėienė (Kaunas University of Technology, Natural Sciences, Physics, N 002),

Prof. Dr. Julija Armalytė (Vilnius University, Natural Sciences, Biochemistry, N 004),

Dr. Aldona Balėiūnaitė (State Research Institute Center for Physical Science and Technology, Natural Sciences, Chemistry, N 003),

Dr. Mantas Šilkūnas (Old Dominion University, Natural Sciences, Biophysics, N 011).

The dissertation shall be defended at a public meeting of the Dissertation Defence Panel at 14:00 on 19th December 2025 in Meeting room A101 of the Center for Physical Science and Technology.

Address: Sauletekio av. 3, A101, LT-10257, Vilnius, Lithuania

Tel. +370 5264 9211; e-mail: office@ftmc.lt

The text of this dissertation can be accessed at the libraries of Vilnius University, as well as on the website of Vilnius University:

www.vu.lt/lt/naujienos/ivykiu-kalendorius

<https://doi.org/10.15388/vu.thesis.874>
<https://orcid.org/0009-0003-8436-3940>

VILNIAUS UNIVERSITETAS
VALSTYBINIS MOKSLINIŲ TYRIMŲ INSTITUTAS
FIZINIŲ IR TECHNOLOGIJOS MOKSLŲ CENTRAS

Neringa Bakutė

Biomedžiagų biologinio suderinamumo, ląstelių adhezijos ir jų pritaikymo mikroskysčių sistemose tyrimai

DAKTARO DISERTACIJA

Gamtos mokslai,
Chemija (N 003)

VILNIUS 2025

Disertacija rengta 2020–2025 metais Valstybinis mokslinių tyrimų institutas
Fizinių ir Technologijos mokslų centras

Mokslinis vadovas – dr. Arūnas Stirė (Valstybinis mokslinių tyrimų institutas
Fizinių ir technologijos mokslų centras, gamtos mokslai, chemija, N 003).

Gynimo taryba:

Pirmininkas – prof. dr. Evaldas Naujalis (Valstybinis mokslinių tyrimų
institutas Fizinių ir technologijos mokslų centras, gamtos mokslai, chemija, N
003)

Nariai:

Doc. dr. Brigita Abakevičienė (Kauno technologijos universitetas, gamtos
mokslai, fizika, N 002),

Prof. dr. Julija Armalytė (Vilniaus universitetas, gamtos mokslai, biochemija,
N 004),

Dr. Aldona Balčiūnaitė (Valstybinis mokslinių tyrimų institutas Fizinių ir
technologijos mokslų centras, gamtos mokslai, chemija, N 003),

Dr. Mantas Šilkūnas (Old Dominion University, gamtos mokslai, biofizika, N
011).

Disertacija ginama viešame Gynimo tarybos posėdyje 2025 m. gruodžio mėn. 19
d. 14:00 val. Fizinių ir technologijos mokslų centro A101 auditorijoje.

Adresas: Saulėtekio al. 3, A101, LT-10257, Vilnius,
tel. +3705264 9211; el. paštas office@ftmc.lt

Disertaciją galima peržiūrėti Vilniaus universiteto bibliotekoje ir VU interneto
svetainėje adresu:

<https://www.vu.lt/naujienos/ivykiu-kalendorius>

SANTRUMPOS

COC - cyclic olefin copolymer
CP-Ti - commercially pure titanium
ECM - extracellular matrix
EIC - electrochemical impedance spectroscopy
FBS – fetal bovine serum
GAG – glycosaminoglycans
LoC – lab-on-a-chip
MPS – microphysiological system
OoC – organ-on-a-chip
OSTE - off-stoichiometry thiol-ene
PBS - phosphate-buffered saline
PC – polycarbonate
PCL - polycaprolactone
PDL - poly-D-lysine
PDMS - polydimethylsiloxane
PEF – pulsed electric field
PEG - polyethylene glycol
PET – polyethylene terephthalate
PG - proteoglycan
PGA - polyglycolic acid
PLA - polylactic acid
PLGA - poly-lactic-co-glycolic acid,
PLL - poly-L-lysine
PMMA – poly(methylmethacrylate)
PTFE – polytetrafluoroethylene
PU - polyurethane
PVA - polyvinyl alcohol
PVP - polyvinylpyrrolidone
SBF – simulated body fluid
SEM – scanning electron microscope
SD – standard deviation
TEER – trans epithelial/endothelial electrical resistance
UHMWPE - ultra-high molecular weight polyethylene

CONTENT

INTRODUCTION	10
Aim and objectives	11
Scientific novelty.....	11
Statements presented for the defence	12
Contribution of the author	13
List of publications	13
Participation in conferences.....	14
1. LITERATURE REVIEW	16
1.1. BIOMATERIALS	16
1.1.1. Description of biomaterials	16
1.1.2. Metals and their alloys	18
1.1.3. Bioceramics	21
1.1.4. Bioceramic alumina.....	22
1.1.5. Synthetic and natural polymeric biomaterials	25
1.1.6. Polycarbonate.....	27
1.1.7. Biocompatibility.....	29
1.2. CELL ADHESION	32
1.2.1. Introduction to adhesion.....	32
1.2.2. Adherent and suspension cells	32
1.2.3. The extracellular matrix	33
1.2.4. Building blocks of ECM	35
1.2.5. Collagen	35
1.2.6. Fibronectin	37
1.2.7. Cell adhesion receptors	37
1.2.8. Focal adhesion.....	38
1.2.9. Process of cell adhesion	39
1.3. CELL ADHESION ON ARTIFICIAL SURFACES	41
1.3.1. Surface topography	42

1.3.2. Surface roughness	43
1.3.3. Surface porosity.....	44
1.3.4. Material stiffness	45
1.3.5. Curvature.....	46
1.3.6. Surface chemical properties	46
1.3.7. Functional groups.....	47
1.3.8. Surface wettability.....	48
1.3.9. Surface energy.....	49
1.3.10. Surface charge.....	50
1.3.11. Modification of surface chemistry	50
1.3.12. Oxidation of the surface	50
1.3.13. Surface coatings for adhesion	52
1.3.14. Future directions in biomaterial surface engineering.....	53
1.4. MICROFLUIDIC TECHNOLOGY	54
1.4.1. Definition of microfluidics.....	54
1.4.2. Microfluidics with flow.....	55
1.4.3. Microfluidic set-up.....	56
1.4.4. Materials for microchip fabrication.....	57
1.4.5. PDMS	58
1.4.6. OSTE.....	60
1.4.7. Microchannel architecture.....	61
1.4.8. Fluid dynamics and transport mechanisms in microfluidic systems..	62
1.4.9. Shear stress.....	65
1.4.10. Biology meets microfluidics	66
2. METHODOLOGY	68
2.1. MATERIALS AND EQUIPMENT	68
2.1.1. Material	68
2.1.2. Cell lines.....	69
2.1.3. Equipment	69
2.2. METHODS	70

2.2.1. Bioceramic coating preparation	70
2.2.2. Water droplet contact angle.....	71
2.2.3. SBF immersion experiments	71
2.2.4. ICP-OES.....	72
2.2.5. Corrosion tests.....	72
2.2.6. SEM imaging	73
2.2.7. Cell line handling	74
2.2.8. Viability assays	74
2.2.9. Cell adhesion on PC membranes.....	75
2.2.10. Biological functionalisation of PC membrane	75
2.2.11. Oxidation of the PC membrane.....	76
2.2.12. Fabrication of a microfluidic chip.....	76
2.2.13. Microfluidic setup	78
2.2.14. PEF treatment experiments	78
2.2.15. Oxygen sensing setup.....	80
2.2.16. pH measurement setup	80
2.2.17. TEER measurement.	82
2.2.18. Statistical analysis	82
3. RESULTS	83
3.1. BIOCOMPATIBILITY STUDIES OF BIOCERAMIC ALUMINA COATINGS ON AL ALLOY 6082	83
3.1.1. Structural characterization of bioceramic coatings	84
3.1.2. Surface wettability.....	87
3.1.3. Ion release and its toxicity.....	87
3.1.4. Electrochemical evaluation of corrosion resistance in Al alloy and Al ₂ O ₃ coatings.....	91
3.1.5. Characterization of bioceramic coatings after SBF immersion.....	94
3.1.6. Biocompatibility test	96
3.1.7. Discussion on biocompatibility of bioceramic coatings.....	99
3.2. OPTIMIZATION OF POLYCARBONATE FOR CELL ADHESION	102

3.2.1. Inherent adhesion properties of PC membrane	102
3.2.2. Chemical treatment of PC membrane	105
3.2.3. Cell adhesion on the modified PC membranes	107
3.2.4. Cell adhesion with different adhesion factors	108
3.2.5. Cell culturing in a microfluidic channel.....	109
3.2.6. Discussion on PC surface treatment for improved cell adhesion	111
3.3. POLYCARBONATE-INTEGRATED MPS FOR PEF TREATMENT OF CELLS.....	113
3.3.1. Design of the microchip	113
3.3.2. Microchip fabrication.....	114
3.3.3. Simulation of the electric field in the microchip.....	115
3.3.4. Cell viability and permeability after PEF treatment in the microchip.....	117
3.3.5. Prediction of affected area in continuous PEF	119
3.3.6. Oxygen measurement experiments	121
3.3.7. pH measurement.....	122
3.3.8. TEER measurement.....	123
3.3.9. Discussion on the MPS	123
SUMMARY	127
CONCLUSIONS	130
REFERENCES	131
SANTRAUKA	153
ACKNOWLEDGEMENT.....	175
Curriculum Vitae	177

INTRODUCTION

The interaction between engineered materials and biological systems – cells and tissues – is a fundamental aspect of material engineering and tissue regeneration research. Biomaterials designed for biomedical applications must support cellular interactions and possess adequate mechanical strength to maintain structural stability under physiological conditions. In addition to mechanical and biocompatible properties, they should promote essential cellular functions, such as adhesion, proliferation, and differentiation. These characteristics are important not only in regenerative medicine but also in fields as tissue engineering and *in vitro* organ modelling.

The functional requirements of biomaterials vary depending on their specific application. In tissue regeneration and implantology, biomaterials serve as scaffolds that facilitate cell adhesion, migration, and tissue integration. In contrast, implants used in the circulatory system, such as artificial heart valves or vascular prostheses, must actively prevent cell adhesion to avoid complications like thrombosis. Therefore, to ensure the effective application of biomaterials, it is crucial to select the appropriate material and modify its surface according to the biological system's requirements. Surface engineering techniques can influence the behaviour of cells through chemical and physical modification. These adjustments affect surface topography, porosity, and roughness, and may also alter surface chemistry through the incorporation of functional groups that modulate hydrophilicity. All of these features impact protein adhesion formation of focal adhesions, and, consequently, cell adhesion.

In recent years, researchers have focused not only on improving surface modification strategies but also on integrating them into advanced *in vitro* systems that better mimic real physiological conditions. Microfluidic technologies offer a powerful way to study how cells behave in dynamic environments, where factors as fluid flow and shear stress are important. These systems combine material engineering with biological modeling and can include various types of stimulation, such as electrical signals, chemical gradients, or mechanical cues. This allows for precise, controlled experiments that reveal how cells respond to specific cues.

This thesis focuses on optimizing biomaterial surfaces and improving their biocompatibility through targeted modification strategies. The research examined two biomaterials - bioceramic alumina and polycarbonate (PC) – each belonging to a distinct biomaterial class. The integration of PC into microfluidic systems enabled the development of functional platforms for cell culture and stimulation. The proposed solution contributes to the advancement of biomaterial science and opens new possibilities in both implantology and tissue engineering.

Aim and objectives

This dissertation aims to systematically evaluate the biocompatibility and cell adhesion properties of biomaterials – anodized Al alloy 6082 and polycarbonate – to assess and optimize their suitability for biomedical applications and integration into a microphysiological system.

Objectives:

1. To evaluate the biocompatibility, chemical stability, and surface characteristics of two distinct Al alloy 6082, anodized with sulfuric and phosphoric acids, to assess their suitability as biomaterials.
2. To chemically modify the surface of a porous polycarbonate membrane to enhance its compatibility for cell adhesion and cultivation within a microfluidic system.
3. To develop a microphysiological system incorporating a track-etched polycarbonate membrane for pulsed electric field treatment and real-time monitoring of microenvironmental parameters.

Scientific novelty

This dissertation presents research that contributes to the advancement of biomaterials engineering and their application in microfluidic systems. The focus is placed on surface optimization, material biocompatibility, and integration of modified materials into microfluidic platforms for *in vitro* studies. The study assesses the impact of surface modification strategies on two distinct classes of biomaterials – bioceramic alumina (Al_2O_3) coatings for orthopaedic implants and polycarbonate (PC) polymer for microfluidic cell culture systems.

The first part of the study investigates ceramic coatings produced via anodization of industrial-grade aluminum (Al) alloy 6082, evaluating their potential as biomedical materials for implantology. Anodization is proposed as an alternative to conventional sintered Al_2O_3 bioceramics, which are brittle, form-limited, and costly to produce. Unlike powder-based manufacturing methods, anodizing enables the formation of mechanically robust, lightweight, and customizable biomaterials.

Although anodizing itself is not a novel technique, this study presents the first systematic evaluation of anodized Al alloy 6082, with emphasis on assessing its suitability as a biomaterial. The evaluation encompasses surface characterisation, chemical stability, and *in vitro* biocompatibility, benchmarked against medical-grade titanium alloy. One of the anodized specimens demonstrated properties consistent with biomaterial classification and shows potential for biomedical applications.

The second part of the research introduces a surface modification strategy for inherently hydrophobic polycarbonate, using wet chemical oxidation with sodium metaperiodate, sulfuric acid, and piranha solution. Although similar surface treatments have been recently reported by other authors using alternative reagents, this pilot study investigates specifically the effectiveness of the above-mentioned reagents in enhancing cell adhesion within microfluidic cell culture. The modified surfaces supported stable and reproducible cell adhesion under both static and dynamic culture conditions, when combined with adhesion-promoting factors such as poly-D-lysine (PDL), fibronectin, and collagen. This approach offers a practical and effective alternative for improving cell adhesion in microfluidic systems, with relevance in tissue engineering and organ-on-a-chip technologies.

The third part of the dissertation introduces a custom-designed and fabricated microphysiological system (MPS) that integrates multiple advanced functionalities into a single unified platform. The MPS combines a track-etched polycarbonate membrane, embedded electrodes within a microchannel, and real-time environmental sensors – an integrated configuration not previously described in the literature. The polycarbonate membrane functions as a semi-permeable barrier between two parallel microchannels, enabling the dual-compartment cell culture to connect through membrane pores. Electrodes embedded directly within the microchannel allow for the localized application of pulsed electric fields (PEF). In parallel, embedded oxygen and pH sensors provide continuous monitoring of the cellular environment, even in devices fabricated from gas-impermeable materials such as off-stoichiometry thio-ene (OSTE) and cyclic olefin copolymer (COC).

Addressing the limitation of conventional microfluidic systems, the pilot MPS presented here represents a novel convergence of electrical stimulation, compartmentalized culture, and real-time sensing within a single microfluidic device, marking a functional advancement in microfluidic and *in vitro* modelling technologies.

Statements presented for the defence

1st statement:

The Al alloy 6082, anodized with sulfuric acid electrolyte, can be classified as a biomaterial due to its chemical stability and biocompatibility properties.

2nd statement:

Chemical oxidation of the polycarbonate membrane followed by coating with poly-D-lysine ensures robust cell adhesion under both static and dynamic culture conditions.

3rd statement:

A microphysiological system has been developed, featuring a track-etched polycarbonate membrane, integrated electrodes, and oxygen and pH sensors, enabling pulsed electric field stimulation of mammalian cells and real-time monitoring of physiological parameters.

Contribution of the author

Bioceramic coating studies: The author conducted immersion experiments, contact angle measurements, all cell-based experiments, and data analysis. The experimental samples and their structural characteristics were provided by Dr. Tadas Matijošius; ICP-OES measurements were conducted by Dr. Aleksey Žarkov; SEM was conducted by Dr. Aušra Selskienė. Electrochemical measurements for corrosion assessments were conducted, analysed, and described by Dr. Asta Grigucevičienė. Both the author and Dr. Tadas Matijošius contributed equally to the drafting and writing of the publication.

PC membrane modification: The author modified the PC membrane, conducted surface characterization, cell-based assays, and data analysis. The chemical modification strategy was initially developed by Dr. Antanas Strakšys.

MPS fabrication and cellular studies: The author carried out the core work related to MPS fabrication and cellular experiments, including technological development, cell handling, data analysis, and publication drafting and writing. The overall project design, including the microchip and MPS layout, was executed by Dr. Arūnas Stirkė. The MPS supporting jig was designed and fabricated using 3D printing technology by Dr. Eivydąs Andriukonis, while the pH monitoring system was designed and built by Dr. Martynas Šapurov. Jorūnas Dobilas conducted numerical modelling and simulations.

List of publications

Matijošius, Tadas; **Bakutė, Neringa**; Padgurskas, Juozas; Selskienė, Aušra; Žarkov, Aleksej; Grigucevičienė, Asta; Kavaliauskaitė, Justina; Stirkė, Arūnas; Asadauskas, Svajus. Corrosion and biocompatibility studies of bioceramic alumina coatings on aluminum alloy 6082. *ACS applied materials & interfaces*. Washington: American chemical society, 2025, vol. 17, iss. 17, pp. 24901-24917. ISSN 1944-8244. eISSN 1944-8252. doi: [10.1021/acsami.5c00532](https://doi.org/10.1021/acsami.5c00532) [Science Citation Index Expanded (Web of Science); Scopus] [Citav. rod.: 4,080, Q1 (2025, SCIE)] [M.kr.: N 003, T 004]

Bakutė, Neringa; Andriukonis, Eivydas; Kasperavičiūtė, Kamilė; Dobilas, Jorūnas; Šapurov, Martynas; Mozolevskis, Gatis; Stirkė, Arūnas. Microphysiological system with integrated sensors to study the effect of pulsed electric field. *Scientific reports*: Springer science and business media LLC, 2024, vol. 14, iss. 1, art. no. 18713, pp. 1-12. eISSN 2045-2322. doi: [10.1038/s41598-024-69693-w](https://doi.org/10.1038/s41598-024-69693-w) [Science Citation Index Expanded (Web of Science); Scopus] [Citav. rod.: 8,300, Q1 (2024, SCIE)] [M.kr.: N 003, T 004]

Abouhagger, Adei; Celiešiūtė-Germanienė, Raimonda; **Bakutė, Neringa;** Stirkė, Arūnas; Martins Antunes de Melo, Wanessa de Cassia. Electrochemical biosensors on microfluidic chips as promising tools to study microbial biofilms: a review. *Frontiers in cellular and infection microbiology*. Lusanne: Frontiers media SA, 2024, vol. 14, pp. 1-16. eISSN 2235-2988. doi: [10.3389/fcimb.2024.1419570](https://doi.org/10.3389/fcimb.2024.1419570) [Science Citation Index Expanded (Web of Science); Scopus] [Citav. rod.: 4,590, Q1 (2024, SCIE)] [M.kr.: N 003, T 004, T008]

Participation in conferences

1. Open Readings 2024. Agnė Damarackaitė, **Neringa Bakutė**, Arūnas Stirkė “Mammalian cells electroporation in the microfluidic chip”. Poster presentation.
2. MicroTAS 2023. **Neringa Bakutė**, Jorūnas Dobilas, Skirmantas Keršulis, Gatis Mozolevskis, Arūnas Stirkė. “OSTE-based microfluidic chip for PEF treatment of mammalian cells”. Poster presentation.
3. ICMN 2023. International Conference on Microfluidics and Nanofluidics. Arūnas Stirkė, **Neringa Bakutė**, Gatis Mazolevskis “PDMS-free microfluidic chip fabrication and utilization for pulsed electric fields application. Oral presentation.
4. Fiztech 2023. **Neringa Bakutė**, Agnė Damarackaitė, Kamilė Kasperavičiūtė, Eivydas Andriukonis, Martynas Šapurov, Jorūnas Dobilas, Vilius Vertelis, Skirmantas Keršulis, Gatis Mazolevskis, Arūnas Stirkė. Microphysiological system for the electroporation of the mammalian cells with oxygen, pH and TEER sensors. Oral presentation.
5. Open Readings 2023. Paulina Kizinievič, **Neringa Bakutė**, Arūnas Stirkė “Adhesion of mammalian cells on polycarbonate membrane” Poster presentation.
6. 4th World Congress on Electroporation & Pulsed Electric Fields in Biology, Medicine, Food and Environmental Technologies. **Neringa Bakutė**, Elinga Bražionytė, Arūnas Stirkė „High-throughput cell transfection in a microfluidic electroporation chip“. Oral presentation.

7. International 3rd Baltic Biohysics conference. **Neringa Bakutė**, Arūnas Stirkė. „Fabrication of microfluidic chip for electroporation of cells“. Poster presentation.
8. Fiztech 2022. **Neringa Bakutė**, Paulina Kizinievič, Elinga Bražionytė, Arūnas Stirkė. „Microfluidic chip fabrication technology for cell electroporation“ Oral presentation
9. Fiztech 2021. **Neringa Bakutė**, Tadas Matijošius, Auksė Kazlauskaitė, Justina Kavaliauskaitė, Arūnas Stirkė. “Biocompatibility of metal surfaces for optoporation studies” Oral presentation.

1. LITERATURE REVIEW

The literature review encompasses three aspects of the dissertation: biomaterials, cell adhesion, and microfluidics. In the first section, I will provide an overview of biomaterials and introduce two specific biomaterials—bioceramic alumina, obtained by anodizing Al alloy, and polycarbonate — that are the focus of my thesis. The second section defines cell adhesion, identifies key cellular and extracellular matrix (ECM) components involved in this process, and explains the underlying mechanism. This section provides essential context for understanding cell adhesion to artificial surfaces, such as biomaterials. Finally, the third section presents an overview of microfluidic systems, reflecting the broader orientation of this dissertation and its experimental foundation in microfluidic device development.

1.1. BIOMATERIALS

1.1.1. Description of biomaterials

A biomaterial is defined as a material specifically engineered to interact with biological systems for medical and biological purposes. Biomaterials are utilized in various fields, including therapeutic and diagnostic applications. Their applications span medical implantation devices, drug delivery systems, tissue engineering, and microfluidic systems for *in vitro* manipulation with cells and tissues. The latter includes organ-on-a-chip and MPS [1].

In the realm of medical devices, biomaterials are used to create artificial heart valves, blood vessels, and other implants. For drug delivery, biomaterials can be engineered to deliver drugs to specific areas of the body in a controlled manner, ensuring effective medication targeting and minimizing side effects. In tissue engineering, biomaterials act as scaffolds that support cell adhesion, proliferation, and biosynthesis, providing a structural framework for tissue formation and regeneration. Organ-on-a-chip systems and MPS, which replicate organ function *in vitro*, rely on biomaterials to mimic the natural environment of an organ. Meanwhile, in wound healing, biomaterials are incorporated into dressings and sutures to enhance healing by creating a supportive environment for cell growth and tissue repair [1].

Biomaterial engineering bridges multiple disciplines, including biology, chemistry, material science, and engineering. The designed biomaterial should mimic the natural environment of cells, promoting tissue regeneration and repair. Establishing strong positive interactions between the biomaterial surface and

cells is entirely dependent on both the materials and the targeted biological system chemistry [2].

Table 1. Types of biomaterials and their most relevant applications [1].

	Benefits and limitations	Examples	Applications
Metals	<p>Benefits:</p> <p>high mechanical properties high fatigue resistance ductility</p> <p>Limitations:</p> <p>poor biocompatibility stiffness high specific weight corrosion</p>	Stainless steel, nickel, platinum, tantalum, titanium, Ti6Al4V, CoCrMo	Orthopedic, orthodontic, cardiovascular
Ceramics	<p>Benefits:</p> <p>biocompatibility chemical inertness high compressive strength corrosion resistance</p> <p>Limitation:</p> <p>low impulsive tensile strength high weight brittleness not easy to process</p>	Alumina, zirconia, hydroxyapatite , beta- tricalcium phosphate, pyrolytic carbon	Orthopedic, orthodontic, cardiovascular
Polymers	<p>Benefits:</p> <p>toughness low weight processability</p> <p>Limitation:</p> <p>low mechanical strength degradability over time deformability over time</p>	Polyethylene, cel- lulose, PU, nylon, PVA, PLGA, PEG, PMMA, PCL, UHMWPE, PC PLA, PGA, PTFE, PLA *	Orthopaedic, orthodontic, cardiovascular, breast implants, scaffolds for soft tissues
Biological material	<p>Benefits:</p> <p>Biocompatibility</p> <p>Limitation:</p> <p>Difficult handling and storage</p>	Porcine/bovine pericardium, skin grafts	Bioprosthetic heart valves, artificial heart, wound healing, tissue regeneration [3]

* Polyurethane (PU), polyvinyl alcohol (PVA), poly-lactic-co-glycolic acid (PLGA), polyethylene glycol (PEG), polymethylmethacrylate (PMMA), polycaprolactone (PCL), ultra-high molecular weight polyethylene (UHMWPE), polylactic acid (PLA), polyglycolic acid (PGA), polytetrafluoroethylene (PTFE), polylactic acid (PLA).

Biomaterials exhibit a wide range of chemical compositions and properties, allowing them to be utilized in various applications. It is therefore quite difficult to define them uniquely. The main groups are metals and alloys, ceramics, and polymers. **Table 1** lists some of the most significant biomaterials from clinical applications.

Each type of biomaterial requires specific biocompatibility considerations. Ensuring safe and effective interaction with biological tissues. Chapter 1.1.8 will discuss biocompatibility in greater detail, outlining its importance in biomaterial selection, testing methods, and impact on medical applications.

1.1.2. Metals and their alloys

Metals are the most widely used scaffold materials for load-bearing implants. Their application includes orthopaedic implants - including wires, screws, fixation plates, and joint prostheses for knees, hips, ankles, and shoulders - as well as in dental implantology and cardiovascular surgeries. Compared with other biomaterials, metallic materials possess superior mechanical properties, including fatigue strength, fracture toughness, yield strength, and ductility.

Historically, metals like gold (Au), platinum (Pt), silver (Ag), tantalum (Ta), palladium (Pd), nickel (Ni), copper (Cu), Al, zinc (Zn), and magnesium (Mg) were used in implantology, starting from the 16th century. The most used materials are stainless steel, titanium (Ti), and Ti alloys, cobalt (Co) -based, and Ta-based alloys. However, it was later realised that these metals often lack essential features such as biocompatibility or mechanical properties. The major limitation of using metals in biological fluids is their tendency to corrode. This led to the development of modern materials such as stainless steel, cobalt-chromium (Co-Cr) alloys, Ti alloys, and others. Among these, Ti and its alloys are considered the most favourable material for implantology due to their excellent combination of mechanical properties, corrosion resistance, and biocompatibility [1], [4].

Modern metallic biomaterials have been developed to address the limitations of earlier materials, offering a unique combination of high strength and corrosion resistance, particularly in Ti and Co-Cr alloys. However, several challenges remain, including ion release, the general susceptibility to corrosion in metals

other than Ti and Co-Cr alloys, and the high stiffness of these materials compared to natural bone. These factors continue to be areas of concern in biomaterial research and development [5]. **Table 2** presents a comparison of the mechanical properties of metallic biomaterials and natural bone. The Young's modulus (or elastic modulus) of a material measures its stiffness and describes how much it deforms under an applied force. It determines how well the biomaterial interacts mechanically with the surrounding tissue. It is important for the stress shielding – this occurs because the implant bears most of the mechanical load; this can result in bone resorption and weakening. The closer match to natural bone minimizes mechanical mismatching. Moreover, the elastic modulus determines how a material withstands repetitive stresses without fracturing.

The second data, presented in **Table 2**, is ultimate tensile strength, which presents the maximum amount of tensile strength that a biomaterial can withstand before it breaks. The third presented data is the fracture toughness, which measures a material's ability to resist crack propagation when subjected to stress. Low fracture toughness is more prone to sudden, brittle fracture, which could lead to implant failure [4].

Table 2. Mechanical properties of metallic alloy materials and cortical bone [4].

Materials	Young's modulus (GPa)	Ultimate tensile strength (MPa)	Fracture toughness (MPa \sqrt{m})
CoCrMo alloys	240	900-1540	~100
316L stainless steel	200	540-1000	~100
Ti alloys	105-125	900	~80
Mg alloys	40-45	100-250	15-40
NiTi alloys	30-50	1355	30-60
Cortical bone	10-30	130-150	2-12

Below is a summary of the main metallic biomaterials.

Stainless steel refers to a class of iron (Fe)-based alloys specifically engineered for enhanced corrosion resistance. This resistance is attributed to the presence of Cr, which forms a thin protective oxide layer on the surface of steel. This layer prevents oxygen and moisture from penetrating and causing corrosion, thereby inhibiting corrosion. However, in a chloride-rich environment, such as bodily fluids and saliva, stainless steel is susceptible to pitting and crevice corrosion. To mitigate this, a modern 316L stainless steel alloy was designed to improve corrosion resistance. The "L" stands for low carbon content, which enhances the corrosion resistance. Additionally, 316L contains Cr, Ni, and molybdenum (Mo), which further improve its durability. However, the release of

Ni and Cr may cause adverse reactions such as allergies or toxicity. Moreover, the corrosion resistance of 316L remains insufficient for long-term implants. Thus, stainless steel can be used only as a biomaterial for short-term implants [4], [6].

Co-based alloys exhibit exceptionally high corrosion resistance, even in a chloride-rich environment. This is due to the spontaneous creation of a passive chromium oxide (Cr_2O_3) layer on their surface [7]. Cobalt-based alloys also offer a balance between biocompatibility and mechanical properties. They demonstrate high wear resistance, fatigue strength, and hardness, making them suitable for long-term loading-bearing applications. However, the cost of Co-based alloy is higher than that of stainless steel. The most commonly used Co-based alloys are Co-Cr-Mo for orthopedic implants and Co-Ni-Cr-Mo for cardiovascular stents and dental materials [4].

Ti-based alloys are the most widely used metallic biomaterials due to their excellent biocompatibility and superior mechanical properties. Ti promotes direct bone apposition and exhibits a lower elastic modulus than stainless steel or Co-based alloys, reducing the risk of stress shielding. The mechanical properties of Ti are further enhanced in Ti-6Al-4V, which contains 6% Al and 4% vanadium (V). However, Al and V ions may be released over time, which are neurotoxic and cytotoxic and can interfere with cellular processes. To address this issue, surface engineering techniques, such as coating, have been developed. Additionally, other Ti-based materials, such as Ti-6Al-7Nb (where V is replaced with niobium (Nb)) and β -Ti alloys, have been introduced to improve biocompatibility and mechanical performance [8], [9].

Ni-Ti alloy, commonly known as nitinol, is another advantageous Ti-based alloy for clinical applications. It typically consists of 54-60 wt% Ni and exhibits unique properties of superelasticity and shape memory. Nitinol has good corrosion resistance and biocompatibility, but there is a significant concern regarding the release of Ni ions. It can cause allergic reactions and is associated with carcinogenic effects. Despite these limitations, nitinol is widely used as guide wires, stents, peripheral vascular devices, and embolic protection filters [4], [10].

Ta-based implants can form a compact passive oxide layer, Ta_2O_5 , on their surface. This oxide layer promotes bone ingrowth by facilitating the formation of apatite, which enhances adhesion of hard and soft tissues. Ta has a low elastic modulus, closely matching that of natural bone. Ta has high fatigue strength and chemical stability. Additionally, Ta can be manufactured as porous structures, further improving bone ingrowth. Ta is considered an excellent biomaterial for biomedicine applications. However, its high cost, stemming from limited

availability and expensive processing, restricts its widespread use. To address this, thin Ta coatings have been developed to promote outstanding properties of Ta to other materials, such as stainless steel, Co-Cr alloys, and Ti-based materials [4], [11], [12].

Mg-based alloys, such as Mg-Zn, Mg-Ca, Mg-strontium (Sr), are resorbable materials, specifically designed for temporary implant applications. These alloys eliminate the need for a second surgery by gradually degrading in the body. Mg-based alloys have a low elastic modulus, which helps reduce stress shielding. Additionally, they support bone growth. Several challenges restrict the use of the implant, including rapid resorption that compromises its structural integrity before healing is completed; hydrogen gas formation, elevated corrosion rate, and limited mechanical strength [4], [13].

1.1.3. Bioceramics

Ceramics can be defined as inorganic non-metallic materials and are commonly described by their chemical composition, which can be generally expressed in two ways; either as weight percentage (wt %) of elements or as the composition of elements, represented by the proportion of atoms of each element's percentage of the number of atoms of each element within the material (expressed as atomic percentage = at %).

Bioceramics are a class of ceramic materials specifically designed for dental restoration and bone-contacting applications. It is characterized by its remarkable combination of excellent strength, high hardness, toughness, and outstanding resistance to both corrosion and mechanical degradation. There are two types bioceramics: oxides, such as silicon oxide (SiO_2), aluminum oxide, also known as alumina (Al_2O_3), and zirconium oxide, also known as zirconia (ZrO_2); and non-oxide, such as silicon carbide (SiC), silicon nitride (Si_3N_4), and aluminum nitride ($\text{Al}(\text{NO}_2)_3$) [14]. In general, bioceramics are considered biocompatible materials. The substances released to the surrounding tissues depend on the ceramic material's composition, mainly Si, Al, Na, K, Mg, and Ca. Local toxicity is considered low, and systemic toxicity is unlikely to occur due to relatively low amounts of released materials, such as lithium and lead [1].

Based on their interaction with adjacent tissues, bioceramics can be classified into three categories:

- 1) Bioinert, such as alumina and zirconia, result in little or no physiological reaction in the human body and tend to exhibit inherently low levels of reactivity, which peak in the order of hundreds of years.

2) Bioactive, such as hydroxyapatite ($\text{Ca}_{10}(\text{PO}_4)_6(\text{OH})_2$), react positively with local cells, i.e., they form direct chemical bonds and exhibit a substantially higher level of reactivity, reaching a peak around 100 days.

3) Biodegradable, such as tricalcium phosphate ($\text{Ca}_3(\text{PO}_4)_2$), which is slowly and gradually replaced by bone, have even higher levels of reactivity, peaking in the order of 10 days [14], [15].

Oxides are highly stable inorganic materials; they do not undergo any additional oxidative processes, meaning no corrosion or ion release would occur. The limitations of the widespread use of bioceramic oxides are stiffness and brittleness, which represent severe drawbacks in many practical applications. Only alumina and zirconia are utilized to produce hip prostheses, while ceramic composite oxides, prevalently made of alumina-zirconia ($\text{Al}_2\text{O}_3\text{-ZrO}_2$), were subsequently developed, seeking improved mechanical performance [16]. Alumina exhibits features of chemical stability, high hardness, and wear resistance, making it a preferred material for load-bearing implants [17], [18]. Its bioinertness to surrounding tissues can be either an advantage or a limitation, depending on the application. To enhance its performance in biomedical devices that require improved cell adhesion, surface modification techniques such as anodization have been developed. These techniques enable alumina to overcome some of its inherent challenges and expand its functional capabilities [19].

1.1.4. Bioceramic alumina

Bioceramic alumina, or aluminum oxide Al_2O_3 , is a type of ceramic material designed for biomedical applications. Al_2O_3 is an inorganic compound of Al and O, with the most common and thermodynamically stable form of crystalline $\alpha\text{-Al}_2\text{O}_3$ known as corundum. $\alpha\text{-Al}_2\text{O}_3$ phase can be formed by calcinating hydrated Al_2O_3 through several different phase structures, or directly from powders using advanced methods [20]. Al_2O_3 is chemically stable and resistant to acids and bases, essentially based on dense Al_2O_3 ceramics with a hexagonal structure [21].

Since the 1960s, bioinert alumina Al_2O_3 has been utilized as a promising candidate in orthopedic joint prostheses due to its exceptional compressive strength and chemically inert properties [16]. Al_2O_3 does not promote bonding with living tissues or body fluids but exhibits resistance to low pH environments for thousands of hours. Alumina demonstrates high chemical inertness, indicating that a significant amount of time is required to establish stable connections between implants and tissues, and it does not induce mutagenicity to cells [22], [23], [24].

Alumina ceramics for implants are typically fabricated from powder through a series of demanding steps, such as mechanical grinding, dry pressing, sintering,

and extrusion at high temperatures and pressures [25]. These processes are costly and time-intensive, and the brittleness of alumina, along with compositional impurities, limits the production of large or complex-shaped structures.

To overcome these limitations and enhance surface properties, Al alloys were introduced as alternative substrates. Al, when combined with alloying additives such as Si, Fe, Co, Mg, Mn, Zn, forms an Al alloy. Al alloy enhances mechanical and corrosion resistance compared to Al. Both pure Al and its alloys rapidly react with the oxygen from the atmosphere at ambient temperatures by creating a thin Al_2O_3 layer of 1–10 nm thickness [26]. However, this native oxide layer is insufficient for robust mechanical protection and corrosion resistance, and may lead to the release of toxic Al^{3+} ions.

To enhance the thickness, uniformity, and functionality of the oxide layer, anodization is employed. Anodization is an electrochemical process that creates a protective oxide layer on the surface of a metal. Anodized alloys demonstrate enhanced surface hardness, corrosion resistance, and other technical properties [19]. This process can be conducted using various electrolytes, including sulfuric, oxalic, phosphoric, and chromic acids, as well as their mixtures. Anodization is commonly employed in industrial applications. During the process, Al reacts with anions (such as HSO_4^- , OH^- , RCOO^- , etc.), resulting in porous anodized coatings of varying thicknesses, which can exceed 100 μm or more. However, it is not possible to achieve coatings thicker than 200 μm due to the high resistivity of Al_2O_3 . Anodized Al_2O_3 coatings feature vertical nanopores of uniform size and distribution [27].

This artificial oxide film forms on Al when a sufficient voltage current flows through an electrolyte, with Al as the anode and a suitable material (often lead (Pb) or stainless steel) as the cathode [28]. The mobile species involved in the anodizing of pure Al in aqueous solutions are Al^{3+} cations, and O^{2-} or OH^- anions. The oxidation of Al at the Al/oxide interface generates Al^{3+} cations, while O^{2-} or OH^- anions form at the oxide/solution interface by the removal of H^+ from H_2O molecules. Ionic migration through the oxide under a high electric field, in the range of 10^8 to 10^9 V/m, facilitates the growth of the anodic oxide film [29].

The anodization process begins with surface cleaning, followed by immersion in an acidic electrolyte bath. Upon applying electric current, the following reactions occur:

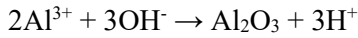
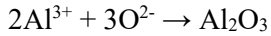
- **Cathode (reduction):**



- **Anode (oxidation):**



- **Formation of Al_2O_3 :**



- **The overall anodic oxidation reaction:**



Oxide growth occurs simultaneously at both the metal/oxide interface by Al^{3+} transport and at the oxide/electrolyte interface by oxygen ion transport. The resulting anodized coating exhibits a well-ordered hexagonal structure, with each cell containing a central pore perpendicular to the surface (**Figure 1**). Beneath the porous layer lies a barrier layer, composed of nanocrystallites with sizes of 2–10 nm, hydrated Al_2O_3 , anions, and water molecules [30]. The barrier layer protects the underlying Al from corrosion and chemical attack, while also acting as an electrical insulator due to its high resistivity. Its thickness increases linearly with voltage by approximately 1.2-1.4 nm/V, but typically does not exceed $1\mu\text{m}$ [31], [32].

The pore size and the interpore distance primarily depend on electrolyte concentration, temperature, and anodization voltage [29]. Self-ordered porous Al_2O_3 structures can be formed under specific conditions. Sulfuric acid electrolyte at 19–25 V yields small nanopores with low interpore distance [33], [34], whereas phosphoric acid at 160–195V produces wider pores with greater interpore distance [20].

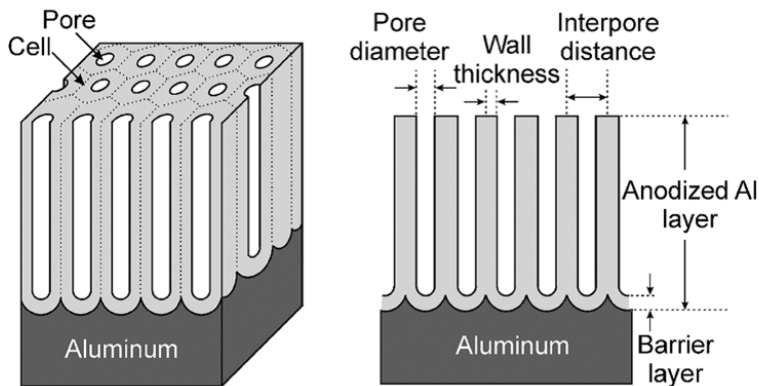


Figure 1. Schematic representation of an ideal porous anodic oxide [28].

1.1.5. Synthetic and natural polymeric biomaterials

Polymers used as biomaterials include both naturally derived and synthetic polymers, which can be either biodegradable or non-biodegradable. Naturally occurring polymers, such as collagen, chitosan, alginate, and gelatin, are often preferred for biomaterials due to their biodegradability and ease of acquisition. In contrast, synthetic polymers are commonly used in various applications, including prosthetic materials, dental materials, disposable medical supplies, and implants. Synthetic and natural biopolymers are also employed in constructing microfluidic systems for *in vitro* cell and tissue studies [35], [36].

Biodegradable natural polymers are materials that degrade into non-toxic byproducts through natural processes such as hydrolysis or enzymatic reactions. Biodegradable biomaterials do not elicit permanent chronic foreign-body reactions and are ideal for temporary implantations. Examples include (**Figure 2**):

1. Proteins and biopolymers:

- gelatin - used in drug delivery formulation and tissue engineering;
- collagen - used in wound dressing and drug delivery;
- alginate, extracted from algae, used in wound healing, tissue engineering, injectable bone cement, and drug delivery applications;
- chitosan (used for the synthesis of hydrogels, in tissue engineering scaffolds, injectable bone implant materials, and wound dressing);

2. Synthetic polymers:

- polylactic acid (PLA) $(C_3H_4O_2)_n$ – thermoplastic aliphatic polyester derived from lactic acid; used in bone fixation, tissue engineering, 3D printing, and packaging);
- poly-lactic-co-glycolic acid (PLGA) $(C_6H_8O_4)_n(C_4H_4O_4)_m$ - is obtained by copolymerization of lactic acid and glycolic acid and used in sutures and tissue engineering.
- polycaprolactone (PCL) $(C_6H_{10}O_2)_n$ - prepared by the ring-opening polymerization of ϵ -caprolactone, used in bone filling, drug delivery devices, suture, and tissue engineering. PCL is cheaper compared to PLA and PLGA, has better processability, and has high thermal stability, which enables it to be shaped by the melting process [37], [38].

Non-degradable synthetic polymers, originally developed for non-medical purposes, are now widely utilized as biomaterials due to their physical and mechanical properties that closely resemble those of human soft tissues. Common examples include (**Figure 2**):

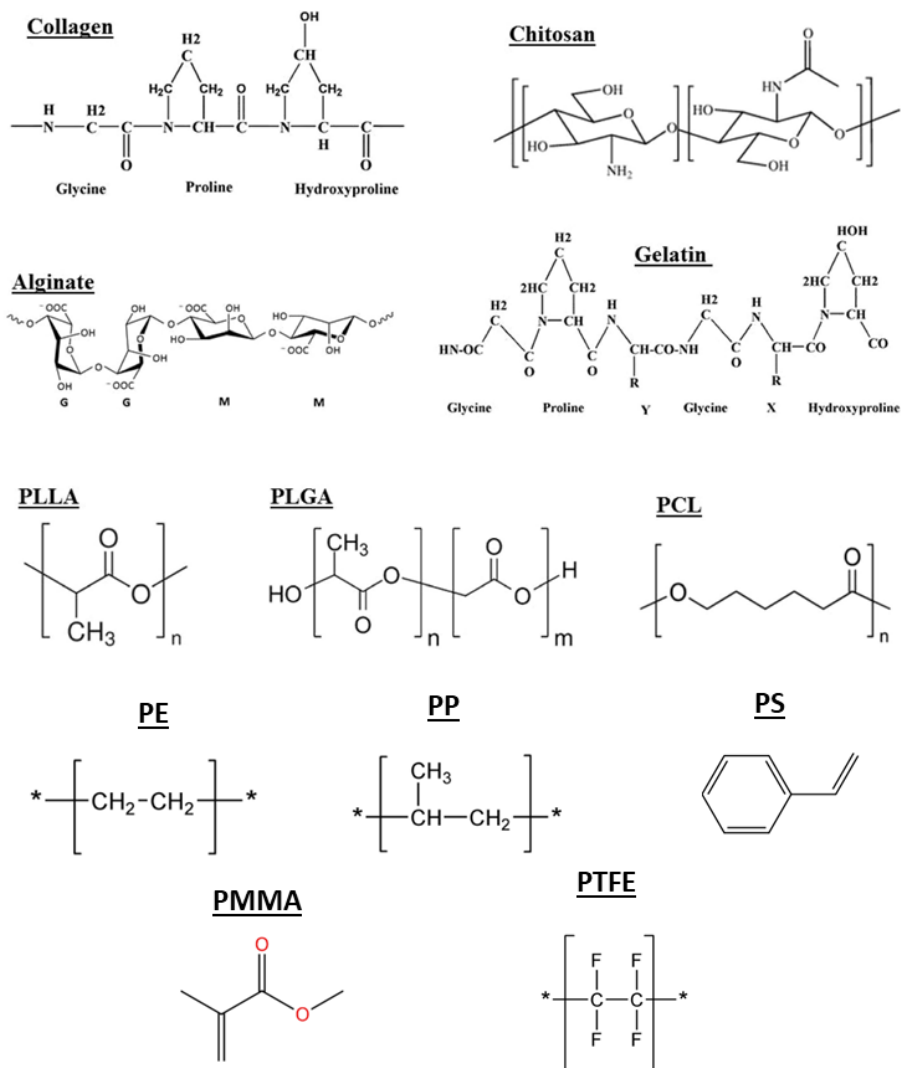


Figure 2. Chemical structures of biodegradable polymers: collagen, gelatin, alginate, chitosan, PLA (poly-L-lactic acid), PLGA (poly-lactic-co-glycolic acid), PCL (polycaprolactone), and non-degradable synthetic polymers: PE (polyethylene), PP (polypropylene), PS (polystyrene), PMMS (polymethylmethacrylate), PTFE (polytetrafluoroethylene). While PLLA is presented in the figure, the text refers to PLA in general [38], <https://commonchemistry.cas.org/>; <https://merckindex.rsc.org/>

- Polyethylene (PE) (C₂H₄)_n is used for pharmaceutical bottles, nonwoven fabric, catheters, pouches, flexible containers, and orthopedic implants;

- Polypropylene (PP) (C_3H_6)_n is used for disposable syringes, blood oxygenator membranes, sutures, nonwoven fabric, and artificial vascular grafts;
- Polystyrene (PS) (C_8H_8)_n is used for tissue culture flasks, roller bottles, and filter wares;
- PMMA ($C_5H_8O_2$)_n is used for a blood pump and reservoirs, membrane for blood dialyzer, implantable ocular lens, and bone cement;
- PTFE (C_2F_4)_n is used for catheter and artificial vascular grafts;
- PC ($C_{16}H_{14}O_3$)_n is used for hemodialyzers, arterial filters, endoscopic devices, intravenous connectors, etc.

These polymers are preferred over metals and ceramics because they can be easily manufactured in various forms (fibers, films, sheets), are cost-effective, and offer customized physical and mechanical properties. However, polymeric biomaterials have some drawbacks, including water and protein adsorption, susceptibility to surface contamination, challenges in sterilization, biodegradation, and wear issues. The use of non-degradable polymers raises environmental concerns related to pollution and waste management. Despite these challenges, their versatility makes polymers a key choice for biomedical applications [39], [40].

Polymeric materials continue to evolve and offer diverse physical forms and properties: from solids to fibers, from thin sheets to thick plates, from hard to soft components, from inert to bioactive products. Advanced fabrication techniques such as electrospinning and 3D printing enable customization of polymeric materials. However, biocompatibility is often compromised by the chemical additives such as polymerization inhibitors/initiators, monomers, plasticizers, pigments, antioxidants, and radiopaque agents [41].

1.1.6. Polycarbonate

Polycarbonate (PC), chemically referred to as poly(bisphenol A carbonate), is a synthetic thermoplastic polymer capable of undergoing repeated cycles of melting upon heating and solidification upon cooling. Its chemical formula is ($C_{16}H_{14}O_3$)_n (**Figure 3**) [42]. It is synthesized through a condensation polymerization reaction between bisphenol A (BPA) and phosgene ($COCl_2$) [43]. Structurally, PC features repeating carbonate groups ($-O-(C=O)-O-$) in its molecular backbone, which contribute to its exceptional properties. The unique combination of aromatic rings from BPA and carbonate linkages imparts high rigidity, strength, and optical clarity to the material [44].

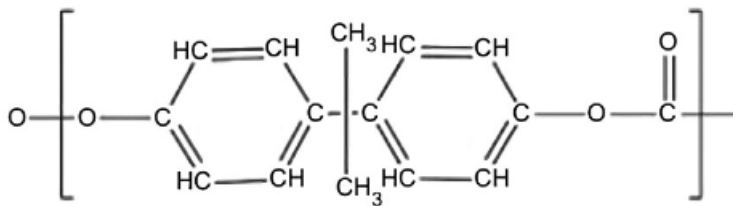


Figure 3. Chemical structure of polycarbonate [44].

PC is widely used in a range of applications, especially in the electronics, automotive, and construction sectors. Acknowledging the significance of biocompatibility, certain grades of PC are specifically engineered to comply with biocompatibility testing standards, such as ISO 10993-1. PC is among the most commonly utilized and rigorously tested engineering thermoplastic materials in the medical device industry today. Known for its strength, high heat distortion temperature, excellent optical clarity, and dimensional stability, it is an ideal material for demanding and critical healthcare applications. With a safety record spanning over 50 years, polycarbonate has become a proven material that offers significant benefits for medical applications. Moreover, it combines robustness with the ability to be sterilized using all common methods (ethylene oxide (EtO), irradiation (both gamma and electron-beam), and steam autoclaving, as well as disinfection with common clinical disinfectants, such as isopropyl alcohol, further solidifying its position as a reliable material [45], [46].

Polycarbonate is commonly used in life-supporting devices, including hemodialysers, anesthetics containers, blood oxygenators, arterial filters, intravenous connectors, endoscopic devices, and others. These devices are lightweight, easy to handle, resistant to breakage, and, above all, transparent and translucent for quick and accurate visual inspection or monitoring of the level, flow rate, or condition of the liquids flowing through them. While offering the clarity of glass, polycarbonate surpasses it in durability and practicality, making it an essential material in modern healthcare.

In cellular studies, PC membranes are widely used for cell adhesion, migration, and co-culture experiments. Commercially available track-etched PC membranes provide precise control over pore size and surface properties, including wettability. While untreated PC membranes are hydrophobic, those treated with polyvinylpyrrolidone (PVP) become hydrophilic. However, despite its hydrophilic nature, PVP-treated PC membranes may exhibit reduced cell adhesion on their surface [47], [48]. Therefore, alternative surface treatments are necessary to fully enhance adhesion and optimize membrane performance for specific applications [49].

In the current research, a track-etched PC membrane was designed for use as a component in microchip fabrication, serving a dual function: as a structural wall separating two subchannels and as a substrate for cell adhesion. To optimize the PC surface for improved cell adhesion, physical and wet chemical oxidation methods were applied. Additionally, the adhesion-promoting factors (PDL, fibronectin, collagen) were added to the oxidised PC. Our results demonstrate how these surface modification techniques influence adhesion properties (see Chapter 3.2).

1.1.7. Biocompatibility

Biocompatibility is a fundamental requirement for any material to be classified as a biomaterial. It defines the material's ability to interact with the biological environment without causing harm, ensuring functional and long-term safety. Since biomaterials are used in direct contact with human tissues, understanding biocompatibility is essential for selecting appropriate materials for medical and biological applications.

A biomaterial must not elicit:

- Toxicity - the potential to harm biological systems through chemical means. This includes systematic toxicity, where adverse reactions occur away from the application site; local toxicity, which affects the contact site; and cytotoxicity, which involves damage to individual cells, such as those in the cell cultures.
- Allergenicity – the potential to trigger an allergic reaction in the body. The dose levels that cause allergic reactions are generally lower than those required to induce toxic effects.
- Immunogenicity – the ability of a substance to provoke an immune response.
- Genotoxicity - an alteration of the base pair sequence in the genomic DNA. Cells have numerous mechanisms to repair genotoxic damage.
- Mutagenicity – occurs when the genetic damage is not repaired, resulting in mutations that are passed to the next generation of cells.
- Carcinogenicity – when alterations in DNA cause cells to grow and proliferate in an unregulated manner [14].

While biocompatibility is universal across all biomaterials, specific materials exhibit distinct mechanical, physical, and chemical properties, making them suitable for different applications:

1) For replacing musculoskeletal parts of the body, crucial features include tensile and fatigue strength, resistance to wear and corrosion, low modulus of

elasticity, and good hardness. Examples are dental and orthopedic implants, such as joint replacements and bone screws [50].

2) In wound dressing, tissue engineering, and drug delivery, soft biomaterials like hydrogels are required. Their primary purpose is to support cell growth and provide a moist environment. Thus, they do not need mechanical strength but rather flexibility and porosity [51].

3) Some materials are designed to react with tissues rather than be ignored by them. Here, chemical properties such as bioactivity are critical. Examples include hydroxyapatite, which promotes osseointegration, and bioactive glass used in dental and orthopaedic implants [14], [52].

4) Materials designed to degrade over time possess chemical properties that allow for gradual resorption and replacement with natural tissue. Examples include PLA and polyglycolic acid PGA, used in sutures and temporary implants, as well as tricalcium phosphate, which serves as a bone graft substitute that degrades over time and is replaced by natural bone [38].

To assess the biocompatibility of a material, a series of tests must be conducted, tailored to its intended use, location, and duration of contact with the tissues. Biocompatibility is evaluated through three categories of biologic tests: *in vitro* tests, animal studies, and clinical trials. **The *in vitro* testing** includes the following experiments:

1) **Surface characterization** – assesses the materials' topography and surface chemistry, which influence protein adsorption and subsequently, cell adhesion.

2) **Ion release analysis** - measures the release of ions from the material into the surrounding environment. Excessive ion release may result in toxicity, adversely affecting cell function and integration.

3) **Corrosion testing** - examines the material's resistance to chemical degradation when exposed to bodily fluid. Materials susceptible to corrosion may release harmful byproducts.

4) **Cell adhesion assays** - determine the material's ability to promote attachment to its surface. Cell adhesion is critical for cell proliferation, tissue integration, and regeneration.

5) **Cytotoxicity tests** - assess whether materials' byproducts or surface interactions lead to decreased cell viability or cell death.

These *in vitro* tests are based on internationally recognized standards for biological evaluation of medical devices, primarily the ISO 10993 series. They represent widely accepted methodologies for assessing biocompatibility in early-stage material screening, before animal or clinical studies. In the present study, all listed *in vitro* biocompatibility assessments were conducted on Al alloy 6082 modified by anodization, to determine its suitability as a biomaterial.

While biocompatibility ensures that biomaterials do not cause harm when interacting with biological systems, their effectiveness in cellular applications depends on their ability to support cell adhesion. The interaction between cells and biomaterial surfaces is dictated by surface chemistry, topography, wettability, and functional groups, all of which influence protein adsorption and cellular attachments. In the next chapter, I explore the mechanism of cell adhesion, highlighting the role of extracellular matrix proteins, integrins, and receptor interactions in guiding cell adhesion. These principles will be applied to biomaterial surfaces, where topographical and surface chemistry determine the success of artificial substrates in supporting cellular functions.

1.2. CELL ADHESION

1.2.1. Introduction to adhesion

Cell adhesion is a biological cellular process by which individual cells form molecular and chemical bonds with neighbouring cells or a substrate. This process is crucial for maintaining cell viability and other essential molecular mechanisms, such as cellular communication, signal transduction, proliferation, tissue, and organ formation [53]. Changes in cell adhesion can cause a wide range of diseases, including cancer [54], [55], arthritis [56], osteoporosis [4], and atherosclerosis [58], [59].

In vivo, a tissue is defined as a collection of similar cells that collaborate to execute a specific function. These cells typically exhibit a common structure and are organized in a manner that enables them to accomplish tasks that a single cell would be unable to perform independently. Cells in a tissue adhere to each other and the ECM. Adhesion is a critical aspect for maintaining tissue integrity and function, contributing to structural stability, barrier formation, and cellular polarization. It also plays a key role in signal transduction, regulating processes such as cell proliferation, differentiation, survival, and migration [60]. Cell adhesion is a crucial feature in cell biology, biomedicine, and tissue engineering, and has been extensively studied. Research on cell adhesion is important for fundamental scientific studies and various applications, including artificial tissues, organs, bones, teeth, implantable sensors, skin regeneration, and organ transplantation [61], [62]. Understanding how to control the behaviour of cells on artificial surfaces, as well as selecting and preparing these surfaces to promote cell adhesion, is essential.

1.2.2. Adherent and suspension cells

Based on adhesion to substrate, there are two types of cells:

1) Adherent cells – cells that require adhesion to a substrate for proper growth and proliferation. These are cells of various tissues – skin, muscle, bone, and others.

2) Suspension cells – non-adherent cells that can proliferate directly in a growth medium without requiring a surface to attach, such as white blood cells or erythrocytes.

When cells are taken from an organism for *in vitro* culture, they are initially considered primary cells. As they adapt and proliferate over time, they may develop into a cell line. Thus, there are two main groups of *in vitro* cells based on their origin and characteristics:

1) Primary cells - cells taken directly from living tissues and cultured for the first time. They retain most of the characteristics of their tissue of origin. This group also includes stem cells, which are undifferentiated cells that have the potential to differentiate into various cell types.

2) Cell lines – cells being adapted to grow continuously in culture, often through genetic modifications or mutations that enable prolonged proliferation. This category encompasses:

- Cancer cell lines – cells derived from cancer that can proliferate indefinitely.

- Immortalised cell lines – genetically altered to proliferate indefinitely. They can be from various origins, including cancer cells.

Both primary and cell lines retain their characteristics as either adherent cells or suspension cells. For example, the cell line SK-MEL 28 (human cutaneous melanoma cells) can grow and divide only when adhered to a surface, while the suspension cell line Jurkat (human T lymphocyte cells) grows in the culture medium in the vial without adhesion.

Adherent cells can, in some cases, be cultured as suspension cells. For example, the widely used HEK293 (human embryonic kidney) and BHK (baby hamster kidney) cell lines can grow either as originally adherent or suspension cells [63], [64], [65]. It has been shown that there is a clear difference in the expression of certain proteins between these lines, indicating that the biochemical processes in these cell lines differ depending on their growth. The mammalian suspension cells have lower expression of adhesion receptors and ECM adhesion molecules, and differences in cytoskeletal proteins have been observed compared to adherent mammalian cell conditions [66], [67]. Other cells that have altered morphology or intracellular molecular mechanisms, which may also alter normal adhesion processes, are the cancer cells [68]. Thus, it is important to have in mind the origin of the adherent cells while studying cell adhesion.

1.2.3. The extracellular matrix

The extracellular matrix (ECM) is a complex assembly of macromolecules - proteins, glycoproteins, proteoglycans, and polysaccharides - that serves as the architectural scaffold for all multicellular organisms. ECM is involved in cell polarisation and migration, organizing cells into tissues, and providing mechanical stability to tissues. Besides structural function, ECMs operate as communication liaisons between the cells in organs and tissues by coordinating multiple signalling inside-out or outside-in commands [69], [70]. It transmits biochemical signals through cell surface receptors, including integrins,

syndecans, and adhesion GPCRs (G protein-coupled receptor). This signalling indicates cellular fate and a wide range of cellular functions, including proliferation, survival, adhesion, migration, wound healing, tissue repair, differentiation, and senescence [71], [72], [73], [20]. Structurally, ECM behaves as a hydrogel. The structural fibers, formed by collagen molecules, create a cross-linked network that captures and retains other ECM components, such as proteoglycan [74]. The negatively charged carboxyl and sulphate groups of proteoglycans attract water molecules and act as an osmotic sponge, allowing the polysaccharide molecules to retain a large amount of water in the ECM. This property is important for the ECM's elasticity to maintain the tissues' compressive strength [75].

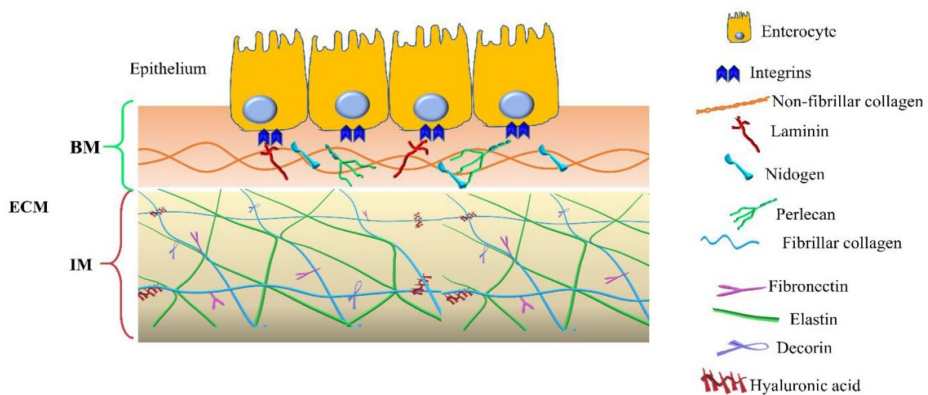


Figure 4. Schematic representation of the main components of the two ECM compartments: basement membrane (BM) and interstitial matrix (IM). The legend indicates ECM components. Adapted from [76].

ECM is composed of two main components: the interstitial matrix and the basement membrane (also known as the basal membrane) (**Figure 4**). Cells attach either directly to components of the interstitial matrix or to the basement membrane. The interstitial matrix is found between various cells, providing structural support and helping to withstand mechanical stress. The basement membrane is a specialized structure that supports epithelial cells and separates them from underlying connective tissue; it covers the basal surfaces of virtually all epithelia, surrounds the surfaces of muscle fibres, and ensheathes nerves. Other functions include sequestering growth factors and cytokines, establishing concentration gradients, and regulating their spatial and temporal distribution [77].

The compositions of the ECM vary from tissue to tissue, allowing it to meet the distinct structural and functional demands of each tissue. For instance, the

ECM of nervous tissue supports signal transduction, while the ECM of connective tissue provides structural support. Nevertheless, the formulation of ECMs can be constantly adapted according to biochemical or mechanical signals, resulting in a fine-tuned, dynamic ECM remodelling procedure [72].

1.2.4. Building blocks of ECM

ECM constitutes an arranged 3-dimensional network structure that offers cells both structural and biochemical assistance. The building blocks of ECM are the proteins (most abundant: collagens, elastin, laminin, fibronectin, and matricellular proteins), glycoproteins, proteoglycans (PG), and glycosaminoglycans (GAG) [78]. ECM comprises 1%–1.5% of the mammalian proteome, which consists of almost 300 proteins, including 43 collagen subunits, more than three dozen proteoglycans, and around 200 glycoproteins [73], [78].

Proteins of the ECM can be divided into two groups: structural and adhesion proteins:

(1) Structural proteins — The primary function of structural proteins is to form fibrils, which maintain the strength and elasticity of the ECM. However, these proteins also support and promote cell adhesion [25]. The main structural proteins are: collagen, which provides structural support and tensile strength; and elastin, which gives elasticity to tissues. The main PGs are aggrecan, versican, and syndecan.

(2) Adhesion proteins interact with cell adhesion receptors on the outside of the cell membrane. From a ligand and receptor perspective, these ECM adhesion proteins can be referred to as adhesion ligands. The main proteins are fibronectin, involved in cell adhesion, growth, migration, and differentiation; laminin, the primary protein of the basement membrane, involved in cell adhesion; and vitronectin, which binds integrins to the ECM. The main glycoproteins are osteopontin – important in bone remodelling; tenascin – involved in tissue repair and morphogenesis, and periostin – which facilitates adhesion and migration of fibroblasts.

For *in vitro* cell culturing, a few elements of ECM are commonly used to facilitate cell adhesion to a surface, which include collagen, fibronectin, elastin, and laminin. While numerous ECM components exist, this thesis emphasizes collagen and fibronectin due to their direct use in the experiments.

1.2.5. Collagen

Collagens are the most abundant proteins of the ECM, comprising ~30% of total ECM protein content [72]. They provide fundamental structural support

across all ECM compartments, including strong fibers of tendons, the organic matrices of bones and cartilages, the laminar sheets of basement membranes, the viscous matrix of the vitreous humor (which is the clear, gel-like substance filling the space between the lens and the retina in the posterior segment of the eye), and the interstitial ECMs of the dermis and of capsules around organs. In these roles, collagens serve as structural support for tissues and, simultaneously with other matrix components, provide both elasticity and stability.

The most abundant collagen types in the human body are collagen I (found in bones, tendons, ligaments, and skin), II (found in cartilage, intervertebral disc), II (found in skin, lung, vascular system), and IV (found in basement membrane). Beyond these predominant types, collagens V through XIII exist in smaller quantities, each specialized in function and location within the body.

Collagens can be categorized into subfamilies according to their supramolecular assemblies: fibrils, beaded filaments, anchoring fibrils, and networks (**Figure 5**). Most collagen fibrils are heterotypic, meaning they are composed of multiple collagen types. Collagen fibrils can also be considered macromolecular alloys, consisting of collagens and non-collagenous proteins or proteoglycans [79].

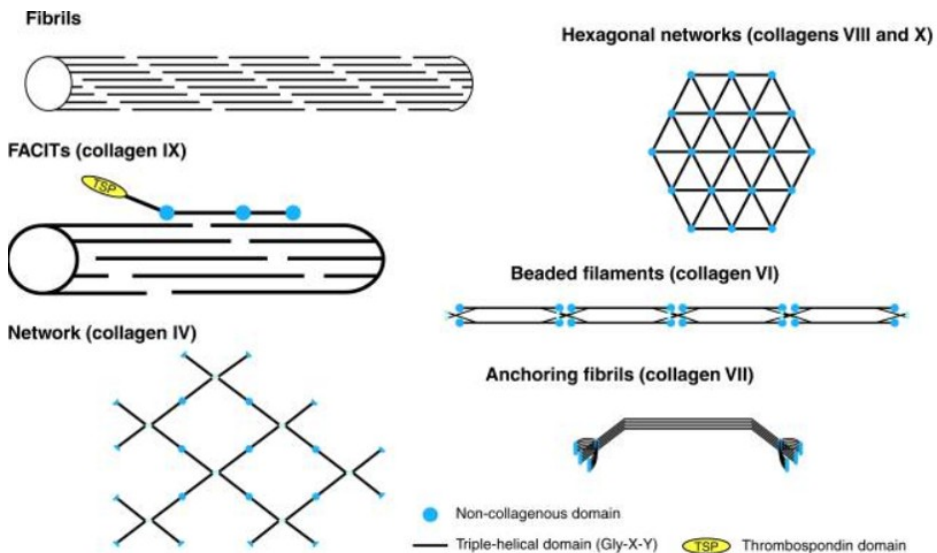


Figure 5. Supramolecular assemblies formed by collagens [79].

1.2.6. Fibronectin

Fibronectin is a large dimeric multidomain protein that can bind simultaneously to cell surface receptors, collagen, proteoglycans, and other fibronectin molecules. Fibronectin outweighs other adhesion proteins (ligands) found in the ECM. It is synthesized by many adherent cells, which then assemble it into a fibrillar network.

Fibronectin forms a fibrillar network by directly interacting with receptors on the cell surface. Newly secreted soluble fibronectin dimers bind to transmembrane integrin receptors on the outside of the cell. These interactions promote fibronectin-fibronectin association and fibril formation by inducing conformational changes in bound fibronectin [80], [81]. During assembly, fibronectin undergoes conformational changes that reveal fibronectin-binding sites, facilitating intermolecular interactions essential for fibril formation. The role of fibrils in ECM involves signal transduction, cell adhesion, and migration, including processes such as wound healing and embryonic development [82].

Fibronectin has two forms: (1) cellular fibronectin – a non-soluble form secreted by fibroblasts and many other cell types and incorporated into ECM; (2) plasma fibronectin – a soluble form secreted by hepatocytes and enriched in blood plasma [82]. Plasma fibronectin plays a crucial role in initiating and regulating the body's response to tissue injury. When a blood vessel is injured, plasma fibronectin is quickly deposited at the injury site, forming a temporary matrix that facilitates platelet adhesion and aggregation. Additionally, the assembly ensures proper clot formation and supports the healing process. The assembly of fibronectin into a complex three-dimensional matrix during physiological repair serves not only as a structural scaffold, but also as a regulator of cell function throughout the tissue [83].

It is important to notice that, despite being a glycoprotein, fibronectin is often referred to simply as a protein in the context of ECM, rather than being categorized as a glycoprotein. This is due to fibronectins' critical role in structural and functional support to the ECM. Its involvement in various biological processes surpasses that of other glycoproteins, which is why it receives special attention. fibronectin receives special mention. The same can be said for another group of glycoproteins – laminins.

1.2.7. Cell adhesion receptors

Cell adhesion receptors are specialized transmembrane proteins that enable cells to detect and respond to external signals. These receptors mediate cell-ECM interactions, supporting tissue structure and signalling. Key types include

integrins, which connect the ECM to the cytoskeleton and facilitate bidirectional signalling, and PG receptors, which often act as co-receptors in cell-ECM communication.

1.2.8. Focal adhesion

Focal adhesions, also known as focal contacts, are specialized sites where adherent cells anchor to substrate surfaces. These multi-protein assemblies are initiated by the binding of integrin receptors to specific adhesion ligands. This binding triggers the clustering of various integrins and the recruitment of several intracellular proteins, including talin, vinculin, and paxillin [60](**Figure 6**). These complexes link the ECM to the actin cytoskeleton within the cell. The cytoskeletal structure supports the nucleus and maintains the shape of the cell. Actin filaments of the cytoskeleton attach to the focal adhesion complexes, providing structural support and facilitating signal transduction. This interaction enables cells to sense and respond to their external environment [60],[84].

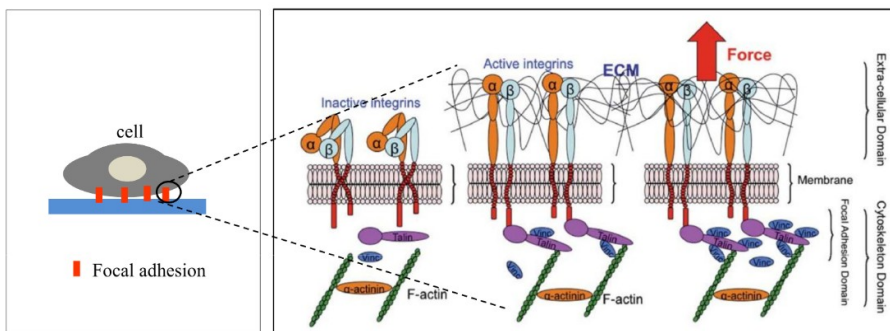


Figure 6. Schematic representation of activated integrins and the formation of ECM-integrin-cytoskeleton linkages at the focal adhesion site upon the application of an external tensile load [60].

Structurally, focal contacts are closed junctions where the distance between the substrate surface and the cell membrane ranges from 10 to 15 nm. Some authors categorize the focal contacts based on their lateral extension of adhesion structures at the cell-surface interface:

- 1) Less than 1 μm in length – focal complexes;
- 2) 1 to 5 μm in length - focal adhesions;
- 3) Greater than 5 μm in length – supermature adhesions [85].

When cells attach to surfaces, they first form nanometer-scale, dot-like focal complexes. These focal complexes are transient and unstable. Some will mature

into micrometer-scale elongated focal adhesions, which serve as anchoring points for cells; others disassemble without progressing further [86], [87].

During cell motion, focal complexes continuously form under the protruding front of the cells, known as the lamellipodium. Lamellipodia are thin, wide sheets of cytoplasm (approximately 200 nm thick and several micrometres in width) composed of actin filaments. Some focal complexes mature into focal adhesions, which grow and extend toward the cell centre, forming thicker actin fibres [88].

1.2.9. Process of cell adhesion

Cells explore the surfaces of materials using membrane-bound receptors, such as integrins, and use them to interact with ECM molecules adsorbed on substrate surfaces. Cell adhesion to a substrate is typically divided into three or four stages [60], [89]. The distinction lies in whether the third and fourth stages are merged or treated as separate stages. In the description below, I present the information according to the four phases for a broader and clearer understanding, while **Figure 7** illustrates three phases. Therefore, the phases of the cell adhesion to the surface are:

1. Van der Waals and ionic forces draw the seeded cells close to the substrate.

2. After a few minutes, the adhesion receptors integrins form contacts with their adhesion ligands. This process triggers the expression of cytoskeletal and other ECM proteins. Focal adhesions begin to form at these contact points, linking the ECM to the cell's cytoskeleton through multi-protein complexes.

3. After a few hours, the cells start to flatten, enabling more receptors to bind to the surface. This leads to the formation of strong focal adhesions and the establishment of the cytoskeleton. The strength of adhesion increases with the duration of a cell's contact with the substrate or another cell. Focal adhesion becomes more stable and mature, facilitating stronger connections between the cell and the ECM. These structures serve as anchor points for the cytoskeleton and are essential for its establishment and reorganization.

4. Finally, the cells fully adhere, initiating the secretion of ECM molecules and other essential proteins into the environment, followed by cell proliferation. Focal adhesions play a crucial role in transmitting mechanical and regulatory signals between the ECM and the cell, influencing cell behaviour and fate.

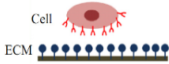
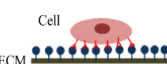
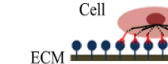
Cell Adhesion Phases	Phase I	Phase II	Phase III
Schematic diagram of cell adhesion			
Schematic diagram of the transformation of cell shape	 Initial attachment	 Flattening	 Fully spreading and structural organization
Cell adhesion intervention	Electrostatic interaction	Integrin bonding	Focal adhesion
Adhesion stages	Sedimentation	Cell attachment	Cell spreading and stable adhesion

Figure 7. Phases of cell adhesion [60].

To conclude, cells sense their surroundings by forming adhesions. A significant factor in cell-material interactions is protein adsorption. Conformation, concentration, distribution, and binding strength influence cell adhesion. Initially, fibronectin, vitronectin, and fibrinogen affect cell adhesion, while collagen and laminin dominate in long-term adhesion [90].

1.3. CELL ADHESION ON ARTIFICIAL SURFACES

Artificial substrates are utilized for *in vitro* cell culturing share functional similarities with biomaterials applied in implantation procedures. The surface of a substrate significantly impacts the cell behaviour and adhesion. Understanding how surface properties affect these interactions is crucial for designing biomaterials that better mimic physiological conditions. This chapter outlines the factors that influence cell adhesion.

In both culturing and implantation scenarios, a material's surface is never simply bare; it is always covered with water and proteins. In *in vitro* cell culturing, cells are seeded in a growth medium. Initially, proteins from the growth medium coat the material's surface, and cells adhere only when they detect these adsorbed proteins (**Figure 8**).

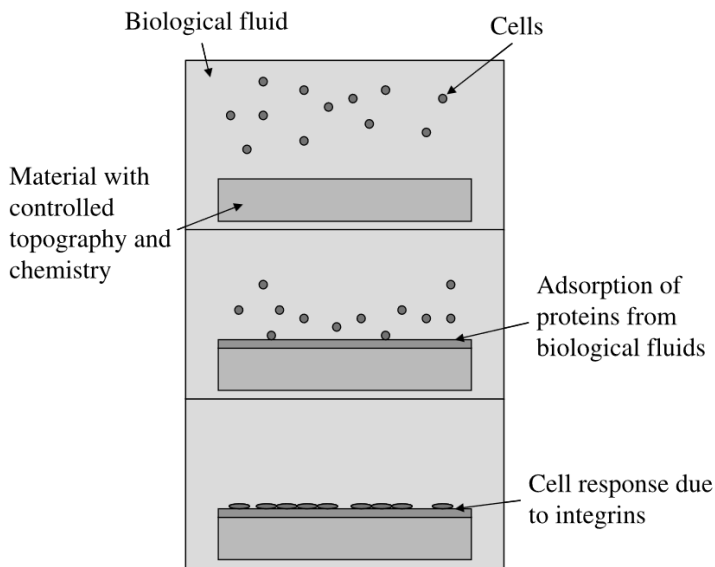


Figure 8. Schematic illustration of the different phases of the interaction of biological elements with the material's surface [89].

This also applies to the implantation process. After implantation, biomaterials are immediately coated with proteins from blood and interstitial fluids. Cells sense the substrate surface through this adsorbed protein layer, meaning their initial reaction is to the adsorbed proteins rather than the surface itself [91].

In addition to sensing the protein composition of their environment, cells also detect the physical and chemical properties of the surrounding material. Cell adhesion is influenced by various characteristics, including surface topography,

porosity, mechanical properties, and hydrophilicity (**Figure 9**). These surface cues affect how proteins conform on the substrate, which in turn governs cell adhesion, morphology, movement, and biological function – protein expression, proliferation, and differentiation. By tailoring the surface properties, biomaterials can be engineered to support improved biocompatibility and cell performance. Studying how these factors influence cellular responses provides valuable insights for designing biomaterials in medical and tissue engineering applications.

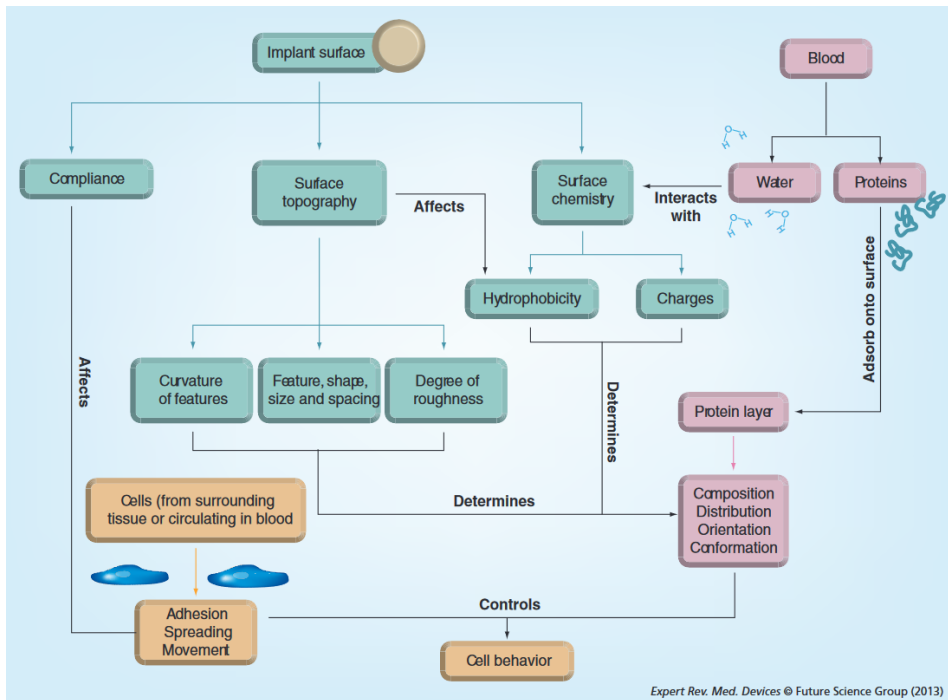


Figure 9. Factors influencing cell behaviour at the implant-tissue interface, including surface properties, adsorbed proteins, and cellular interactions [92].

1.3.1. Surface topography

Topographic features of the surface, including shape, size, and geometric structures, provide biophysical and biochemical signals to the cells. Those signals influence the cytoskeleton organization, protein orientation, and folding; thereby determining the fate of the cell, including its adhesion, polarisation, migration, and proliferation. This phenomenon, known as contact guidance, occurs when cells interact with surface topography, leading to alignment and orientation along specific patterns or structures [93]. This is particularly important in tissue

engineering and regenerative medicine when designing biomaterial surfaces. By tailoring specific topographic cues, it is possible to direct cell responses toward desired functional outcomes. While flat surfaces provide a two-dimensional platform for cell spreading, curved or structured surfaces create a three-dimensional architecture that enables cells to infiltrate and grow within the material [92].

Surface topographical parameters important for contact guidance are surface roughness, pattern size and geometry, regularity, stiffness, surface wettability, and surface energy. In addition to topography, the presence and type of functional groups of a surface have a huge impact in modulating cell adhesion and behavior. The most important features of a biomaterial for cell adhesion are discussed below.

1.3.2. Surface roughness

Surface roughness describes the degree of irregularity or texture on a surface, typically characterized by deviation from an ideal smooth plane. The roughness of a given surface is quantitatively described by the roughness average (Ra), which represents the mean deviation of the surface profile from a central line over a specified length. The value of Ra usually can be given in micrometers (μm): higher values of Ra refer to a surface with higher irregularities and a rough surface, while lower values correspond to smoother, flatter texture [94]. The surface roughness can be categorized based on the size of the irregularities present:

1) Macroscopic roughness refers to the surface irregularities with features larger than 1 mm, Ra typically greater than 10 μm . These are visible to the naked eye. The cells have sufficient space to spread and grow between macroscopic irregularities, with minimal impact on cell adhesion.

2) Surface roughness on micron and submicron scales (1 μm to 1 mm) is usually not visible with the naked eye but can be observed under a microscope. Ra values between 0.1 μm and 10 μm . This scale promotes cell adhesion as it provides enough irregularities for cells to attach.

3) Submicron roughness includes features in the range of 100 nm to 1 μm . Ra values between 0.01 μm and 0.1 μm . This group provides an increased surface area that can further enhance cell attachment and spreading.

4) Nano roughness features smaller than 100 nm. Ra values lower than 0.01 μm . These extremely fine features can affect molecular interactions and cell behaviour. Nano roughness is considered to be the closest to natural tissue morphology, and it is an ideal factor that has a positive effect on cell adhesion, growth, and maturation [53].

Surface roughness increases cell adhesion, and this effect depends on both the degree of roughness and the size of the cells. Generally, cells adhere better to surfaces with roughness that is equal to or slightly greater than the size of the cell, as demonstrated with human osteoblasts and osteosarcoma cells. Those cells exhibit varying adhesion levels on surfaces with different roughness, with optimal adhesion often occurring on surfaces whose roughness parameters align with the size of the cells [80], [81]. Large cells like human primary bone cells ($\sim 50\ \mu\text{m}$) will react differently to the same surface topography than smaller cells like monocytes ($\sim 10\ \mu\text{m}$) or platelets ($\sim 2\ \mu\text{m}$). However, excessively rough surfaces with high peaks and deep valleys may hinder cell adhesion and spreading. Additionally, cell type plays a crucial role as different cell phenotypes respond differently to the same surface relief. Overall, the interaction between surface roughness and cell adhesion is complex, and careful consideration of the specific cell type and the extent of surface properties is essential for achieving the desired result in biomaterials development [89].

1.3.3. Surface porosity

Surface porosity refers to the presence of tiny voids or pores on the surface of a material. It can significantly affect the physical and chemical properties of the material, increasing the available surface area for processes such as adsorption, catalysis, and diffusion. Additionally, it impacts cell adhesion, migration, proliferation, and differentiation. The primary factor affecting cell adhesion is pore size. The pore size classification is as follows:

- 1) milipore – pore size between 0.1 mm and 100 μm ,
- 2) micropore – pore size between 0.1 μm and 100 nm,
- 3) nanopore – pore size between 0.1 nm and 100 nm [97].

The study involving mesenchymal stem cells (MSC) and collagen-glucosaminoglycan scaffold with varying milipores, ranging from 80 μm to 320 μm , demonstrated a consistent increase in adhesion corresponding to larger pore sizes [98]. In contrast, the same scaffold tested with osteoblasts demonstrated that cell adhesion occurred in a non-linear pattern. Specifically, increased adhesion was observed with larger pores up to 320 μm , the same as in the case of osteoblasts. However, a secondary peak was observed at the pore size 120 μm . This phenomenon can be attributed to the fact that smaller pores provide a larger surface area, while large pores provide a higher ligand density. Nevertheless, the secondary peak disappeared following cell proliferation, indicating that while specific surface area may be important for initial cell adhesion, improved cell migration provided by scaffolds with pores above 300 μm overcomes this effect [99].

When examining micropores, a study involving osteoblasts and porous polycarbonate membrane with pore sizes ranging from 0.2 μm to 8 μm was conducted. The cells were fully adhered and spread on the surface with 0.2–1 μm pores, whereas cells became spherical with few filopodia and lamellipodia on membranes with larger micropores (3.0–8.0 μm in diameter) [100].

Another study involving fibroblasts and anodic aluminium oxides of different pore sizes, ranging from 0.075 μm to 0.3 μm , demonstrated the highest adhesion and proliferation with 0.075 μm pores compared to wider pores, owing to increased focal adhesion densities [25]. Thus, both studies revealed the highest cell adhesion with the smallest pore size.

To sum up, cell adhesion is influenced by pore size, with smaller pores typically providing a larger surface area and promoting higher adhesion. Meanwhile, larger pores offer higher density and improved cell migration.

1.3.4. Material stiffness

Material stiffness refers to a material's resistance to deformation under an applied force. In tissue engineering, stiffness and elasticity are often used interchangeably; however, in this context, I will use the term stiffness to discuss the mechanical properties of biomaterial surfaces. Stiffness is quantified by Young's modulus, which measures material elasticity. A higher Young's modulus indicates increased material stiffness.

In vivo, tissue stiffness is determined by the stiffness of the ECM, primarily influenced by the composition of collagen and elastin. This stiffness varies significantly, ranging from approximately 0.1 kPa in brain tissue to around 100 GPa in bone tissue [101]. Cells perceive these mechanical properties of the ECM through a process called mechanotransduction, which involves the application of traction, compressive, and tensile forces, as well as the assessment of the resulting deformations. In response, cells form focal adhesions. The stiffness of the ECM affects various cell activities, including gene transcription, cytoskeletal remodelling, and intercellular interactions [53].

In tissue engineering, designing biomaterials with the appropriate stiffness can help mimic the natural environment of tissues, thereby promoting cell behaviour and tissue regeneration [2], [102]. Stiffer surfaces provide a more stable foundation for cells to anchor to and generally enhance the organization and dynamics of the cytoskeleton. On these stiffer surfaces, cells develop more pronounced stress fibres - specialized bundles of actin filaments within the cytoskeleton that generate contractile forces and are involved in cell adhesion, migration, and morphogenesis. These conditions also lead to stronger focal adhesions, resulting in more spread-out morphologies. In contrast, on softer

surfaces, cells display a more rounded shape, less organized cytoskeletal structures, reduced stability of focal adhesions, and decreased cell movement [2], [103].

Different cell types respond differently to material stiffness. The actin stress fibres of fibroblast cells form when the Young's modulus exceeds 2 kPa, while neutrophils remain insensitive to a wide range of stiffness variations. This suggests that cells may rely on their internal standards of mechanical sensing [53].

1.3.5. Curvature

Surface curvature influences cell behaviour both directly, by altering the cytoskeleton, and indirectly, by affecting protein concentration and folding. On flat surfaces, cells extend their cytoskeleton within a two-dimensional field. Conversely, on curved surfaces, cells adapt their cytoskeleton to conform to the geometry. Convex surfaces (e.g., spheres) compel cells to wrap around them, which results in stretching and distortion of the cytoskeleton. In contrast, concave surfaces (e.g., pits) enable cells to expand into the curvature (**Figure 10**) [104], [105], [92].

Cell adhesion is inherently dependent on protein adsorption, which is also influenced by curvature. The orientation, unfolding, or denaturation of these proteins thereby impacts cell adhesion. Fibrinogen and albumin display structural changes in response to varying levels of curvature. Additionally, the presence of sharp and smooth edges influences receptor ligand accessibility, while specific patterns, such as honeycomb pores, guide the formation of focal adhesions [92], [106], [107].



Figure 10. The effect of surface curvature on cell shape [92].

1.3.6. Surface chemical properties

Surface chemistry encompasses functional groups, wettability, and surface energy, and surface charge. The first three characteristics are inherently

interconnected, as a change in one aspect influences the others. For instance, the presence of hydroxyl (-OH) functional groups on a surface determines its hydrophilicity; this heightened hydrophilicity corresponds to increased surface energy, which enhances the material's tendency to interact with water and other polar substances. This relationship can be summarized as follows:

- **Functional groups.** These are chemical groups present on a surface, such as hydroxyl (-OH), carboxyl (-COOH), amine (-NH₂) and methyl (CH₃) groups.

- **Surface energy.** It is influenced by the types of functional groups present. Hydrophilic groups (e.g., -OH, -COOH) increase surface energy, enhancing the ability of the surface to interact with polar substances, such as water molecules. In contrast, hydrophobic groups (e.g., -CH₃) reduce surface energy, limiting such interactions.

- **Wettability.** This refers to a surface's ability to attract or repel water, typically quantified by measuring the contact angle. Hydrophilic surfaces with high surface energy display low contact angles, indicating strong water interactions. In contrast, hydrophobic surfaces with low surface energy exhibit high contact angles - low wettability - reflecting weaker interactions with water.

All those features determine the conformation of a protein, leading to the impact on cell adhesion. One example is fibronectin, which exhibits two conformations: globular and linear. Material surface properties, such as hydrophobicity and hydrophilicity, influence their conformations: linear conformation is more prevalent on hydrophilic surfaces, whereas globular conformation is more dominant on hydrophobic surfaces. This is due to the exposure of negatively charged groups on hydrophilic surfaces, which may interfere with the stabilizing ionic interactions within the protein. Importantly, the linear conformation of fibronectin enhances cell adhesion by exposing the integrin-binding sites RGD motif. Other factors, including temperature, pH, and ionic strength, also influence the protein conformation of ECM [108], [109], [110].

Although distinguishing among these properties can be challenging, the primary features relevant to cell adhesion are outlined below.

1.3.7. Functional groups

Surface chemistry refers to the chemical composition and functional groups present on a material's surface. These groups can interact with liquids, proteins, and cells, influencing various properties, including cell adhesion. Surfaces with functional groups such as carboxyl (-COOH), amine (-NH₂), and hydroxyl (-OH) tend to enhance cell adhesion due to their ability to form hydrogen bonds and

electrostatic interactions with ECM proteins. Conversely, surfaces with hydrophobic groups, such as a methyl group (-CH₃), discourage cell attachment [92].

Chemical modification can also be used to either promote or inhibit cell attachment directly to the surface. By introducing functional groups with varying hydrophobicity and surface charges, these modifications influence the orientation and conformation of adsorbed proteins. Such alterations in protein behaviour can, in turn, impact cellular differentiation processes [109].

1.3.8. Surface wettability

Surface wettability, characterized by hydrophobicity and hydrophilicity, influences cellular responses by altering protein adsorption and conformation. It reflects how a liquid interacts with a solid surface. It is commonly assessed by measuring the contact angle formed between a water droplet and the surface. Wettability primarily depends on factors such as chemical composition, morphology, and surface roughness, and it strongly correlates with biological interactions [111]. A water droplet contact angle exceeding 90° signifies a hydrophobic surface, characterized by low surface energy and poor wetting. In contrast, a contact angle below 90° indicates a hydrophilic surface with better wetting and higher surface energy. Surface wettability can be categorized as hydrophobic (contact angle >80°), moderately wettable (contact angle 48–62°), and strongly hydrophilic (contact angle <35°) [112].

Cells are more likely to adhere to hydrophilic surfaces. For instance, the adhesion of fibroblasts is the highest with the water drop contact angle from 60° to 80° [113]. The super-hydrophilic matrix surface, characterized by a contact angle of less than 5°, exhibits a strong attraction to water molecules. This strong hydrophilicity inhibits the proper binding of adhesion proteins, thereby impairing cell adhesion. Conversely, the super-hydrophobic surface, with a contact angle exceeding 150°, strongly repels water. On such surfaces, adhesion proteins are adsorbed in a denatured state, which compromises their ability to support cell adhesion (**Figure 11**) [1], [53].

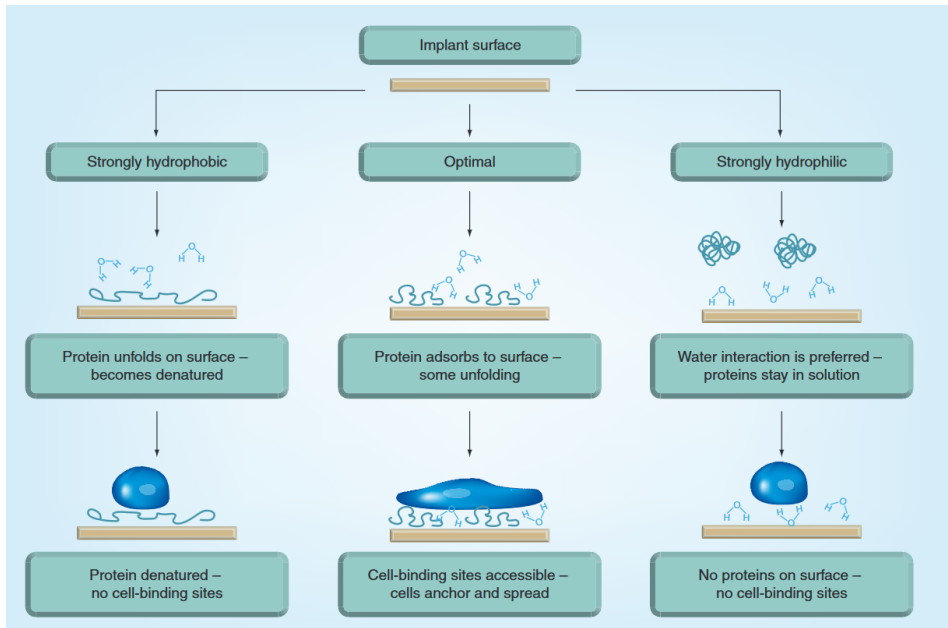


Figure 11. Effect of surface wettability on protein adsorption and cell adhesion [92].

1.3.9. Surface energy

Surface energy refers to the energy required to create a new surface by breaking bonds within a material. Mathematically, it is described as

$$\gamma = \frac{W}{A} \quad (1)$$

where

γ – surface energy, [J/m²];

W -work done to create the new surface, [J];

A – area of the new surface, [m²].

Surface energy is determined by the interactions of molecules at the interface with the environment. It influences how a material interacts with liquids, gases, and biological tissues. The surface with high surface energy attracts water and other polar molecules, leading to better wettability and adhesion.

The material's wettability is closely related to its surface energy:

- High surface energy surfaces are typically hydrophilic, promoting better interactions with water
- Low surface energy surfaces are hydrophobic materials, repelling water [114].

For cell adhesion, high surface energy is desirable. A hydrophilic surface encourages protein adsorption, creating a favourable cell attachment and spreading environment. This enhanced protein adhesion directly contributes to improved cell adhesion [115].

1.3.10. Surface charge

Surface charge influences how proteins from the growth medium interact with surfaces. Positively or negatively charged surfaces attract oppositely charged regions of proteins, which affects their orientation, conformation, unfolding, and adsorption [116]. This, in turn, affects the cell adhesion.

The cell membrane typically has a negative charge due to phospholipids and glycoproteins. Positively charged surfaces enhance adhesion through electrostatic attractions, leading cells to adhere better to positively charged surfaces than to negatively charged ones [53], [117].

1.3.11. Modification of surface chemistry

As described above, the quality of cell adhesion to the substrate is influenced by the physical and chemical properties of the material. To control this adhesion, the surface of the biomaterial can be modified according to these parameters. Techniques for modifying the topography of biomaterials include electrospinning, etching, laser ablation, and 3D printing. The surface chemistry can also be altered to enhance or inhibit hydrophilicity, depending on the desired application. This can be achieved through physical methods, such as plasma treatment, UV-activation, CO₂-pulsed laser treatments [118], [119], [120]. Chemical methods include grafting functional groups, covalent bonding, and silanization, while biological approaches involve immobilization of peptides, proteins, and growth factors [2], [92], [121].

One of the most effective strategies for modifying surface chemistry is oxidation, which plays a crucial role in controlling surface hydrophilicity and improving cell adhesion.

1.3.12. Oxidation of the surface

Surface oxidation can be conducted through either chemical or physical modification to increase a polymer's hydrophilicity and surface energy, thereby enhancing its suitability for cell adhesion and biocompatibility [122].

Chemical modification introduces oxygen-containing functional groups - such as hydroxyl, carbonyl, and carboxyl - to a biomaterial's surfaces, increasing hydrophilicity and surface energy. This is typically accomplished through wet

oxidation, using strong acids, alkalis, or other oxidizing agents [123], [124]. Commonly used oxidizers include nitric acid, sulfuric acid, hydrogen peroxide, potassium permanganate, and sodium hydroxide. These chemicals react with the polymer surface, enabling further functionalization or biomolecule grafting. Chemical oxidation modifies only the surface while preserving the basic properties of the polymer, making it an effective method for enhancing cell adhesion.

Physical oxidation of a surface can be achieved through plasma treatment, a widely used technique for modifying material surfaces. Plasma, known as the fourth state of matter, is an ionized gas containing positive and negative ions, electrons, and charged radicals. Various types of plasma discharges are employed for surface modification, making this approach highly versatile [125]. Plasma states can be broadly categorized into hot (thermal) plasma and cold (non-thermal) plasma. Hot plasma is characterized by high-temperature electrons and heavy particles, such as ions and neutral atoms, resulting in a high degree of ionization. In contrast, cold plasma features low-temperature heavy particles and high-energy electrons, leading to a lower degree of ionization [126].

Cold plasmas are routinely used for surface modification in laboratory conditions because they activate surfaces without causing thermal damage to the material. Plasma treatment of polymers has long been recognized as an effective method for modifying surfaces to enhance cell adhesion [127]. It has been demonstrated that when synthetic polymers are exposed to oxygen gas plasma, oxygen-containing polar groups such as C-O, O=C-O, and C=O form on the surface. These groups increase the hydrophilicity and roughness of the surface, facilitating the adhesion of ECM proteins [128].

Chemical oxidation maintains the stability of the surface structure. In contrast, plasma oxidation allows the surface to revert to its original state after a certain period, a process known as surface aging. This reversal results in a loss of some of the induced hydrophilicity effects, necessitating repeated plasma oxidation [129]. The duration for which the surface remains hydrophilic depends on the storage conditions. Plasma-mediated surface restructuring slows significantly when the polymer is incubated at lower temperatures in a less humid environment [130]. Therefore, when working with different surfaces, it is crucial to identify the appropriate conditions and oxidation method to maintain the surface's suitability for cell adhesion for as long as possible.

Nevertheless, plasma oxidation has several advantages over chemical oxidation. Firstly, it does not involve hazardous substances to health and the environment, which ultimately become chemical waste that must be disposed of safely. Secondly, surface plasma treatment is a time-saving method, requiring only a few seconds of plasma modification to achieve effective surface changes.

Third, plasma modification alters the surface uniformly, regardless of geometry, whether it involves micro or nanoparticles, thin films, or complex 3D structures [131], [132].

Other physical methods, including ozone treatment combined with UV treatment, photografting, and gamma irradiation, have also been noted and widely used to incorporate various chemical groups into material surfaces. However, radiation can lead to material degradation, resulting in changes to the surface structure. These modifications are often discontinuous and non-specific, which may limit their stability and targeted functionalization in certain applications [133], [134]. Despite these challenges, these methods remain valuable tools in surface engineering due to their ability to enhance surface characteristics in terms of adhesion, wettability, and compatibility with the biological environment [122], [135].

Oxidation techniques significantly enhance adhesion properties, yet additional strategies, such as surface coatings, further optimize biomaterial interactions with cells.

1.3.13. Surface coatings for adhesion

In vitro cell culture often requires specialized surfaces to optimize adhesion. While commercially pretreated cultureware is widely available, for specific applications researchers need to modify surfaces to enhance cell adhesion. Beyond adjusting surface topography and chemistry, adhesion proteins from the ECM, such as collagen, fibronectin, laminin, and the artificial RGD loop, facilitate cell adhesion. A drawback of using these proteins is their cost and short shelf life. An alternative approach involves using synthetic polymers as adhesion-promoting coatings. Among these polylysins offer a convenient and cost-effective alternative. Poly-L-lysine (PLL) and PDL can be used alone or in combination with other adhesive molecules. Positively charged PLL interacts with negatively charged cell membrane proteins, supporting adhesion [136]. Cells metabolize PLL, whereas its stereoisomer PDL provides a more stable substrate for mammalian cell attachment. PDL is commonly used in neuronal cell adhesion studies due to its durability. This polymer can coat glass, plastic, or other surfaces, offering a cost-effective alternative for initiating cell adhesion [137]. Surface coating complements oxidation methods by creating a chemically tailored environment for optimal cell interaction.

1.3.14. Future directions in biomaterial surface engineering

To optimise the interaction of biomaterials with cells, modifications of the substrate surface are crucial. Cell adhesion is affected by surface topography, chemical composition, and wettability, it can be improved by modifying these properties. The main strategies include the regulation of surface roughness, the introduction of functional groups, and the use of adhesion-promoting coatings.

Physical methods such as plasma treatment and microstructuring are used to modify material topography and surface energy. Plasma treatment also introduces oxygen-containing functional groups. Chemical modifications further enable controlled surface reactivity, improving hydrophilicity and compatibility with biological molecules. In addition, biochemical coatings, including extracellular matrix proteins and synthetic alternatives, create a tailored environment for cell attachment.

Biomaterials engineering is a highly interdisciplinary field that brings together chemists, biologists, materials scientists, engineers, and medical researchers to develop biological alternatives capable of restoring or enhancing tissue and organ function. The primary goal of this interdisciplinary field is to leverage the potential of biomaterials engineering to create biological alternatives, ultimately advancing tissue engineering and regenerative medicine. As this field evolves, biomaterial surface engineering is applied to advanced platforms such as microfluidic systems. These systems require precise control of the cellular microenvironment is essential, including surface properties that support cell adhesion under dynamic culture conditions, enabling the study of cell behaviour under shear stress, nutrient gradient, and spatial confinement. To ensure optimal cell adhesion in such systems, substrate surfaces must be engineered with tailored chemical and physical characteristics that maintain adhesion during flow. The ability to modify biomaterials plays an important role in the development of microfluidic technology, drug screening, and next-generation tissue engineering strategies.

1.4. MICROFLUIDIC TECHNOLOGY

1.4.1. Definition of microfluidics

According to George M. Whiteside, microfluidics is defined as the science and technology of systems that process or manipulate small amounts of fluids (10^{-9} to 10^{-18} L), using channels that measure tens to hundreds of micrometers [138]. Since the inception of microfluidics in the early 1990s, research in this field has primarily focused on the chemistry and physics of the microscale. Only after a solid understanding of fundamental microscale principles was established, could these concepts be applied to the study of cells, which are objects of a micron scale [139]. Microfluidics has shifted towards cell research, and today it integrates seamlessly with cell biology and tissue engineering techniques [140]. Currently, microfluidics has found applications in various domains, ranging from microarrays to cellular biophysics (**Figure 12**).

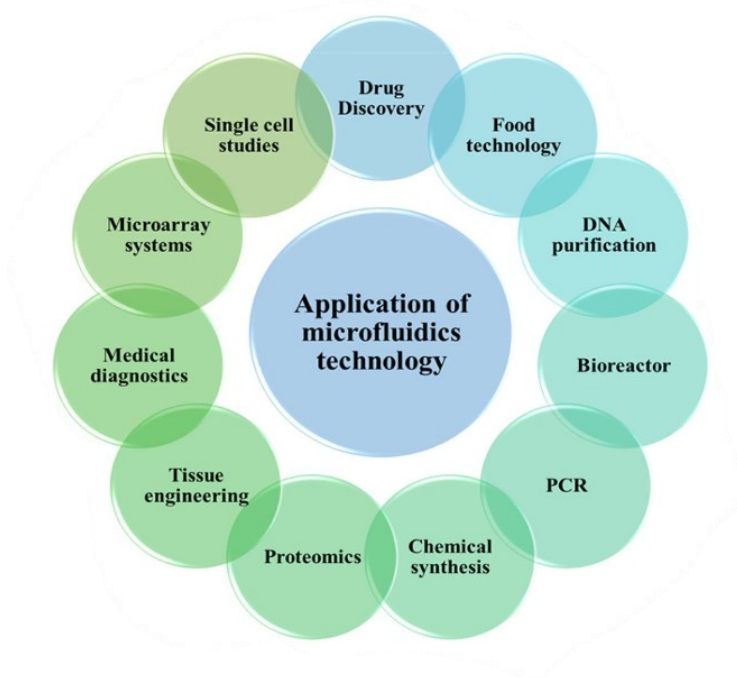


Figure 12. Application of the microfluidic technology [141].

Microfluidics is a rapidly developing technology. The annual number of new publications on the topic of microfluidics is increasing rapidly and continuously every year: more than 88 thousand publications published by the end of 2024, as presented in ScienceDirect, under the search of „microfluidic“.

The technology of microfluidics consists of two main subsections:

1) Microfluidics with flow. This technology involves the movement of liquid through a microchannel, enabling functions such as mixing, separation, chemical reactions, and cell nourishment. It is crucial for applications that demand steady and controlled fluid movement, including lab-on-a-chip (LoC), organ-on-a-chip (OoC), and microphysiological systems (MPS).

2) Droplet-based microfluidics. This subsection focuses on generating and manipulating discrete droplets within another immiscible fluid. These droplets function as individual microreactors, allowing for high-throughput screening, single-cell analysis, and precise encapsulation. This technique is particularly valuable for applications that benefit from the compartmentalization and isolation of reactions.

In this work, I focus exclusively on flow-based microfluidics. Information regarding droplet-based microfluidics will not be presented further. Consequently, in the text that follows, flow-based microfluidics will simply be referred to as microfluidics.

1.4.2. Microfluidics with flow

LoC, OoC and MPS are three categories of microfluidic platforms with distinct applications: laboratory, biomedical, and physiological, respectively. These closely related technologies complement each other in chemical, biochemical, and cellular research.

LoC are primarily designed for laboratory applications – they miniaturize and automate analytical processes such as diagnostics, chemical analysis, or sample preparation. Historically, the term LoC referred to microfluidic systems in general, but today it is associated with compact laboratory tools that integrate multiple functions on a single microchip [142], [143], [144].

OoC platforms, in contrast, are engineered to replicate the function of a specific human organ or tissue *in vitro*. These systems simulate physiological conditions such as fluid flow, mechanical stress, and biochemical gradients. OoCs allow researchers to study organ-level responses. e.g., heart, liver, kidney, gut, or blood-brain-barrier-on-a-chip [145].

MPS represents a broader category and a more advanced category. While often used interchangeably with OoC, MPS typically includes features that extend beyond the single-organ model:

1) Integrated sensors for real-time monitoring of the microphysiological environment. While this feature is frequently found in OoC, it is also considered a defining aspect of MPS [146], [147].

2) Multi-organ-on-chip systems, such as liver-kidney-chips and heart-lung-chips, which integrate multiple organ models to simulate inter-organ interactions. These systems are also referred to as multi-OoCs [148], [149].

3) Applications involving spheroids and organoids, which represent three-dimensional cellular structures but do not strictly fall within the definition of OoC [150].

1.4.3. Microfluidic set-up

Contrary to the expectation that microfluidics would achieve full miniaturization - hence the name lab-on-a-chip - these devices often resemble a "chip in the lab" setup due to extensive ancillary equipment required. This includes components such as pumps, reservoirs, incubators, sensors, valves, etc. (**Figure 13**). Furthermore, an incubator is essential for maintaining the optimal conditions for *in vitro* cell culture, ensuring proper environmental parameters are upheld throughout the process.

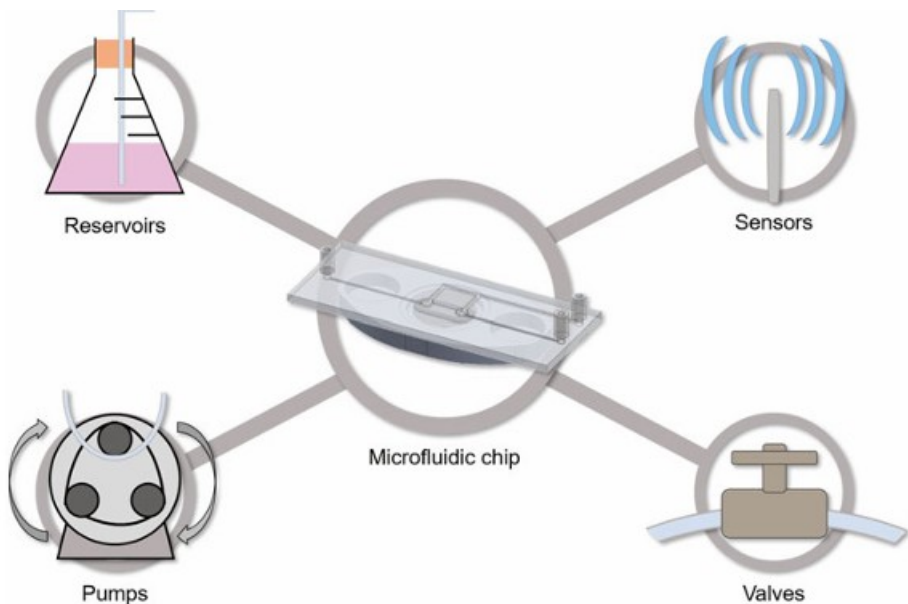


Figure 13. The general equipment for microfluidics in flow [151].

Unlike microfluidic systems designed for physical or chemical studies, those intended for cell and tissue research have specific features of particular importance:

1. Material from which the microchip is made – it should be biocompatible to ensure the proper conditions for cell culture, as well as transparent to allow optical imaging techniques.

2. The design of the microchannel, along with the flow type, determines the flow dynamics and directly impacts cell behaviours, including adhesion, morphology, and viability.

Both aspects are described below.

1.4.4. Materials for microchip fabrication

The choice of material for microchip fabrication is critical in ensuring desired performance. Biocompatibility is a key requirement for the material used in the fabrication of microchips for cell research. The materials must be optically transparent to allow observation under an optical microscope. The materials must also be chemically inert and resistant to physical influences. Lastly, the materials should be capable of being fabricated into microscale channels and must support surface functionalization to ensure effective cell adhesion.

Microchip manufacturing has historically moved through several materials: silicon in the 1960s, then glass in the 1970s, with the eventual introduction of polymers in the 1990s, and paper chips in the 2000s. Silicon chips are very precise; however, they lack optical transparency, which renders them unsuitable for optical microscopy observations and cellular research.

Glass-based microchips are fabricated using various types of glass: borosilicates [152], quartz [153], soda lime glass [154], pyrex [155], ultra-thin glass [156]. Glass slides are quite commonly applied as the cell culturing plate in traditional static culturing conditions and this material was adopted for microfluidic cell culture as well. Glass is biocompatible, resistance to most solvents and has exceptional optical transparency [11]. The microchip itself consists of two main wafers. One wafer contains the microchannel patterns created by etching, laser ablation, embossing, or mechanical erosion. The second wafer contains inlet and outlet ports and acts as a lid to enclose the microchip. The wafers are aligned and *thermally* bonded.

Glass-based microchips offer a simpler and more convenient method compared to silicon. However, when bonding multiple layers of glass, it is difficult to ensure precise alignment and adhesion of the layers. The bonding

process is quite complex, the productivity is low, and it needs experience in manual handling [157].

The fabrication of both glass and silicon microchips requires intricate and time-consuming processes. These microchips are highly fragile, and their cost is extremely high. As a result, they are less appealing compared to next-generation polymer-based microchips, such as PMMA, COC, and polydimethylsiloxane (PDMS). These polymers offer significant ease of fabrication.

PMMA is a transparent thermoplastic synthesized from the methyl methacrylate monomer. Multi-layer PMMA chips are fabricated using laser cutting and plasma-activated thermal bonding [158], [159]. This material provides excellent mechanical stability and rigidity and is transparent within the visible light spectrum, making it ideal for applications in optical detection, such as fluorescence microscopy and absorbance spectroscopy. However, PMMA's interaction with certain solvents or reagents may alter its properties or lead to monomer leaching. Additionally, it is prone to scratching and can become brittle, particularly in thinner structures.

COC is another replacement for glass in the microchips, composed of cyclic olefin monomers (norbornene) and linear olefins (ethylene). It offers several advantages, including good biocompatibility, low water absorption, high heat-resistance, good chemical resistance, and high transparency in the deep UV range, which minimizes interference in fluorescence-based assays [160]. However, the price is higher than PMMA or PDMS.

Two other polymers – PDMS and OSTE - are of exceptional importance to this thesis and are discussed in detail in the following chapters.

1.4.5. PDMS

PDMS – polydimethylsiloxane, also known as dimethicone, is the most popular and widely used polymer for microchip fabrication. It is a mineral-organic polymer composed of carbon and silicon, belonging to the siloxane family. It is achieved by combining an elastomer (base polymer) with a curing agent (a cross-linker) and fine-tuning its thermosetting properties, such as temperature, curing time, degree of cross-linking, and final hardness or strength.

PDMS is remarkably soft and deformable, with elasticity that enables it to withstand significant deformations without sustaining damage. This feature makes it suitable [141] [161]. PDMS has the flexibility to bend, stretch, and precisely adapt to various shapes. PDMS can be molded, cased, and patterned to

create intricate microchip structures. Multilayer microchips are fabricated using soft lithography, which transfers microscale patterns from a master mold, and the layers are permanently sealed using plasma bonding [189], [190], [191].

In addition to its ease of fabrication, PDMS offers several advantageous features. Its optical transparency allows for microscopic observations, while its gas permeability facilitates the exchange of gases, including oxygen and carbon dioxide, between the surrounding atmosphere and the medium within culture chambers, which is essential for cell culture. Furthermore, PDMS is non-toxic and biocompatible, making it ideal for long-term cell culture, cell screening, and biochemical studies [162], [163].

While PDMS is regarded as the gold standard for microchip fabrication, it has its limitations. Once cross-linked, PDMS becomes a hydrophobic elastomer. However, hydrophilic properties are essential for microfluidic applications because they facilitate fluid flow control, minimize bubble formation, and improve cell adhesion. The hydrophobic surface of PDMS can be altered through oxidation, such as radiofrequency or oxygen plasma treatment, leading to the formation of silanol groups (SiOH) on its surface. Additionally, the material can be functionalized with organic compounds, such as 2-hydroxyethyl methacrylate (HEMA), PEG, PVP, PU, and others, temporarily rendering it hydrophilic [164], [165].

During the curing process, some residual polymer chains remain incompletely cross-linked, resulting in residual oligomers that can diffuse within the PDMS material and may leach out when exposed to a solution [35], [166]. Additionally, the porous nature of PDMS enables it to absorb small molecules, including components in cell culture media and test substances, which may impact experimental outcomes. Organic solvents could also be absorbed [35], [166], [167], [168], [169]. Moreover, the expansion and deformation of PDMS microchannels can be caused by high flow rates [170].

The characteristics of PDMS suggest that this material may introduce artifacts in microfluidic cell culture results due to the interaction of PDMS with culture medium and cells. However, the underlying mechanisms remain unclear. It is uncertain whether these effects are caused by molecules leaching into or out of the PDMS or by some other process. One possibility is that uncrosslinked monomers, leaching from the PDMS into the medium, could potentially partition into the hydrophobic portions of the cells, such as the plasma membrane, endoplasmic reticulum, or nuclear envelope. This could disrupt cellular signalling

or metabolism via an unknown mechanism. Thus, it makes PDMS-based microchips less suitable for pharmaceutical testing. [35], [167], [171].

To overcome these limitations, various strategies can be used, which include surface modification of microchannels using non-stick and inert materials such as sol-gel-based silica nanoparticles, Parylene, and perfluorinated polymers like Teflon AF and Cytop [35], [172], [173], [174]. An alternative to PDMS is off-stoichiometry thiol-ene (OSTE), and it is described in the next chapter.

1.4.6. OSTE

OSTE, off-stoichiometry thiol-ene, was introduced in 2011 as the first polymer designed for microchip fabrication. It is composed of two types of monomers: one featuring thiol functional groups, $xR_1-(SH)_m$, and the other containing allyl functional groups, $yR_2-(CH_2-CH=CH_2)_n$. Here, x and y represent the number of each type of monomer, while m and n indicate the number of functional groups present on each. Off-stoichiometric thiol-ene formulations contain an excess of one type of functional group ($xm \neq yn$), resulting in unreacted functional groups both within the bulk material and on the surface. The density of these unreacted functional groups remains stable over time and is evenly distributed, allowing for precise control by adjusting the degree of off-stoichiometry. This characteristic makes the OSTE polymer particularly well-suited for direct UV-initiated grafting of functional molecules through highly specific thiol-ene “click” reactions [175], [176].

OSTE polymers are unique due to their dual-curing mechanism. In the first curing stage, UV light initiates the thiol-ene reaction, solidifying the material and allowing for precise shaping of microstructures. This process preserves unreacted thiol and alkene groups on the surface, making it sticky and enabling the polymer to bond covalently with other surfaces or graft functional molecules. The second curing stage involves applying heat to eliminate the remaining reactive groups, resulting in a fully cross-linked, chemically stable material with robust mechanical properties. This dual-curing process allows OSTE to combine versatility during fabrication with long-term stability performance [177].

Microchip fabrication often involves assembling multiple layers, which presents challenges in bonding and sealing. Conventional bonding methods, such as thermal bonding, solvent bonding, plasma activation, and UV-curable adhesives, can deform microchannels, compromise surface modification, or obstruct tiny microstructures [168]. In contrast, OSTE polymer employs its reactive surface groups to form covalent bonding to other surfaces, allowing for gentle bonding without the drawbacks of traditional methods. Furthermore,

OSTE features low shrinkage during curing, high chemical resistance, and tunable mechanical properties, making OSTE an excellent material for microfluidic devices [175], [177], [178].

1.4.7. Microchannel architecture

Microchips are very versatile in design and are adapted to the field of application. These designs can differ substantially, ranging from the simple linear channel, which may feature one, two, or several parallel channels, to more complex configurations as mixing channels. Advanced designs include multilayered chips for 3D fluid flow, porous devices for diffusion and filtration studies, and topographical chips whose surface features influence cell behaviour or fluid dynamics [179]. The versatility of microchip architecture limits the standardization and commercialization of microchips, which is why many laboratories design and manufacture their own microchips according to their specific research needs.

To properly design a microfluidic system, the parameters – geometry and dimension - of the microfluidic device must be accurately calculated. In single cell studies, the width and height of the microchannel are typically measured in the tens of micrometres. Additionally, when trapping or sorting the cells, the microchannel may incorporate specific traps or curved geometries [180], [181]. For cellular culture, microchannel sizes often range from 100 to 1000 μm . The microchannel should accommodate a sufficient number of cells within the microchannel, enabling population-based analysis [182].

To achieve more complex microchannel geometries, PC and PET track-etched membranes are used to create a three-dimensional network. These networks are formed by integrating the membranes into the device during fabrication. The membrane functions as a semi-permeable barrier that separates microchannels on different horizontal planes, while permitting interactions exclusively at the points where the channels intersect [183], [184].

Fluid velocity within the microchannel exhibits distinctive behaviour based on geometry. In a circular channel, fluid moves fastest at the center and slows down symmetrically near the channel, resulting in a parabolic velocity profile. In rectangular channels, the velocity distribution varies according to the width-to-height ratio, with fluid slowing near the walls and corners due to boundary effects. The velocity profile is critical as it dictates the shear stress experienced by cells. Shear stress influences cellular morphology, signalling, and mechanotransduction. Additionally, variation in the velocity profile can lead to differences in nutrient and oxygen distribution, ultimately affecting cellular behaviour, viability, and function [185].

The architecture of microchannels, including their geometry and dimensions, directly influences critical parameters such as Reynolds number, flow type, which collectively govern fluid behaviour and cellular interactions in microfluidic systems. These aspects are described below.

1.4.8. Fluid dynamics and transport mechanisms in microfluidic systems

In fluid dynamics, the fluid flow behaviour within the microchannel is characterized by a Reynolds number (Re) – a dimensionless quantity representing the ratio of inertial to viscous forces [138], [186]. It provides insight into the fluid flow regimes and is defined as:

$$Re = \frac{uL}{\nu} = \frac{\rho uL}{\mu} \quad (2)$$

where

ρ is the density of the fluid [kg/m^3],

u is the flow velocity [m/s],

L is a height [m],

μ is the dynamic viscosity of the [$\text{Pa}\cdot\text{s}$ or $\text{N}\cdot\text{s}/\text{m}^2$ or $\text{kg}/(\text{m}\cdot\text{s})$],

ν is the kinematic viscosity of the fluid [m^2/s].

In microfluidic systems, flow behaviour is strongly influenced by microscale dimensions. Unlike macroscale systems, microfluidics typically operates under low Reynolds numbers, where viscous forces dominate and flow remains highly predictable [45]. Microfluidic systems exhibit several distinct flow types, which include: laminar, turbulent, electroosmotic, capillary, and centrifugal flows. Among these, laminar and turbulent flows are particularly important in microfluidic applications involving cells.

1) **Laminar flow** is the predominant flow type in microfluidic systems. It is characterised by the orderly movement of fluid particles in parallel layers without disruption or mixing between layers. Dominated by viscous forces, laminar flow exhibits highly predictable behaviour, typically occurring at low Reynolds numbers ($Re < 2000$). This orderly flow enables precise control over fluid positioning and reagent delivery, which is essential for cell-based microfluidic applications.

2) **Turbulent flow** is characterized by chaotic and unpredictable fluid movement, often accompanied by eddies and instabilities. In this regime, inertial forces dominate over viscous forces. Reynolds numbers typically exceed 4000. Although turbulent flow is uncommon in microfluidic systems, it can be intentionally induced to enhance mixing efficiency. Its potential impact on shear stress and flow uniformity must be carefully considered during microchip design

to ensure optimal performance and prevent unintended flow disturbance (**Figure 14**) [187].

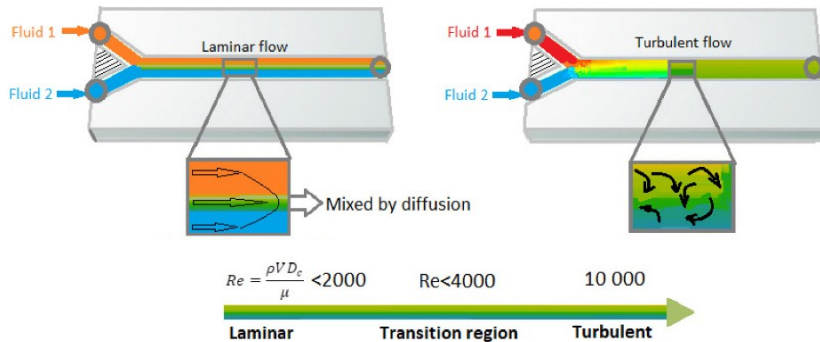


Figure 14. Laminar versus turbulent flow in the microfluidic channels [187].

In microfluidic cell systems, fluid is transported between different regions either by active or passive pumping mechanisms. Microchip inlet and outlet ports connect microchannels - where cultured cells reside - to the external environment. Tubing is used to link these ports to the fluid reservoir and the flow generator.

As **active pumping methods**, syringe pumps and peristaltic pumps are commonly employed in OoC and MPS. **Syringe pumps** are designed for non-recirculatory flow, employing a stepper motor to pull or push a syringe (**Figure 15**). This mechanism produces a steady, pulse-free flow, required for applications with precise control of fluid rates.

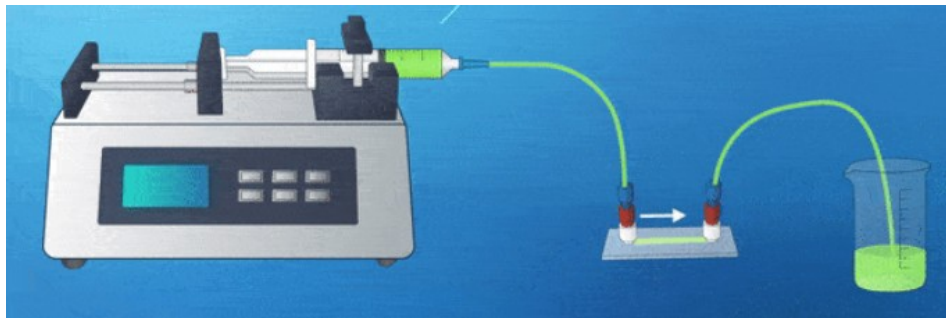


Figure 15. Schematic representation of a microfluidic system with flow driven by a syringe pump. Picture sourced from <https://www.elveflow.com>

In contrast, **peristaltic pumps** generate recirculating, pulsatile flow by mechanically compressing flexible tubing using rotating rollers. This mimics physiological blood flow and is suitable for dynamic stimulations. The pump head contains multiple rollers mounted on a rotating wheel. As the wheel turns:

1. The first roller compresses the tubing at the inlet, sealing it and initiating forward movement.
2. As the roller continues along the arc, it presses the tubing against the manifold, creating a pressure wave that propels the fluid forward.
3. Before the fluid reaches the outlet, the second roller closes the tubing behind the first, preventing backflow.
4. Once the first roller passes the outlet, the second roller continues the cycle, generating the next pressure wave. This sequential compression mimics the natural rhythm of physiological blood flow (**Figure 16**).

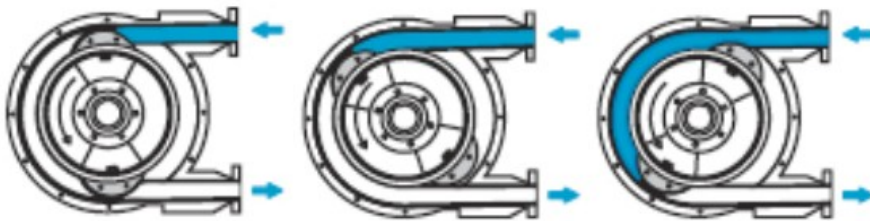


Figure 16. Peristaltic pump flow scheme [188].

An alternative to active flow generators is **passive pumping**, which relies on surface tension differences between droplets at the inlet and outlet to drive fluid flow. The mechanism is based on the pressure difference created by droplets of different sizes, placed at the inlet and outlet (**Figure 17**) [182]. According to Laplace's law, the internal pressure of a droplet is inversely proportional to its radius:

$$\Delta P = \frac{2\gamma}{R} \quad (3)$$

where

ΔP is the pressure difference across the liquid-air interface [Pa],

γ is the surface tension of the liquid [N/m],

R is the radius of the droplet [m].

Figure 17 illustrates this principle. In this context, a smaller droplet (radius R_i) at the outlet has a higher internal pressure (P_i) than a larger droplet (radius R_0 and pressure P_0) at the inlet. Since $R_i < R_0$, it follows that $P_i > P_0$. This pressure gradient drives fluid from the inlet to the outlet through the microchannel.

Passive pumping eliminates the need for external tubing or interconnections, as the flow is initiated by pipetting drops directly to the inlets. This approach is advantageous for microchip applications for process automation

[189]. However, passive pumping is restricted to low flow rates and pressures, making it less suitable for systems requiring continuous and uninterrupted fluid movement. While drops can theoretically be replenished during a passive pump cycle, external flow generators are generally preferred for microfluidic applications for long-duration microfluidic experiments.

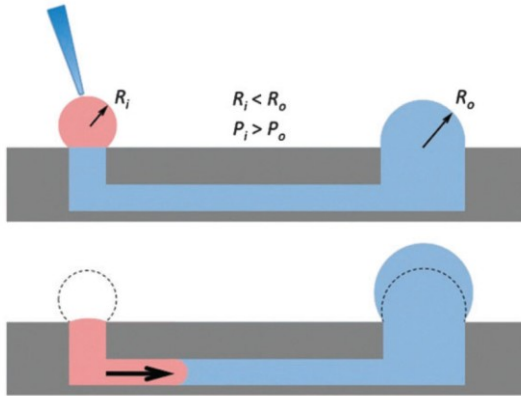


Figure 17. Schematics of passive pumping. Fluid flow is driven by pressure differences between droplets of varying radii, based on Laplace's law [182].

1.4.9. Shear stress

Shear stress is defined as the stress created when a tangential force acts on a surface. In biology and microfluidics, it can be described as the frictional force of a biological fluid flow acting on cells or tissues.

In vivo, mechanical forces act as physiological signals that elicit cellular responses. Cells detect and react to these forces through mechanosensors, which convert the mechanical signals into chemical signals. This process is called mechanotransduction. In microfluidics, mechanotransduction is initiated by shear stress and influences the cell adhesion, migration, and proliferation [190].

Shear stress is closely related to channel geometries and dimensions. *In vivo*, it is present in blood vessels, where it regulates endothelial cell function and vascular homeostasis. The magnitude of shear forces that cells are subjected to varies depending on the location and environment. For instance, endothelial cells lining arteries experience higher shear stress than those in veins (**Table 3**). Besides the vascular endothelium, cells from other tissues also experience shear stress – interstitial endothelium (0-0.003 Pa), respiratory endothelium, lymphatic endothelium, cartilage, bone, corneal cells (0.05-1.5 Pa), and renal glomerular cells, in all cases with different shear stress parameters (**Table 3**) [191].

Understanding this variability is crucial for designing devices that accurately replicate physiological or pathological conditions.

Table 3. Shear stress in various physiological contexts.

Blood vessel	Shear stress [192]	Other tissue environments	Shear stress
Arteries	1-6 Pa	Lymphatic vessel	0.64 Pa with peaks of 4 – 12 Pa [193]
Veins	0.1-1 Pa	Gut (intestinal endothelium)	0 - 0.003 Pa [191]
Ascending aorta	1.2 Pa	Bone (osteoblasts)	0.8 - 1.0 Pa [194]
Descending aorta	0.5-0.8 Pa	Bone (osteocytes)	0.8 - 3.0 Pa [195]
Pulmonary artery	0.5 Pa	Cornea	0.005 -1.5 Pa [191]
Small veins	1.1 Pa	Kidney (glomerular endothelium)	0.5 – 2 Pa [196]
Large veins	0.5 Pa		

1.4.10. Biology meets microfluidics

The convergence of biology, chemistry, biochemistry, physics, and engineering is essential for cell research at the microscale. A thorough understanding of cell, tissue, and organ biology, alongside the dynamics of the microenvironment, is important to replicate them *in vitro*. Equally important is a strong foundation in microfluidic technologies, which enable the creation of controlled, miniaturized systems for biological experiments.

Traditionally, cells have been cultured under static conditions, and a straightforward approach has massively contributed to our knowledge. However, advances in microfluidics now enable more precise studies of cells within three-dimensional environments and continuous flow systems. Controlled fluid flow is essential for nutrient delivery, waste removal, and gas exchange within microfluidic systems. These functions are essential for maintaining cell viability and mimicking *in vivo* conditions. Additionally, these systems can also incorporate sensors to monitor key physiological parameters, such as pH and oxygen levels, in real-time.

One of the primary advantages of microfluidic systems is their ability to overcome the limitations of conventional cell culture methods, allowing for more dynamic and precisely controlled experimental setups. These innovations not only increase the precision and relevance of *in vitro* research but also open the way to groundbreaking applications, including personalized medicine, OoC, MPS technologies, and high-throughput drug screening. As the field of microfluidics continues to evolve, it promises to revolutionize biological research and bridge the gap between experimental models and real biological systems.

2. METHODOLOGY

2.1. MATERIALS AND EQUIPMENT

2.1.1. Material

Biomaterials of the study:

- **Al alloy 6082 anodized with sulphuric acid**, with a diameter of 15 or 16 mm and a sheet thickness of 2 mm (provided by Dr. Tadas Matijošius)
- **Al alloy 6082 anodized with phosphoric acid**, with a diameter of 15 or 16 mm and a sheet thickness of 2 mm (provided by Dr. Tadas Matijošius)
- **Al alloy 6082** - with the purity of 96.52 wt % (2.28 wt % Mg; 0.53 wt % Si; 0.36 wt % Fe; 0.31 wt % Mn), with a diameter of 16 mm and a sheet thickness of 2 mm (FXB-Niemet UAB, Lithuania)
- **Ti alloy BT1** - with the purity of 96.32% (1.76 wt % Mn; 1.75 wt % Al; 0.11 wt % Fe; 0.06 wt Si) with a diameter of 16 mm and a sheet thickness of 2 mm (SP MET UAB, Lithuania)
- **PC** - track-etched PC membrane, pore size of 3 μm or 0.4 μm (ipPORE, Belgium)

Materials for microchip fabrication

- Zortrax white resin - (Zortrax Ikspire, Poland).
- PDMS - Sylgard 184 silicone elastomer kit (Dow Corning, USA)
- OSTE - Ostemer322 resin (Mercene Labs, Sweden)
- COC – microscopy slide format (Microfluidic Microchip Shop, Germany)
- Track-etched PC membrane - 3 μm pores with 21.2 % porosity and 22 μm thickness (it4ip, Germany)
- Silicon tubing – 1 mm inner diameters (Darwin Microfluidics, France)
- Mini Luer ports - (Microfluidic ChipShop, Germany)
- Oxygen sensors - SP-PSt6-YAU point oxygen sensors (PreSens Precision Sensing GmbH, Germany)
- MD® medical adhesive 1403-M - (Dymax, Wiesbaden, Germany)
- Sil-Poxy™ silicone adhesive (Smooth-on Inc., PA, USA).
- PTFE tubing with 0.8 mm inner diameter and silicon tubing with 1 mm inner diameter (Darwin Microfluidics, Paris, France)

Materials for cell handling:

- RPMI 1640 growth media - (Corning, USA)

- F-12K growth media - (*Corning*, USA)
- FBS – Fetal Bovine Serum (*Gibco*, USA)
- Penicillin - Streptomycin solution (*Gibco*, USA)
- Glutamine - (*Lonza*, USA)
- PBS – Phosphate Buffered Saline (*Sigma-Aldrich*, USA)
- Trypsin-EDTA - (*Gibco*, USA)
- Trypan Blue Solution – 0.4% (*Gibco*, USA)
- PDL - (*Gibco*, USA)
- Collagen I - (*Sigma-Aldrich*, USA)
- Fibronectin - (*Sigma-Aldrich*, USA)
- Resazurin – (*Applichem*, Germany)
- XTT kit - (*Roche*, Germany)
- DAPI - (*Thermofisher Scientific*, USA)

2.1.2. Cell lines

- L929 - mouse fibroblast cell line (NCTC clone 929 [L cell, [L-929, derivative of Strain L], cultured in RPMI-1640 supplemented with 10% FBS, 2 mM Glutamine, 100 U/ml penicillin, and 100 µg/ml streptomycin.
- CHO-K1 – chinese hamster ovary cell line, epithelial-like (ATCC, CCL-TM), cultured in RPMI-1640 supplemented with 10% FBS, 100 U/ml penicillin, and 100 µg/ml streptomycin.
- SK-MEL-28 – human melanoma cell line, polygonal, epithelial-like (ATCC, HTB-72TM), cultured in RPMI-1640 supplemented with 10% FBS, 100 U/ml penicillin, and 100 µg/ml streptomycin.
- U2OS – human bone osteosarcoma cell line, epithelial (ATCC, HTB-96TM), cultured in F-12K supplemented with 10% FBS, 100 U/ml penicillin, and 100 µg/ml streptomycin.
- C6 – rat glioma cell line, fibroblast, (ATCC, CCL-107TM), cultured in RPMI-1640 supplemented with 10% FBS, 100 U/ml penicillin, and 100 µg/ml streptomycin.

2.1.3. Equipment

1. Ultrasonic bath VTUSC3 (Velleman, Belgium)
2. Ultrasonic bath DT100H (Bandelin Electronics, Germany)
3. Dualscope MPOR-FP (Helmut Fisher, USA)
4. Profilometer SurfTest SJ-210 (Mitutoyo, Aurora, USA)
5. Nanoindenter Hysitron Ti Premier (Bruker, USA)

6. Microindenter PMT-3 (Kirova, Russia)
7. Potentiostat system Solartron 1280C (Ametek, Inc.).
8. Spectrometer Optima 7000 DV (PerkinElmer, USA)
9. Scanning electron microscope Helios NanoLab 650 (FEI, The Netherlands).
10. INCA spectrometer equipped with X-Max 20 mm² silicon-drift detector (Oxford Instruments, UK).
11. Contact angle measurement system EasyDrop (KRÜSS, Germany).
12. 3D printer Anycubic Photon (Shenzhen Anycubic Technologies, China).
13. UV lamp - 365 nm UV light, intensity approx. 2.04 mW/cm² (custom-made, FTMC, Lithuania).
14. UV lamp - 405 nm UV light, intensity approx. 1.95 mW/cm², custom-made, FTMC, Lithuania).
15. LCR-6000 meter (Gwinstek, USA).
16. Plasma cleaner Zepto B (Diener electronics, Germany)
17. neMESYS low-pressure syringe pump (Cetoni, Germany)
18. Electroporator Elpora (FTMC, Lithuania)
19. Oscilloscope TDS 1012B (Tektronix, USA)
20. Fluorescent spectrophotometer LS50B – (Perkin Elmer, USA)
21. Confocal microscope ECLIPSE Ti (Nikon, USA)
22. Hemocytometer (BLAUBRAND, Germany)
23. Oscilloscope TDS 1012B (Tektronix, JAV)
24. Oxygen measurement system Oxy-4 SMA (G3) meter (PreSens Precision Sensing, Germany)
25. Photodiode optical glass filter FGL515 (Thorlabs, USA)
26. White LED LEDWE-15 (Thorlabs, USA)
27. Laminar hood AURA VERTICAL S.D.4 - (BioAir, Italy)
28. CO₂ incubator ICO (Mettler, Germany)

2.2. METHODS

2.2.1. Bioceramic coating preparation

Al alloy 6082 underwent electrochemical oxidation (anodizing) in sulfuric acid (H₂SO₄) and phosphoric acid (H₃PO₄) electrolytes. Initially, the alloys were degreased with acetone and subsequently cleaned by immersion in an alkaline solution (30 g/L sodium hydroxide (NaOH) + 25 g/L trisodium phosphate (Na₃PO₄) + 75 g/L sodium carbonate (Na₂CO₃)) for 45 seconds at 60°C, followed by a 10% nitric acid (HNO₃) treatment for 60 seconds at 21°C, with deionized water rinsing after each step.

The prepared specimens were mounted in a titanium holder and immersed in a continuously mixed 3 L aqueous electrolyte bath with a titanium cathode. The type III hard anodizing process was conducted in a solution containing 18 wt % H_2SO_4 , 2 wt % oxalic acid, and approximately 0.4 wt % Al^{3+} concentration at $15^\circ C$, using an anodic current density of $200 A/m^2$ for 70 minutes, resulting in thick bioceramic Al_2O_3 coatings ($\sim 60 \mu m$ thickness) with ~ 15 nm nanopores [20].

The addition of oxalic acid was employed to minimize coating dissolution and promote the formation of denser, more stable Al_2O_3 during the anodization process. Incorporating the oxalic acid into the sulfuric acid electrolyte enhances the thickness and hardness of the alumina coating, thereby improving its corrosion resistance [29], [197], [198].

Phospho-anodizing was conducted in a 4 wt % H_3PO_4 electrolyte at $15^\circ C$ and 150 V direct current for 150 minutes, producing thin ($\sim 10 \mu m$ thickness) coatings with ~ 200 nm micropores [199].

2.2.2. Water droplet contact angle

Water droplet contact angle measurements were conducted using the EasyDrop instrument and analysed with Drop Shape Analysis v.1.70-02 software. The dosing process utilized a syringe pump, delivering droplet volumes of $24.7 \pm 3.6 \mu L$. Each liquid sample formed a free-hanging droplet that detached due to mechanical action. To determine the actual contact angle, a minimum of five water droplets were measured at various locations, and their average value was calculated.

2.2.3. SBF immersion experiments

Specimens were in simulated body fluid (SBF) to evaluate their behaviour under physiologically relevant conditions. SBF was prepared according to the method, described by Kokubo and Takadama [200], with the following concentration of cations: 142 mM Na^+ , 5 mM K^+ , 1.5 mM Mg^{2+} , 2.5 mM Ca^{2+} , and anions: 147.8 mM Cl^- , 4.2 mM HCO_3^- , 1 mM HPO_4^{2-} , 0.5 mM SO_4^{2-} , adjusted to pH=7.4 at $36.5^\circ C$. Each component was accurately weighted, dissolved in a minimal volume of deionized water, and gradually added into the SBF solution dropwise, following the prescribed order. Prior the use, the anhydrous materials were heat-dried and sterilized with 70% ethanol, thoroughly washed with sterile deionized water, and UV-dried for 30 min. Specimens (16 mm diameter) were immersed in 50 mL SBF solution for periods ranging from 1 to 28 days at

37°C. pH measurements were conducted to monitor changes in the SBF solution. After immersion, samples were subjected for inductively coupled plasma optical emission spectroscopy (ICP-OES), and potentiometry to assess ion release and electrochemical behaviour. In addition, scanning electron microscopy (SEM) was employed to examine the surface characteristics of specimens.

2.2.4. ICP-OES

Release of ions from specimens into SBF for 1 to 28 days was analysed by inductively coupled plasma optical emission spectroscopy (ICP-OES) using a PerkinElmer Optima 7000 DV spectrometer. Before analysis, SBF samples were diluted 10-fold with deionized water, and the concentrations of Al, Fe, Mg, Mn, Si, Ti, P, and S analytes were measured in mg/L.

2.2.5. Corrosion tests

Corrosion is an electrochemical process involving at least two half-reactions: metal oxidation (anodic) and oxidant (typically dissolved oxygen) reduction (cathodic). The rate of corrosion is directly linked to the intensity of these reactions and is quantified by the corrosion current density (j_{corr}). Near the corrosion potential ($\pm 5\text{-}20$ mV from the open circuit potential, E_{ocp}), the current potential (I-E) relationship is approximately linear, allowing the use of Tafel extrapolation to estimate j_{corr} .

The corrosion rate can be calculated using the following equation:

$$CR = \frac{K \times j_{\text{corr}} \times EW}{\rho}, \quad (4)$$

where

CR – corrosion rate [mm/year],

K – constant [3.27×10^{-3}]

j_{corr} – corrosion current density [$\mu\text{A}/\text{cm}^2$],

EW – equivalent weight [g/equiv]

ρ - density of the material [g/cm^3]

The corrosion tests and calculations were conducted by Dr. Asta Grigučevičienė. Electrochemical voltammetric (j/E) and impedance (Z) measurements were conducted in SBF at 37°C using the potentiostat system. An Ag/AgCl electrode in saturated KCl solution served as the reference electrode, while a Pt plate was used as the counter electrode. The working electrode was

mounted in a holder and immersed in an electrochemical glass cell containing approximately 100 mL of SBF, ensuring an exposed electrode area of 0.5 cm².

Electrochemical measurements began 10-15 min after immersion to allow the open circuit potential (OCP) to reach a quasi-steady state. Tafel polarization curves were recorded in a potentiodynamic mode with a potential at a scan rate of 1 mV/s. Corrosion current densities (j_{corr}) were determined by extrapolating linear regions of the anodic and cathodic Tafel slopes to the open circuit potential value (E_{ocp} or E_{corr}) before and after immersion periods from 1 to 28 days in SBF. The electrochemical impedance spectroscopy (EIS) spectra was conducted at E_{ocp} over a frequency range from 1000 kHz to 10 mHz to further characterize the corrosion behaviour and surface properties of the specimen.

2.2.6. SEM imaging

Specimens without cells were washed with deionized water and air-dried before SEM imaging. The samples were then analysed using a dual-beam scanning electron microscope, enabling the detailed visualization of surface features. Characteristics of surface pores were analysed using the open-source image processing program ImageJ 1.53t, based on using SEM images captured at 100,000. A thresholding process distinguished the black and white areas, representing the pores and the Al₂O₃ surface, respectively, enabling accurate outlining of surface pores. The average nanopore density was determined by counting nanopores within a 1 μm² segment of the surface in three random spots. Characteristics of surface pores were determined by the open-source image analysis program ImageJ 1.53t using SEM images at 100,000× magnification. Thresholding was carried out in the black and white areas representing the pores and Al₂O₃ surface, respectively, which enabled the outlining of surface pores. Average nanopore density was determined by calculating the number of nanopores in a 1 μm² segment area of the surface in three randomly selected areas. Surface porosity (%) was calculated as the ratio of nanopore openings to the total selected oxide surface area.

To visualize cell adhesion onto biomaterials, cells were cultured on them for 24 hours. After incubation, specimens with adherent cells were rinsed twice with PBS and subsequently fixed with 2% glutaraldehyde in PBS for 1–2 hours at +4°C. Following fixation, samples were then dehydrated through a series of ethanol concentrations (50%, 70%, 85%, 96%, 96%) each for 15 min, and finally air-dried in a desiccator. Dry cellular constructs were sputter-coated with Cr (1–2 nm thickness) to obtain the necessary electrical conductivity. The prepared samples were

subsequently analysed using SEM for high-resolution visualization of cell adhesion and surface interaction.

2.2.7. Cell line handling

Cell lines were grown in their respective culture media (see Chapter 2.1.2) at 37°C, 5% CO₂ atmosphere in a humidified chamber. The culture medium was replaced, or cells were passed twice a week and always a day before an experiment. To collect cells for experiments, cells were detached by trypsinization (trypsin 0.025% and EDTA 0.02% solution) and resuspended either in the full medium or in a buffer required for the experiment: Cells subjected to PEF treatment were resuspended in electroporation buffer (7 mM NaCl, 1 mM KCl, 10 mM HEPES, 3 mM NaOH, 250 mM saccharose, pH 7.4) at a concentration of 5-10×10⁶ cells/ml [201].

2.2.8. Viability assays

To evaluate the impact of alloys and their bioceramic coating on cell viability, the cytotoxicity was assessed by evaluating the viability of L929 cells exposed to the specimens' extracts. These extracts were prepared using an elution test method, in which each specimen was incubated in cell culture medium for 4 days at 37°C. Following incubation, the conditioned media, now containing potential leachables from the materials, were collected and used to culture the cells. As a control, the same culture medium was incubated under identical conditions without the specimen immersion.

To assess cell growth, adhesion, and proliferation, L929 cells were detached using trypsin, resuspended in the specimen extracts, and seeded at a density of 10⁵ cells/well in a 6-well plate. The cells were subsequently incubated for 48 hours to allow for cell attachment and proliferation. Following incubation, cells were washed with PBS and exposed to resazurin at a concentration of 20 µg/mL in a buffer containing 7 mM NaCl, 1 mM KCl, 10 mM HEPES, 3 mM NaOH, 250 mM saccharose, pH 7.4. Cells were incubated with resazurin for 30-60 min, after which fluorescence measurements were recorded using a fluorescent spectrophotometer with an excitation wavelength of 571 nm and emission at 584 nm. Each sample was prepared in duplicate, and the experiments were repeated three times for consistency. Relative cell viability was calculated as the ratio of the test specimen to the control specimen, expressed as a percentage.

To evaluate the impact on cell proliferation, a pre-cultured cell monolayer was used. Cells were seeded at a density of 5×10³ cells/well in a 96-well plate and precultured for 24 hours before exposure to the extracts. Finally, cells were

incubated with the extracts for 24 hours. Following incubation, cell viability measurements were taken using the XTT assay kit with an incubation time of 15-45 min. Absorbance was recorded at 490 nm, with 620 nm used as the reference wavelength. Each sample was prepared in quadruplicate, and the experiments were repeated three times for reproducibility. Relative cell viability was calculated as the ratio of the test specimen to the control specimen, expressed as a percentage.

2.2.9. Cell adhesion on PC membranes

To evaluate the cell adhesion capacity of PC membranes, their ability to support cell adhesion was assessed under standard culture conditions. Cells were plated onto a 35 mm diameter PC membrane placed in 6-well plates and incubated overnight. After incubation, the growth media were collected to estimate the number of non-adherent cells, and the cells were detached by trypsinization to estimate the number of adherent cells. Experiments were conducted in triplicate.

PC membranes were subjected to different pre-treatment conditions to examine their influence on cell adhesion. These include PC's incubation with PBS, FBS, PDL, fibronectin, and collagen, and PC's oxidation with oxygen plasma and wet chemical oxidation.

2.2.10. Biological functionalisation of PC membrane

To prepare PC membranes for cell adhesion studies, various coatings and pre-treatment methods were applied. These included pre-incubation with PBS, FBS, as well as functionalisation with PDL, collagen I, and fibronectin.

To assess whether the PC membrane inherently supports cell adhesion, it was pre-incubated with PBS for 1 h before cell seeding. Similarly, to determine whether the PC membrane facilitates adhesion through factors present in FBS, membranes were incubated with FBS for 1 h prior to cell seeding.

PC membranes were coated with PDL following a modified protocol from B-27™ Plus Neuronal Culture System (Gibco™, ThermoFisher Scientific, USA). PDL was diluted in PBS to 0.05 µg/mL, applied to the membranes in a 6-well plate, and incubated for 1 h at room temperature. The coating was designed to achieve a final surface concentration of 0.01µg/cm². After incubation, the solution was removed, and membranes were washed three times with sterile distilled water before being dried in a laminar hood for 2 hours. When coating membranes within a microchannel, the microchannel was thoroughly washed with 10x volume of PBS.

The PC membranes were coated with collagen I at a concentration of 30 $\mu\text{g/mL}$, dissolved in 20 mM acetic acid. The membranes with collagen I were incubated for 2 hours at room temperature, after which the solution was removed, and the membranes were dried overnight in a laminar flow hood. The coating was designed to achieve a final surface concentration of 10 $\mu\text{g/cm}^2$

The PC membranes were coated with fibronectin at 2 $\mu\text{g/mL}$ in PBS. The membranes with fibronectin were incubated for 1 h at room temperature, washed twice with PBS, and dried thoroughly before seeding the cells. Fibronectin coating was applied to achieve a final surface concentration of 2 $\mu\text{g/cm}^2$.

2.2.11. Oxidation of the PC membrane

PC membranes were cut into circular specimens with a diameter of approximately 35 mm (surface area $\sim 9,6 \text{ mm}^2$) to ensure compatibility with 6-well cell culture plates following oxidation. For oxidation of the PC membrane within the microchip, the chemical reagents were introduced directly into the microchannels of the fabricated device.

Plasma oxidation. Both sides of the PC membrane were exposed to oxygen plasma in Plasma Cleaner Zepto, supplied with oxygen gas. The treatments were conducted for 30 seconds at 70% power and 0.35 mbar pressure to induce surface modification.

Wet chemical oxidation of PC membranes was conducted using sodium metaperiodate (NaIO_4), H_2SO_4 , and Piranha solution as oxidizing agents.

1. Oxidation with NaIO_4 : The PC membrane was immersed in a 25g/L NaIO_4 solution and incubated at room temperature in the dark for 30 min to avoid photochemical interference.

2. Oxidation with H_2SO_4 . PC membrane was immersed in 10% H_2SO_4 and incubated for 30 min at room temperature.

3. Oxidation with piranha solution. Piranha solution was prepared with 12.5% H_2SO_4 , which was mixed with H_2O_2 in a 4:1 ratio. PC membranes were immersed in this highly reactive solution and incubated for 2 h at room temperature.

After incubation, all membranes were thoroughly rinsed with deionized water and dried at room temperature. Before the experimentation, membranes were sterilized using 70% ethanol and UV light to ensure aseptic conditions.

2.2.12. Fabrication of a microfluidic chip

The OSTE moulding technology using PDMS mold was adapted for microchip fabrication, with the integration of additional elements - electrodes,

sensors [202], [203]. The brief description of our microchip fabrication process is presented in **Figure 18**.

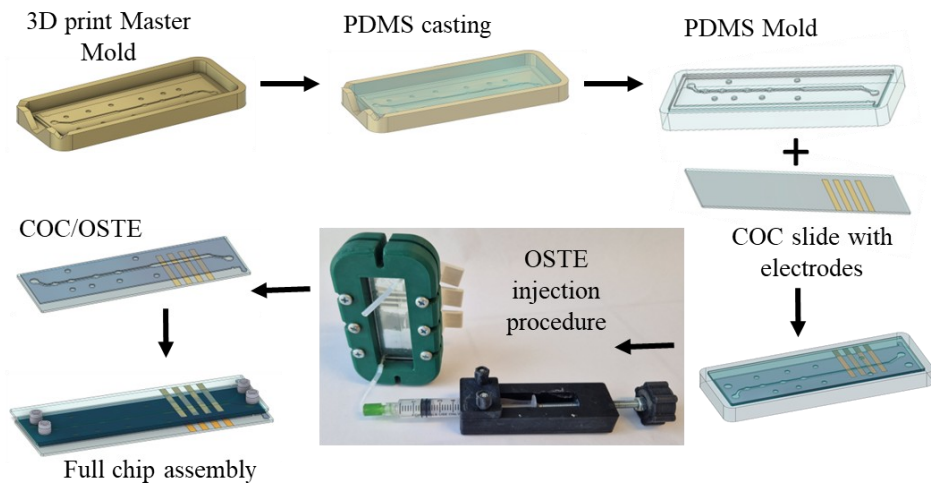


Figure 18. Microchip fabrication process.

The fabrication requires two molds. A master mold is 3D printed using Zortrax white resin. A Sylgard 184 silicone elastomer kit was mixed with the crosslinker and the substrate in a 1:10 (w/w) ratio, degassed in a vacuum chamber. Master mold was pre-coated with a thin layer of organic mold-releasing wax, and the PDMS mixture was cast into the 3D-printed master mold. To achieve the correct dimensional height, the PDMS was pressed against glass surfaces and cured at 60°C overnight. The cured PDMS mold was then removed from the master mold, and inlets were punched with a biopsy punch.

A COC in microscopy slide format was employed as a substrate material for the microchip. Two COC slides were pre-washed with acetone and rinsed with isopropanol using an ultrasonic cleaning bath for 10 min, followed by an oxygen plasma treatment for 30 seconds at 70% power and 0.35 mbar pressure. A thin layer of gold with a chrome sublayer for adhesion was deposited onto COC slides via thermal evaporation through a mechanical mask.

The bottom COC slide with electrodes was placed into a PDMS mold and secured in a custom 3D-printed holder. Two PTFE tubes were attached to the injection ports for the injection of OSTE. OSTE was prepared according to the manufacturer's instructions (1.09:1 PartA:PartB, w/w), degassed, and injected into the cavities of the COC/PDMS construct. Initial curing of OSTE was conducted using 365 nm UV light at an intensity of approximately 2.04 mW/cm²

for 1 min. This results in the OSTE taking shape while still containing unreacted functional groups, which make the surface sticky. The device was then disassembled, and a porous PC, pre-treated with oxygen plasma, was pressed onto the cured but still sticky OSTE layer. A PC membrane, with 3 μm pores with 21.2 % porosity and 22 μm thickness, is attached to the sticky OSTE surface of the bottom slide, forming a COC/OSTE/PC slide.

The UV-cured upper slide of the chip was then prepared likewise. Two SP-PSt6-YAU point oxygen sensors were glued to the designated channel locations using Sil-Poxy™ silicone adhesive. The upper COC/OSTE/O₂ sensor slide was then aligned with pressed onto the lower COC/OSTE/PC slide and cured at 60°C for 2 hours to complete assembly. Finally, mini-Luer ports are glued to the inlet and outlet holes of the microchip channels, allowing connections to all required tubing.

The channel height of the fabricated microchip was measured using a Vernier calliper to ensure dimensional accuracy. Mini Luer ports were mounted with MD® medical adhesive 1403-M and cured under 405 nm UV light for 1 min (intensity approx. 1.95 mW/cm²). Finally, electrode performance was validated by measuring the impedance with a precision LCR-meter.

2.2.13. Microfluidic setup

The neMESYS low-pressure syringe pump was used to regulate laminar flow type and flow rate within the microfluidic channel, controlled via computer software Cetoni Elements. For fluid connections, PTFE tubing were utilized to link the syringe pump to the microchip. Before the experimentation, microchannels were sequentially washed with 70% ethanol, followed by sterile deionized water, and finally with either electroporation buffer or cell growth medium RPMI-1640, depending on the experimental conditions. The flow rate was set to 1 $\mu\text{l/s}$ for cell injection and 5 $\mu\text{l/s}$ for cell collection and channel washing.

2.2.14. PEF treatment experiments

Pulsed electric field treatment (PEF) was applied using a high-power square wave pulse electroporator Elpora [204]. The voltage of PEF treatment was determined using an oscilloscope.

Stop flow PEF. Cells were injected into the electrode area at a flow rate of 1 $\mu\text{l/s}$, allowed to settle for one minute, and then subjected to PEF ranging from 0-10 kV/cm. A sequence of 8 or 16 rectangular pulses (100 μs duration, 1 Hz repetition frequency) was applied for pulsation, followed by a 1-minute

incubation period. The cells were then moved along the microchannel by a volume corresponding to the space between one electrode pair, and the PEF treatment was repeated.

To ensure that all cells received PEF treatment, the entire process was repeated twice, based on the initial injected cell volume. The volume between one electrode pair (V_0) is calculated using the following formula:

$$V_0 = l \times w \times h \quad (5)$$

where

V_0 – volume between parallel electrodes [μl],

l – electrode length [μm],

w – electrode width [μm],

h – microchannel height [μm].

Continuous flow PEF. Cells were injected into the microchip and remained in continuous flow while receiving 8 to 128 rectangular pulses (100 μs duration, 1 Hz repetition rate). To achieve a specific number of pulses in continuous flow mode, the flow rate (v) was calculated using the following formula:

$$v = \frac{4 \times V_0 \times f}{n}, \quad (6)$$

where

v – flow rate [$\mu\text{l/s}$]

4 – number of electrodes,

V_0 – volume between parallel electrodes [μl],

f – repetition rate [Hz],

n – pulse number.

For the viability studies, cells were collected after PEF treatment, seeded into a 24-well plate, and incubated for 16 hours at 37°C, in a humidified chamber with 5 % CO₂ atmosphere. The number of viable cells was determined with a trypan blue exclusion assay.

For the permeability studies, cells were suspended with DAPI to a 1 μM concentration and incubated for 20 min before the PEF treatment. After incubation, cells were injected into the microchip, and PEF treatment was conducted. In continuous flow experiments, cells were incubated without flow for 5 min after PEF treatment. Fluorescence emission at 455 nm was measured for excitation of 395 nm using a fluorescent spectrophotometer.

2.2.15. Oxygen sensing setup

The oxygen measurement system Oxy-4 SMA (G3) meter was connected to the support jig via polymer optical fiber, which transfers the excitation light to the sensor embedded within the microchip. The sensor's response was recorded and analysed using the PreSens Measurement Studio 2 software.

Oxygen microsensors were calibrated using a two-point conventional calibration method. The first calibration point (0) was established in oxygen-free water, prepared with 80 mM sodium sulphite and 0.25 mM cobalt nitrate. The second calibration point (21) corresponded to air-saturated water, ensuring accurate oxygen concentration measurements.

The variation of oxygen content between the two built-in sensors was assessed during stop flow electroporation experiments. The oxygen levels were recorded before and immediately after PEF treatment, which involved different electric field strengths and 16 pulses. Measurements were conducted simultaneously with both sensors, and the results were expressed as the difference in oxygen concentration ($\Delta\%$) between sensor 2 (post-PEF-treatment) and sensor 1 (pre-PEF-treatment).

2.2.16. pH measurement setup

The developed pH sensor module incorporates a photodiode optical glass filter FGL515, 515 nm long-pass, and a white LED (LEDWE-15, forward current 25 mA, power 13.0 mW [205]). The pH measurement system was developed by Martynas Šapurov [206]. The sensor system records measurement data via RealTerm software, utilizing a 10-bit analog-to-digital converter for signal processing. To ensure high-quality measurement, a current-to-voltage converter with a floating reference, based on the operational amplifier (opamp), is employed. Additionally, a second-stage amplifier, designed as a non-inverting amplifier with variable gain, is incorporated to enhance the magnitude of the offset signal (**Figure 19**). The floating reference enables the extraction of precise measurement data by eliminating unnecessary DC components.

The pH sensor consists of a white LED (D1) and a photodiode (S1) current produced by the photodiode depends on pH measurements. An opamp (OP1) based current-to-voltage converter is employed in order to produce a voltage signal of the desired amplitude range. The floating reference is connected to the circuit employing opamp OP3 buffer for impedance alignment. Reference is adjusted according to the environmental ambient exposure during. The second stage opamp OP2-based amplifier, is dedicated to extracting essential measurements, discarding ambient exposure.

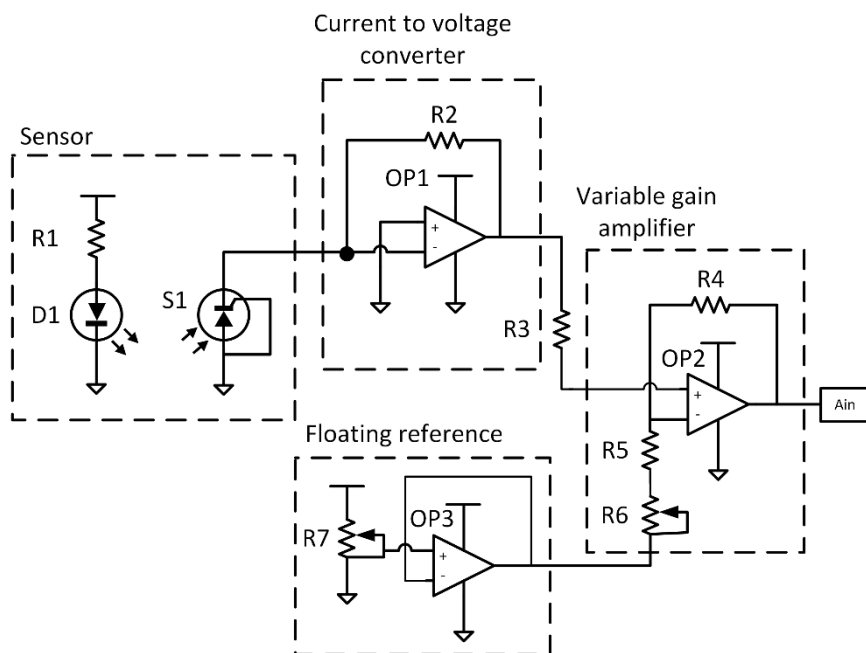


Figure 19. Circuit diagram of pH measurement consists of sensor LED D1 with current limiting resistor R1, and photodiode S1, current to voltage converter (opamp OP1 and feedback resistor R2), floating reference (potentiometer R7 and opamp OP3 as a buffer), variable gain amplifier (noninverting opamp OP2, feedback resistor R4, gain resistors R5, R6 and input resistor R3), treated reading is passed to an analog input Ain [206].



Figure 20. Visual representation of the colour variation in phenol red-containing cell culture medium corresponding to different pH levels.

The optical pH-meter operates on the principle of the colour change of phenol red (**Figure 20**). The pH was calibrated using RPMI medium containing sodium bicarbonate and HEPES, spanning four pH values ranging from 6.0 to 8.0 (**Figure 21**). The pH of the cell suspension was measured during stop flow electroporation experiments, conducted at electric field strengths of 0, 1.8, and 2.4 kV/cm with 16 pulses. The pH values were calculated using the calibration curve.

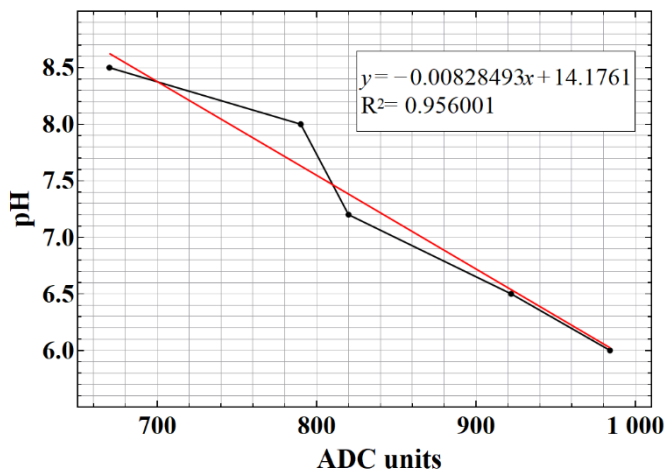


Figure 21. pH calibration curve.

2.2.17. TEER measurement.

The LCR-6000 meter was connected to two adjacent electrodes positioned in a single plane and utilized for transendotelial electrical resistance (TEER) measurement during stop flow electroporation experiments.

2.2.18. Statistical analysis

All data are presented as the mean \pm standard deviation (SD). One-way analysis of variance (ANOVA) was used for multifactorial comparisons in this study. A P value < 0.05 was considered statistically significant. All experiments were conducted with independent replicates of $n \geq 3$ to ensure reproducibility and statistical reliability.

3. RESULTS

This chapter consists of three sections, each contributing to the appropriate defensive statement. The first section focuses on biocompatibility studies of bioceramic alumina, evaluating its suitability for biomedical applications. The second section examines the properties of polycarbonate as a biomaterial, specifically its potential for enhancing cell adhesion. Finally, the third section explores the integration of PC into a microfluidic system, a core component of MPS, evaluating its performance and suitability for PEF treatment and real-time monitoring of the microenvironment.

3.1. BIOCOMPATIBILITY STUDIES OF BIOCERAMIC ALUMINA COATINGS ON AL ALLOY 6082

This chapter presents the research on bioceramic biomaterial alumina Al_2O_3 , a promising candidate for orthopedic joint prostheses due to its exceptional compressive strength and chemically inert properties [16]. Traditionally, alumina implants are produced from powder through multistep processes, including mechanical grinding, pressing, sintering, and extrusion at high temperatures and pressures [25]. While this method yields high-performance bioceramics, it faces notable limitations: alumina's brittleness, susceptibility to impurities, and compositional variation can hinder the fabrication of complex shapes and large implants. Moreover, the manufacturing process is time-consuming, costly, and constrained by machining challenges due to alumina's high hardness.

To address this challenge, this study explores an alternative approach for utilizing bioceramic alumina for implantology through anodization of Al alloy substrates. This approach enables the formation of porous Al_2O_3 layers directly on the Al alloy surface and simplifies implant preparation. Two distinct types of anodized Al alloy 6082 were evaluated to determine their potential as biomaterials for biomedical applications. The evaluation encompasses mechanical, chemical, and biocompatibility properties, with particular attention to parameters critical for biocompatibility and functional performance.

It should be emphasized that the use of Al in biomedical research often raises concerns due to its reputation for cytotoxicity and poor biocompatibility, particularly in its pure form. These concerns stem from uncontrolled ion release and surface reactivity, which can adversely impact surrounding tissues. However, it is essential to recognize that metallic alloys differ significantly from their pure elemental counterparts, as the presence of alloying elements alters their structural and chemical behaviour. Likewise, Al alloy 6082 used to prepare the specimens with anodization technique, consists of 96.52 wt% Al, 2.28 wt% Mg, 0.53 wt%

Si, 0.36 wt% Fe, and 0.31 wt% Mn. These alloying elements in Al alloy 6082 contribute to its enhanced mechanical properties and its corrosion resistance: Mg and Si improve the mechanical strength, Si improves corrosion resistance by reducing microcracks; Fe increases hardness by forming brittle intermediates, while Mn refines these phases and stabilizes the microstructure [207].

Although pure Al is considered unsuitable for biocompatibility, Al alloy 6082 may not share this limitation. In this study, the untreated alloy was not treated as a negative control, but instead served as a reference point to assess whether anodization enhances its surface and functional properties. This distinction is crucial, as the original alloy exhibited favourable performance across several tests.

To evaluate the qualification of the anodized specimens as biomaterials, medical-grade Ti alloy was used as a reference material. Ti alloys are widely regarded as the gold standard in implantology due to their excellent biocompatibility, corrosion resistance, and mechanical performance. The comparison with Ti alloy provides a meaningful context for interpreting the performance of specimens in biomedical applications.

3.1.1. Structural characterization of bioceramic coatings

The original Al alloy 6082 was selected for this study owing to its relatively high strength and corrosion resistance [208]. To modify its surface properties, Al alloy 6082 was anodized using two different electrolytes to produce porous Al_2O_3 coatings. Two distinct anodized coatings were obtained using sulfuric acid and phosphoric acid, designated $\text{Al}_2\text{O}_3^{\text{S}}$ and $\text{Al}_2\text{O}_3^{\text{P}}$, respectively. The electrolyte composition and anodizing conditions are summarized in **Table 4**.

Table 4. Electrolyte composition and anodizing conditions of Al alloy 6082.

Specimen	Electrolyte composition	Time	Temperature	Current density/voltage
$\text{Al}_2\text{O}_3^{\text{S}}$	18% H_2SO_4 2% oxalic acid 0.4% Al^{3+}	70 min	15°C	200 A/m ² (~20 V)
$\text{Al}_2\text{O}_3^{\text{P}}$	4% H_3PO_4	150 min	15°C	150 V

Table 5. Characteristics of bioceramic alumina coatings and corresponding specimens produced by anodizing Al alloy in different electrolytes.

Specimen	Coating thickness, μm	Pore diameter, nm	Pore density, pores/ μm^2	Interpore distance, nm	Porosity, %
$\text{Al}_2\text{O}_3^{\text{S}}$	58.4 \pm 2.3	13.7 \pm 0.1	912.0 \pm 83.8	30.9 \pm 4.4	13.5 \pm 1.4
$\text{Al}_2\text{O}_3^{\text{P}}$	8.7 \pm 1.1	177.2 \pm 15.5	19.7 \pm 4.0	284.3 \pm 29	47.6 \pm 2.4
Mechanical properties					
	Surface roughness, μm	Mechanical hardness			
		Indentation, GPa	Vickers, HV		
$\text{Al}_2\text{O}_3^{\text{S}}$	1.5 \pm 0.2	4.6 \pm 0.5	279 \pm 39		
$\text{Al}_2\text{O}_3^{\text{P}}$	1.5 \pm 0.1	1.0 \pm 0.5	115 \pm 12		
Al alloy	1.3 \pm 0.1	1.5 \pm 0.2	139 \pm 10		
Ti alloy	1.2 \pm 0.1	nd	245 \pm 20		

SEM analysis revealed notable differences in the surface morphology of anodized alloys. The $\text{Al}_2\text{O}_3^{\text{S}}$ coatings were relatively thick (\sim 60 nm) and featured narrow nanopores ($<$ 20 nm), while $\text{Al}_2\text{O}_3^{\text{P}}$ coatings were thinner (\sim 10 nm) with significantly larger micropores (\sim 200 nm). Surface porosity was approximately 3.5 times higher in $\text{Al}_2\text{O}_3^{\text{P}}$ (**Table 5, Figure 22**). Notably, the smaller pores may be more favourable for cell adhesion; therefore, it is likely that nanoporous $\text{Al}_2\text{O}_3^{\text{S}}$ coatings would exhibit enhanced cell adhesion performance.

Surface roughness is an important feature influencing osseointegration. Macro-roughness contributes to mechanical stability, while micro- and nanoscale roughness enhances biological response, such as cell adhesion, proliferation, and osteogenic gene expression [209]. In this study, the Ra values of the original Al alloy were 1.28 \pm 0.08 μm . The anodization led to a slight increase in surface roughness, with $\text{Al}_2\text{O}_3^{\text{S}}$ and $\text{Al}_2\text{O}_3^{\text{P}}$ coatings exhibiting Ra values of 1.45 \pm 0.23 μm and 1.49 \pm 0.14 μm . This increased roughness may support enhanced cell adhesion and integration with surrounding tissues.

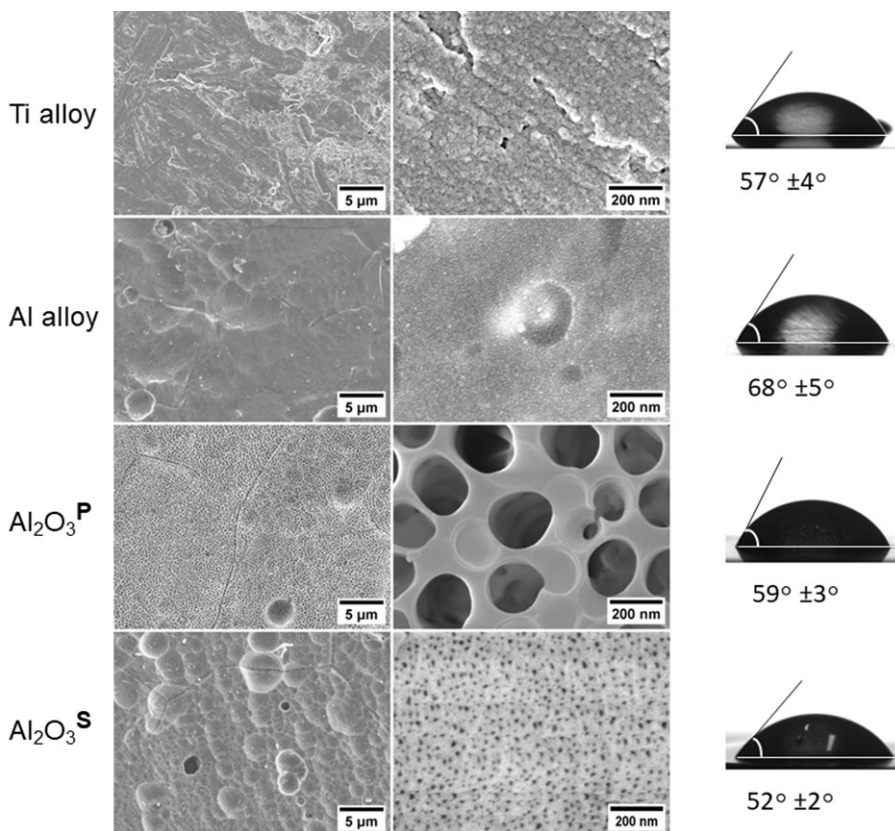


Figure 22. SEM topography (left) of the tested specimens under low and high magnifications and their water droplet contact angles (right).

Mechanical hardness is a critical parameter for load-bearing implants, as higher hardness improves wear resistance and contributes to long-term stability and biocompatibility by minimizing surface degradation. The hardness values of anodized Al_2O_3 coatings provide insight into their potential for biomedical use, particularly when compared to established materials such as Ti alloys. The $\text{Al}_2\text{O}_3^{\text{S}}$ specimen exhibited the highest mechanical hardness, with values of 4.6 ± 0.5 GPa and 279 ± 39 HV, indicating a robust surface comparable to that of Ti alloy (245 ± 20 HV). In contrast, $\text{Al}_2\text{O}_3^{\text{P}}$ coatings exhibited significantly lower hardness - 1.0 ± 0.5 GPa and 115 ± 12 HV, similar to the original Al alloy (1.5 ± 0.2 GPa and 139 ± 10 HV). These data demonstrate that anodization in sulfuric acid not only enhances surface hardness but also yields mechanical properties approaching those of Ti alloy. This reinforces its potential for biomedical applications. Conversely, phosphoric acid anodization does not improve mechanical performance over the untreated Al alloy.

3.1.2. Surface wettability

Surface wettability is a key parameter in evaluating the biological performance of biomaterials, particularly in relation to protein adsorption, cell adhesion, and tissue integration. The wettability reflects how a liquid interacts with a solid surface and is influenced by surface chemistry and surface topography, both of which correlate with biological interaction [111]. Moderate hydrophilicity (contact angle between 50–80°) is associated with enhanced cell growth and improved biocompatibility, as noted in previous studies [111], [112], [210].

The wettability was assessed by measuring the contact angle between a liquid droplet and the surface. All tested specimens exhibited moderately hydrophilic properties with a water droplet contact angle below 90° (**Figure 22**). The untreated Al alloy demonstrated the lowest hydrophilicity, with a contact angle of 68°±5°. The anodized samples exhibited variable wetting behaviour, initially recording higher values, which subsequently decreased and stabilized within approximately 60 seconds: from 75°±8° to 59°±3° for the porous Al₂O₃^P, and from 60°±9° to 52°±2° for the nanoporous Al₂O₃^S. The reduction in contact angles is likely attributed to the porous nature of the Al₂O₃ coating. Meanwhile, the Ti alloy exhibited a contact angle of 57°±4°, similar to anodized specimens.

All tested surfaces demonstrated moderate hydrophilicity, which supports cell growth and adhesion.

3.1.3. Ion release and its toxicity

Biomaterials implanted in the body are subject to a hostile corrosive environment comprising various body fluids, including blood, water, sodium, chlorine, plasma, amino acids, and proteins. These interactions can lead to ion release from the biomaterial, degradation, and corrosion of the biomaterial [211]. SBF is commonly used to replicate physiological conditions, providing a controlled assessment of implant behaviour in a real biological environment. This method provides insight into surface oxidation, the integrity of the passive film, and the possible biological effects of the released ions [200].

Highly porous and rough surfaces can influence the release of metal ions, particularly in materials that are not chemically pure. To evaluate the stability and biocompatibility of the specimens, they were immersed in SBF for 28 days to monitor ion release, corrosion resistance, and surface changes. This duration aligns with established *in vitro* protocols for accelerated corrosion evaluation, and is recognized as sufficient for simulating long-term physiological exposure and assessing degradation behaviour of biomaterials under controlled laboratory

conditions. To ensure the experiment closely simulates *in vivo* degradation behaviour, the pH of SBF should remain within a physiological range of ± 7.4 , as fluctuations can significantly influence the degradation of these specimens [212]. For this reason, the pH of the SBF was continuously monitored throughout the entire immersion process.

The starting pH of SBF was 7.4 at 36.5°C. After three days, a slight increase in pH was observed, although it remained below 7.50 (**Figure 23**) – a level that does not interfere with physiological conditions [213]. Significant changes were observed only by day 28, when the pH of plain SBF and $\text{Al}_2\text{O}_3^{\text{S}}$ decreased to 7.29. By the end of the immersion experiment (day 28), the SBF buffer was nearing expiration, which may account for the anticipated pH shift [200]. Additionally, the precipitation began on day 7 and progressively increased throughout the immersion period, potentially contributing to the observed pH changes. Taking these factors into account, the pH monitoring data confirmed the accuracy of the immersion test, with questionable results noted for $\text{Al}_2\text{O}_3^{\text{S}}$ only on day 28.

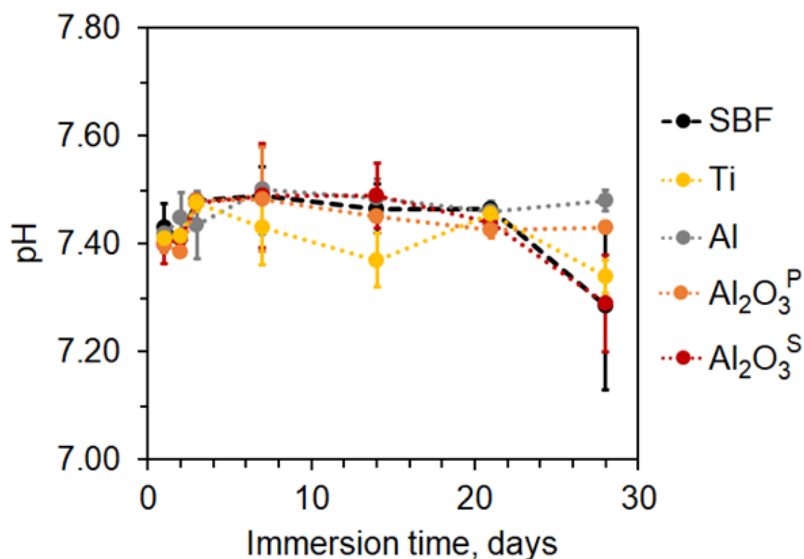


Figure 23. pH of SBF during the immersion of the specimens.

When studying biomaterials, especially those implanted into the human body, it is important to analyse the release of specific ions - Al, Fe, Mg, Mn, Si, sulphur (S) and phosphorus (P) – to assess the material's safety, stability and biological activity. The following section presents the impact of each ion on the human body, as well as the results of ion release from the tested samples into the surrounding environment.

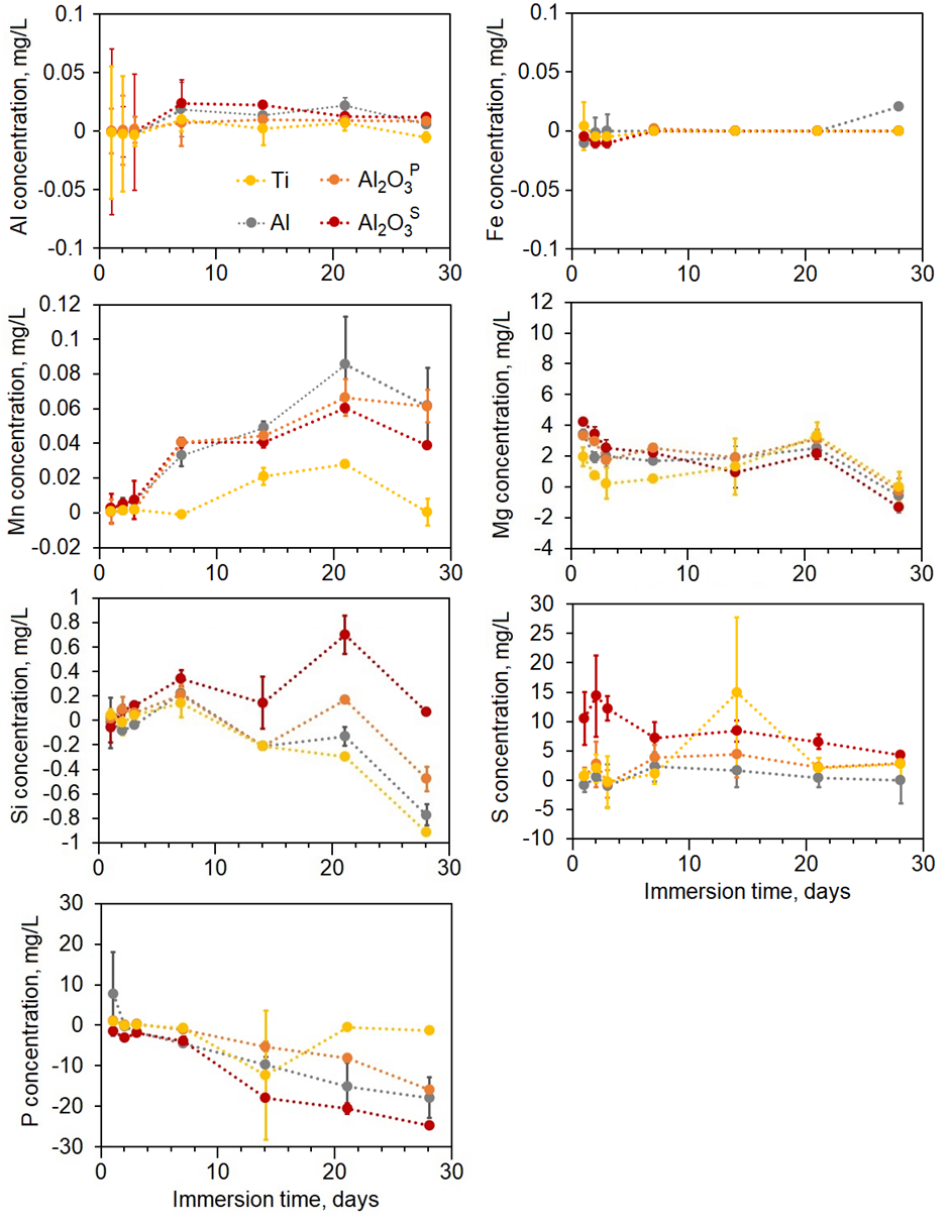


Figure 24. Total ion release from tested specimens after 1 to 28 days of immersion in SBF, as determined by ICP-OES.

Al ions are known to be toxic at high concentrations, potentially leading to local and systemic toxicity, inflammation, bone erosion, and implant rejection due to migration to surrounding tissues and organs [214], [215]. To prevent adverse health effects, the blood serum concentration of Al should not exceed

30 µg/L for Al alloy [215]. However, the estimated daily intake of Al is much higher, ranging between 0.10–0.12 mg Al/kg/day for adults [216]. Immersion tests conducted over 28 days in SBF revealed no significant release of Al ions from tested alloys and coatings, suggesting the effectiveness of surface passivation in minimizing ion release (**Figure 24**).

Iron is one of the essential elements that regulates oxygen and electron transport, DNA synthesis, enzymatic reactions, and other physiological processes. However, the excessive Fe ions can contribute to lipid peroxidation, cell damage, and diseases such as liver cancer, atherosclerosis, and haematological diseases [217]. The normal Fe concentration in blood serum ranges from 0.6–1.8 mg/L, while concentrations above 5 mg/L are considered toxic [215]. Experimental results showed no detectable release of Fe ions from any of the tested specimens immersed in SBF.

Manganese poses potential neurotoxicity risks due to its accumulation in the brain and other tissues and organs upon excessive exposure [218]. The normal Mn concentration in human tissues is approximately 1 mg/kg, while in blood serum, it ranges from 4 to 15 µg/L [215]. Results showed a gradual release of Mn ions in SBF, though average experimental values did not exceed 0.1 mg/L. The highest Mn ion release was detected with the Al alloy, reaching up to 0.08 ± 0.02 mg/L on the 21st day. Porous Al₂O₃ coatings released lower quantities, up 0.06 ± 0.001 mg/L for Al₂O₃^S and 0.066 ± 0.01 mg/L for Al₂O₃^P. Mn release from Ti alloy was the lowest – 0.03 mg/L.

The release of non-toxic Mg ions remained relatively stable across all specimens, with the average concentration mostly below 4 mg/L. Since Mg plays a vital physiological role, its release does not pose a risk to the biological environment.

Silicon is an essential trace element, playing a critical role in bone formation, osteogenesis, and osseointegration at the bone-to-implant interface [219], [220]. During the immersion period, Si ion release exhibited a decreasing trend in most of the tested samples. While Al₂O₃^S coating showed slightly higher Si ion dissolution, the peak remained below 1 mg/L, which is far lower than the optimal range (30 to 52 mg/L) required for enhancing cellular response [221].

Phosphates are essential for skeletal biomineralization, membrane integrity, and homeostasis [222]. During the anodization process, significant amounts of phosphates and sulphates become incorporated into Al₂O₃ coatings, affecting their long-term stability. In this study, the average sulfur and phosphorus concentrations within the coating were 3.90 at% and 1.00 at%, respectively. Immersion tests revealed that S and P concentrations steadily decreased over time due to precipitate formation, particularly in Al alloys and Al₂O₃ coatings. By day 7, visible precipitate formation indicated active chemical interactions between

phosphates and the Al alloy, leading to surface changes in SBF. Over the 28-day immersion period, the decline in P concentration was more pronounced due to AlPO_4 formation, which has much lower solubility than $\text{Al}_2(\text{SO}_4)_3$ salt. Additionally, sulfate anion release was most evident for $\text{Al}_2\text{O}_3^{\text{S}}$ coatings, particularly in the early immersion stages, suggesting its potential role in modifying local acidity [223].

The data revealed limited or negligible release of potential toxic ions from the anodized Al alloys, indicating good chemical stability and effective surface passivation.

3.1.4. Electrochemical evaluation of corrosion resistance in Al alloy and Al_2O_3 coatings

The electrochemical corrosion behavior of Al alloy and both Al_2O_3 coatings was evaluated using electrochemical impedance spectroscopy (EIS) and potentiodynamic polarization tests. Immersion in SBF at 37°C was conducted over 28 days. Nyquist plots revealed distinct differences in electrochemical behavior. **Figure 25** illustrates the evolution of Tafel polarization curves and Nyquist plots for each specimen over the 28-day immersion period.

1) **Al alloy** initially displays a wider semicircle, indicating strong impedance and the likely presence of a passive film. However, by day 28, the semicircle shrinks drastically, reflecting a significant drop in impedance. This change indicates deterioration of the surface film, increased exposure to electrolyte, and reduced corrosion resistance over time.

2) **$\text{Al}_2\text{O}_3^{\text{P}}$ coating** begins with a moderately sized semicircle, indicating partial protection by the porous structure. As immersion progresses, the semicircle contracts considerably, implying that the barrier effect weakens.

3) **$\text{Al}_2\text{O}_3^{\text{S}}$ coating** demonstrates a consistently large semicircle that expands further with time. This trend highlights the coating's exceptional barrier performance and supports excellent long-term corrosion resistance.

Across all specimens, reduced Z_{re} values at early time points (1 and 7 days) reflected damage to surface oxides and increased ion diffusion. However, impedance values increased after 21 days, indicating the development of protective layers composed of insoluble corrosion products.

Key electrochemical parameters, including corrosion potential (E_{corr}), corrosion current density (j_{corr}), polarization resistance (R_p), and corrosion rates, are summarized in **Table 6**. Higher E_{corr} and lower j_{corr} values correlate with greater corrosion resistance. The R_p value is defined from the slope of the voltametric curve at open-circuit potential. This value is directly correlated with the corrosion rate: a higher R_p value indicates better corrosion resistance.

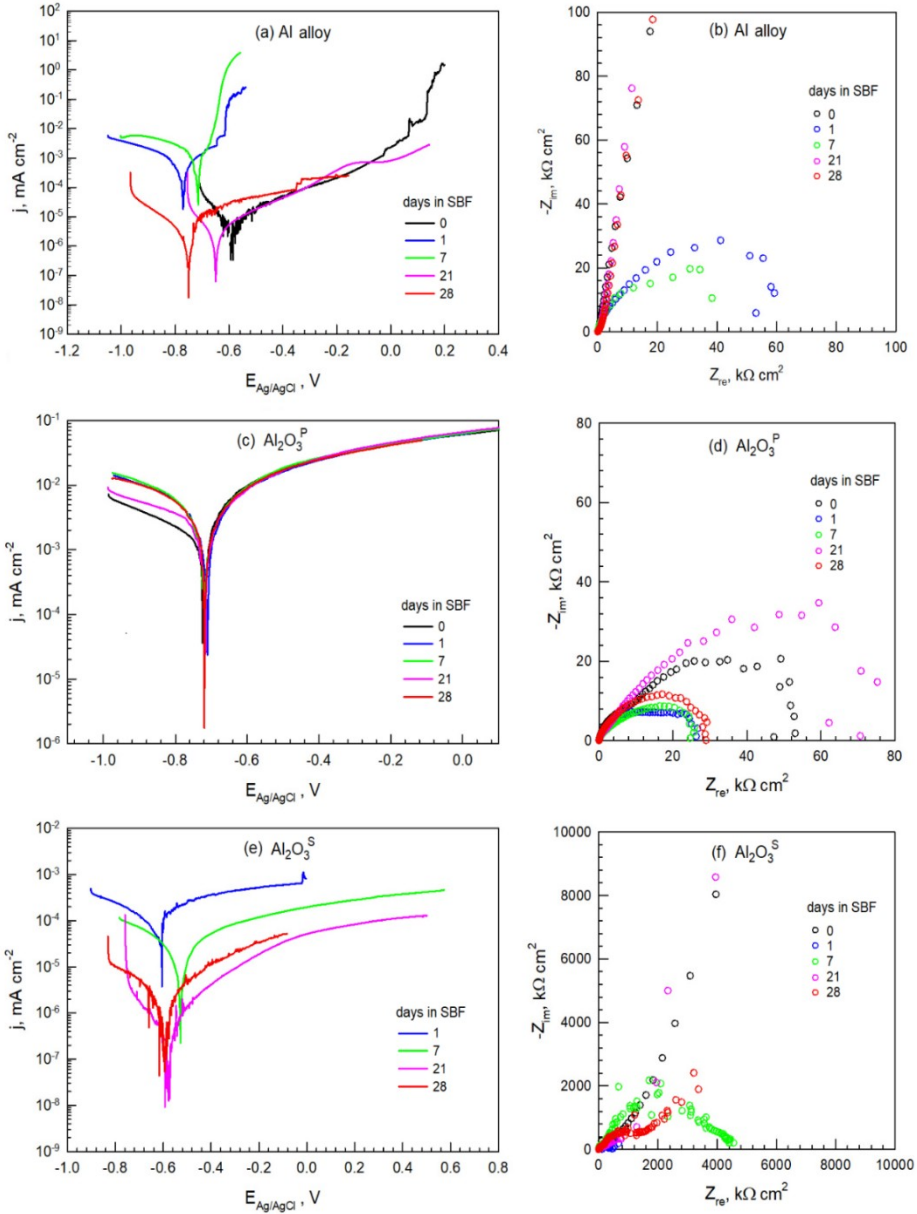


Figure 25. Potentiodynamic polarisation (Tafel) curves and Nyquist plots (right) of EIS spectra for (a, b) Al alloy, (c, d) $\text{Al}_2\text{O}_3^{\text{P}}$, and (e, f) $\text{Al}_2\text{O}_3^{\text{S}}$ before and after immersion in SBF for 1 to 28 days.

Table 6. Summary of electrochemical corrosion parameters of Al alloy and Al₂O₃ coatings after immersion in SBF.

Specimen	Days in SBF	E_{corr} , V	j_{corr} , $\mu\text{A cm}^{-2}$	R_p , $\text{M}\Omega \text{ cm}^2$	Corrosion rate, mm/year
Al alloy	0	-0.593	0.0027	10.50	14.6×10^{-6}
	1	-0.769	0.2820	0.15	1.5×10^{-3}
	7	-0.713	0.4260	0.05	2.3×10^{-3}
	21	-0.648	0.0010	24.70	5.3×10^{-6}
	28	-0.752	0.0012	17.30	6.8×10^{-6}
Al ₂ O ₃ ^P	0	-0.704	1.2200	0.05	6.7×10^{-3}
	1	-0.711	2.2500	0.04	24.6×10^{-3}
	7	-0.719	2.1700	0.04	11.8×10^{-3}
	21	-0.718	1.3100	0.05	7.2×10^{-3}
	28	-0.719	1.4000	0.04	7.6×10^{-3}
	0	-0.620	0.056	1.44	290×10^{-6}
Al ₂ O ₃ ^S	1	-0.605	0.0570	1.40	285×10^{-6}
	7	-0.528	0.0010	6.80	76.5×10^{-6}
	21	-0.577	0.0003	177.00	1.4×10^{-6}
	28	-0.594	0.0009	55.50	5.4×10^{-6}

The results demonstrated:

1) **Al alloy** initially exhibited high corrosion resistance due to its native protective oxide layer. However, exposure to Cl⁻ ions in SBF disrupted this layer after 1 day, resulting in a sharp increase in corrosion rate by day 7. After 21-28 days, surface re-passivation due to salt deposition restored its protective capabilities, reducing the corrosion rate to 6.8×10^{-6} mm/year.

2) **Al₂O₃^P coating** exhibited significantly higher corrosion rates throughout the immersion period (up to 6.7×10^{-3} mm/year at day 1), attributed to their high surface reactivity and porous morphology. Although these coatings promoted bioactivity through hydroxyapatite formation, their electrochemical performance indicated limited corrosion resistance.

3) **Al₂O₃^S coating** provided the most effective protection. Their nanoporous architecture, formed via anodization using H₂SO₄ electrolyte, yielded exceptionally high R_p values and corrosion rates up to 50 times lower than those of the Al alloy. Their performance also exceeded that of commercially pure titanium (CP-Ti), a widely used biomedical alloy.

4) **Comparative data** show that the CP-Ti alloy had an initial corrosion rate of 3.54×10^{-2} mm/year [224] compared to 1.46×10^{-5} mm/year for the Al alloy and 6.7×10^{-3} mm/year for the Al₂O₃^P under similar testing conditions. Other scientists

reported a lower corrosion rate of 7×10^{-4} mm/year for etched CP-Ti [225], these values still did not surpass the performance of $\text{Al}_2\text{O}_3^{\text{S}}$ coatings.

The combined EIS and potentiodynamic data confirm that $\text{Al}_2\text{O}_3^{\text{S}}$ coating offers exceptional long-term corrosion resistance in SBF, far surpassing both Al alloy and $\text{Al}_2\text{O}_3^{\text{P}}$. $\text{Al}_2\text{O}_3^{\text{S}}$ performance not only exceeds that of CP-Ti [224], [226], but also positions $\text{Al}_2\text{O}_3^{\text{S}}$ as a promising candidate for biomedical surface protection and implant applications.

3.1.5.Characterization of bioceramic coatings after SBF immersion

Bioactivity refers to the ability of a material to interact with the biological environment, facilitating mineralization and tissue integration. A key indicator of bioactivity in biomaterials is the formation of hydroxycarbonate apatite (HCAp) - a mineral, structurally similar to hydroxyapatite ($\text{Ca}_{10}(\text{PO}_4)_6(\text{OH})_2$), which is naturally found in human bones and teeth. The presence of HCAp after SBF immersion suggests enhanced biocompatibility, improving the potential for osseointegration and implant success [227].

Bone tissue is a complex composite material, composed of organic collagen and inorganic calcium phosphate, primarily in the form of hydroxyapatite. Since surface topography significantly influences mineral deposition, rough and porous surfaces enhance adhesion of deposited minerals, thus ultimately improving osseointegration and the success of implantation [228].

Specimen surfaces were examined after 21 and 28 days of immersion in SBF, revealing notable differences in the morphology and distribution of deposited salts (**Figure 26**):

1) Ti alloy developed large filament-like structures, while Al alloy exhibited smaller pellet-like formations that tended to coalesce over time.

2) $\text{Al}_2\text{O}_3^{\text{P}}$ coatings formed large salt clusters ($>50 \mu\text{m}$) with visible cracks by day 21. However, these clusters exhibited poor adhesion, resulting in their complete removal by day 28.

3) $\text{Al}_2\text{O}_3^{\text{S}}$ coatings, however, displayed no visible salt deposition, suggesting a significant difference in surface chemistry and wettability.

In biomaterial integration, Ca/P ratio is important. A stoichiometric ratio of 1.67 closely resembles natural bone composition, making it the most desirable for bioceramic coatings [228]. However, hydroxyapatites formed from SBF often exhibit a lower Ca/P ratio due to reduced crystallinity [227]. EDS analysis revealed the following CA/P ratios in deposited salts:

1) Ti alloy had the highest ratio (1.00 ± 0.12), while the Al alloy exhibited the lowest ratio (0.33 ± 0.09).

2) Al_2O_3 coatings demonstrated higher Ca/P ratio values than untreated, measured at 0.39 ± 0.10 for $\text{Al}_2\text{O}_3^{\text{P}}$ and 0.62 ± 0.06 for $\text{Al}_2\text{O}_3^{\text{S}}$.

3) Negatively charged phosphate ions, accumulated within the pores of Al_2O_3 coatings, to a greater extent than Ca^{2+} cations, suggesting that Al_2O_3 coatings possess a positively charged surface and a negatively charged interior. This highlights the importance of surface chemistry in mineralization and implant integration

Overall, the apatites with distinct morphology were formed across all tested specimens, with higher Ca/P amounts on Ti and Al_2O_3 coatings compared to the Al alloy. Despite these findings, the Ca/P ratios observed remained lower than those of natural bone, suggesting that additional surface modifications may be necessary to optimise biomaterial performance for enhanced osseointegration.

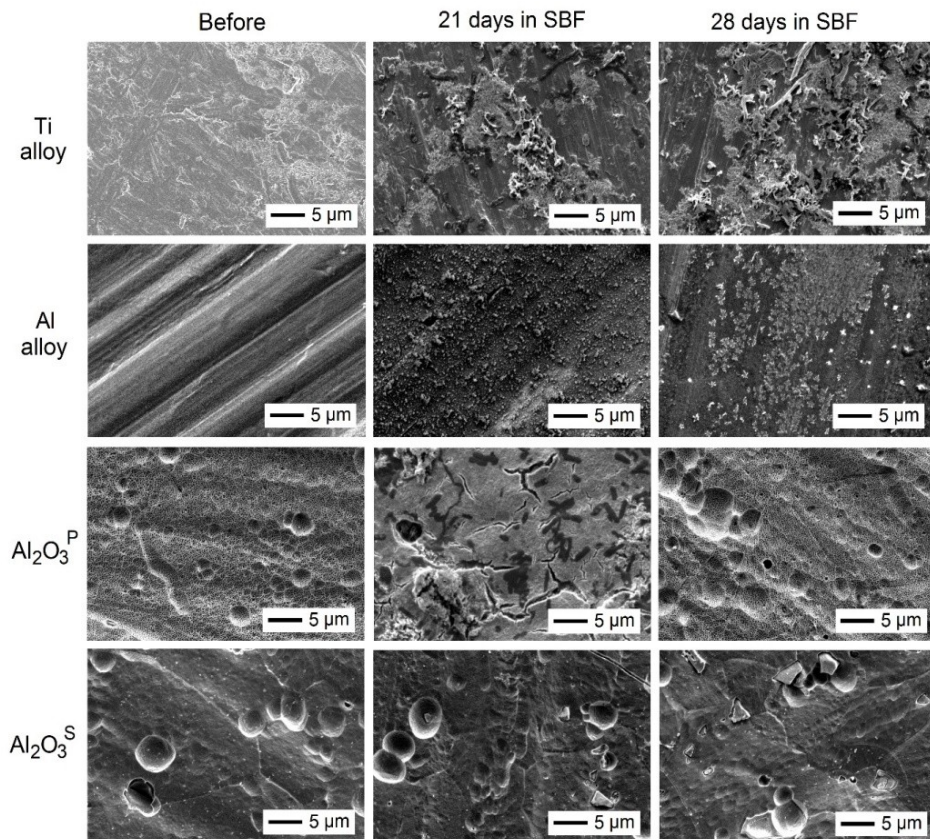


Figure 26. SEM topography of tested specimens.

3.1.6. Biocompatibility test

Biocompatibility is an important parameter in evaluating the suitability of a biomaterial for medical applications. This chapter presents a comprehensive assessment of the biocompatibility of the tested specimens, while analysing two aspects: cell adhesion and morphology, and cytotoxicity. Together, these analyses provide insight into the biomaterial's biological properties and its potential for successful integration with host tissue. Fibroblasts, particularly the L929 mouse fibroblast cell line, are widely used as a standard model due to their essential role in cell adhesion, wound healing, and ECM production. This cell line ensures reproducibility and comparability, making it a reliable comparison of analysis of the biological response of a biomaterial.

Adhesion and morphology of L929 fibroblast cells grown onto the specimen's surfaces were analysed from SEM images (**Figure 27**). Analysis revealed a high abundance of cells on Ti and $\text{Al}_2\text{O}_3^{\text{P}}$ specimens, suggesting favourable conditions for cell attachments. In contrast, Al alloy and $\text{Al}_2\text{O}_3^{\text{S}}$ exhibited lower image contrast, which limited the reliability of quantitative cell evaluation. However, this reduced contrast does not necessarily imply diminished adhesion.

Cell morphology is a reliable indicator of cellular physiology. Under normal conditions, cells display three features: an extended shape, a flattened shape, and prominent filopodial protrusions. The presence of all three characteristics simultaneously suggests intact cytoskeletal organization, robust adhesion and active cellular processes. In contrast, the absence or alteration of any of these morphological features signals physiological disruption [229].

Morphological assessment revealed that cells, cultured on Ti alloy, Al alloy, and $\text{Al}_2\text{O}_3^{\text{S}}$, maintained consistent and distinguished morphologies. Some cells appeared elongated while others displayed flattened morphologies, with visible filopodia extension and ECM expression. These features indicate normal physiological behaviour of those cells, supporting the suitability of $\text{Al}_2\text{SO}_4^{\text{S}}$ coatings for normal cell adhesion.

In contrast, cells on $\text{Al}_2\text{O}_3^{\text{P}}$ surfaces displayed predominantly flattened morphologies. These effects are likely influenced by the surface topography and microporous pore size of the coating [20],[253]. Filopodia were either embedded within surface pores or spread across them, making visualization in SEM images challenging. The predominance of single cell shape suggests impaired physiological processes, which may adversely impact the biomaterial's integration with surrounding tissues and compromise its long-term functionality.

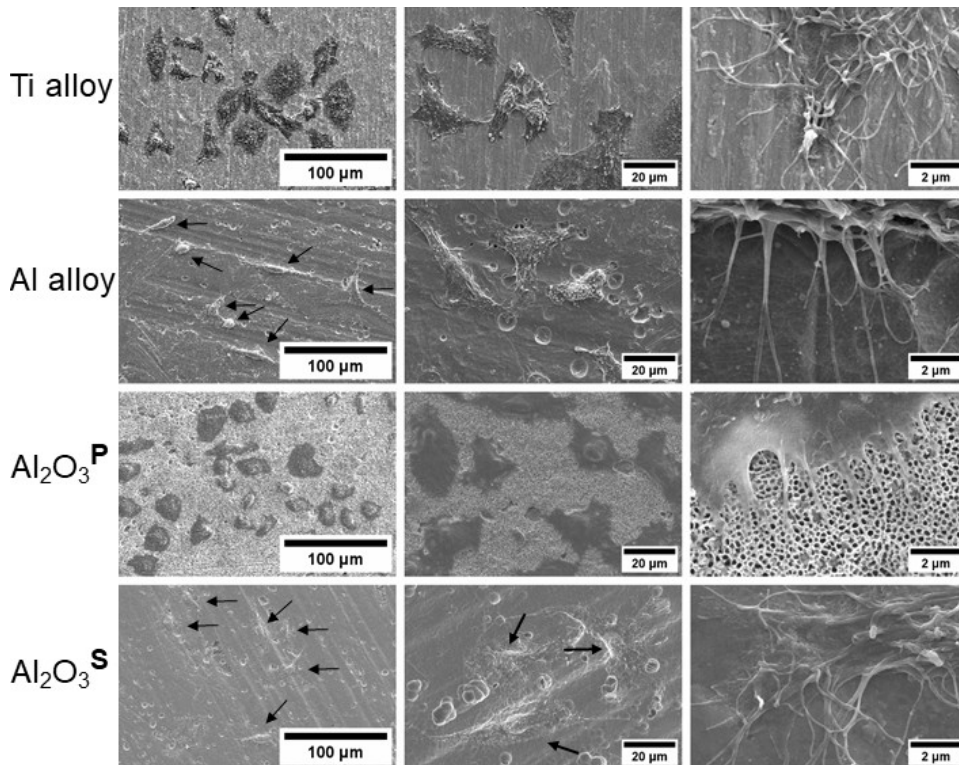


Figure 27. SEM images of L929 cells cultured on Ti alloy, Al alloy, $\text{Al}_2\text{O}_3^{\text{P}}$, and $\text{Al}_2\text{O}_3^{\text{S}}$ samples at various magnifications. Arrows indicate cells with low contrast.

To complement the morphological assessment and gain a more comprehensive understanding of the coatings' biocompatibility, a **cytotoxicity test** was conducted to evaluate the biological impact of alloy-derived extracts on direct cell-surface interactions. Extract-based assays were used for identifying potential leachables that may affect cell viability in the surrounding environment.

The viability of L929 cells was assessed after 24-hour incubation with extracts obtained from each specimen. To analyse attachment, adhesion, and proliferation, L929 cells were collected, suspended in specimen extracts, and seeded. After 24 hours of incubation, the mitochondrial activity of adhered cells was measured to assess cell viability. The relative viability (%) of cells treated with different extracts was:

- Ti alloy - $108.2 \pm 11.0\%$,
- Al alloy - $103.7 \pm 4.3\%$,
- $\text{Al}_2\text{O}_3^{\text{P}}$ - $101.7 \pm 9.0\%$,
- $\text{Al}_2\text{O}_3^{\text{S}}$ - $96.6 \pm 13.3\%$ (**Figure 28a**).

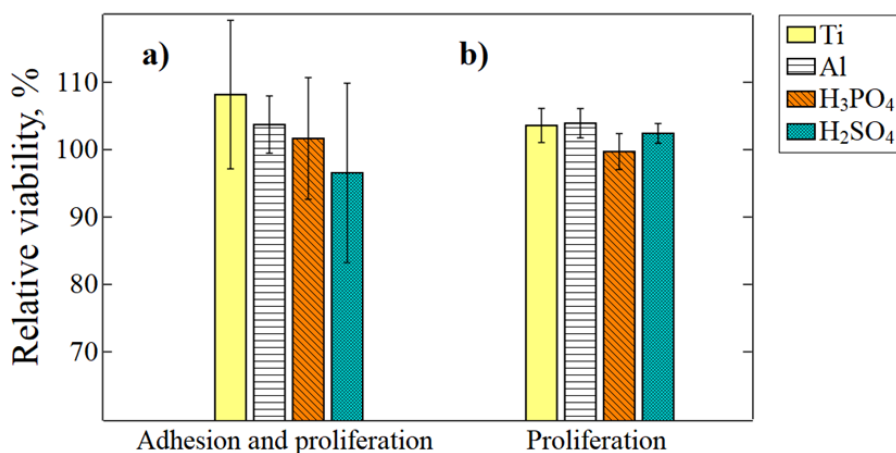


Figure 28. Effect of alloy extracts on the relative viability of L929 cells: (a) overall cell growth, including adhesion and proliferation, and (b) proliferation only. One-way ANOVA analysis revealed no significant differences in overall cell growth ($p=0.61$) or proliferation ($p=0.66$).

To evaluate the impact on cell proliferation (excluding adhesion), L929 cells were first allowed to adhere, after which the growth medium was replaced with specimen extracts. After 24 hours, mitochondrial activity was measured using the XTT assay (**Figure 28 b**). The relative viability (%) of cells treated with different extracts was:

- Ti alloy – $105.5 \pm 2.5\%$,
- Al alloy - $101.4 \pm 2.2\%$,
- $\text{Al}_2\text{O}_3^{\text{P}}$ - $99.4 \pm 2.7\%$,
- $\text{Al}_2\text{O}_3^{\text{S}}$ - $101.5 \pm 1.5\%$ (**Figure 28b**).

No significant differences were detected in overall growth ($p=0.61$) or proliferation ($p=0.66$) across both experimental conditions. The greater variability in the error bars in adhesion tests may be attributed to experimental conditions and instrument sensitivity. These results confirm that all tested specimens are non-cytotoxic, with relative cell viability exceeding 95% after incubation with extracts. Adhesion results demonstrated effective adhesion, with filopodia and ECM expression observed.

In summary, all tested materials supported cell viability and adhesion. While $\text{Al}_2\text{O}_3^{\text{P}}$ coatings exhibited morphological limitations likely due to microporous structure, $\text{Al}_2\text{O}_3^{\text{S}}$ coatings with their nanoporous architecture provided a more favorable environment for cell adhesion and physiological functions.

3.1.7. Discussion on biocompatibility of bioceramic coatings

Biocompatibility is strongly influenced by the surface structure of biomaterials and the release of metal ions, both of which play a crucial role in cell adhesion, viability, and integration. Studies have shown that TiO₂/Al₂O₃-reinforced hydroxyapatite coatings deposited on stainless steel 316L significantly improved cell viability (99.5%), whereas hydroxyapatite coatings on stainless steel and bare stainless steel exhibited reduced viability rates (75% and 51%, respectively) after 72 hours of seeding [231]. This decline is primarily due to high surface cracking and porosity of hydroxyapatite coatings, which expose the underlying stainless steel to SBF, resulting in corrosion and toxic Fe ion release. Similarly, TiO₂/hydroxyapatite nanocomposite with TiO₂ and Ag nanoparticles applied on Ti6Al4V/TiO₂ coatings reported cell viability of 98.8%, attributed to enhanced uniformity, crack-free structure, and suppressed migration of toxic Al and V ions [232]. Furthermore, research demonstrated that Ti6Al4V alloy combined with a 20% ZrO₂ ceramic composite enhanced biocompatibility, increasing cell viability up to 98.25%, while ZrO₂-hydroxyapatite hybrid composite achieved the highest viability (107.53%) [233]. These data underscore the importance of optimizing surface morphology, chemical composition, and structural integrity in biomaterial coatings to enhance cell viability and ensure long-term implant success.

This study examined the biocompatibility of Al alloy 6082 and its porous bioceramic Al₂O₃ coatings, which were obtained through anodization of Al alloy 6082 using two different electrolytes: phosphoric acid and sulfuric acid. The evaluation focused on ion leakage, corrosion resistance, cell growth, and cytotoxicity, with comparable results against medical-grade Ti alloy; the results are summarized in **Table 7**.

The Al₂O₃^S bioceramic coating, anodized in sulfuric acid, exhibited multiple beneficial properties regarding biocompatibility. The Al₂O₃^S coating effectively suppressed Fe and Al ion release, preventing toxicity, inflammation, and implant rejection [215]. Mn ion release remained within safe limits (0.04 mg/L, below the 0.1 mg/L threshold) [215]. Mg and Si ions, essential for biological functions, were released in non-toxic quantities. Moreover, a higher Si ion dissolution supports osteogenesis, cell adhesion, and proliferation, thereby improving osseointegration [219], [220]. The release of sulfates from the Al₂SO₃^S specimen was a concern, as these ions contribute to local acidity within the body [223]. Therefore, additional long-term studies on sulfate migration are recommended to assess its potential impact on biocompatibility and systemic ion levels under prolonged physiological conditions. The corrosion resistance following a 28-day immersion of the specimen in SBF demonstrated that Al₂O₃^S exhibited superior

Table 7. Summary of biomedical-relevant properties of $\text{Al}_2\text{SO}_3^{\text{S}}$, $\text{Al}_2\text{SO}_3^{\text{P}}$, and Ti alloy.

Property	$\text{Al}_2\text{SO}_3^{\text{S}}$ (sulfuric acid)	$\text{Al}_2\text{SO}_3^{\text{P}}$ (phosphoric acid)	Ti alloy (medical grade)
Surface structure	Nanoporous (supports adhesion)	Microporous	Dense
Hardness/durability	High	Low	High
Ion release: Fe and Al	Suppressed	Suppressed	Suppressed
Ion release: Mn	0.04 mg/L (safe)	0.06 mg/L (highest; still safe)	Lowest
Ion release: Si and Mg	Low levels (biologically favourable)	Low levels	None
Hydroxyapatite formation	Minimal	Pronounced	Absent
Corrosion resistance	Excellent	Poor	Excellent
Cell morphology	Flattened and elongated	Flattened, Limited spreading	Flattened and elongated
Cell viability (short-term)	High	High	High
Mechanical integrity	Robust	Reduced	Strong
Biomedical suitability	Promising candidate for implants	Not recommended for implants	Standard clinical material

corrosion resistance, compared to the original Al alloy and $\text{Al}_2\text{O}_3^{\text{P}}$. Among the tested specimens, $\text{Al}_2\text{O}_3^{\text{S}}$ exhibited the highest corrosion resistance, demonstrating a continuous increase in protective oxide formation that effectively suppressed corrosion via stabilization of the passive film. The corrosion rate of $\text{Al}_2\text{O}_3^{\text{S}}$ was either lower or comparable to that of CP-Ti [224],

[226]. This enhanced stability and longevity minimize the release of harmful ions, thereby reinforcing biomaterial integrity over prolonged exposure.

The immersion tests confirmed that alumina coatings significantly influence ion release and corrosion behaviour. $\text{Al}_2\text{O}_3^{\text{S}}$ coatings exhibited enhanced stability, lower ion dissolution, and superior corrosion resistance, making them suitable for biomedical applications requiring durable implant materials. $\text{Al}_2\text{O}_3^{\text{S}}$ retains the lightweight properties of Al alloy while demonstrating mechanical properties comparable to Ti alloy, making it an excellent candidate for implant applications. The nanoporous structure of $\text{Al}_2\text{O}_3^{\text{S}}$ provides a favorable environment for cellular activity, as evidenced by viability assays and fibroblast morphology. Cells exhibited both extended and flattened shapes and expressed filopodia, characteristics of healthy adhesion and intact physiological function. The biocompatibility of $\text{Al}_2\text{O}_3^{\text{S}}$ is underscored by its enhanced stability, hardness, and supportive cellular environment, rendering it highly suitable for implantation.

The second bioceramic coating, $\text{Al}_2\text{O}_3^{\text{P}}$, produced by anodizing Al alloy with phosphoric acid, also demonstrated adequate ion release control, preventing Fe and Al ion release. However, the Mn ion released from $\text{Al}_2\text{O}_3^{\text{P}}$ was the highest among all specimens, though still within the safe limits (0.06 mg/L) [215]. Immersion tests in SBF confirmed the formation of a hydroxyapatite layer on $\text{Al}_2\text{O}_3^{\text{P}}$ coatings. This is a desirable feature in implantology due to its role in promoting bone integration. However, the high corrosion rate observed in this specimen is a significant drawback, as biomaterials require long-term stability to ensure implant durability and functionality. The presence of micropores in $\text{Al}_2\text{O}_3^{\text{P}}$ contributes to both reduced hardness and compromised structural integrity, impacting its long-term stability as a biomaterial. Additionally, the surface features influence cell morphology, leading to a predominantly flattened shape, which may interfere with essential cellular processes, such as spreading and migration [234], [235]. The altered morphology indicates compromised cell physiology and could negatively impact its long-term performance.

In summary, the $\text{Al}_2\text{O}_3^{\text{S}}$ and $\text{Al}_2\text{O}_3^{\text{P}}$ bioceramic coatings demonstrated different properties. $\text{Al}_2\text{O}_3^{\text{P}}$ bioceramic coating, while capable of hydroxyapatite formation and maintaining a safe ion release level, exhibited a higher corrosion rate and reduced mechanical stability, and impaired cell morphology, limiting its suitability for biomedical applications. In contrast, $\text{Al}_2\text{O}_3^{\text{S}}$ exhibited superior corrosion resistance, mechanical integrity, and favourable cellular interactions, positioning it as a promising candidate for long-term implant use. Overall, these findings support the classification of Al alloy 6082, anodized in sulfuric acid electrolyte, as a chemically stable, biocompatible biomaterial.

3.2. OPTIMIZATION OF POLYCARBONATE FOR CELL ADHESION

PC is a second biomaterial analysed in this thesis due to its potential role in microfluidic systems designed for cell culture. Specifically, a track-etched porous PC membrane was considered for integration into a custom-fabricated microchip (see Chapter 3.3), where the membrane serves a dual function: as a substrate for cell adhesion and a porous barrier separating two parallel subchannels. The membrane as a barrier enables molecular exchange between compartments while maintaining spatial separation of cell populations, making the membrane an essential component of the device for an organ-on-a-chip function.

Among various PC forms, track-etched PC membranes are especially suitable for microdevices. However, despite these advantages, PC presents a significant limitation for cell-based applications: its surface is inherently hydrophobic and chemically inert, lacking the functional groups necessary for effective cell adhesion [236], [237]. Thus, the inherent hydrophobicity poses a challenge for applications requiring direct cell-material interaction. Without surface modification, the PC membrane does not provide a biological supportive interface for cell adhesion and growth.

This chapter introduces the strategy for optimizing the track-etched PC membrane to support cell adhesion. A combination of physical, chemical, and biological surface treatments was applied to improve the membranes' wettability and biocompatibility. The experimental work that follows evaluates how these modifications influence surface hydrophilicity and the ability of the membrane to affect surface hydrophilicity and the membrane's ability to support cell adhesion. By comparing untreated, plasma-treated, chemically oxidized, and biologically functionalized membranes, the study aims to identify a robust and reproducible strategy for PC modifications suitable for cell adhesion. For successful operation, the membrane must support stable cell attachment under both static and dynamic culture conditions, necessitating effective surface modification.

3.2.1. Inherent adhesion properties of PC membrane

To enhance the adhesion-supporting properties of track-etched PC membrane, three types of surface modifications were applied and evaluated: physical, chemical, and biological. Physical surface modification was conducted using plasma treatment with oxygen gas only. Therefore, in the following text, the term “plasma” refers specifically to oxygen-based plasma. Chemical modification was carried out using selected reagents, while biological functionalization involved adhesion-promoting molecules. The effectiveness of

each approach was assessed by measuring membrane wettability and endothelial cell adhesion under static culture conditions.

Baseline adhesion was first evaluated using untreated PC membranes either with PBS or FBS. In both cases, minimal cell adhesion was observed, with fewer than 3% of CHO-K1 cells adhering to the membrane surface (**Figure 29** and **Figure 30a**). This result confirms the membrane's inability to support adhesion without active surface modification.

To improve cell adhesion, the PC membrane was coated with PDL, a cost-effective and widely used adhesion factor. It significantly increased the PC membrane's ability to accommodate CHO-K1 cells, increasing adhesion to approximately 24% (**Figure 29** and **Figure 30b**). To further improve the PC membrane's adhesion properties, surface oxidation was applied using plasma, followed by incubation with PDL. This combined plasma and PDL treatment strategy resulted in a drastic improvement in PC membrane-mediated cell adhesions, reaching up to 94% of adherent cells (**Figure 29** and **Figure 30c**). Notably, upon forming a monolayer with the highest adhesion rate (**Figure 30c**), the optical contrast under microscopy decreases, likely due to the loss of structural distinctiveness and changes in light refraction.

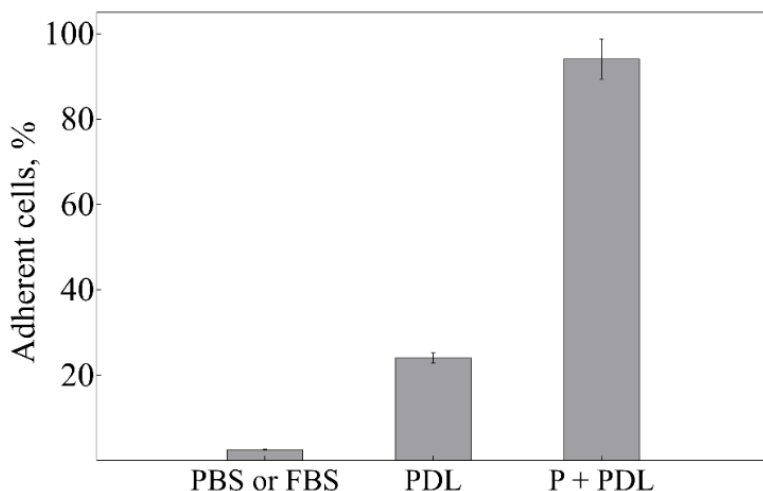


Figure 29. Percentage of CHO-K1 cells adhered to PC membrane under three distinct surface treatment conditions: 1) incubation with PBS or FBS; 2) coating with PDL; 3) plasma treatment (indicated as P) followed by PDL coating.

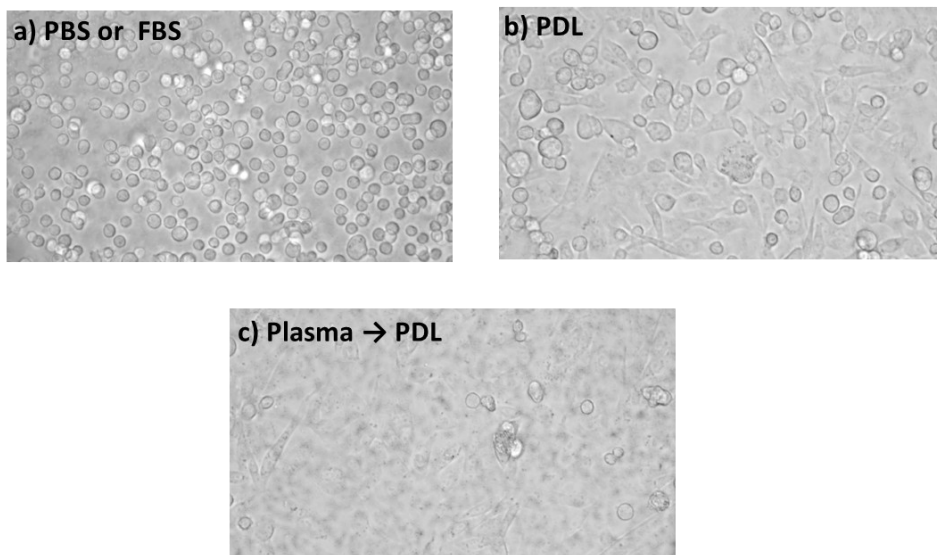


Figure 30. Cell adhesion pattern of CHO-K1 cells to PC membrane under three different surface treatment conditions: a) incubation with PBS or FBS; b) coating with PDL; b) plasma treatment followed by PDL coating.

In parallel, surface wettability of PC membranes was characterized using water contact angle measurements. This parameter directly reflects the material's hydrophilic or hydrophobic character: lower contact angles indicate enhanced hydrophilicity, whereas higher angles correspond to increased hydrophobicity. The untreated membrane exhibited a contact angle of $84 \pm 2^\circ$ (**Figure 31**, none), indicating a hydrophobic surface. Plasma treatment significantly reduced the contact angle to $62 \pm 6^\circ$ (**Figure 31**, P₀), confirming a substantial increase in hydrophilicity (* $p < 0.05$, Tukey HSD post-hoc test following one-way ANOVA). Nevertheless, after 9 days post-treatment, the contact angle increased to $83 \pm 6^\circ$, showing no significant difference from the untreated samples (* $p > 0.05$) (**Figure 31**, P₉). These results suggest surface aging and a reversion to the initial hydrophobic state. Such behaviour underscores the transient nature of plasma-induced oxidation and indicates the necessity of employing alternative oxidation strategies capable of achieving long-term and stable surface modifications.

Together, these data demonstrate that oxidation combined with PDL coating, substantially improves both wettability and cell adhesion on PC membranes. Moreover, the temporary nature of plasma-induced hydrophilicity underscores the importance of optimizing surface chemistry to obtain more stable and long-lasting modifications.

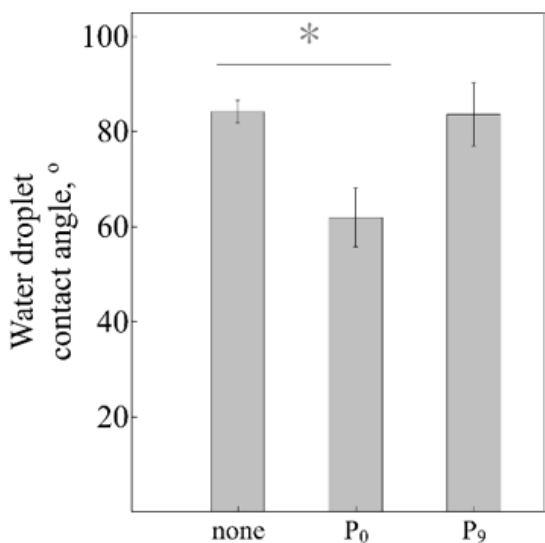


Figure 31. Wettability of untreated and modified PC membranes after plasma and chemical treatments. P₀ – plasma-treated and measured immediately; P₉ – plasma-treated and measured 9 days post-treatment.

3.2.2. Chemical treatment of PC membrane

Given the reversible nature of plasma-induced oxidation and the wettability results obtained in this study, alternative chemical oxidation strategies were explored. Sodium metaperiodate (NaIO₄, 0.117 M), sulfuric acid (10%), and Piranha solution (10%) – all well-established reagents for polymer surface oxidation – were selected to treat the PC membranes. The choice of reagents and their concentrations was guided by the need to maintain compatibility with other microchip components, particularly OSTE and COC, which are sensitive to aggressive chemicals.

NaIO₄ is a crystalline inorganic salt and a strong oxidizing agent widely employed in organic and polymer chemistry for the functionalization of materials [277]. It is primarily used to oxidize materials which have vicinal diols (C(OH) – C(OH)), resulting in cleavage of the C-C bond and producing the aldehyde and ketone functional groups. Although the inherent PC lacks vicinal diols. However, environmental and chemical factors such as UV exposure, acid or base treatment, heat, and mechanical damage may introduce surface rearrangements [238], [239]. Moreover, in the case of track-etched PC membrane, produced through high-energy ion irradiation followed by alkaline etching, the pore structures are chemically altered [240]. After such an impact,

the PC surface could be modified with NaIO_4 and may form oxygen-containing groups such as hydroxyl, aldehyde, and ketone groups.

Sulfuric acid is a strong oxidizing and degrading agent that, at high concentration, can cause complete degradation of various materials, particularly PC [241]. In the present study, a 10% sulfuric acid solution was used, as this concentration does not lead to full or partial degradation of PC or other polymeric components within the microchip. Notably, OSTe, a polymer employed in microchip fabrication, exhibits chemical resistance only up to 10% of sulfuric acid. Therefore, it was assumed that a 10% solution may be sufficient to induce surface modifications on the PC membrane. According to the literature, oxidation of polymers with sulfuric acid results in the formation of sulfonic groups, which gives the hydrophilicity and wettability of the material. In addition, the hydrolysis process may introduce hydroxyl groups on the polymer surface [241].

Piranha solution is also a strong oxidizing agent, which is formed from the H_2SO_4 and H_2O_2 , and is stronger than sulfuric acid alone. The volume ratio of sulfuric acid and hydrogen peroxide typically ranges between 3:1 to 5:1. In the present study, 10% Piranha solution was used for the same reason as with sulfuric acid: sulfuric acid concentration higher than 10% deteriorates other polymeric components of the microchip. When combined, sulfuric acid reacts with hydrogen peroxide to generate peroxymonosulfuric acid (H_2SO_5), also referred to as Caro's acid. The formed Caro acid is unstable and decomposes rapidly, generating hydroxyl radicals and regenerating sulfuric acid. Under these highly oxidative conditions, H_2SO_5 and the resulting hydroxyl radical can modify the PC surface by introducing functional groups such as sulfonic (SO_3H), hydroxyl, or peroxide groups [242], [243], [244]. Consequently, the Piranha solution may enhance the hydrophilicity and wettability of the PC membrane.

PC membranes treated with chemical oxidants (NaIO_4 , H_2SO_4 , and Piranha solution) exhibited moderate changes in water droplet contact angles, which were not significantly different compared to the untreated control. The measured contact angles were $78 \pm 8^\circ$ for NaIO_4 , $75 \pm 1^\circ$ for H_2SO_4 , and $75 \pm 7^\circ$ for Piranha solution (**Figure 32**), none of which demonstrated a significant difference in hydrophilicity compared to unoxidized PC with $84 \pm 2^\circ$ (* $p > 0.05$, Tukey HSD post-hoc test following one-way ANOVA). These results prompt further consideration of whether the chemical oxidation methods can effectively alter surface characteristics relevant to biological applications, including cell adhesion.

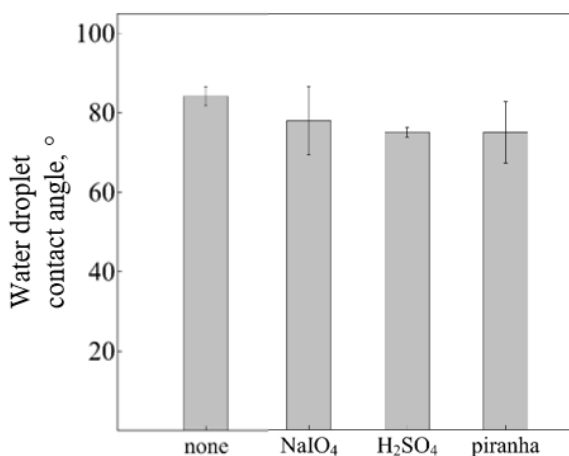


Figure 32. Wettability of untreated and modified PC membranes after chemical treatments.

3.2.3. Cell adhesion on the modified PC membranes

To evaluate the effect of surface modification on cell adhesion, SK-MEL-28 cells were cultured on PC membranes subjected to various oxidative treatments. All modified membranes were coated with PDL before cell seeding to ensure consistent presentation of adhesion-promoting molecules. Quantification of adherent cells following overnight incubation revealed significantly improved adhesion on oxidized membranes compared to untreated controls. Specifically, adhesion rates were 94±3% for oxygen plasma, 95±6% for NaIO₄, 80±9% for H₂SO₄, and 83±13% for piranha solution, while the untreated PC membrane yielded only 24±2% (**Figure 33**). Statistical analysis confirmed that all oxidized conditions resulted in significantly greater adhesion to the control ($p < 0.005$, determined using a one-way ANOVA followed by Tukey's HSD post-hoc test), although no significant differences were observed among the chemically treated groups. Overall, the combination of chemical surface modification of the PC membrane and an additional adhesion factor improved cell adhesion by 4.3-fold with NaIO₄, 3.2-fold with H₂SO₄, and 4.3-fold with piranha solution. These results highlight the effectiveness of oxidation-based surface functionalization in enhancing the cell-adhesive properties of the PC membrane. Similar adhesion trends observed with additional cell lines (CHO-K1 and C6, data not shown) further support the reproducibility of this approach across different cell lines.

In summary, these pilot experiments confirmed the effectiveness of NaIO₄, H₂SO₄, and piranha solution in introducing stable surface modification without compromising the integrity of other microchip materials. While oxygen plasma treatment also facilitated cell adhesion, its reversible nature and rapid surface

aging posed limitations for extended workflow. Chemical treatment offered consistent performance, longer shelf life, and compatibility with preassembled microchip. This strategy simplifies fabrication and enables timely surface activation. By piloting chemical oxidation, the study validated its use as a robust alternative to plasma, expanding the surface functionalisation toolkit for microfluidic systems requiring reliable cell support.

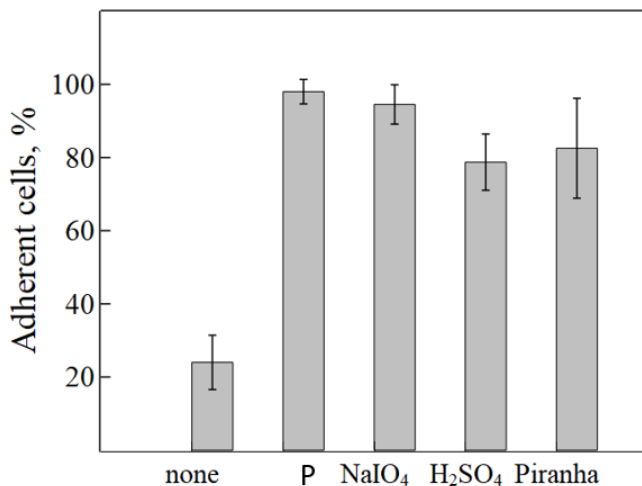


Figure 33. Influence of surface treatment on SK-MEL-28 cell adhesion. PC membranes treated with plasma are denoted as P.

3.2.4. Cell adhesion with different adhesion factors

To investigate the effect of varying adhesion molecules on SK-MEL-28 cell adhesion, an experiment was conducted on a fresh oxygen plasma-oxidized PC membrane using three adhesion factors: PDL, collagen, and fibronectin in various combinations.

The results revealed that all combinations of these adhesion factors, except for fibronectin alone, exhibited more than 90% of cell adhesion to the PC membrane in static culture (**Figure 34**). Fibronectin alone was the least favourable adhesion option, providing 87±8% of adherent cells, which was a statistically significant difference compared to all other adhesion factors ($p < 0.05$, one-way ANOVA followed by Tukey's HSD post-hoc test). To summarize, these results suggest that all three factors and their combinations enhance cell adhesion. Considering the cost and convenience, a simple cell culturing approach with chemically modified PC membranes can be selected in the following order: PDL, collagen, and fibronectin.

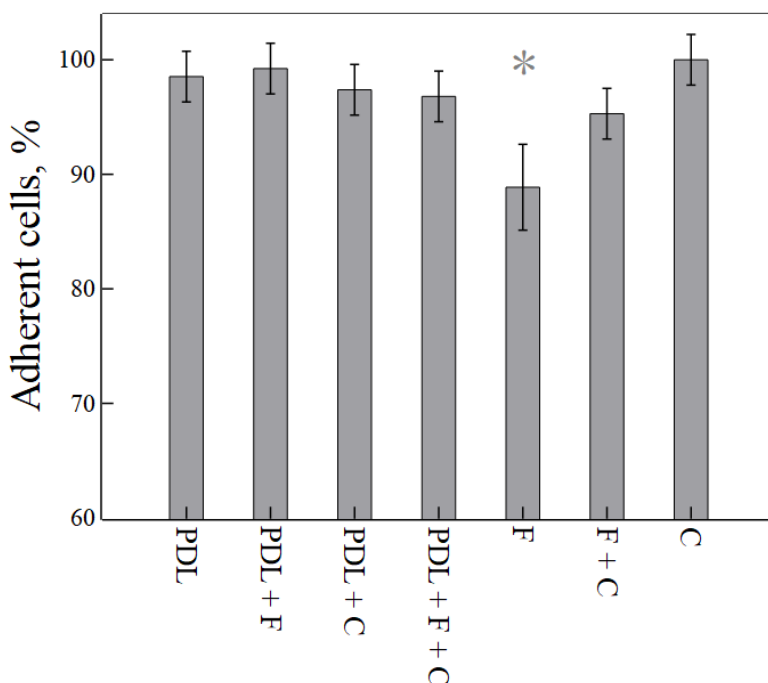


Figure 34. Effect of adhesion-promoting factors on SK-MEL-28 cell adhesion to oxygen plasma-treated PC membrane. Groups included PDL, fibronectin (F), and collagen (C). Significant difference was observed only between F and all other groups (* $p < 0.05$).

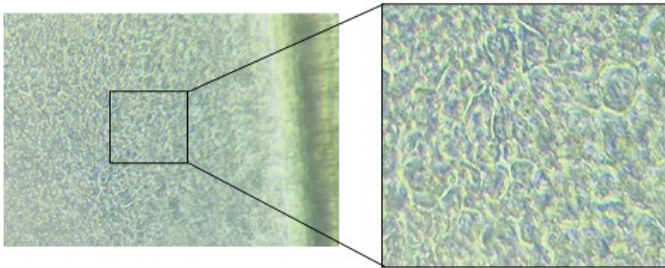
3.2.5. Cell culturing in a microfluidic channel

The previous section demonstrated successful mammalian cell adhesion to oxidized PC membranes under static culture conditions. This initial step confirmed the positive impact of PC oxidation on cell adhesion. To extend this study and better simulate physiological conditions, the adhesion of U2OS cells to oxidized PC membrane under flow culture was analysed next. The microchip with an integrated PC membrane (see Chapter 3.3.1) was used for the experiment.

Shear stress is a key mechanical force experienced by cells in fluid environments, influencing cell adhesion, morphology, and signalling. While the U2OS cell line originates from cancerous cells in bone tissue, its physiological shear stress is not defined. As a reference, physiological shear stress for mesenchymal cells, such as that generated by interstitial flow, can be considered. Interstitial flow refers to the slow movement of fluid through the ECM, specifically through the fluid-filled spaces called interstitial spaces. This flow exerts a low shear stress, typically $\leq 0.1 \text{ dyn/cm}^2$ [245], [246].

To analyse the impact of the PC membrane's oxidation on cell adhesion and culturing underflow, the piranha solution was used as an oxidizing agent, PDL was used as an adhesion molecule, and U2OS cells were used as an object. The cells were injected and allowed to adhere without the flow overnight. The following day, the flow was initiated at a shear stress of 0.08 dyn/cm^2 and was increased gradually by a factor of two every day up to 0.64 dyn/cm^2 . Throughout the two-week experiment, U2OS cells remained intact, forming a progressively denser monolayer while maintaining their adhesion, with the cell monolayer becoming denser (**Figure 35**). With this experiment, it was confirmed that oxidised PC membrane and adhesion molecules, such as PDL, can ensure stable cell adhesion even with the flow supplied.

a) No flow, 0 dyn/cm^2



b) With flow, 0.64 dyn/cm^2

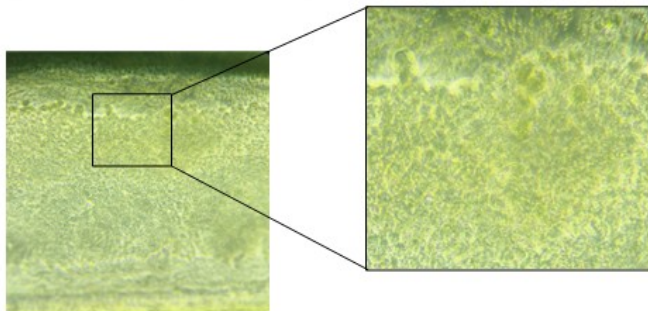


Figure 35. U2OS cell adhesion on the oxidized PC membrane in the microchannel, pretreated with piranha solution and functionalized with PDL. Cell adhesion is shown (a) at the beginning of the experiment under static conditions, and (b) at the end of the experiment under flow conditions.

3.2.6. Discussion on PC surface treatment for improved cell adhesion

The track-etched PC membranes offer mechanical strength, transparency, and compatibility with microfluidic system fabrication, making them suitable candidates for microfluidic applications. In the prototype microchip, fabricated in this thesis (see Chapter 3.3), a commercial PC membrane was integrated as a structural element forming two parallel microchannels and serving as a cell culture surface. Although cells are expected to adhere and proliferate on the membrane, the hydrophobic and chemically inert properties of PC make its native surface unfavourable for cell adhesion, as confirmed by control experiments, conducted without specific surface modification or adhesion-promoting factors. Therefore, surface functionalization of PC is necessary to enhance the membrane's cell-adhesive properties.

To address this limitation, oxidative surface treatments were investigated to enhance the cell's ability to accommodate cell adhesion in PC. Two complementary strategies were employed: physical modification via oxygen plasma and chemical modification using wet reagents. Oxygen plasma treatment is a reagent-free and time-efficient technique widely used for polymer functionalization. It introduces polar oxygen-containing groups onto the surface, such as hydroxyl, carbonyl, and carboxyl moieties. In this study, plasma oxidation combined with PDL coating demonstrated notable adhesion performance. However, the oxidized PC surface gradually reverted to its original state in terms of surface wettability, as confirmed by contact angle measurements after 9 days post-treatment. The obtained results come in line with literature data on surface aging, following the plasma exposure [129], [130]. Therefore, the instability of the plasma-treated PC surface – especially considering the extended fabrication process and the treatment of UV and high temperature (see Chapter 2.2.12) – limits the applicability of plasma oxidation for long-term use.

Reports in literature indicate that chemical oxidation reagents, such as NaIO_4 and piranha solution, are effective in incorporating functional groups into the polymer surface without causing significant material degradation [242], [243], [247]. This approach is a more stable solution for microfluidic applications requiring longer production times. Consequently, alternative chemical oxidation methods, including NaIO_4 , H_2SO_4 , and Piranha solution, were tested as potential substitutes. While water droplet contact angle measurements revealed no significant difference in the wettability of PC following chemical treatment, cell adhesion assays demonstrated a clear improvement in adhesion with modified membranes compared to untreated controls.

To further augment the cell-adhesive properties of treated PC membranes, surface coatings with adhesion-promoting ECM molecules, fibronectin, collagen,

and PDL, were assessed individually or in combination. These proteins adsorb onto the modified PC surface and mediate cell adhesion through integrin-ligand interactions. Quantitative analysis revealed that all tested combinations, except fibronectin alone, yielded adhesion rates above 90%. In contrast, fibronectin-coated membrane demonstrated lower cell adhesion ($87\pm 8\%$), suggesting the fibronectin's conformational changes upon adsorption potentially masking or limiting exposure to the integrin binding domains, critical for cell adhesion [248]. This phenomenon aligns with literature emphasizing the critical role of protein folding and surface orientation in modulating cell surface interactions [53].

Following confirmation of effective cell adhesion for the static culture conditions, the experimental setup was extended to assess retention of adhesion under shear flow, simulating physiological shear stress conditions. U2OS cells cultured on modified PC membrane exhibited sustained adhesion within the microfluidic channel, even under shear stress levels up to six times higher than physiological interstitial flow. These results demonstrate that the modified PC surfaces effectively support robust cell adhesion and retain adherent cells under elevated shear stress.

Taken together, these pilot experiments demonstrate that combining surface oxidation with ECM protein coatings provides an effective strategy for functionalizing otherwise inert PC membranes, enabling their integration into microfluidic systems designed for cell culture. While oxygen plasma treatment enables rapid surface modification, its short-lived hydrophilicity limits its applicability. In contrast, chemical modification methods using NaIO_4 , H_2SO_4 , and piranha solution proved to be stable, compatible with fabrication processes, and capable of achieving comparable biological performance. Importantly, this approach is cost-effective and does not require sophisticated and expensive equipment, making it practical for routine laboratory use.

These findings confirm chemical surface modification as a practical and easily adaptable strategy for enhancing PC membrane functionality within an enclosed microfluidic system. The additional PDL to the piranha-treated PC surface enhanced its ability to support sustained cell adhesion under both static and dynamic culture conditions.

3.3. POLYCARBONATE-INTEGRATED MPS FOR PEF TREATMENT OF CELLS

In the previous chapter, the PC membrane was modified using physical, chemical, and biological treatment. Building on these findings, this chapter introduces a MPS that incorporates the PC membrane as a functional component within a microfluidic chip. The integrated porous PC membrane mimics the complexity of biological tissues and organs. It serves two essential purposes:

1) Providing a surface for cell growth on both sides of the membrane, thereby preventing direct mixing of cell populations in adjacent microchannels.

2) Enabling interchannel communication through its pores, which allow the diffusion of gases, nutrients, and signalling molecules while maintaining physical separation between compartments. This configuration supports the formation of physiologically relevant tissue interfaces, closely resembling *in vivo* conditions.

The MPS is specifically designed for PEF, or electroporation, studies. PEF treatment has emerged as a powerful tool in biomedical science due to its ability to induce transient membrane permeabilization, facilitate targeted drug delivery, gene transfer, and controlled modulation of cellular activity. PEF-based approaches are particularly valuable in cancer therapy, where they enhance chemotherapeutic uptake and enable non-thermal tumour ablation [249]. Additionally, PEF plays a growing role in tissue engineering and regenerative medicine by promoting cell stimulation, migration, and ECM remodelling [250].

In this chapter, I present the MPS for PEF studies, which was designed, fabricated, and analysed in the lab from scratch. Due to its adaptable architecture and compatibility with standard cell culture protocols, the system can be applied to a wide range of cell types, enabling comparative studies across different biological models. The MPS is specifically designed for investigating cellular responses to PEF treatment. The microchip was fabricated using OSTE as the base material, rather than the widely used PDMS. The microchip incorporates electrodes for PEF treatment. Real-time monitoring can be performed with integrated sensors for oxygen and pH, and cell or tissue integrity can be analysed using TEER measurements.

3.3.1. Design of the microchip

The microfluidic chip is designed with dimensions of 75 x 25 mm. It contains one main channel that begins at the inlet, passes through the PEF treatment chamber, and then through the pH sensing area, exiting the microchip through the outlet (**Figure 36**). The channel width is 2 mm in the electroporation area and 1 mm in the pH sensing area. The channel, with the height ranging from

0.75 to 0.85 mm, is separated into two subchannels by a porous PC membrane (Figure 35b), serving as a surface for cell adhesion and growth.

The PEF treatment chamber incorporates four independent pairs of parallel plate electrodes, each measuring 2 x 2 mm, with a spacing of 2 mm between them. For PEF treatment, any combination of the electrode pairs can be used together, based on their connection to the power source. In the upper subchannel, two oxygen sensor spots, each with a diameter of 3 mm, are integrated upstream and downstream of the PEF treatment chamber.

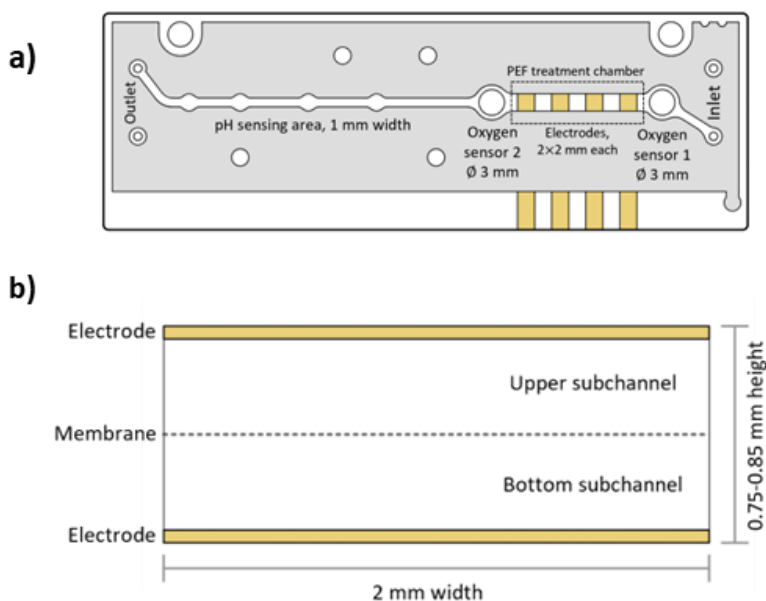


Figure 36. Schematic representation of the microchip. a) Illustration of the upper COC/OSTE/O₂ slide and b) cross-sectional view of the channel at the electrodes in the PEF treatment chamber.

3.3.2. Microchip fabrication

A primary material for microchip production, PDMS, is considered the gold standard. Indeed, PDMS has favourable properties, such as biocompatibility, optical transparency, gas permeability, ease of fabrication, and straightforwardness of tubing directly into PDMS. However, significant issues such as the absorption of small molecules, leaching of uncrosslinked oligomers, and microchannel deformation due to high flow rates and organic solvents limit the full application of microchips, particularly in pharmaceutical applications [35], [166], [167], [171]. This encourages the search for new suitable polymers

for microchip production. A decade ago, the dual-curable polymer OSTE was introduced specifically for microchip production. This polymer avoids the negative properties associated with PDMS [175], [251].

For the microchip to perform the MPS function, it is placed in a custom-made support jig. This jig has electrical contacts in both the top and bottom sections for PEF processing, while the top section also incorporates components for monitoring oxygen and pH (**Figure 37**).

The presented technology has two key aspects:

(1) Microchip fabrication is achieved through soft lithography, enabling easy modifications of channel geometry, number of electrodes, and positioning according to specific needs.

(2) The use of COC, OSTE, and PC membranes to constrain the channel eliminates the adverse properties associated with PDMS, such as molecular absorption, gas permeation, and channel deformation.

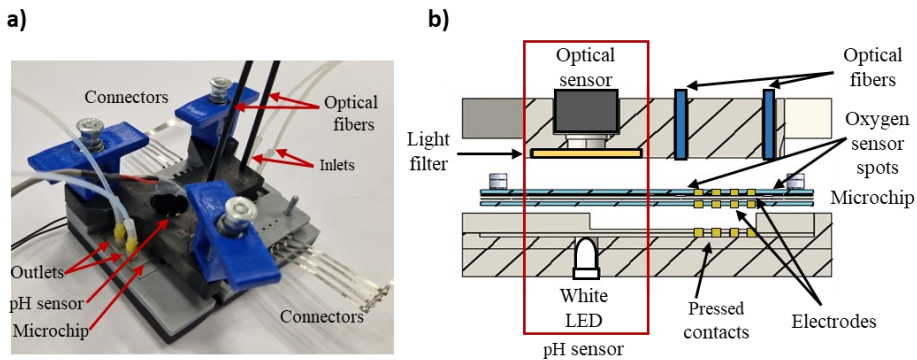


Figure 37. (a) MPS prototype, (b) Schematic cross-section and decomposition of the supporting jig.

3.3.3. Simulation of the electric field in the microchip

The fabricated microchip is intended for PEF treatment of cells. The upper and lower walls of the microchip channel in the PEF treatment chamber have integrated electrodes that generate an electric field. A schematic depiction of the electric field distribution within the microchannel is presented in Figure 38a. The electric field is generated only in the area between parallel plate electrodes. Meanwhile, the electric field is absent in the gaps between the electrodes.

In terms of channel height, the channel is divided approximately in half by a porous insulating PC membrane (**Figure 38b**, **Figure 38c**). To evaluate the impact of the membrane on the electric field, a simulation of it was conducted with two membranes with different pore sizes and porosity: (1) PC membrane -

0.4 μm pores with 18.8 % porosity and 25 μm thickness; (2) PC membrane - 3 μm pores with 21.2 % porosity and 22 μm thickness; (3) no membrane.

The electric field simulation across two parallel plane electrodes, measuring $2 \times 2 \text{ mm}$ with a height of 0.8 mm, was conducted using the COMSOL Multiphysics software package. An 800 V potential difference was selected for the simulation to achieve up to 10 kV/cm electric field.

The electric field simulations revealed a nearly uniform distribution of the electric field in the subchannels, measuring approximately 9 kV/cm (Figure 38b). This represents a slight decrease compared to the channel without a membrane, which measured 10 kV/cm. Notably, the electric field near the membrane was amplified by about a factor of 2. Additionally, the electric field strength oscillates spatially, reaching its maximum peak above the void space (Figure 38c). The distribution of the electric field above the membrane is influenced by the membrane's characteristics. The membrane with a pore size of 3 μm exhibits greater electric field distribution and higher oscillation amplitude near the membrane compared to the membrane with smaller pores (0.4 μm). Conversely, the smaller pore membrane shows a more uniform electric field distribution and lower oscillation amplitude.

Concluding from the simulation data, the electric field throughout the subchannel is consistent with the set parameters. However, at the membrane, the electric field is enhanced twofold, while inside the pores it is fourfold. This enhancement must be considered when culturing cells that adhere directly to the membrane.

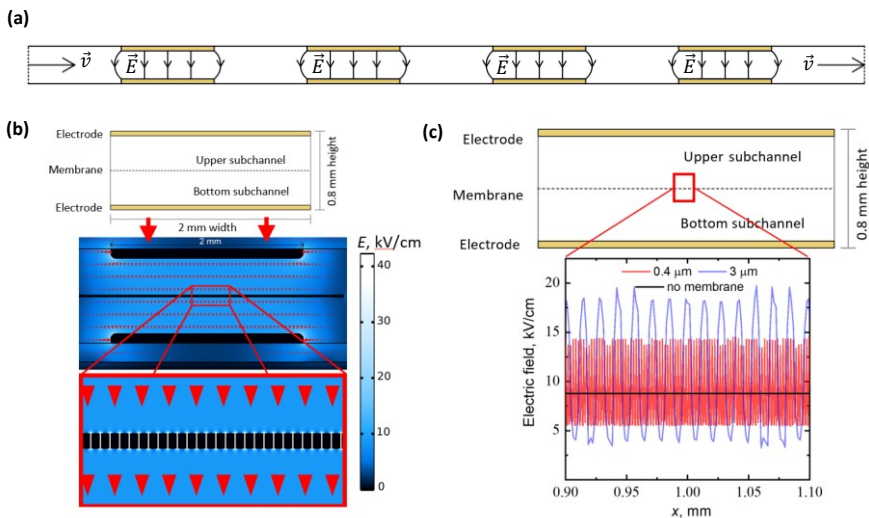


Figure 38. Electric field distribution in the microchip. (a) Schematic representation of electric field lines in the PEF treatment chamber, where \vec{v} is the

fluid flow rate and \vec{E} – the electric field vector. (b) Visualisation of electric field distribution in the microchip simulated using COMSOL Multiphysics with the membrane with a pore size of 3 μm and porosity of 21.2 %. A voltage potential of 800 V is applied, producing a 10 kV/cm electric field in the channel without the membrane. The colour gradient illustrates the electric field strength in kV/cm, with the red triangles indicating the direction of the electric field. (c) Simulation results comparing the electric field strength distribution across the microchip without the membrane (black line) and 0.5 μm above the membrane. Blue and red lines correspond to oscillations in the microchip with pore sizes of 3 μm and 0.4 μm , respectively.

3.3.4. Cell viability and permeability after PEF treatment in the microchip

In order to confirm the suitability of MPS for investigating the effect of IEL on cells, electroporation experiments were performed on mammalian cells in suspension.

The PEF treatment chamber contains four identical pairs of independent electrodes and three equally sized gaps of the same dimensions between them (Figure 35a, 38a). This configuration means that when cells are injected into the chamber, only 4/7 of the total cell volume will be subjected to the electric field. To guarantee the electroporation of the remaining cells, the cell suspension must be directed across the volume of one electrode pair. This volume is calculated using formula (5) (Materials and Methods). The experimental procedure could be significantly improved by conducting the PEF treatment in continuous flow mode, where the flow and PEF treatment occur simultaneously. In this setup, cells move through the entire PEF treatment chamber, which contains the electrodes and gaps, resulting in varying exposure to the electric field. Therefore, it is essential to calculate the flow rate (using formula (6), as outlined in the Materials and Methods section) to determine the precise number of pulses to be applied to the cells as they pass through the entire chamber. This specific number of pulses is referred to as pulses per cell.

Studies assessing the efficacy of the PEF treatment in microchips were carried out under two flow modes: stop and continuous. For electroporation experiments, we used the suspension of rat glioma cell line C6, applying the electric field in the range of 0 to 10 kV/cm, with a pulse duration of 100 μs , and a repetition rate of 1 Hz. Stop flow electroporation was performed using an electric field from 1.8 kV/cm to 10 kV/cm (Figure 39a). The results revealed no change in cell viability after PEF treatment with 8 pulses across all tested electric fields.

The permeability under stop flow post-PEF treatment with 8 and 16 pulses was examined using a non-permeable fluorescent dye DAPI. Since DAPI cannot enter intact cells, membrane permeabilization is required, which can be achieved via PEF treatment. This permeabilization effect was evident in the stop flow IEL experiment, where permeability increased progressively with higher electric field strengths when using 8 pulses, as indicated by the fluorescence ratio compared to the non-PEF-treated control (**Figure 39a**). When comparing the effects of 8 and 16 pulses, a similar level of membrane permeability was observed using 16 pulses at 1.8 kV/cm as with 8 pulses at 10 kV/cm. Thus, under stop flow electroporation, the most favourable parameters for achieving maximum permeabilization were 16 pulses at an electric field strength of 1.8 kV/cm.

In continuous flow mode, permeability increased slightly with 32 pulses per cell at 1.8 kV/cm, reaching a maximum increase at 64 and 128 pulses (**Figure 39b**). This increase was comparable to the 1.8 kV/cm observed in stop flow experiments with 16 pulses. Moreover, exposure to continuous flow PEF treatment at the highest electric field strength of 10 kV/cm with 8-32 pulses per cell did not significantly impact cell viability compared to the control. However, continuous flow electroporation with 64 and 128 pulses per cell led to a substantial reduction in cell viability - by 80% and 93%, respectively (**Figure 39b**) – indicating that these IEL parameters are unsuitable for achieving maximal membrane permeabilization without inducing cell death.

These conducted experiments confirm that the fabricated microchip with integrated PC membrane is suitable for PEF treatment of mammalian cells, enabling effective control of membrane permeabilization under both stop flow and continuous parameters.

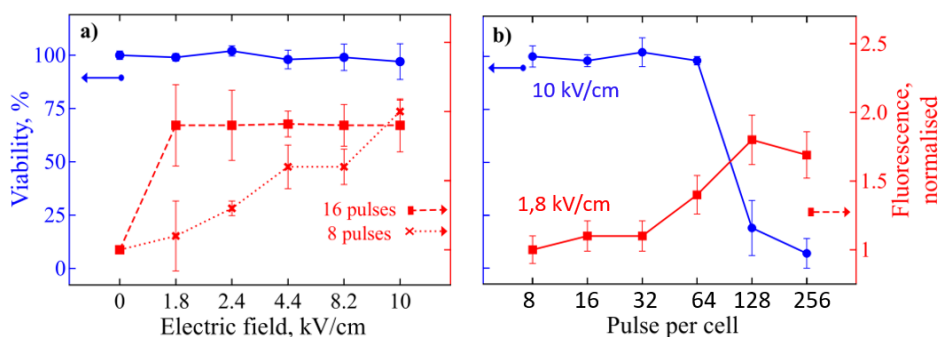


Figure 39. The impact of PEF treatment on C6 cells and permeability under (a) stop flow and (b) continuous flow electroporation modes. Blue colour with blue circles represents viability data; red colour – permeability data For (a) an electric field range of 0 to 10 kV/cm electric field range was applied with either 8 (red cross) or 16 pulses (red squares). For (b) a 10 kV/cm electric field was used

for viability experiments, while permeability experiments employed a 1.8 kV/cm field with 0 to 128 pulses per cell. In both (a) and (b), PEF treatment was conducted using a 100 μ s pulse duration and a 1 Hz repetition rate. Permeability quantified as fluorescence normalised to the non-treated control; the number of experiments $n \geq 3$; with error bars indicating standard deviation.

3.3.5. Prediction of affected area in continuous PEF

The viability results indicate that 64 pulses are necessary to reduce cell viability at an electric field of 10 kV/cm in continuous flow electroporation. In contrast, no change in cell viability in stop flow electroporation with 8 pulses at 10 kV/cm demonstrated no change in cell viability. Permeability studies revealed that the maximum permeability was achieved at an electric field of 1.8 kV/cm with 16 pulses in stop flow mode, whereas continuous flow required 64 pulses at the same electric field strength. This suggests that continuous flow electroporation requires four times as many pulses to achieve equivalent permeability as stop flow mode. These results can be explained by the following assumptions: (1) the electric field gradient affects only a specific area of the membrane; (2) in stop flow, cells are in semi-stationary conditions, i.e., cells remain relatively stationary during the entire pulsation process, allowing energy to be delivered multiple times (successfully electroporated area, **Figure 40a**). In contrast, during continuous flow, cells rotate randomly throughout PEF treatment (**Figure 40b**), leading to a more even distribution of energy across the cell surface and resulting in fewer pulses being directed at any particular area.

A theoretical model for determining the affected area of the membrane was developed using MATLAB software. In continuous flow, a portion of the total cell area is influenced by the electric field. The cell is then allowed to randomly rotate by a certain angle θ , affecting different locations of the cell membrane by an electric field.

This process is repeated N times until the affected area overlaps at least n times in a single spot. In stop flow mode, it is assumed that cells remain approximately stationary, leading to overlapping affected areas, where n represents the number of pulses required. The size of the affected area is determined by the effective ratio N/n , as illustrated in Figure 6. Based on experimental results, the effective ratio of N/n was found to be equal to 4, indicating the affected area was 16% (intersection of red lines in **Figure 41**). This means that 16% of the cell membrane must receive pulses to achieve the same permeability level as observed in stop flow mode.

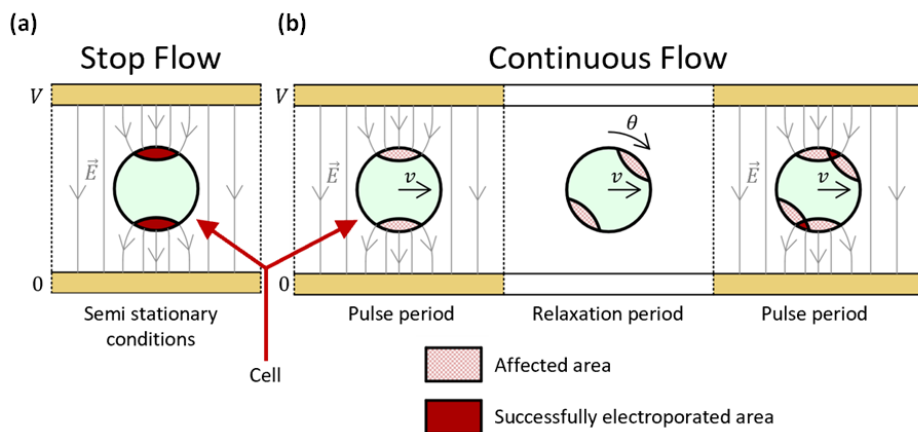


Figure 40. Schematic representation of how cells are affected in (a) stop flow and (b) continuous flow PEF. v stands for fluid flow rate, \vec{E} – electric field vector, θ – random angle of rotation, V - applied voltage on the electrode, and 0 – ground voltage on the electrode.

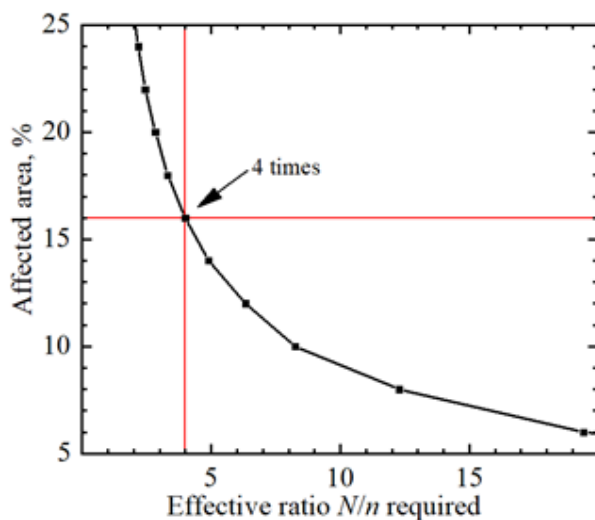


Figure 41. Surface area and pulse ratio relationship of continuous and stop flow electroporation modes as calculated in MATLAB software. N and n correspond to pulse number in continuous flow and stop flow modes, respectively; red lines mark the match with experimental data.

3.3.6. Oxygen measurement experiments

When culturing cells *in vitro*, ensuring a constant supply of the necessary gases is essential – O₂ and CO₂. Oxygen is required for cell respiration, while CO₂ ensures the correct pH of the culture medium. A distorted O₂ and pH level will interfere with cell survival and is associated with the development of various pathologies, including cancer [252], [253].

The materials of our microchip - OSTE and COC- are impermeable to gases. For monitoring of O₂ and pH levels, the MPS system has incorporated sensors for monitoring both features. The microchip features two oxygen sensors — one positioned upstream and the other downstream of the PEF treatment chamber (Figure 2a). Both sensors are equidistant from the edge electrodes. When the flow is activated, Sensor 1 measures the oxygen concentration in the fresh medium that passes through the electrodes, while Sensor 2 measures the concentration in the medium after it has undergone potential PEF treatment. To assess the effectiveness of MPS in detecting changes in oxygen concentrations, experiments were conducted with C6 cell suspension using PEF as the stimulus. Data on oxygen concentration were collected from both sensors before and immediately after the cessation of PEF.

In the absence of PEF treatment (0kV/cm), oxygen concentration at sensor 2 decreased by $0.14 \pm 0.07\%$ compared to sensor 1 (**Figure 42a**). This decline was substantial when compared to the control sample, which contained only buffer and exhibited a smaller decrease of $0.01 \pm 0.07\%$. However, when cells were subjected to PEF treatment, there was a noticeable increase in oxygen concentration of 0.14%, 0.13%, 0.09%, and 0.03% at electric fields of 1.8 kV/cm, 2.4 kV/cm, 4.4 kV/cm, and 8.0 kV/cm, respectively. Importantly, the buffer samples at lower electric fields (1.8 kV/cm and 2.4 kV/cm) displayed distinct variations compared to the cell suspension, indicating that these differences were specifically due to the effect of PEF on the cells. In contrast, at 4.4 and 8.0 kV/cm, both the cells and buffer showed similar changes in oxygen concentration.

The obtained results confirm that the fabricated MPS is suitable for precise monitoring of oxygen concentration.

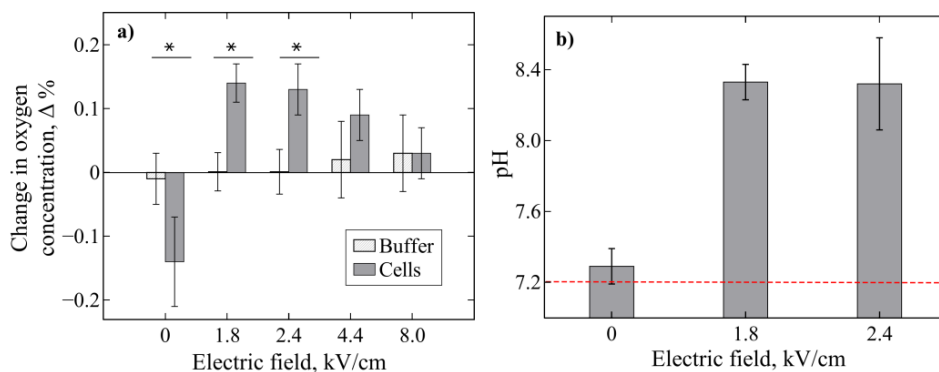


Figure 42. Effect of PEF treatment on (a) the difference in oxygen concentration between two sensors and (b) pH, immediately after PEF. The PEF treatment was performed in stop flow mode using various electric fields, with 16 pulses, a 100 μ s pulse duration, and a 1 Hz repetition rate. The number of experiments $n \geq 3$; asterisks* indicate statistically significant differences ($p < 0.00001$). The dashed line in (b) represents the buffer baseline.

3.3.7. pH measurement

The optimal pH for mammalian cell culture media is approximately 7.2-7.4. Drastic changes in pH can significantly impact cell viability, so it is crucial to maintain the pH within this range. Bicarbonate is a commonly used buffering agent in culture media, with its effectiveness highly dependent on the CO_2 level. In contrast, the buffering agent HEPES is not influenced by CO_2 . For simple monitoring of pH levels in the media in stationary culturing, phenol red is typically used as an indicator, changing colour from yellow in acidic conditions to purple in alkaline conditions. Cellular metabolic processes tend to shift the medium's pH towards the acidic side, and PEF treatment may also induce changes in pH levels [254], [255].

To assess the performance of the pH-meter, pH fluctuations were measured after applying PEF treatment to C6 cells resuspended in media containing phenol red, bicarbonate, and HEPES. The inclusion of these two buffering agents helps maintain a stable pH level, even with a lower CO_2 concentration compared to a CO_2 incubator. PEF treatment was administered at electric field strengths of 1.8 kV/cm and 2.4 kV/cm, utilizing 16 pulses, as these parameters are optimal for enhancing permeability. The effect of pH on the PEF-treated cell suspension was compared to non-treated one. The initial pH of the media was 7.2. For cells not subjected to PEF, the pH was recorded at 7.29 ± 0.06 . In contrast, PEF treatment raised the pH to 8.3 ± 0.14 at 1.8 kV/cm and 8.3 ± 0.26 at 2.4 kV/cm (**Figure 42b**).

The obtained results confirm that the fabricated MPS is suitable for precise monitoring of oxygen concentration.

3.3.8. TEER measurement

TEER (transepithelial electrical resistance) measurement is commonly utilized in MPS to assess the integrity and functionality of biological barriers, including epithelial and endothelial cell layers. Since the fabricated microchip includes integrated electrodes, it can be used for both PEF treatment and TEER measurement. To evaluate whether TEER measurement is applicable in the developed MPS, experiments were conducted using cells in suspension. No significant change in TEER was observed before and after PEF treatment, which was expected due to the absence of a confluent cell layer. Upon cell injection, impedance decreased by $60\pm 4\%$ reduction compared to the plain buffer. As TEER represents a specific case of impedance measurement, characterizing electrical resistance across a cell layer, this result indicates that the system is sensitive to the presence of cells. The obtained data, along with the microchip design enabling the use of the same electrodes for both PEF and TEER applications, suggests that the microchip design may be suitable for TEER measurements within existing MPS applications.

3.3.9. Discussion on the MPS

MPS development encounters several significant challenges. First, standard instruments for monitoring physiological parameters are not suitable for microfluidic applications, necessitating the creation and integration of specific sensors for *in situ* monitoring of microfluidic systems. The second challenge involves PDMS, a polymer commonly used in soft lithography for microchip fabrication. While PDMS offers several advantages, it also has undesirable properties, such as the absorption of small molecules, channel expansion, and the release of unbound crosslinkers into the inner channel. Third, to mimic an organ in OoC and MPS, two or more cells need to be cultured in contact with each other without mixing. A porous membrane can facilitate the separation. However, integrating a membrane into the microchip often requires additional additives, which may influence cellular processes. These issues can distort experimental results and hinder the adoption of MPS in pharmaceutical applications.

PEF, a physical method for electrotransfer, for inactivation of the cells, is utilized in both the medical and food industries. Currently, PEF research is shifting towards the microfluidics scale, allowing for experiments that monitor the effects of PEF on cells under more controlled conditions within microfluidic

research. Integrated real-time monitoring sensors and instruments in MPS systems facilitate the collection of experimental data *in situ*.

In this study, OSTE-based microchip fabrication was employed for microchip production [203]. The microchip incorporates a track-etched PC membrane and electrodes for PEF treatment. To evaluate the porous membrane's impact on electric field distribution, mathematical simulations with and without membranes were conducted. The presence of a porous insulating membrane in the centre of the channel did not significantly change the electric field in the subchannel, measuring 9 kV/cm with the membrane compared to 10 kV/cm without the membrane. However, just a few microns above the membrane's surface, the electric field strength approximately doubled. Since the PEF treatments were applied to suspension cells, distributed throughout the full height of a single subchannel (0.4 mm), the enhancement of the electric field had a negligible effect on the PEF results. However, this enhancement becomes relevant in experiments involving cells positioned near the membrane, such as adherent cells cultured directly on the surface.

Our microchip features parallel plate electrodes that replicate the structure of conventional electroporation systems currently available in the market. To assess the microchip's effectiveness as an electroporation cuvette, PEF treatment on mammalian cells in suspension was executed. In stop flow experiments, cell viability remained unchanged after 8 pulses of electric field 0–10 kV/cm were applied (**Figure 39a**). In contrast, continuous flow electroporation resulted in decreased cell viability with 64 and 128 pulses delivered at 10 kV/cm (**Figure 39**).

The permeability was assessed using the impermeable fluorescent dye DAPI, whose uptake indicates the membrane disruption. Stop flow electroporation indicated a gradual increase in permeability as the electric field increased up to 10 kV/cm with 8 pulses (**Figure 39a**). Achieving an electric field of 10 kV/cm requires applying 800 V, which is relatively high and may lead to electrode deterioration after only a few sets of experiments. Therefore, we tested 16 pulses, which demonstrated that permeability saturated at 1.8 kV/cm, significantly lower than the initial target (**Figure 39a**). To achieve the same level of permeability under continuous flow, 64 pulses per cell were necessary (**Figure 41b**). Based on the pulse ratios in stop and continuous flow, MATLAB calculations estimated that the affected cell surface in continuous flow mode is approximately 16%.

These data demonstrated that cells experience membrane permeabilization during PEF treatment in the microchip, while maintaining a high level of cell viability. The high viability observed during electroporation is attributed to lower voltage, shorter pulse duration, and improved heat dissipation in the microfluidic

device [248]. A conceptual model was developed illustrating how cells are affected by electric fields in both stop flow and continuous flow electroporation. It is suggested that the cells display semi-stationary behaviour in stop flow mode, while they experience random rotation in continuous flow. The model does not account for fluid turbulence caused by bubbles on the electrodes during PEF applications [256], [257], which may have influenced cell rotation in both continuous and stop flow modes. Cell rotation can be beneficial as it facilitates an even distribution of increased permeability across the entire cell surface [258].

The performance of integrated sensors was evaluated by applying an electric field. We monitored changes in oxygen concentration immediately after PEF treatment (**Figure 42a**). A slight change in oxygen concentration was observed in both the presence and absence of PEF treatment in the cell suspension. This indicates that accurate oxygen monitoring can be achieved using the described microfluidic system.

To observe the pH changes following PEF treatment, pH levels at electric fields of 1.8 kV/cm and 2.4 kV/cm were measured and compared to non-electroporated samples. Both treated samples demonstrated a shift from pH 7.2 to pH 8.3 with PEF treatment (**Figure 42b**). This shift of one pH unit toward alkalinity was smaller than what was reported by other authors [254], [259]. This can be explained by differences in the buffers used in other publications: (1) we utilize two buffering agents, bicarbonate and HEPES, which accelerate the significant pH shift; (2) the change was measured not immediately but rather a few minutes after PEF treatment; and (3) we do not measure the change occurring at the electrode's surface, where the localized change is expected to be the strongest [254]. Despite these, it enables reliable monitoring of pH dynamics following electroporation.

Finally, TEER measurement capabilities were validated using cell culture media, both with and without suspension cells, through the same integrated electrode used for PEF treatment. The changes in TEER were clearly detectable. It is important to note that TEER measurements are typically taken in the presence of a functional barrier, where disruptions in it can be observed. However, this experiment involves suspension cells, which do not form such a barrier. Despite this limitation, the results indicate that the microfluidic device is capable of capturing impedance differences, as demonstrated by the change of impedance observed in the buffer alone compared to the cell suspension. These data support the suitability of the device for TEER measurements.

To summarize, the viability and permeability results following PEF treatment confirmed that the microchip with integrated track-etched PC membrane is well suited for PEF treatment of mammalian cells. The integrity and performance of the integrated sensors were successfully confirmed,

demonstrating their ability to compensate for the non-permeability of OSTE and COC by continuously monitoring oxygen levels and pH. These results collectively demonstrate that the developed MPS, featuring the PC membrane, embedded electrodes, and integrated oxygen and pH sensors, successfully enables PEF treatment and real-time physiological monitoring within the microfluidic environment, fully supporting the statement for defence.

SUMMARY

This thesis explores the design and evaluation of biomaterials - specially engineered materials designed for interaction with biological systems in medical and biological research applications. Two distinct material groups were studied: ceramic-type and polymeric materials, each of which aligns with different clinical and technological goals.

The first material investigated was bioceramic alumina, proposed as a candidate for orthopaedic and dental implantology. While conventional sintered alumina is already used in medical settings, particularly in dental prosthetics, its broader application is limited by intrinsic brittleness, manufacturing complexity, cost, and geometry constraints. This work introduces an alternative approach: producing bioceramic alumina by anodising industrial aluminium alloy 6082 to use it in implantology, such as an osteosynthesis plate. This method allows for more versatile sample geometries and leverages the lightweight nature and high post-anodization hardness of alumina alloys, offering potential replacement for heavier, more expensive titanium-based implants.

A primary objective was to determine whether anodized alumina alloys treated with phosphoric or sulfuric acid electrolytes could qualify as a biocompatible material. A comprehensive assessment was conducted to analyse their mechanical and chemical properties, corrosion resistance, and interaction with cells. These evaluations included quantification of ion release into SBF, biological assay for cell adhesion, viability, and proliferation, and comparative analysis with both non-anodized Al alloy and medical grade Ti alloy.

The results revealed that bioceramic coatings formed via phosphoric acid anodization produced a microporous surface with insufficient mechanical strength and increased corrosion rate. Additionally, the impaired cell adhesion profiles indicate that such bioceramic alumina coatings are unsuitable for biomedical use. In contrast, anodization in sulphuric acid yielded nanoporous bioceramic alumina coatings with superior hardness, low ion release, and excellent corrosion resistance. Cell-based assays demonstrated high short-term viability and strong adhesion on these surfaces with performance comparable to or exceeding that of Ti alloy. Minor concerns included elevated sulphur and manganese ion release, though the latter remained within the safe biological limits. Future long-term studies and refinement of sample preparation would be necessary to validate the safety and durability of these coatings. Overall, sulfuric acid anodized Al alloy 6082 represents a promising platform for bioceramic implant applications.

The second biomaterial studied was PC, evaluated for its suitability in a microfluidic system. A microchip, fabricated in this thesis from scratch,

incorporated a track-etched PC membrane, which spatially divided the central microchannel into two parallel subchannels. Cells cultured on opposing sides of the PC membrane were expected to interact through its pores, thereby mimicking physiological tissue barriers found in organ-on-a-chip systems.

PC's intrinsic hydrophobicity limits its use in cell-based applications, as such surfaces do not support cell adhesion. To address this, a sequence of physical and chemical surface modification strategies was employed. Initial plasma treatment using oxygen gas rapidly increased hydrophilicity and improved adhesion, but the effect diminished over a short time due to surface aging nine days post-plasma treatment.

To achieve long-term stability, wet chemical oxidation was applied using sodium metaperiodate, sulphuric acid, and piranha solution. These treatments effectively functionalised the PC surface, enhancing cell attachment in static culture. To further improve adhesion, ECM proteins – fibronectin, collagen, and PDL- were introduced. Single adhesion molecules and their combinations yielded consistently high adhesion levels on modified PC surfaces. PDL alone also proved to be effective in dynamic flow experiments. Importantly, epithelial-type U2OS cells have maintained adhesion under shear stress conditions up to six times higher than physiological interstitial flow, demonstrating that these optimised PC surface supports cell growth across experimental modes.

With these pilot studies, the need for customized surface chemistries and adhesion protocols tailored to specific cell types was highlighted. The versatile PC membrane treatment process developed here lays the groundwork for future cell and tissue-specific designs. Modification of the PC membrane with these substances favourably affected cell adhesion on the modified membrane.

Additional adhesion factors are needed to achieve optimal cell adhesion and PDL, fibronectin and collagen were used in the study. The oxidised PC membrane, together with the adhesion molecules and their various combinations, provided high cell adhesion under static culture conditions. In a flow experiment, the cheapest and most accessible adhesion molecule, PDL, was chosen as the adhesion molecule, and epithelial bone tissue cells grew on the surface of the oxidized PC membrane, even under 6 times higher shear force than physiological conditions. This confirmed that the modified PC surface is suitable for cell growth under both static and flow conditions. It should be noted that these studies were carried out as pilot experiments, and therefore, specific cells and specific adhesion molecules would have to be tested for each cell type individually.

Building on these results, the PC membrane was successfully integrated into a microfluidic microchip, designed for PEF studies. The MPS, developed in this study, incorporated not only the PC membrane and embedded electrodes but also integrated oxygen and pH sensors to enable real-time monitoring of the

microenvironment. Mathematical simulation of electric field distribution revealed that the presence of the porous membrane did not significantly alter the field strength across the microchannel, except in the immediate vicinity of the membrane surface. This localized amplification must be considered in future experiments involving adherent cells cultured directly on the membrane.

Initial electroporation experiments were conducted using suspension cells to assess the effectiveness of PEF treatment in both stop flow and continuous flow conditions. The results demonstrated that the optimal PEF parameters vary depending on flow mode, but effective membrane permeabilization and high cell viability can be achieved in both modes. Measurements from the integrated oxygen and pH sensors confirmed the system's ability to monitor physiological changes in real-time. Additionally, TEER measurements, although performed with non-adherent cells, revealed detectable differences between cell-containing and cell-free media, suggesting that the system is suitable for future studies of barrier integrity and epithelial function.

Taken together, the results of this thesis demonstrate the potential of surface-engineered biomaterials to regulate cell-material interactions with precision in both static and dynamic settings. Whether enhancing corrosion resistance and biological compatibility in implant coatings or enabling membrane-integrated cellular communication in microfluidic devices, the strategies explored here respond to the evolving demand of biomedical engineering. The modularity, chemical stability, and biological efficacy of these materials support future developments in regenerative medicine, pharmacological research, and next-generation organ-on-a-chip technologies.

CONCLUSIONS

1. Al alloy 6082 anodized in sulphuric acid electrolyte increased the specimen's hardness twofold, did not alter ion release compared to the non-anodized alloy, and improved corrosion resistance by 1.5 times compared to the titanium alloy.

2. The morphology of mouse fibroblast L929 cells on Al alloy 6082 anodized in sulphuric acid electrolyte confirms normal physiological behaviour. Cell viability results indicate the alloy's biocompatibility. These characteristics, closely resembling those of medical-grade titanium alloy, support the suitability of this material for biomedical applications.

3. Polycarbonate membranes modified with sodium metaperiodate, sulfuric acid, and piranha solution, followed by poly-D-lysine coating, increased cell adhesion by more than threefold.

4. Polycarbonate membrane modified with piranha solution and coated with poly-D-lysine enhanced cell adhesion by 4.3-fold under static conditions. Under dynamic conditions, epithelial U2OS cells withstood shear stress that was six times higher than the physiological interstitial flow.

5. The porous polycarbonate membrane was successfully incorporated into the microchip designed for pulsed electric field (PEF) treatment. The membrane's porous architecture enhanced the electric field strength by up to 200% at the membrane surface, when compared to the identical channel without a membrane, while maintaining over 90% electric field strength within the microchannel.

6. A microphysiological system (MPS) designed for PEF treatment of mammalian cells was developed. PEF treatment resulted in increased cell membrane permeability without compromising cell viability. Recorded changes in oxygen concentration and pH confirm the MPS applicability for physiological monitoring.

REFERENCES

- [1] S. Todros, M. Todesco, and A. Bagno, 'Biomaterials and Their Biomedical Applications: From Replacement to Regeneration', *Processes*, vol. 9, no. 11, Art. no. 11, Nov. 2021, doi: 10.3390/pr9111949.
- [2] M. Rahmati, E. A. Silva, J. E. Reseland, C. A. Heyward, and H. J. Haugen, 'Biological responses to physicochemical properties of biomaterial surface', *Chemical Society Reviews*, vol. 49, no. 15, pp. 5178–5224, 2020, doi: 10.1039/D0CS00103A.
- [3] K. Vig *et al.*, 'Advances in Skin Regeneration Using Tissue Engineering', *International Journal of Molecular Sciences*, vol. 18, no. 4, p. 789, Apr. 2017, doi: 10.3390/ijms18040789.
- [4] P. Balakrishnan, M. S. Sreekala, and S. Thomas, *Fundamental Biomaterials: Metals*. Woodhead Publishing, 2018.
- [5] S. Ali *et al.*, 'Biocompatibility and corrosion resistance of metallic biomaterials', *Corrosion Reviews*, vol. 38, no. 5, pp. 381–402, Oct. 2020, doi: 10.1515/corrrev-2020-0001.
- [6] J. S. Lu, Q. S. Lu, and J. Xue, 'Corrosion Resistance of Three 316 Stainless Steels', *Advanced Materials Research*, vol. 936, pp. 1097–1101, 2014, doi: 10.4028/www.scientific.net/AMR.936.1097.
- [7] Cramer, Stephen D. and Covino, Bernanrd S., *Corrosion: Materials*. in Volume 13B. ASM International, 2005. doi: 10.31399/asm.hb.v13b.9781627081832.
- [8] P. Bocchetta, L.-Y. Chen, J. D. C. Tardelli, A. C. dos Reis, F. Almeraya-Calderón, and P. Leo, 'Passive Layers and Corrosion Resistance of Biomedical Ti-6Al-4V and ?-Ti Alloys', *Coatings*, vol. 11, no. 5, Art. no. 5, May 2021, doi: 10.3390/coatings11050487.
- [9] M. Sepúlveda *et al.*, 'Enhancement of biocompatibility of anodic nanotube structures on biomedical Ti-6Al-4V alloy via ultrathin TiO₂ coatings', *Front. Bioeng. Biotechnol.*, vol. 12, Dec. 2024, doi: 10.3389/fbioe.2024.1515810.
- [10] S. A. Shabalovskaya, 'Surface, corrosion and biocompatibility aspects of Nitinol as an implant material', *Biomed Mater Eng*, vol. 12, no. 1, pp. 69–109, 2002.
- [11] A. Liu *et al.*, 'Progress of porous tantalum surface-modified biomaterial coatings in bone tissue engineering', *J Mater Sci: Mater Med*, vol. 36, no. 1, p. 26, Mar. 2025, doi: 10.1007/s10856-025-06871-w.
- [12] F. Carraro and A. Bagno, 'Tantalum as Trabecular Metal for Endosseous Implantable Applications', *Biomimetics (Basel)*, vol. 8, no. 1, p. 49, Jan. 2023, doi: 10.3390/biomimetics8010049.
- [13] M. M. Jamel, M. M. Jamel, and H. F. Lopez, 'Designing Advanced Biomedical Biodegradable Mg Alloys: A Review', *Metals*, vol. 12, no. 1, Art. no. 1, Jan. 2022, doi: 10.3390/met12010085.
- [14] W. Elshahawy, 'Biocompatibility', 2011. doi: 10.5772/18475.

- [15] K. S. Naik, 'Chapter 25 - Advanced bioceramics', in *Advances in Biological Science Research*, S. N. Meena and M. M. Naik, Eds, Academic Press, 2019, pp. 411–417. doi: 10.1016/B978-0-12-817497-5.00025-2.
- [16] C. Piconi, G. Maccauro, F. Muratori, and E. B. Del Prever, 'Alumina and Zirconia Ceramics in Joint Replacements', *Journal of Applied Biomaterials and Biomechanics*, vol. 1, no. 1, pp. 19–32, Jan. 2003, doi: 10.1177/228080000300100103.
- [17] J. B. Park, 'Aluminum Oxide: Biomedical Applications', in *Concise Encyclopedia of Advanced Ceramic Materials*, R. Brook, Ed., Oxford: Pergamon, 1991, pp. 13–16. doi: 10.1016/B978-0-08-034720-2.50013-7.
- [18] H. Al-Moameri, Z. Nahi, D. Raheem, and N. Al-sharify, 'A REVIEW ON THE BIOMEDICAL APPLICATIONS OF ALUMINA', *Journal of Engineering and Sustainable Development*, vol. 24, Feb. 2020, doi: 10.31272/jeasd.24.5.5.
- [19] W. Bensalah, K. Elleuch, M. Feki, M. Wery, and H. F. Ayedi, 'Optimization of anodic layer properties on aluminium in mixed oxalic/sulphuric acid bath using statistical experimental methods', *Surface and Coatings Technology*, vol. 201, no. 18, pp. 7855–7864, June 2007, doi: 10.1016/j.surfcoat.2007.03.027.
- [20] T. Matijošius *et al.*, 'Friction reduction using Nanothin Titanium layers on anodized aluminum as potential bioceramic material', *Ceramics International*, vol. 46, no. 10, Part A, pp. 15581–15593, July 2020, doi: 10.1016/j.ceramint.2020.03.105.
- [21] Y. Rao, Q. Wang, D. Oka, and C. S. Ramachandran, 'On the PEO treatment of cold sprayed 7075 aluminum alloy and its effects on mechanical, corrosion and dry sliding wear performances thereof', *Surface and Coatings Technology*, vol. 383, p. 125271, Feb. 2020, doi: 10.1016/j.surfcoat.2019.125271.
- [22] L. Vaiani *et al.*, 'Ceramic Materials for Biomedical Applications: An Overview on Properties and Fabrication Processes', *Journal of Functional Biomaterials*, vol. 14, no. 3, Art. no. 3, Mar. 2023, doi: 10.3390/jfb14030146.
- [23] C. Piconi and S. Sprio, 'Oxide Bioceramic Composites in Orthopedics and Dentistry', *Journal of Composites Science*, vol. 5, no. 8, Art. no. 8, Aug. 2021, doi: 10.3390/jcs5080206.
- [24] Y. Takami, T. Nakazawa, K. Makinouchi, J. Glueck, and Y. Nosé, 'Biocompatibility of alumina ceramic and polyethylene as materials for pivot bearings of a centrifugal blood pump', *Journal of Biomedical Materials Research*, vol. 36, no. 3, pp. 381–386, 1997, doi: 10.1002/(SICI)1097-4636(19970905)36:3%3C381::AID-JBM12%3E3.0.CO;2-H.
- [25] J. Hu *et al.*, 'Cell culture on AAO nanoporous substrates with and without geometry constrains', *Microelectronic Engineering*, vol. 88, no. 8, pp. 1714–1717, Aug. 2011, doi: 10.1016/j.mee.2010.12.055.

- [26] T. J. Webster, R. W. Siegel, and R. Bizios, 'Osteoblast adhesion on nanophase ceramics', *Biomaterials*, vol. 20, no. 13, pp. 1221–1227, July 1999, doi: 10.1016/S0142-9612(99)00020-4.
- [27] H. Kim, D. Kim, W. Lee, S. J. Cho, J.-H. Hahn, and H.-S. Ahn, 'Tribological properties of nanoporous anodic aluminum oxide film', *Surface and Coatings Technology*, vol. 205, no. 5, pp. 1431–1437, Nov. 2010, doi: 10.1016/j.surfcoat.2010.07.056.
- [28] G. D. Sulka, 'Highly Ordered Anodic Porous Alumina Formation by Self-Organized Anodizing', in *Nanostructured Materials in Electrochemistry*, John Wiley & Sons, Ltd, 2008, pp. 1–116. doi: 10.1002/9783527621507.ch1.
- [29] M. Paz Martínez-Viademonte, S. T. Abrahami, T. Hack, M. Burchardt, and H. Terryn, 'A Review on Anodizing of Aerospace Aluminum Alloys for Corrosion Protection', *Coatings*, vol. 10, no. 11, Art. no. 11, Nov. 2020, doi: 10.3390/coatings10111106.
- [30] J. Konieczny, K. Labisz, W. Jakub, and L. Dobrzanski, 'Stereometry specification of anodised and PVD coated surface of aluminium alloy', *Archives of Materials Science and Engineering*, vol. 38, Aug. 2009.
- [31] K. Habib and K. A.- Muhanna, 'Structures and Properties of Oxide Barrier-Film of Anodized Aluminum by Electrochemical Impedance Spectroscopy at the Nano-metere Scale', *J Membra Sci Technol*, vol. 02, no. 02, 2012, doi: 10.4172/2155-9589.1000114.
- [32] H.-J. Oh and C.-S. ChF, 'The Electrochemical Behaviors of Barrier-Type Anodic Films on Aluminum in Ammonium Adipate SO₄ solution'.
- [33] C. V. Manzano, J. P. Best, J. J. Schwiedrzik, A. Cantarero, J. Michler, and L. Philippe, 'The influence of thickness, interpore distance and compositional structure on the optical properties of self-ordered anodic aluminum oxide films', *J. Mater. Chem. C*, vol. 4, no. 32, pp. 7658–7666, Aug. 2016, doi: 10.1039/C6TC01904H.
- [34] A.-P. Li, F. Muller, A. Birner, K. Nielsch, and U. Gosele, 'Hexagonal Pore Arrays with a 50–420 nm Interpore Distance Formed by Self-Organization in Anodic Alumina', *J. Appl. Phys.*, vol. 84, pp. 6023–6026, Dec. 1998, doi: 10.1063/1.368911.
- [35] Yisu Wang, Han Sun, Wanbo Li, Chong Hu, and Kangning Ren, 'Recent progresses in microfabricating perfluorinated polymers (Teflons) and the associated new applications in microfluidics', *Microphysiological Systems*, vol. 2, no. 6, 2018, [Online]. Available: <http://dx.doi.org/10.21037/mps.2018.08.02>
- [36] J. Ma, Y. Wang, and J. Liu, 'Biomaterials Meet Microfluidics: From Synthesis Technologies to Biological Applications', *Micromachines*, vol. 8, no. 8, Art. no. 8, Aug. 2017, doi: 10.3390/mi8080255.
- [37] P. Parida, A. Behera, and S. C. Mishra, 'Classification of Biomaterials used in Medicine', *International Journal of Advances in Applied Sciences*, vol. 1, no. 3, Art. no. 3, Sept. 2012, doi: 10.11591/ijaas.v1.i3.pp125-129.

- [38] M. M. Farag, ‘Recent trends on biomaterials for tissue regeneration applications: review’, *J Mater Sci*, vol. 58, no. 2, pp. 527–558, Jan. 2023, doi: 10.1007/s10853-022-08102-x.
- [39] A. Rohani Shirvan, A. Nouri, and C. Wen, ‘12 - Structural polymer biomaterials’, in *Structural Biomaterials*, C. Wen, Ed., in Woodhead Publishing Series in Biomaterials. , Woodhead Publishing, 2021, pp. 395–439. doi: 10.1016/B978-0-12-818831-6.00010-0.
- [40] A. J. T. Teo, A. Mishra, I. Park, Y.-J. Kim, W.-T. Park, and Y.-J. Yoon, ‘Polymeric Biomaterials for Medical Implants and Devices’, *ACS Biomater. Sci. Eng.*, vol. 2, no. 4, pp. 454–472, Apr. 2016, doi: 10.1021/acsbiomaterials.5b00429.
- [41] S. S. Bhatti and J. Singh, ‘3D printing of biomaterials for biomedical applications: a review’, *Int J Interact Des Manuf*, Oct. 2023, doi: 10.1007/s12008-023-01525-z.
- [42] D. C. Clagett and S. J. Shafer, ‘Polycarbonate resins’, *Polymer Engineering & Science*, vol. 25, no. 8, pp. 458–461, 1985, doi: 10.1002/pen.760250805.
- [43] J. A. King and Jr, ‘Synthesis of Polycarbonates’, in *Handbook of Polycarbonate Science and Technology*, CRC Press, 1999.
- [44] Md. T. Siraj *et al.*, ‘12.47 - Eco-friendly food packaging innovations: A review of recent progress on recyclable polymers’, in *Comprehensive Materials Processing (Second Edition)*, S. Hashmi, Ed., Oxford: Elsevier, 2024, pp. 693–709. doi: 10.1016/B978-0-323-96020-5.00077-7.
- [45] Leonard, LaVerne, ‘Sterilization - Tough on Germs, Tough on Plastics, too’, doczz.net. Accessed: Mar. 14, 2025. [Online]. Available: <https://doczz.net/doc/7551595/sterilization---tough-on-germs--tough-on-plastics--too>
- [46] McKeen, L, ‘The Effect of Sterilization on Plastics and Elastomers: Fourth Edition’, ResearchGate. Accessed: Mar. 14, 2025. [Online]. Available: https://www.researchgate.net/publication/329984794_The_Effect_of_Sterilization_on_Plastics_and_Elastomers_Fourth_Edition
- [47] K. Kokubo *et al.*, ‘Effects of increased surface coverage of polyvinylpyrrolidone over a polysulfone hemofilter membrane on permeability and cell adhesion during continuous hemofiltration’, *J Artif Organs*, vol. 18, no. 3, pp. 257–263, Sept. 2015, doi: 10.1007/s10047-015-0826-0.
- [48] Y. Kurihara *et al.*, ‘In vitro evaluation of the platelet adhesion and interferon- γ production capacity of mononuclear cells coming in contact with a hydrophilic polymer-embedded polysulfone dialyzer’, *Renal Replacement Therapy*, vol. 10, no. 1, p. 28, Apr. 2024, doi: 10.1186/s41100-024-00542-2.
- [49] R. Podgórski *et al.*, ‘Different Strategies for Modifying Polycarbonate Membranes to Control Cell Adhesion’, *BioNanoSci.*, vol. 15, no. 3, p. 388, June 2025, doi: 10.1007/s12668-025-01993-5.

- [50] F. D. Al-Shalawi *et al.*, ‘Biomaterials as Implants in the Orthopedic Field for Regenerative Medicine: Metal versus Synthetic Polymers’, *Polymers*, vol. 15, no. 12, Art. no. 12, Jan. 2023, doi: 10.3390/polym15122601.
- [51] S. Jacob, A. B. Nair, J. Shah, N. Sreeharsha, S. Gupta, and P. Shinu, ‘Emerging Role of Hydrogels in Drug Delivery Systems, Tissue Engineering and Wound Management’, *Pharmaceutics*, vol. 13, no. 3, Art. no. 3, Mar. 2021, doi: 10.3390/pharmaceutics13030357.
- [52] R. Ma and D. Guo, ‘Evaluating the bioactivity of a hydroxyapatite-incorporated polyetheretherketone biocomposite’, *Journal of Orthopaedic Surgery and Research*, vol. 14, no. 1, p. 32, Jan. 2019, doi: 10.1186/s13018-019-1069-1.
- [53] S. Cai, C. Wu, W. Yang, W. Liang, H. Yu, and L. Liu, ‘Recent advance in surface modification for regulating cell adhesion and behaviors’, *Nanotechnology Reviews*, vol. 9, no. 1, pp. 971–989, Jan. 2020, doi: 10.1515/ntrev-2020-0076.
- [54] S. Hirohashi and Y. Kanai, ‘Cell adhesion system and human cancer morphogenesis’, *Cancer Sci*, vol. 94, no. 7, pp. 575–581, July 2003, doi: 10.1111/j.1349-7006.2003.tb01485.x.
- [55] T. Okegawa, R.-C. Pong, Y. Li, and J.-T. Hsieh, ‘The role of cell adhesion molecule in cancer progression and its application in cancer therapy’, *Acta Biochim Pol*, vol. 51, no. 2, pp. 445–457, 2004.
- [56] Z. Szekanecz and A. E. Koch, ‘Cell-cell interactions in synovitis. Endothelial cells and immune cell migration’, *Arthritis Res*, vol. 2, no. 5, pp. 368–373, 2000, doi: 10.1186/ar114.
- [57] H. Perinpanayagam, R. Zaharias, C. Stanford, R. Brand, J. Keller, and G. Schneider, ‘Early cell adhesion events differ between osteoporotic and non-osteoporotic osteoblasts’, *J Orthop Res*, vol. 19, no. 6, pp. 993–1000, Nov. 2001, doi: 10.1016/S0736-0266(01)00045-6.
- [58] S. I. Simon and C. E. Green, ‘Molecular Mechanics and Dynamics of Leukocyte Recruitment During Inflammation’, *Annual Review of Biomedical Engineering*, vol. 7, no. Volume 7, 2005, pp. 151–185, Aug. 2005, doi: 10.1146/annurev.bioeng.7.060804.100423.
- [59] C. N. Serhan and J. Savill, ‘Resolution of inflammation: the beginning programs the end’, *Nat Immunol*, vol. 6, no. 12, pp. 1191–1197, Dec. 2005, doi: 10.1038/ni1276.
- [60] A. A. Khalili and M. R. Ahmad, ‘A Review of Cell Adhesion Studies for Biomedical and Biological Applications’, *International Journal of Molecular Sciences*, vol. 16, no. 8, Art. no. 8, Aug. 2015, doi: 10.3390/ijms160818149.
- [61] J. Mitchell and K. W.-H. Lo, ‘The Use of Small-Molecule Compounds for Cell Adhesion and Migration in Regenerative Medicine’, *Biomedicines*, vol. 11, no. 9, Art. no. 9, Sept. 2023, doi: 10.3390/biomedicines11092507.
- [62] W. Wu *et al.*, ‘Advances in biomaterials for preventing tissue adhesion’, *Journal of Controlled Release*, vol. 261, pp. 318–336, Sept. 2017, doi: 10.1016/j.jconrel.2017.06.020.

- [63] F. L. Graham, J. Smiley, W. C. Russell, and R. Nairn, 'Characteristics of a human cell line transformed by DNA from human adenovirus type 5', *J Gen Virol*, vol. 36, no. 1, pp. 59–74, July 1977, doi: 10.1099/0022-1317-36-1-59.
- [64] A. Garnier, J. Côté, I. Nadeau, A. Kamen, and B. Massie, 'Scale-up of the adenovirus expression system for the production of recombinant protein in human 293S cells', *Cytotechnology*, vol. 15, no. 1–3, pp. 145–155, 1994, doi: 10.1007/BF00762389.
- [65] O.-W. Merten, 'Advances in cell culture: anchorage dependence', *Philosophical Transactions of the Royal Society B: Biological Sciences*, vol. 370, no. 1661, p. 20140040, Feb. 2015, doi: 10.1098/rstb.2014.0040.
- [66] M. Malm *et al.*, 'Evolution from adherent to suspension: systems biology of HEK293 cell line development', *Sci Rep*, vol. 10, p. 18996, Nov. 2020, doi: 10.1038/s41598-020-76137-8.
- [67] V. Dill, F. Pfaff, A. Zimmer, M. Beer, and M. Eschbaumer, 'Adherent and suspension baby hamster kidney cells have a different cytoskeleton and surface receptor repertoire', *PLoS One*, vol. 16, no. 6, p. e0246610, June 2021, doi: 10.1371/journal.pone.0246610.
- [68] J. Yayan, K.-J. Franke, M. Berger, W. Windisch, and K. Rasche, 'Adhesion, metastasis, and inhibition of cancer cells: a comprehensive review', *Mol Biol Rep*, vol. 51, no. 1, p. 165, 2024, doi: 10.1007/s11033-023-08920-5.
- [69] L. J. Dooling, K. Saini, A. A. Anlaş, and D. E. Discher, 'Tissue mechanics coevolves with fibrillar matrisomes in healthy and fibrotic tissues', *Matrix Biol*, vol. 111, pp. 153–188, Aug. 2022, doi: 10.1016/j.matbio.2022.06.006.
- [70] J. D. Humphrey, E. R. Dufresne, and M. A. Schwartz, 'Mechanotransduction and extracellular matrix homeostasis', *Nat Rev Mol Cell Biol*, vol. 15, no. 12, pp. 802–812, Dec. 2014, doi: 10.1038/nrm3896.
- [71] K. M. Yamada *et al.*, 'Extracellular matrix dynamics in cell migration, invasion and tissue morphogenesis', *International Journal of Experimental Pathology*, vol. 100, no. 3, pp. 144–152, 2019, doi: 10.1111/iep.12329.
- [72] N. K. Karamanos, A. D. Theocharis, T. Neill, and R. V. Iozzo, 'Matrix modeling and remodeling: A biological interplay regulating tissue homeostasis and diseases', *Matrix Biology*, vol. 75–76, pp. 1–11, Jan. 2019, doi: 10.1016/j.matbio.2018.08.007.
- [73] A. Naba, 'Mechanisms of assembly and remodelling of the extracellular matrix', *Nat Rev Mol Cell Biol*, vol. 25, no. 11, pp. 865–885, Nov. 2024, doi: 10.1038/s41580-024-00767-3.
- [74] S. Tadimalla, M. C. Tourell, R. Knott, and K. I. Momot, 'Quantifying collagen fibre architecture in articular cartilage using small-angle X-ray scattering', *Biomedical Spectroscopy and Imaging*, vol. 6, no. 1–2, pp. 37–57, Jan. 2017, doi: 10.3233/BSI-170164.
- [75] F. Horkay and P. J. Bassar, 'Osmotic Properties of Cartilage', Nov. 2016, doi: 10.1039/9781782623663-00044.
- [76] S. Pompili, G. Latella, E. Gaudio, R. Sferra, and A. Vetuschi, 'The Charming World of the Extracellular Matrix: A Dynamic and Protective

- Network of the Intestinal Wall', *Front. Med.*, vol. 8, Apr. 2021, doi: 10.3389/fmed.2021.610189.
- [77] R. Hallmann, N. Horn, M. Selg, O. Wendler, F. Pausch, and L. M. Sorokin, 'Expression and Function of Laminins in the Embryonic and Mature Vasculature', *Physiological Reviews*, vol. 85, no. 3, pp. 979–1000, July 2005, doi: 10.1152/physrev.00014.2004.
- [78] R. O. Hynes and A. Naba, 'Overview of the Matrisome—An Inventory of Extracellular Matrix Constituents and Functions', *Cold Spring Harb Perspect Biol*, vol. 4, no. 1, p. a004903, Jan. 2012, doi: 10.1101/cshperspect.a004903.
- [79] S. Ricard-Blum, 'The Collagen Family', *Cold Spring Harb Perspect Biol*, vol. 3, no. 1, p. a004978, Jan. 2011, doi: 10.1101/cshperspect.a004978.
- [80] P. J. McKeown-Longo and D. F. Mosher, 'Interaction of the 70,000-mol-wt amino-terminal fragment of fibronectin with the matrix-assembly receptor of fibroblasts', *J Cell Biol*, vol. 100, no. 2, pp. 364–374, Feb. 1985, doi: 10.1083/jcb.100.2.364.
- [81] F. J. Fogerty and D. F. Mosher, 'Mechanisms for organization of fibronectin matrix', *Cell Differentiation and Development*, vol. 32, no. 3, pp. 439–450, Dec. 1990, doi: 10.1016/0922-3371(90)90061-Z.
- [82] Y. Mao and J. E. Schwarzbauer, 'Fibronectin fibrillogenesis, a cell-mediated matrix assembly process', *Matrix Biology*, vol. 24, no. 6, pp. 389–399, Sept. 2005, doi: 10.1016/j.matbio.2005.06.008.
- [83] W. S. To and K. S. Midwood, 'Plasma and cellular fibronectin: distinct and independent functions during tissue repair', *Fibrogenesis & Tissue Repair*, vol. 4, no. 1, p. 21, Sept. 2011, doi: 10.1186/1755-1536-4-21.
- [84] D. E. Ingber, 'Mechanical signaling and the cellular response to extracellular matrix in angiogenesis and cardiovascular physiology', *Circ Res*, vol. 91, no. 10, pp. 877–887, Nov. 2002, doi: 10.1161/01.res.0000039537.73816.e5.
- [85] M. J. P. Biggs, R. G. Richards, S. McFarlane, C. D. W. Wilkinson, R. O. C. Oreffo, and M. J. Dalby, 'Adhesion formation of primary human osteoblasts and the functional response of mesenchymal stem cells to 330nm deep microgrooves', *J R Soc Interface*, vol. 5, no. 27, pp. 1231–1242, Oct. 2008, doi: 10.1098/rsif.2008.0035.
- [86] J. T. Parsons, A. R. Horwitz, and M. A. Schwartz, 'Cell adhesion: integrating cytoskeletal dynamics and cellular tension', *Nat Rev Mol Cell Biol*, vol. 11, no. 9, pp. 633–643, Sept. 2010, doi: 10.1038/nrm2957.
- [87] R. Zaidel-Bar, C. Ballestrem, Z. Kam, and B. Geiger, 'Early molecular events in the assembly of matrix adhesions at the leading edge of migrating cells', *J Cell Sci*, vol. 116, no. Pt 22, pp. 4605–4613, Nov. 2003, doi: 10.1242/jcs.00792.
- [88] A. Bershadsky, M. Kozlov, and B. Geiger, 'Adhesion-mediated mechanosensitivity: a time to experiment, and a time to theorize', *Current Opinion in Cell Biology*, vol. 18, no. 5, pp. 472–481, Oct. 2006, doi: 10.1016/j.ceb.2006.08.012.

- [89] K. Anselme, L. Ploux, and A. Ponche, 'Cell/Material Interfaces: Influence of Surface Chemistry and Surface Topography on Cell Adhesion', *Journal of Adhesion Science and Technology*, vol. 24, no. 5, pp. 831–852, Jan. 2010, doi: 10.1163/016942409X12598231568186.
- [90] J. Luo, M. Walker, Y. Xiao, H. Donnelly, M. J. Dalby, and M. Salmeron-Sanchez, 'The influence of nanotopography on cell behaviour through interactions with the extracellular matrix – A review', *Bioact Mater*, vol. 15, pp. 145–159, Dec. 2021, doi: 10.1016/j.bioactmat.2021.11.024.
- [91] C. J. Wilson, R. E. Clegg, D. I. Leavesley, and M. J. Percy, 'Mediation of biomaterial-cell interactions by adsorbed proteins: a review', *Tissue Eng*, vol. 11, no. 1–2, pp. 1–18, 2005, doi: 10.1089/ten.2005.11.1.
- [92] A. G. Harvey, E. W. Hill, and A. Bayat, 'Designing implant surface topography for improved biocompatibility', *Expert Rev Med Devices*, vol. 10, no. 2, pp. 257–267, Mar. 2013, doi: 10.1586/erd.12.82.
- [93] A. M. Ross, Z. Jiang, M. Bastmeyer, and J. Lahann, 'Physical Aspects of Cell Culture Substrates: Topography, Roughness, and Elasticity', *Small*, vol. 8, no. 3, pp. 336–355, 2012, doi: 10.1002/sml.201100934.
- [94] M. Dashti and A. Albannai, 'A Review on Surface Roughness (Ra) Ranges for Some Finishing Processes', vol. 11, no. 4, 2020.
- [95] M. Bigerelle, K. Anselme, B. Noël, I. Ruderman, P. Hardouin, and A. Iost, 'Improvement in the morphology of Ti-based surfaces: a new process to increase in vitro human osteoblast response', *Biomaterials*, vol. 23, no. 7, pp. 1563–1577, Apr. 2002, doi: 10.1016/S0142-9612(01)00271-X.
- [96] O. Zinger *et al.*, 'Time-dependent morphology and adhesion of osteoblastic cells on titanium model surfaces featuring scale-resolved topography', *Biomaterials*, vol. 25, no. 14, pp. 2695–2711, June 2004, doi: 10.1016/j.biomaterials.2003.09.111.
- [97] T. Mays, 'A new classification of pore sizes', *Studies in Surface Science and Catalysis - STUD SURF SCI CATAL*, vol. 160, pp. 57–62, Dec. 2007, doi: 10.1016/S0167-2991(07)80009-7.
- [98] C. M. Murphy, G. P. Duffy, A. Schindeler, and F. J. O'Brien, 'Effect of collagen-glycosaminoglycan scaffold pore size on matrix mineralization and cellular behavior in different cell types', *J Biomed Mater Res A*, vol. 104, no. 1, pp. 291–304, Jan. 2016, doi: 10.1002/jbm.a.35567.
- [99] C. M. Murphy, M. G. Haugh, and F. J. O'Brien, 'The effect of mean pore size on cell attachment, proliferation and migration in collagen-glycosaminoglycan scaffolds for bone tissue engineering', *Biomaterials*, vol. 31, no. 3, pp. 461–466, Jan. 2010, doi: 10.1016/j.biomaterials.2009.09.063.
- [100] S. J. Lee, J. S. Choi, K. S. Park, G. Khang, Y. M. Lee, and H. B. Lee, 'Response of MG63 osteoblast-like cells onto polycarbonate membrane surfaces with different micropore sizes', *Biomaterials*, vol. 25, no. 19, pp. 4699–4707, Aug. 2004, doi: 10.1016/j.biomaterials.2003.11.034.

- [101] A. Padhi and A. S. Nain, 'ECM in Differentiation: A Review of Matrix Structure, Composition and Mechanical Properties', *Ann Biomed Eng*, vol. 48, no. 3, pp. 1071–1089, Mar. 2020, doi: 10.1007/s10439-019-02337-7.
- [102] K. H. Vining and D. J. Mooney, 'Mechanical forces direct stem cell behaviour in development and regeneration', *Nat Rev Mol Cell Biol*, vol. 18, no. 12, pp. 728–742, Dec. 2017, doi: 10.1038/nrm.2017.108.
- [103] T. Yeung *et al.*, 'Effects of substrate stiffness on cell morphology, cytoskeletal structure, and adhesion', *Cell Motil Cytoskeleton*, vol. 60, no. 1, pp. 24–34, Jan. 2005, doi: 10.1002/cm.20041.
- [104] V. Vogel and M. Sheetz, 'Local force and geometry sensing regulate cell functions', *Nat Rev Mol Cell Biol*, vol. 7, no. 4, pp. 265–275, Apr. 2006, doi: 10.1038/nrm1890.
- [105] S. J. P. Callens *et al.*, 'Emergent collective organization of bone cells in complex curvature fields', *Nat Commun*, vol. 14, no. 1, p. 855, Mar. 2023, doi: 10.1038/s41467-023-36436-w.
- [106] L.-C. Sang and M.-O. Coppens, 'Effects of surface curvature and surface chemistry on the structure and activity of proteins adsorbed in nanopores', *Phys. Chem. Chem. Phys.*, vol. 13, no. 14, pp. 6689–6698, Apr. 2011, doi: 10.1039/C0CP02273J.
- [107] P. Roach, D. Farrar, and C. C. Perry, 'Interpretation of protein adsorption: surface-induced conformational changes', *J Am Chem Soc*, vol. 127, no. 22, pp. 8168–8173, June 2005, doi: 10.1021/ja042898o.
- [108] S. Mitra, 'Protein Adsorption on Biomaterial Surfaces: Subsequent Conformational and Biological Consequences -A Review', *Journal of Surface Science and Technology*, vol. 36, pp. 7–38, June 2020, doi: 10.18311/jsst/2020/23282.
- [109] B. G. Keselowsky, D. M. Collard, and A. J. García, 'Integrin binding specificity regulates biomaterial surface chemistry effects on cell differentiation', *Proc Natl Acad Sci U S A*, vol. 102, no. 17, pp. 5953–5957, Apr. 2005, doi: 10.1073/pnas.0407356102.
- [110] M. Bergkvist, J. Carlsson, and S. Oscarsson, 'Surface-dependent conformations of human plasma fibronectin adsorbed to silica, mica, and hydrophobic surfaces, studied with use of Atomic Force Microscopy', *J Biomed Mater Res A*, vol. 64, no. 2, pp. 349–356, Feb. 2003, doi: 10.1002/jbm.a.10423.
- [111] J. I. Rosales-Leal *et al.*, 'Effect of roughness, wettability and morphology of engineered titanium surfaces on osteoblast-like cell adhesion', *Colloids and Surfaces A: Physicochemical and Engineering Aspects*, vol. 365, no. 1, pp. 222–229, Aug. 2010, doi: 10.1016/j.colsurfa.2009.12.017.
- [112] G. Giridhar, R. K. N. R. Manepalli, and G. Apparao, 'Chapter 8 - Contact Angle Measurement Techniques for Nanomaterials', in *Thermal and Rheological Measurement Techniques for Nanomaterials Characterization*, S. Thomas, R. Thomas, A. K. Zachariah, and R. K. Mishra, Eds, Elsevier, 2017, pp. 173–195. doi: 10.1016/B978-0-323-46139-9.00008-6.

- [113] J. Wei *et al.*, ‘Adhesion of mouse fibroblasts on hexamethyldisiloxane surfaces with wide range of wettability’, *Journal of Biomedical Materials Research Part B: Applied Biomaterials*, vol. 81B, no. 1, pp. 66–75, 2007, doi: 10.1002/jbm.b.30638.
- [114] N. J. Hallab, K. J. Bundy, K. O’Connor, R. L. Moses, and J. J. Jacobs, ‘Evaluation of metallic and polymeric biomaterial surface energy and surface roughness characteristics for directed cell adhesion’, *Tissue Eng*, vol. 7, no. 1, pp. 55–71, Feb. 2001, doi: 10.1089/107632700300003297.
- [115] B. Majhy, P. Priyadarshini, and A. K. Sen, ‘Effect of surface energy and roughness on cell adhesion and growth – facile surface modification for enhanced cell culture’, *RSC Adv.*, vol. 11, no. 25, pp. 15467–15476, Apr. 2021, doi: 10.1039/D1RA02402G.
- [116] M. Aramesh, O. Shimoni, K. Ostrikov, S. Praver, and J. Cervenka, ‘Surface charge effects in protein adsorption on nanodiamonds’, *Nanoscale*, vol. 7, no. 13, pp. 5726–5736, Mar. 2015, doi: 10.1039/C5NR00250H.
- [117] M. R. Bet, G. Goissis, S. Vargas, and H. S. Selistre-de-Araujo, ‘Cell adhesion and cytotoxicity studies over polyanionic collagen surfaces with variable negative charge and wettability’, *Biomaterials*, vol. 24, no. 1, pp. 131–137, Jan. 2003, doi: 10.1016/s0142-9612(02)00270-3.
- [118] D. Ujino, H. Nishizaki, S. Higuchi, S. Komasa, and J. Okazaki, ‘Effect of Plasma Treatment of Titanium Surface on Biocompatibility’, *Applied Sciences*, vol. 9, no. 11, Art. no. 11, Jan. 2019, doi: 10.3390/app9112257.
- [119] M. Ouyang, C. Yuan, R. J. Muisener, A. Boulares, and J. T. Koberstein, ‘Conversion of Some Siloxane Polymers to Silicon Oxide by UV/Ozone Photochemical Processes’, *Chem. Mater.*, vol. 12, no. 6, pp. 1591–1596, June 2000, doi: 10.1021/cm990770d.
- [120] M. T. Khorasani and H. Mirzadeh, ‘Laser surface modification of silicone rubber to reduce platelet adhesion in vitro’, *J Biomater Sci Polym Ed*, vol. 15, no. 1, pp. 59–72, 2004, doi: 10.1163/156856204322752237.
- [121] S. Roh, Y. Jang, J. Yoo, and H. Seong, ‘Surface Modification Strategies for Biomedical Applications: Enhancing Cell–Biomaterial Interfaces and Biochip Performances’, *BioChip J*, vol. 17, no. 2, pp. 174–191, June 2023, doi: 10.1007/s13206-023-00104-4.
- [122] T. Jacobs, R. Morent, N. De Geyter, P. Dubruel, and C. Leys, ‘Plasma Surface Modification of Biomedical Polymers: Influence on Cell-Material Interaction’, *Plasma Chem Plasma Process*, vol. 32, no. 5, pp. 1039–1073, Oct. 2012, doi: 10.1007/s11090-012-9394-8.
- [123] T. I. Croll, A. J. O’Connor, G. W. Stevens, and J. J. Cooper-White, ‘Controllable surface modification of poly(lactic-co-glycolic acid) (PLGA) by hydrolysis or aminolysis I: physical, chemical, and theoretical aspects’, *Biomacromolecules*, vol. 5, no. 2, pp. 463–473, 2004, doi: 10.1021/bm0343040.
- [124] Y.-P. Jiao and F.-Z. Cui, ‘Surface modification of polyester biomaterials for tissue engineering’, *Biomed. Mater.*, vol. 2, no. 4, p. R24, Nov. 2007, doi: 10.1088/1748-6041/2/4/R02.

- [125] A. Bogaerts, E. Neyts, R. Gijbels, and J. van der Mullen, 'Gas discharge plasmas and their applications', *Spectrochimica Acta Part B: Atomic Spectroscopy*, vol. 57, no. 4, pp. 609–658, Apr. 2002, doi: 10.1016/S0584-8547(01)00406-2.
- [126] F. S. Denes and S. Manolache, 'Macromolecular plasma-chemistry: an emerging field of polymer science', *Progress in Polymer Science*, vol. 29, no. 8, pp. 815–885, Aug. 2004, doi: 10.1016/j.progpolymsci.2004.05.001.
- [127] W. Liu *et al.*, 'Effects of plasma treatment to nanofibers on initial cell adhesion and cell morphology', *Colloids and Surfaces B: Biointerfaces*, vol. 113, pp. 101–106, Jan. 2014, doi: 10.1016/j.colsurfb.2013.08.031.
- [128] N. De Geyter, R. Morent, C. Leys, L. Gengembre, and E. Payen, 'Treatment of polymer films with a dielectric barrier discharge in air, helium and argon at medium pressure', *Surface and Coatings Technology*, vol. 201, no. 16, pp. 7066–7075, May 2007, doi: 10.1016/j.surfcoat.2007.01.008.
- [129] J. Nakamatsu, Delgado-Aparicio, Luis F., Da Silva, Rafael, and F. and Soberon, 'Ageing of plasma-treated poly(tetrafluoroethylene) surfaces', *Journal of Adhesion Science and Technology*, vol. 13, no. 7, pp. 753–761, Jan. 1999, doi: 10.1163/156856199X00983.
- [130] N. De Geyter, R. Morent, and C. Leys, 'Influence of ambient conditions on the ageing behaviour of plasma-treated PET surfaces', *Nuclear Instruments and Methods in Physics Research Section B: Beam Interactions with Materials and Atoms*, vol. 266, no. 12, pp. 3086–3090, June 2008, doi: 10.1016/j.nimb.2008.03.167.
- [131] R. Morent, N. De Geyter, and C. Leys, 'Effects of operating parameters on plasma-induced PET surface treatment', *Nuclear Instruments and Methods in Physics Research Section B: Beam Interactions with Materials and Atoms*, vol. 266, no. 12, pp. 3081–3085, June 2008, doi: 10.1016/j.nimb.2008.03.166.
- [132] P. Thevenot, W. Hu, and L. Tang, 'SURFACE CHEMISTRY INFLUENCE IMPLANT BIOCOMPATIBILITY', *Curr Top Med Chem*, vol. 8, no. 4, pp. 270–280, 2008, Accessed: Feb. 02, 2025. [Online]. Available: <https://www.ncbi.nlm.nih.gov/pmc/articles/PMC3230929/>
- [133] N. Sinyavsky and I. Korneva, 'Study of Optical Properties of Polymeric Materials Subjected to Degradation', *J Polym Environ*, vol. 25, no. 4, pp. 1280–1287, Dec. 2017, doi: 10.1007/s10924-016-0908-y.
- [134] M. Curcic *et al.*, 'Plasma, Uv Radiation and Ozone for Microplastics Degradation: Optical Characterization of Polystyrene, Polyethylene and Polypropylene Degradation Using Ftir and Raman Spectroscopy', Oct. 02, 2024, *Social Science Research Network, Rochester, NY*: 4974167. doi: 10.2139/ssrn.4974167.
- [135] T. Goda, R. Matsuno, T. Konno, M. Takai, and K. Ishihara, 'Photografting of 2-methacryloyloxyethyl phosphorylcholine from polydimethylsiloxane: tunable protein repellency and lubrication property', *Colloids Surf B Biointerfaces*, vol. 63, no. 1, pp. 64–72, May 2008, doi: 10.1016/j.colsurfb.2007.11.014.

- [136] C. Tomba, C. Migdal, D. Fuard, C. Villard, and A. Nicolas, ‘Poly-l-lysine/Laminin Surface Coating Reverses Glial Cell Mechanosensitivity on Stiffness-Patterned Hydrogels’, *ACS Appl. Bio Mater.*, vol. 5, no. 4, pp. 1552–1563, Apr. 2022, doi: 10.1021/acsabm.1c01295.
- [137] Y. H. Kim, N. S. Baek, Y. H. Han, M.-A. Chung, and S.-D. Jung, ‘Enhancement of neuronal cell adhesion by covalent binding of poly-d-lysine’, *Journal of Neuroscience Methods*, vol. 202, no. 1, pp. 38–44, Oct. 2011, doi: 10.1016/j.jneumeth.2011.08.036.
- [138] G. M. Whitesides, ‘The origins and the future of microfluidics’, *Nature*, vol. 442, no. 7101, pp. 368–373, July 2006, doi: 10.1038/nature05058.
- [139] D. J. Beebe, G. A. Mensing, and G. M. Walker, ‘Physics and applications of microfluidics in biology’, *Annu Rev Biomed Eng*, vol. 4, pp. 261–286, 2002, doi: 10.1146/annurev.bioeng.4.112601.125916.
- [140] D. Huh, G. A. Hamilton, and D. E. Ingber, ‘From 3D cell culture to organs-on-chips’, *Trends in Cell Biology*, vol. 21, no. 12, pp. 745–754, Dec. 2011, doi: 10.1016/j.tcb.2011.09.005.
- [141] P. Pattanayak *et al.*, ‘Microfluidic chips: recent advances, critical strategies in design, applications and future perspectives’, *Microfluid Nanofluid*, vol. 25, no. 12, p. 99, Oct. 2021, doi: 10.1007/s10404-021-02502-2.
- [142] G. Minas, ‘Lab-on-a-Chip Devices for Chemical Analysis’, in *Encyclopedia of Microfluidics and Nanofluidics*, D. Li, Ed., Boston, MA: Springer US, 2008, pp. 910–927. doi: 10.1007/978-0-387-48998-8_774.
- [143] P. Parthasarathy and M. Venkatesh, ‘Developments in Microfluidic Integrated Lab-on-Chip Devices for DNA Biosensing Towards Unifying the Emergence of Nanobiosensor’, *Biomedical Materials & Devices*, Nov. 2024, doi: 10.1007/s44174-024-00257-2.
- [144] S. Surappa *et al.*, ‘Integrated “lab-on-a-chip” microfluidic systems for isolation, enrichment, and analysis of cancer biomarkers’, *Lab Chip*, vol. 23, no. 13, pp. 2942–2958, June 2023, doi: 10.1039/D2LC01076C.
- [145] K. Ronaldson-Bouchard and G. Vunjak-Novakovic, ‘Organs-on-a-Chip: A Fast Track for Engineered Human Tissues in Drug Development’, *Cell Stem Cell*, vol. 22, no. 3, pp. 310–324, Mar. 2018, doi: 10.1016/j.stem.2018.02.011.
- [146] A. T. Young, K. R. Rivera, P. D. Erb, and M. A. Daniele, ‘Monitoring of Microphysiological Systems: Integrating Sensors and Real-Time Data Analysis toward Autonomous Decision-Making’, *ACS Sens*, vol. 4, no. 6, pp. 1454–1464, June 2019, doi: 10.1021/acssensors.8b01549.
- [147] E. Ferrari, C. Palma, S. Vesentini, P. Occhetta, and M. Rasponi, ‘Integrating Biosensors in Organs-on-Chip Devices: A Perspective on Current Strategies to Monitor Microphysiological Systems’, *Biosensors*, vol. 10, no. 9, Art. no. 9, Sept. 2020, doi: 10.3390/bios10090110.
- [148] P. Loskill, S. G. Marcus, A. Mathur, W. M. Reese, and K. E. Healy, ‘ μ Organo: A Lego®-Like Plug & Play System for Modular Multi-Organ-Chips’, *PLOS ONE*, vol. 10, no. 10, p. e0139587, Oct. 2015, doi: 10.1371/journal.pone.0139587.

- [149] M. Jang and H. N. Kim, 'From Single- to Multi-organ-on-a-Chip System for Studying Metabolic Diseases', *BioChip J*, vol. 17, no. 2, pp. 133–146, June 2023, doi: 10.1007/s13206-023-00098-z.
- [150] J. Bai and C. Wang, 'Organoids and Microphysiological Systems: New Tools for Ophthalmic Drug Discovery', *Front. Pharmacol.*, vol. 11, Apr. 2020, doi: 10.3389/fphar.2020.00407.
- [151] A. R. Atif, 'Evaluation of Biological Biomaterial Properties using Microfluidic Systems', *Acta Universitatis Upsaliensis*, 2023. Accessed: Mar. 28, 2025. [Online]. Available: <https://urn.kb.se/resolve?urn=urn:nbn:se:uu:diva-497537>
- [152] M. Pinti, T. Kambham, B. Wang, and S. Prakash, 'Fabrication of Centimeter Long, Ultra-Low Aspect Ratio Nanochannel Networks in Borosilicate Glass Substrates', *Journal of Nanotechnology in Engineering and Medicine*, vol. 4, no. 020905, Oct. 2013, doi: 10.1115/1.4025366.
- [153] Y. Xu and B. Xu, 'An Integrated Glass Nanofluidic Device Enabling In-situ Electrokinetic Probing of Water Confined in a Single Nanochannel under Pressure-Driven Flow Conditions', *Small*, vol. 11, no. 46, pp. 6165–6171, 2015, doi: 10.1002/sml.201502125.
- [154] S. Prakash, M. Pinti, and B. Bhushan, 'Theory, fabrication and applications of microfluidic and nanofluidic biosensors', *Philosophical Transactions of the Royal Society A: Mathematical, Physical and Engineering Sciences*, vol. 370, no. 1967, pp. 2269–2303, May 2012, doi: 10.1098/rsta.2011.0498.
- [155] H. C. Jung, W. Lu, S. Wang, L. J. Lee, and X. Hu, 'Etching of Pyrex glass substrates by inductively coupled plasma reactive ion etching for micro/nanofluidic devices', *Journal of Vacuum Science & Technology B: Microelectronics and Nanometer Structures Processing, Measurement, and Phenomena*, vol. 24, no. 6, pp. 3162–3164, Dec. 2006, doi: 10.1116/1.2388959.
- [156] Y. Yalikun, Y. Hosokawa, T. Iino, and Y. Tanaka, 'An all-glass 12 μm ultra-thin and flexible micro-fluidic chip fabricated by femtosecond laser processing', *Lab Chip*, vol. 16, no. 13, pp. 2427–2433, June 2016, doi: 10.1039/C6LC00132G.
- [157] Y. Han, Z. Jiao, J. Zhao, Z. Chao, and Z. You, 'A simple approach to fabricate multi-layer glass microfluidic chips based on laser processing and thermocompression bonding', *Microfluid Nanofluid*, vol. 25, no. 9, p. 77, Aug. 2021, doi: 10.1007/s10404-021-02479-y.
- [158] X. Chen, T. Li, and Q. Gao, 'A novel method for rapid fabrication of PMMA microfluidic chip by laser cutting and sealing integration', *Surface Review and Letters*, vol. 26, Sept. 2018, doi: 10.1142/S0218625X19500422.
- [159] K. T. L. Trinh, D. A. Thai, W. R. Chae, and N. Y. Lee, 'Rapid Fabrication of Poly(methyl methacrylate) Devices for Lab-on-a-Chip Applications Using Acetic Acid and UV Treatment', *ACS Omega*, vol. 5, no. 28, pp. 17396–17404, July 2020, doi: 10.1021/acsomega.0c01770.

- [160] J. Y. Shin, J. Y. Park, C. Liu, J. He, and S. C. Kim, ‘Chemical structure and physical properties of cyclic olefin copolymers (IUPAC Technical Report)’, *Pure and Applied Chemistry*, vol. 77, no. 5, pp. 801–814, Jan. 2005, doi: 10.1351/pac200577050801.
- [161] M. Rahimnejad *et al.*, ‘Engineered Biomimetic Membranes for Organ-on-a-Chip’, *ACS Biomater Sci Eng*, vol. 8, no. 12, pp. 5038–5059, Dec. 2022, doi: 10.1021/acsbiomaterials.2c00531.
- [162] A. W. Auner, K. M. Tasneem, D. A. Markov, L. J. McCawley, and M. S. Hutson, ‘Chemical-PDMS binding kinetics and implications for bioavailability in microfluidic devices’, *Lab Chip*, vol. 19, no. 5, pp. 864–874, Feb. 2019, doi: 10.1039/C8LC00796A.
- [163] T. C. Merkel, V. I. Bondar, K. Nagai, B. D. Freeman, and I. Pinnau, ‘Gas sorption, diffusion, and permeation in poly(dimethylsiloxane)’, *Journal of Polymer Science Part B: Polymer Physics*, vol. 38, no. 3, pp. 415–434, 2000, doi: 10.1002/(SICI)1099-0488(20000201)38:3%3C415::AID-POLB8%3E3.0.CO;2-Z.
- [164] S. Hemmilä, J. V. Cauich-Rodríguez, J. Kreutzer, and P. Kallio, ‘Rapid, simple, and cost-effective treatments to achieve long-term hydrophilic PDMS surfaces’, *Applied Surface Science*, vol. 258, no. 24, pp. 9864–9875, Oct. 2012, doi: 10.1016/j.apsusc.2012.06.044.
- [165] M. Kalulu and R. Ngulube, ‘One-step Reversal Technique towards Hydrophilic Surface Modification of Polydimethylsiloxane-co-Polyurethane (PDMS-PU)’, *RDMS*, vol. 13, no. 4, pp. 1451–1459, July 2020, Accessed: Mar. 24, 2025. [Online]. Available: <https://crimsonpublishers.com/index.php>
- [166] K. Regehr *et al.*, ‘Biological implications of polydimethylsiloxane-based microfluidic cell culture’, *Lab on a chip*, vol. 9, pp. 2132–9, Sept. 2009, doi: 10.1039/b903043c.
- [167] M. W. Toepke and D. J. Beebe, ‘PDMS absorption of small molecules and consequences in microfluidic applications’, *Lab Chip*, vol. 6, no. 12, pp. 1484–1486, Dec. 2006, doi: 10.1039/b612140c.
- [168] K. Raj M and S. Chakraborty, ‘PDMS microfluidics: A mini review’, *Journal of Applied Polymer Science*, vol. 137, no. 27, p. 48958, 2020, doi: 10.1002/app.48958.
- [169] A. Paguirigan and D. Beebe, ‘From the cellular perspective: Exploring differences in the cellular baseline in macroscale and microfluidic cultures’, *Integrative biology : quantitative biosciences from nano to macro*, vol. 1, pp. 182–95, Feb. 2009, doi: 10.1039/b814565b.
- [170] F. Jia, Y. Gao, and H. Wang, ‘Recent Advances in Drug Delivery System Fabricated by Microfluidics for Disease Therapy’, *Bioengineering (Basel)*, vol. 9, no. 11, p. 625, Oct. 2022, doi: 10.3390/bioengineering9110625.
- [171] X. Su, E. W. K. Young, H. A. S. Underkofler, T. J. Kamp, C. T. January, and D. J. Beebe, ‘Microfluidic Cell Culture and Its Application in High-Throughput Drug Screening: Cardiotoxicity Assay for hERG Channels’, *J*

- Biomol Screen*, vol. 16, no. 1, pp. 101–111, Jan. 2011, doi: 10.1177/1087057110386218.
- [172] R. Gomez-Sjoberg, A. A. Leyrat, B. T. Houseman, K. Shokat, and S. R. Quake, ‘Biocompatibility and Reduced Drug Absorption of Sol–Gel-Treated Poly(dimethyl siloxane) for Microfluidic Cell Culture Applications’, *Anal. Chem.*, vol. 82, no. 21, pp. 8954–8960, Nov. 2010, doi: 10.1021/ac101870s.
- [173] H. Sasaki, H. Onoe, T. Osaki, R. Kawano, and S. Takeuchi, ‘Parylene-coating in PDMS microfluidic channels prevents the absorption of fluorescent dyes’, *Sensors and Actuators B: Chemical*, vol. 150, no. 1, pp. 478–482, Sept. 2010, doi: 10.1016/j.snb.2010.07.021.
- [174] H. Teng, ‘Overview of the Development of the Fluoropolymer Industry’, *Applied Sciences*, vol. 2, pp. 496–512, Dec. 2012, doi: 10.3390/app2020496.
- [175] C. F. Carlborg, T. Haraldsson, K. Öberg, M. Malkoch, and W. van der Wijngaart, ‘Beyond PDMS: off-stoichiometry thiol–ene (OSTE) based soft lithography for rapid prototyping of microfluidic devices’, *Lab Chip*, vol. 11, no. 18, pp. 3136–3147, Sept. 2011, doi: 10.1039/C1LC20388F.
- [176] C. E. Hoyle, A. B. Lowe, and C. N. Bowman, ‘Thiol-click chemistry: a multifaceted toolbox for small molecule and polymer synthesis’, *Chem. Soc. Rev.*, vol. 39, no. 4, pp. 1355–1387, Mar. 2010, doi: 10.1039/B901979K.
- [177] C. F. Carlborg, A. Vastesson, Y. Liu, W. van der Wijngaart, M. Johansson, and T. Haraldsson, ‘Functional off-stoichiometry thiol-ene-epoxy thermosets featuring temporally controlled curing stages via an UV/UV dual cure process’, *Journal of Polymer Science Part A: Polymer Chemistry*, vol. 52, no. 18, pp. 2604–2615, 2014, doi: 10.1002/pola.27276.
- [178] P. Aubrecht *et al.*, ‘Performance and biocompatibility of OSTEMER 322 in cell-based microfluidic applications’, *RSC Advances*, vol. 14, no. 6, pp. 3617–3635, 2024, doi: 10.1039/D3RA05789E.
- [179] S. Pérez-Rodríguez, J. M. García-Aznar, and J. Gonzalo-Asensio, ‘Microfluidic devices for studying bacterial taxis, drug testing and biofilm formation’, *Microb Biotechnol*, vol. 15, no. 2, pp. 395–414, Feb. 2022, doi: 10.1111/1751-7915.13775.
- [180] V. Narayanamurthy and M. M. S. Biomedical-Staff, ‘Microfluidic Microchannel (Size And Shape) for Single Cell Analysis by Numerical Optimization: Lateral Trapping Method’, *International Journal of Engineering and Advanced Technology (IJEAT)*, Jan. 2019, Accessed: Mar. 26, 2025. [Online]. Available: https://www.academia.edu/42353669/Microfluidic_Microchannel_Size_And_Shape_for_Single_Cell_Analysis_by_Numerical_Optimization_Lateral_Trapping_Method
- [181] I. Petruzzellis *et al.*, ‘Lab-on-Chip Systems for Cell Sorting: Main Features and Advantages of Inertial Focusing in Spiral Microchannels’,

- Micromachines (Basel)*, vol. 15, no. 9, p. 1135, Sept. 2024, doi: 10.3390/mi15091135.
- [182] E. W. K. Young and D. J. Beebe, 'Fundamentals of microfluidic cell culture in controlled microenvironments', *Chem. Soc. Rev.*, vol. 39, no. 3, pp. 1036–1048, Feb. 2010, doi: 10.1039/B909900J.
- [183] Chung, Henry H., Mireles, Marcela, Kwart, Bradley J., and Gaborski, Thomas R., 'Use of porous membranes in tissue barrier and co-culture models', *Lab on a Chip*, vol. 12, 2018. Accessed: Mar. 28, 2025. [Online]. Available: <https://pubs.rsc.org/en/content/articlelanding/2018/lc/c7lc01248a>
- [184] H. M. Eslam, F. Hataminia, H. Asadi-Saghandi, F. Fayazbakhsh, N. Tabatabaei, and H. Ghanbari, 'Characterization and numerical simulation of a new microfluidic device for studying cells-nanofibers interactions based on collagen/PET/PDMS composite', *Front. Lab Chip Technol.*, vol. 3, July 2024, doi: 10.3389/frlct.2024.1411171.
- [185] H. A. Stone, A. D. Stroock, and A. Ajdari, 'Engineering Flows in Small Devices: Microfluidics Toward a Lab-on-a-Chip', *Annual Review of Fluid Mechanics*, vol. 36, no. Volume 36, 2004, pp. 381–411, Jan. 2004, doi: 10.1146/annurev.fluid.36.050802.122124.
- [186] E. Verpoorte and N. F. De Rooij, 'Microfluidics meets MEMS', *Proceedings of the IEEE*, vol. 91, no. 6, pp. 930–953, June 2003, doi: 10.1109/JPROC.2003.813570.
- [187] N. Azizpour, R. Avazpour, D. H. Rosenzweig, M. Sawan, and A. Ajji, 'Evolution of Biochip Technology: A Review from Lab-on-a-Chip to Organ-on-a-Chip', *Micromachines (Basel)*, vol. 11, no. 6, p. 599, June 2020, doi: 10.3390/mi11060599.
- [188] J. Klespitz and L. Kovacs, 'Peristaltic pumps — A review on working and control possibilities', in *2014 IEEE 12th International Symposium on Applied Machine Intelligence and Informatics (SAMi)*, Herl'any, Slovakia: IEEE, Jan. 2014, pp. 191–194. doi: 10.1109/SAMI.2014.6822404.
- [189] I. Meyvantsson, J. W. Warrick, S. Hayes, A. Skoien, and D. J. Beebe, 'Automated cell culture in high density tubeless microfluidic device arrays', *Lab Chip*, vol. 8, no. 5, pp. 717–724, May 2008, doi: 10.1039/b715375a.
- [190] L.-J. Chen, W.-L. Wang, and J.-J. Chiu, 'Vascular Endothelial Mechanosensors in Response to Fluid Shear Stress', in *Molecular and Cellular Mechanobiology*, S. Chien, A. J. Engler, and P. Y. Wang, Eds, New York, NY: Springer, 2016, pp. 29–56. doi: 10.1007/978-1-4939-5617-3_2.
- [191] J. A. Espina, M. H. Cordeiro, M. Milivojevic, I. Pajić-Lijaković, and E. H. Barriga, 'Response of cells and tissues to shear stress', *Journal of Cell Science*, vol. 136, no. 18, p. jcs260985, Sept. 2023, doi: 10.1242/jcs.260985.

- [192] S. Chatterjee, ‘Endothelial Mechanotransduction, Redox Signaling and the Regulation of Vascular Inflammatory Pathways’, *Frontiers in Physiology*, vol. 9, June 2018, doi: 10.3389/fphys.2018.00524.
- [193] J. B. Dixon, S. T. Greiner, A. A. Gashev, G. L. Cote, J. E. MOORE Jr., and D. C. Zawieja, ‘Lymph Flow, Shear Stress, and Lymphocyte Velocity in Rat Mesenteric Prenodal Lymphatics’, *Microcirculation*, vol. 13, no. 7, pp. 597–610, 2006, doi: 10.1080/10739680600893909.
- [194] P. V. Hinton, K. J. Genoud, J. O. Early, F. J. O’Brien, and O. D. Kennedy, ‘Impact of Fluid Flow Shear Stress on Osteoblast Differentiation and Cross-Talk with Articular Chondrocytes’, *International Journal of Molecular Sciences*, vol. 23, no. 16, Art. no. 16, Jan. 2022, doi: 10.3390/ijms23169505.
- [195] S. Weinbaum, S. C. Cowin, and Y. Zeng, ‘A model for the excitation of osteocytes by mechanical loading-induced bone fluid shear stresses’, *Journal of Biomechanics*, vol. 27, no. 3, pp. 339–360, Mar. 1994, doi: 10.1016/0021-9290(94)90010-8.
- [196] H. S. Bevan *et al.*, ‘Acute laminar shear stress reversibly increases human glomerular endothelial cell permeability via activation of endothelial nitric oxide synthase’, *American Journal of Physiology-Renal Physiology*, vol. 301, no. 4, pp. F733–F742, Oct. 2011, doi: 10.1152/ajprenal.00458.2010.
- [197] M. Remešová *et al.*, ‘Effects of anodizing conditions and the addition of Al₂O₃/PTFE particles on the microstructure and the mechanical properties of porous anodic coatings on the AA1050 aluminium alloy’, *Applied Surface Science*, vol. 513, p. 145780, May 2020, doi: 10.1016/j.apsusc.2020.145780.
- [198] M. Sieber, R. Morgenstern, I. Scharf, and T. Lampke, ‘Effect of Nitric and Oxalic Acid Addition on Hard Anodizing of AlCu4Mg1 in Sulphuric Acid’, *Metals*, vol. 8, no. 2, Art. no. 2, Feb. 2018, doi: 10.3390/met8020139.
- [199] S. J. Asadauskas, G. Stalnionis, G. Bikulcius, S. Jankauskas, L. Stasiunus, and T. Matijosius, ‘Nanoscale deposition of Group IVB elements on anodized surfaces to reduce friction’, *Materials Today Communications*, vol. 29, p. 103008, Dec. 2021, doi: 10.1016/j.mtcomm.2021.103008.
- [200] T. Kokubo and H. Takadama, ‘How useful is SBF in predicting in vivo bone bioactivity?’, *Biomaterials*, vol. 27, no. 15, pp. 2907–2915, May 2006, doi: 10.1016/j.biomaterials.2006.01.017.
- [201] J. J. Sherba, S. Hogquist, H. Lin, J. W. Shan, D. I. Shreiber, and J. D. Zahn, ‘The effects of electroporation buffer composition on cell viability and electro-transfection efficiency’, *Sci Rep*, vol. 10, no. 1, Art. no. 1, Feb. 2020, doi: 10.1038/s41598-020-59790-x.
- [202] R. Rimsa *et al.*, ‘Lung on a Chip Development from Off-Stoichiometry Thiol-Ene Polymer’, *Micromachines (Basel)*, vol. 12, no. 5, p. 546, May 2021, doi: 10.3390/mi12050546.
- [203] M. Priedols *et al.*, ‘Bifurcated Asymmetric Field Flow Fractionation of Nanoparticles in PDMS-Free Microfluidic Devices for Applications in

- Label-Free Extracellular Vesicle Separation’, *Polymers*, vol. 15, no. 4, Art. no. 4, Jan. 2023, doi: 10.3390/polym15040789.
- [204] V. Stankevic *et al.*, ‘Compact Square-Wave Pulse Electroporator with Controlled Electroporation Efficiency and Cell Viability’, *Symmetry*, vol. 12, no. 3, Art. no. 3, Mar. 2020, doi: 10.3390/sym12030412.
- [205] S. A. Mousavi Shaegh *et al.*, ‘A microfluidic optical platform for real-time monitoring of pH and oxygen in microfluidic bioreactors and organ-on-chip devices’, *Biomicrofluidics*, vol. 10, no. 4, p. 044111, Aug. 2016, doi: 10.1063/1.4955155.
- [206] N. Bakute *et al.*, ‘Microphysiological system with integrated sensors to study the effect of pulsed electric field’, *Sci Rep*, vol. 14, no. 1, p. 18713, Aug. 2024, doi: 10.1038/s41598-024-69693-w.
- [207] B. Callegari, T. N. Lima, and R. S. Coelho, ‘The Influence of Alloying Elements on the Microstructure and Properties of Al-Si-Based Casting Alloys: A Review’, *Metals*, vol. 13, no. 7, p. 1174, July 2023, doi: 10.3390/met13071174.
- [208] A. Elhadi, S. Amroune, A. Houari, and M. Kouder, ‘Normal Temperature Mechanical Properties of 6082 Aluminium Alloy as a Function of Tempering Temperature: Experimental and Numerical Approach’, *Acta Mechanica et Automatica*, vol. 18, no. 3, pp. 385–392, July 2024, doi: 10.2478/ama-2024-0042.
- [209] R. R. Sarbandi, M.-M. Khani, K. Hassani, M. Tafazzoli-Shadpour, A. Ardeshirylajimi, and M. Tabatabaei, ‘Nanoindentation Characteristics of Stem Cells Towards Osteogenic Differentiation in a Nanoscale Vibratory Bioreactor’, *BioNanoSci.*, vol. 14, no. 3, pp. 2435–2445, Sept. 2024, doi: 10.1007/s12668-024-01547-1.
- [210] M. Ermis, E. Antmen, and V. Hasirci, ‘Micro and Nanofabrication methods to control cell-substrate interactions and cell behavior: A review from the tissue engineering perspective’, *Bioactive Materials*, vol. 3, no. 3, pp. 355–369, Sept. 2018, doi: 10.1016/j.bioactmat.2018.05.005.
- [211] Mohammed, Mohsin T., Khan, Zahid A., and Siddiquee, Arshad N., ‘Corrosion in Biomedical Grade Titanium Based Materials: A Review’, *Indian Journal of Applied Research*, 2013, Accessed: Feb. 06, 2025. [Online]. Available: <https://www.worldwidejournals.com/indian-journal-of-applied-research-%28IJAR%29/article/corrosion-in-biomedical-grade-titanium-based-materials-a-review/MjIIMw==/?form=MG0AV3>
- [212] M. Schinhammer, J. Hofstetter, C. Wegmann, F. Moszner, J. F. Löffler, and P. J. Uggowitzer, ‘On the Immersion Testing of Degradable Implant Materials in Simulated Body Fluid: Active pH Regulation Using CO₂’, *Advanced Engineering Materials*, vol. 15, no. 6, pp. 434–441, 2013, doi: 10.1002/adem.201200218.
- [213] Z. Xu, M. A. Hodgson, and P. Cao, ‘Effect of Immersion in Simulated Body Fluid on the Mechanical Properties and Biocompatibility of Sintered Fe–Mn-Based Alloys’, *Metals*, vol. 6, no. 12, Art. no. 12, Dec. 2016, doi: 10.3390/met6120309.

- [214] R. Messous, B. Henriques, H. Bousbaa, F. S. Silva, W. Teughels, and J. C. M. Souza, 'Cytotoxic effects of submicron- and nano-scale titanium debris released from dental implants: an integrative review', *Clin Oral Invest*, vol. 25, no. 4, pp. 1627–1640, Apr. 2021, doi: 10.1007/s00784-021-03785-z.
- [215] R. V. Badhe, O. Akinfosile, D. Bijukumar, M. Barba, and M. T. Mathew, 'Systemic toxicity eliciting metal ion levels from metallic implants and orthopedic devices – A mini review', *Toxicology Letters*, vol. 350, pp. 213–224, Oct. 2021, doi: 10.1016/j.toxlet.2021.07.004.
- [216] Q. Niu, 'Overview of the Relationship Between Aluminum Exposure and Human Health', in *Neurotoxicity of Aluminum*, Q. Niu, Ed., Singapore: Springer Nature, 2023, pp. 1–32. doi: 10.1007/978-981-99-1592-7_1.
- [217] X. Wang, Y. Li, L. Han, J. Li, C. Liu, and C. Sun, 'Role of Flavonoids in the Treatment of Iron Overload', *Front. Cell Dev. Biol.*, vol. 9, July 2021, doi: 10.3389/fcell.2021.685364.
- [218] J. Crossgrove and W. Zheng, 'Manganese toxicity upon overexposure', *NMR in Biomedicine*, vol. 17, no. 8, pp. 544–553, 2004, doi: 10.1002/nbm.931.
- [219] T. Wang *et al.*, 'Immunoregulatory silicon-deposited implant promotes osseointegration', *Composites Part B: Engineering*, vol. 255, p. 110618, Apr. 2023, doi: 10.1016/j.compositesb.2023.110618.
- [220] Q. Zhao *et al.*, 'Promotion of bone formation and antibacterial properties of titanium coated with porous Si/Ag-doped titanium dioxide', *Front. Bioeng. Biotechnol.*, vol. 10, Oct. 2022, doi: 10.3389/fbioe.2022.1001514.
- [221] J. Turner, A. Nandakumar, N. Anilbhai, A. R. Boccaccini, J. R. Jones, and G. Jell, 'The effect of Si species released from bioactive glasses on cell behaviour: A quantitative review', *Acta Biomaterialia*, vol. 170, pp. 39–52, Oct. 2023, doi: 10.1016/j.actbio.2023.09.012.
- [222] K. Kritmetapak and R. Kumar, 'Phosphate as a Signaling Molecule', *Calcif Tissue Int*, vol. 108, no. 1, pp. 16–31, Jan. 2021, doi: 10.1007/s00223-019-00636-8.
- [223] D. Markovich, 'Physiological Roles and Regulation of Mammalian Sulfate Transporters', *Physiological Reviews*, vol. 81, no. 4, pp. 1499–1533, Jan. 2001, doi: 10.1152/physrev.2001.81.4.1499.
- [224] K. Venkateswarlu *et al.*, 'Fabrication of corrosion resistant, bioactive and antibacterial silver substituted hydroxyapatite/titania composite coating on Cp Ti', *Ceramics International*, vol. 38, no. 1, pp. 731–740, Jan. 2012, doi: 10.1016/j.ceramint.2011.07.065.
- [225] D. Durgalakshmi, R. A. Rakkesh, and S. Balakumar, 'Stacked Bioglass/TiO₂ nanocoatings on titanium substrate for enhanced osseointegration and its electrochemical corrosion studies', *Applied Surface Science*, vol. 349, pp. 561–569, Sept. 2015, doi: 10.1016/j.apsusc.2015.04.142.
- [226] N. F. E. Boraei, M. A. M. Ibrahim, S. S. A. E. Rehim, and I. H. Elshamy, 'Electrochemical corrosion behavior of β -Ti alloy in a physiological saline solution and the impact of H₂O₂ and albumin', *J Solid State Electrochem*,

- vol. 28, no. 7, pp. 2243–2256, July 2024, doi: 10.1007/s10008-023-05751-z.
- [227] H. Miyajima, H. Touji, and K. Iijima, ‘Hydroxyapatite Particles from Simulated Body Fluids with Different pH and Their Effects on Mesenchymal Stem Cells’, *Nanomaterials*, vol. 11, no. 10, Art. no. 10, Oct. 2021, doi: 10.3390/nano11102517.
- [228] M. Demirel and A. I. Kaya, ‘Effect of strontium-containing compounds on bone grafts’, *J Mater Sci*, vol. 55, no. 15, pp. 6305–6329, May 2020, doi: 10.1007/s10853-020-04451-7.
- [229] M.-C. Kim, D. M. Neal, R. D. Kamm, and H. H. Asada, ‘Dynamic Modeling of Cell Migration and Spreading Behaviors on Fibronectin Coated Planar Substrates and Micropatterned Geometries’, *PLOS Computational Biology*, vol. 9, no. 2, p. e1002926, Feb. 2013, doi: 10.1371/journal.pcbi.1002926.
- [230] S. A. Abdellatef, A. Ohi, T. Nabatame, and A. Taniguchi, ‘The Effect of Physical and Chemical Cues on Hepatocellular Function and Morphology’, *International Journal of Molecular Sciences*, vol. 15, no. 3, Art. no. 3, Mar. 2014, doi: 10.3390/ijms15034299.
- [231] R. Ahmadi and A. Afshar, ‘In vitro study: Bond strength, electrochemical and biocompatibility evaluations of TiO₂/Al₂O₃ reinforced hydroxyapatite sol–gel coatings on 316L SS’, *Surface and Coatings Technology*, vol. 405, p. 126594, Jan. 2021, doi: 10.1016/j.surfcoat.2020.126594.
- [232] R. Ahmadi, N. Asadpourchallou, and B. K. Kaleji, ‘In vitro study: Evaluation of mechanical behavior, corrosion resistance, antibacterial properties and biocompatibility of HAp/TiO₂/Ag coating on Ti6Al4V/TiO₂ substrate’, *Surfaces and Interfaces*, vol. 24, p. 101072, June 2021, doi: 10.1016/j.surfin.2021.101072.
- [233] M. Pul, Ü. Erdem, B. M. Bozer, T. Şimşek, R. Yılmazel, and M. Y. Erten, ‘Synthesis of biocompatible Ti-6Al-4V composite reinforced with ZrO and bioceramic produced by powder metallurgy: Morphological, structural, and biocompatibility analysis’, *Microscopy Research and Technique*, vol. 87, no. 11, pp. 2728–2744, 2024, doi: 10.1002/jemt.24646.
- [234] A. H. Mohammed Mohammed, K. A. Shariff, D. A. Wahjuningrum, M. H. A. Bakar, and H. Mohamad, ‘A comprehensive review of the effects of porosity and macro- and micropore formations in porous β -TCP scaffolds on cell responses’, *J Aust Ceram Soc*, vol. 59, no. 4, pp. 865–879, Sept. 2023, doi: 10.1007/s41779-023-00880-0.
- [235] J. Zhou *et al.*, ‘Study on the influence of scaffold morphology and structure on osteogenic performance’, *Front. Bioeng. Biotechnol.*, vol. 11, Mar. 2023, doi: 10.3389/fbioe.2023.1127162.
- [236] R. O. F. Verkuijlen, M. H. A. van Dongen, A. A. E. Stevens, J. van Geldrop, and J. P. C. Bernardis, ‘Surface modification of polycarbonate and polyethylene naphthalate foils by UV-ozone treatment and μ Plasma printing’, *Applied Surface Science*, vol. 290, pp. 381–387, Jan. 2014, doi: 10.1016/j.apsusc.2013.11.089.

- [237] P. Pedrosa, J.-M. Chappé, C. Fonseca, A. V. Machado, J. M. Nóbrega, and F. Vaz, 'Plasma Surface Modification of Polycarbonate and Poly(propylene) Substrates for Biomedical Electrodes', *Plasma Processes and Polymers*, vol. 7, no. 8, pp. 676–686, 2010, doi: 10.1002/ppap.200900176.
- [238] S. Redjala, R. Ferhoum, N. Aït Hocine, and S. Azem, 'Degradation of Polycarbonate Properties Under Thermal Aging', *J Fail. Anal. and Preven.*, vol. 19, no. 2, pp. 536–542, Apr. 2019, doi: 10.1007/s11668-019-00630-0.
- [239] S. Redjala, N. Aït Hocine, R. Ferhoum, M. Gratton, N. Poirot, and S. Azem, 'UV Aging Effects on Polycarbonate Properties', *J Fail. Anal. and Preven.*, vol. 20, no. 6, pp. 1907–1916, Dec. 2020, doi: 10.1007/s11668-020-01002-9.
- [240] A. Kiy *et al.*, 'Ion track etching of polycarbonate membranes monitored by in situ small angle X-ray scattering', *Phys. Chem. Chem. Phys.*, vol. 23, no. 26, pp. 14231–14241, July 2021, doi: 10.1039/D1CP02063C.
- [241] H. Abedsoltan, 'Concentrated Sulfuric Acid as a Catalyst for Chemical Recycling of Polycarbonate in Water', *Waste Biomass Valor.*, vol. 15, no. 5, pp. 2793–2806, May 2024, doi: 10.1007/s12649-023-02326-x.
- [242] F. S. F. dos Santos *et al.*, 'Use of Piranha Solution as An Alternative Route to Promote Bioactivation of PEEK Surface with Low Functionalization Times', *Molecules*, vol. 28, no. 1, Art. no. 1, Jan. 2023, doi: 10.3390/molecules28010074.
- [243] N. AlRubaie and A. AlKhafaji, 'Investigation the effect of piranha solution surface treatment on poly-methylmethacrylate', *Adv. J. Chem. A*, no. Online First, Aug. 2024, doi: 10.48309/ajca.2025.469485.1607.
- [244] T. Li *et al.*, 'Piranha Solution-Assisted Surface Engineering Enables Silicon Nanocrystals with Superior Wettability and Lithium Storage', *Crystals*, vol. 13, no. 7, Art. no. 7, July 2023, doi: 10.3390/cryst13071127.
- [245] Y. Zhang, A. O'Mahony, Y. He, and T. Barber, 'Hydrodynamic shear stress' impact on mammalian cell properties and its applications in 3D bioprinting', *Biofabrication*, vol. 16, no. 2, p. 022003, Feb. 2024, doi: 10.1088/1758-5090/ad22ee.
- [246] M. A. Swartz and M. E. Fleury, 'Interstitial Flow and Its Effects in Soft Tissues', *Annual Review of Biomedical Engineering*, vol. 9, no. Volume 9, 2007, pp. 229–256, Aug. 2007, doi: 10.1146/annurev.bioeng.9.060906.151850.
- [247] A. Sudalai, A. Khenkin, and R. Neumann, 'Sodium periodate mediated oxidative transformations in organic synthesis', *Org. Biomol. Chem.*, vol. 13, no. 15, pp. 4374–4394, Mar. 2015, doi: 10.1039/C5OB00238A.
- [248] A. J. García, M. D. Vega, and D. Boettiger, 'Modulation of Cell Proliferation and Differentiation through Substrate-dependent Changes in Fibronectin Conformation', *MBoC*, vol. 10, no. 3, pp. 785–798, Mar. 1999, doi: 10.1091/mbc.10.3.785.
- [249] L. G. Campana *et al.*, 'Pulsed Electric Fields in Oncology: A Snapshot of Current Clinical Practices and Research Directions from the 4th World

- Congress of Electroporation', *Cancers*, vol. 15, no. 13, p. 3340, Jan. 2023, doi: 10.3390/cancers15133340.
- [250] C. Berry-Kilgour, L. Wise, J. King, and I. Oey, 'Application of pulsed electric field technology to skin engineering', *Front. Bioeng. Biotechnol.*, vol. 12, Apr. 2024, doi: 10.3389/fbioe.2024.1386725.
- [251] T. Haraldsson, C. Carlborg, and W. Wijngaart, 'OSTE: A novel polymer system developed for Lab-on-Chip', *Proceedings of SPIE - The International Society for Optical Engineering*, vol. 8976, Feb. 2014, doi: 10.1117/12.2041918.
- [252] E. K. Rofstad, 'Microenvironment-induced cancer metastasis', *Int J Radiat Biol*, vol. 76, no. 5, pp. 589–605, May 2000, doi: 10.1080/095530000138259.
- [253] N. Raghunand, R. A. Gatenby, and R. J. Gillies, 'Microenvironmental and cellular consequences of altered blood flow in tumours', *Br J Radiol*, vol. 76 Spec No 1, pp. S11–22, 2003, doi: 10.1259/bjr/12913493.
- [254] Y. Li *et al.*, 'Electroporation on microchips: the harmful effects of pH changes and scaling down', *Sci Rep*, vol. 5, no. 1, Art. no. 1, Dec. 2015, doi: 10.1038/srep17817.
- [255] P. Turjanski *et al.*, 'The Role of pH Fronts in Reversible Electroporation', *PLOS ONE*, vol. 6, no. 4, p. e17303, Apr. 2011, doi: 10.1371/journal.pone.0017303.
- [256] Y. (焦云鹏) Jiao, L. (王利民) Wang, and J. (陈建华) Chen, 'A mesoscale bubble-induced turbulence model and simulation of gas–liquid flows', *Physics of Fluids*, vol. 35, no. 1, p. 013314, Jan. 2023, doi: 10.1063/5.0132961.
- [257] I. A. Rodriguez Osuna, P. Cobelli, and N. Olaiz, 'Bubble Formation in Pulsed Electric Field Technology May Pose Limitations', *Micromachines (Basel)*, vol. 13, no. 8, p. 1234, July 2022, doi: 10.3390/mi13081234.
- [258] J. Wang, Y. Zhan, V. M. Ugaz, and C. Lu, 'Vortex-assisted DNA delivery', *Lab Chip*, vol. 10, no. 16, pp. 2057–2061, July 2010, doi: 10.1039/C004472E.
- [259] M. Grys, Z. Madeja, and W. Korohoda, 'Avoiding the side effects of electric current pulse application to electroporated cells in disposable small volume cuvettes assures good cell survival', *Cellular & Molecular Biology Letters*, vol. 22, no. 1, p. 1, Jan. 2017, doi: 10.1186/s11658-016-0030-0.
- [260] R. Varala, N. Dubasi, V. Seema, and V. Kotra, 'Sodium Periodate (NaIO₄) in Organic Synthesis', *SynOpen*, vol. 07, pp. 548–554, Oct. 2023, doi: 10.1055/a-2183-3678.

SANTRAUKA

ĮVADAS

Sąveika tarp biomedžiagų ir biologinių sistemų - tokių kaip ląstelės ir audiniai - yra esminis medžiagų inžinerijos ir audinių regeneracijos tyrimų aspektas. Biomedžiagos turi pasižymėti pakankamu mechaniniu tvirtumu ir gebėjimu palaikyti gretimų ląstelių adheziją, proliferaciją bei kitas gyvybiškai svarbias funkcijas. Šios savybės yra itin svarbios tiek regeneracinėje medicinoje, tiek audinių inžinerijoje ir *in vitro* organų modeliavime.

Biomedžiagų savybės gali smarkiai skirtis priklausomai nuo jų specifinio pritaikymo. Audinių regeneracijos ir implantologijos srityse jos dažnai tarnauja kaip pastoliai, suteikdami struktūrinę atramą ląstelėms, prie kurių jos prisitvirtina ir funkcionuoja. Tuo tarpu kraujotakos sistemoje naudojamos biomedžiagos, pavyzdžiui, dirbtiniuose širdies vožtuvuose ar kraujagyslių protezuose, turi visiškai slopinti ląstelių adheziją, kad būtų išvengta kaip trombozės. Todėl efektyviam biomedžiagų pritaikymui būtina kruopščiai parinkti biomedžiagą ir modifikuoti jos paviršių taip, kad atitiktų konkrečios biologinės sistemos reikalavimus. Paviršiaus inžinerijos metodais galima efektyviai reguliuoti ląstelių elgseną sąlytyje su biomedžiagomis. Cheminės ir fizinės paviršiaus modifikacijos, apimančios topografijos, porėtumo, šurkštumo, hidrofiliškumo keitimą bei funkcinių grupių integravimą, leidžia kontroliuoti baltymų adsorbciją, ir, atitinkamai, ląstelių adheziją.

Pastaraisiais metais vis daugiau dėmesio skiriama ne tik biomedžiagų paviršiaus modifikavimo strategijoms, bet ir jų integracijai į pažangias *in vitro* sistemas, kurios leidžia tiksliau atkurti realias fiziologines sąlygas. Mikroskysčių technologijos, sujungdamos medžiagų inžineriją ir biologinius modelius, leidžia tirti ląstelių atsaką dinaminėje aplinkoje, kur svarbų vaidmenį atlieka skysčių tėkmė, šlyties įtempis. Be to, į mikroskysčių sistemas galima integruoti įvairius stimuliavimo modulius, pavyzdžiui, elektrinius signalus, cheminius gradientus ar mechaninius dirgiklius. Tokios sistemos leidžia atlikti tikslus, kontroliuojamus eksperimentus, skirtus specifinių ląstelių atsakų analizavimui.

Ši disertacija orientuota į biomedžiagų paviršiaus optimizavimą ir jų biosuderinamumo gerinimą, taikant tikslingas modifikavimo strategijas. Tyrime analizuotos dvi biomedžiagos – anoduotas Al lydinys bei polimerų klasei priklausantis polikarbonatas bei polimeras polikarbonatas (PC). PC integravimas į mikroskysčių sistemą leido sukurti funkcionalią platformą žinduolių ląstelių tyrimams bei stimuliacijai elektriniais impulsais. Aprašyti sprendimai prisideda prie biomedžiagų mokslo pažangos ir atveria naujas galimybes tiek implantologijoje, tiek audinių inžinerijoje.

Tyrimo tikslas ir uždaviniai

Disertacijos tikslas – sistemiškai įvertinti anodine danga padengto aliuminio Al 6082 lydinio ir polikarbonato biologinį suderinamumą bei ląstelių adhezijos savybes, siekiant nustatyti ir optimizuoti šių medžiagų tinkamumą biomedicininiam taikymui ir integravimą į mikrofiziologinę sistemą.

Tyrimo uždaviniai:

1) Įvertinti dviejų Al 6082 lydinių su Al_2O_3 dangomis, gautų anoduojant sieros ir fosforo rūgščių elektrolitais, biosuderinamumą, cheminio stabilumą ir paviršiaus savybes, siekiant nustatyti jų tinkamumą biomedicininiam taikymui.

2) Chemiškai modifikuoti porėtą polikarbonato membraną, siekiant pritaikyti šią biomedžiagą ląstelių adhezijai ir auginimui mikroskysčių sistemose.

3) Sukurti mikrofiziologinę sistemą su integruota porėta polikarbonato membrana, skirtą impulsinio elektrinio lauko poveikio tyrimams bei mikroaplinkos parametrų stebėsenai.

Mokslinis naujumas

Šioje disertacijoje aprašyti tyrimai prisideda prie medžiagų bioinžinerijos mokslo bei pritaikymo pažangiose mikroskysčių sistemose. Disertacijoje gilinamasi į medžiagų paviršiaus optimizavimą, biosuderinamumą bei pritaikymą integruotų mikroskysčių platformose *in vitro* tyrimams. Tyrimai apima dvi biomedžiagų klases – biokeraminę aliuminio oksido (Al_2O_3) dangą ir polimerą polikarbonatą, kurios taikomos skirtinguose biomedicininuose kontekstuose: ortopedinių implantų gamyboje ir ląstelių kultūrai mikroskysčių sistemose.

Pirmuoju atveju tirtos biokeraminės dangos, gautos anoduojant pramoninį Al lydinį 6082, kaip potenciali biomedžiaga implantologijos reikmėms. Anodavimas siūlomas kaip alternatyva tradiciniam biokeramikų sinteravimui, kurių produktai pasižymi trapumu, o pati technologija - ribotomis formavimo galimybėmis ir dideliais gamybos sąnaudomis. Priešingai nei milteliais pagrįsti gamybos metodai, anodavimas leidžia suformuoti mechaniškai tvirtus lydinius ir individualiai pritaikomus paviršius.

Nors pats anodavimo metodas nėra naujas, šiame tyrime pirmą kartą sistemiškai įvertintas du skirtingomis sąlygomis anoduoti Al 6082 lydiniai, analizuojant jų paviršiaus charakteristikas bei *in vitro* biosuderinamumą. Vertinimas atliktas lyginant su medicininės klasės titano lydiniu. Vienas iš tiriamųjų mėginių pasižymėjo savybėmis, leidžiančiomis jį priskirti biomedžiagoms ir potencialiai taikyti biomedicininės paskirties gaminiuose.

Antroje tyrimų dalyje analizuotas hidrofobinio polikarbonato paviršiaus modifikavimas naudojant cheminius oksidatorius – natrio metaperjodatą, sieros

rūgštį ir piranijos tirpalą. Nors pastaruoju metu kiti autoriai aprašė panašius paviršiaus apdorojimo metodus taikant kitus reagentus, šis pilotinis tyrimas tiria išvardintų reagentų efektyvumą optimizuojant ląstelių adheziją mikroskysčių sistemoje. Cheminės modifikacijos kartu su adheziją skatinančiomis molekulėmis – fibronektinu, kolagenu ir poli-D-lizinu (PDL) padidina ląstelių adheziją ant polikarbonato paviršiaus. Siūlomas metodas yra technologiškai prieinamesnis ir lankstesnis, nei apdorojimas plazma, todėl išplečia polikarbonato panaudojimo galimybes mikroskysčių ląstelių kultūrų sistemose.

Trečiojoje disertacijos dalyje pristatoma specialiai suprojektuota ir pagaminta mikrofiziologinė sistema (MPS), integruojanti kelias pažangias funkcijas į vieną vientisą platformą. MPS apjungia porėtą polikarbonato membraną, mikrokanaluose integruotus elektrodus ir realaus laiko aplinkos jutiklius – tokia konfigūracija iki šiol nebuvo aprašyta mokslinėje literatūroje kaip vieninga sistema. Polikarbonato membrana veikia kaip pusiau pralaidus barjeras taro dviejų lygiagrečių mikrokanalų, sudarydama dviejų kompartamentų ląstelių kultūros sąlygas, kurias kontaktuoja per membranoje esančias poras. Mikrokanaluose integruoti elektrodai leidžia lokaliai indukuoti impulsinį elektrinį lauką (IEL). Tuo tarpu deguonies ir pH jutikliai užtikrina galimybę registruoti fiziologinės aplinkos parametrus, kas yra svarbu mikrolusto gamyboje naudojant dujoms nelaidžias medžiagas OSTE ir COC. Tokios MPS poreikis susijęs su didėjančio *in vitro* modelių taikymų mastu, kurie tiksliai atkuria žmogaus audinių aplinką, kas ypač reikalinga vaistų bandymams, ligų modeliavimui ir regeneracinei medicinai. Įprastos mikroskysčių platformos dažnai neturi galimybės vienu metu teikti lokalizuotus stimuliavimus ir stebėti aplinkos parametrus realiuoju laiku.

MPS modulinė struktūra leidžia ją taikyti ligų modeliavimui ir vaistų testavimui, kai būtina dinamiška ir kontroliuojama mikroaplinka. Atsižvelgiant į įprastų mikroskysčių sistemų ribotumus, šioje disertacijoje pristatoma MPS žymi elektrinės stimuliacijos, kompartmentizuotos ląstelių kultūros ir realaus laiko stebėsenos integraciją vienoje platformoje. Tai prisideda prie technologinio proveržio mikroskysčių ir *in vitro* modeliavimo srityse.

Ginamieji teiginiai

- 1) Al 6082 lydinys, anoduotas naudojant sieros rūgšties elektrolitą, gali būti priskirtas biomedžiagoms dėl cheminio stabilumo bei biosuderinamumo savybių.
- 2) Polikarbonato membranos paviršiaus cheminis oksidavimas ir padengimas poli-D-lizinu užtikrina ląstelių adheziją esant statinėms ir dinaminėms auginimo sąlygomis.

3) Sukurta mikrofiziologinė sistema su porėta polikarbonato membrana, elektrodais bei deguonies ir pH jutikliais, tinkanti impulsinio elektrinio lauko poveikio taikymui žinduolių ląstelėms ir fiziologinių parametrų stebėsenai.

METODIKA

Biokeraminių dangų tyrimas. Ti lydinio, Al lydinio bei anoduotus mėginius paruošė bei struktūrinės analizės duomenis pateikė dr. Tadas Matijošius. Imersijos eksperimentai atlikti naudojant SBF (simuliuotas kūno skystis) pagamintą pagal metodiką [47], jonų išsiskyrimas matuotas induktyviai susietos plazmos optinės emisijos spektroskopija (ICP-OES) (atliko dr. Aleksej Žarkov), korozijos įvertinimas atliktas atliekant elektrocheminę impedanso spektroskopija (EIS) ir potenciodinaminės poliarizacijos testais (atliko dr. Asta Grigucevičienė). Mėginiai vizualizuoti SEM (atliko dr. Aušra Selskienė). Vandens lašo kontaktinis kampas matuotas naudojant EasyDrop instrument (VU GMC).

Ląstelių auginimas, adhezijos bei gyvybingumo eksperimentai atlikti standartinėmis žinduolių ląstelių auginimo sąlygomis, išskyrus ląstelių auginimą mikroskysčių sistemoje, kuomet auginimas vykdomas pajungiant švirkštinę pompą ir nuolatos leidžiant skystį per ląstelių auginimo kanalą. Ląstelės vizualizuotos šviesiniu ir konfokaliniu mikroskopais, absorbciją matuojant spektrofotometru ir fluorescenciją matuojant spektrofotometru.

PC modifikavimui naudota plazmos technologija, pasitelkiant deguonies dujas. Cheminė modifikacija atlikta inkubuojant membraną konkretaus reagento vonelėje.

MPS gamybai naudota 3D spausdinimo technologija (atliko dr. Arūnas Stirkė ir dr. Eivydąs Andriukonis). PDMS ir OSTE medžiagos paruoštos pagal standartines procedūras. IEL eksperimentai atlikti taikant didelio galingumo kvadratinį impulsų elektroporacijos metodą elektriniai parametrai registruoti osciloskopu. Deguonies koncentracijos matuotos deguonies matavimo sistema Oxy-4 SMA, pH matavimai – pagal dr. Martynas Šapurov paruoštą metodiką.

Statistinė analizė. Duomenys pateikiami kaip vidurkis \pm standartinis nuokrypis (SD). Daugiafaktoriniams palyginimams naudota vienkryptė dispersinė analizė (ANOVA). P vertė $< 0,05$ buvo laikoma statistiškai reikšminga. Visi eksperimentai buvo atliekami su nepriklausomais pakartojimais $n \geq 3$, siekiant užtikrinti atkuriamumą ir statistinį patikimumą.

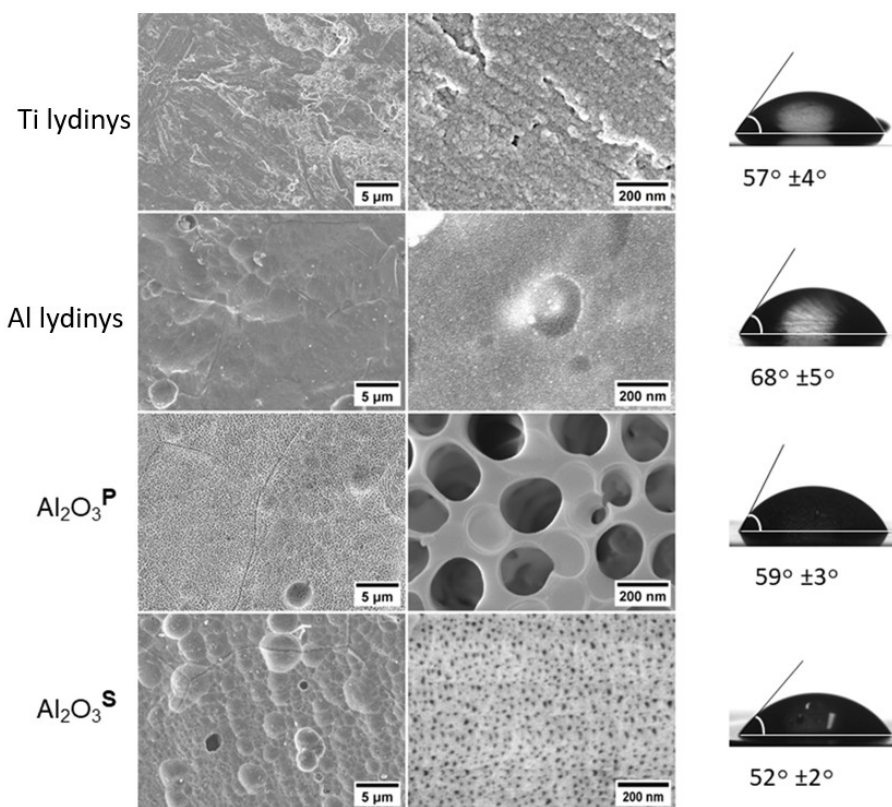
1. BIOKERAMINIO ALIUMINIO OKSIDO DANGŲ, SUSIFORMAVUSIŲ ANT ALIUMINIO 6028 LYDINIO, BIOSUDERINAMUMO TYRIMAI

Šiame skyriuje pristatomi biokeraminio aliuminio oksido (Al_2O_3) tyrimai. Dėl savo išskirtinio atsparumo gniuždymui ir cheminio inertiškumo, ši biomedžiaga galėtų būti naudojama ortopediniam protezavimui [16]. Al_2O_3 jau seniai yra naudojama dantų protezavimo technologijose [23]. Aliuminio oksido keramika paprastai gaminama iš miltelių, taikant daugiaetapį procesą, apimančią mechaninį malimą, sausą presavimą, sukepinimą ir ekstruziją aukštoje temperatūroje ir slėgyje [25]. Vis dėlto, aliuminio oksido trapumas, priemaišų buvimas ir sudėties netolygumai kelia iššūkių gaminant implantus, ypač sudėtingų formų ir didelių gabaritų. Be to, jų gamybos procesas yra brangus ir ilgai trunkantis.

Alternatyvus metodas biokeraminio aliuminio oksido gamybai yra Al lydinio anodavimas. Anodavimo metu suformuojamos biokeraminės Al_2O_3 dangos lydinio paviršiuje. Šioje disertacijoje analizuoti du Al 6028 lydiniai su biokeraminėmis aliuminio oksido dangomis, gautomis anoduojant fosforo ir sieros rūgšties elektrolitais, ir vertintas jų potencialas taikymui implantologijoje. Buvo ištirtos gautų mėginių cheminis atsparumas ir biosuderinamumas ir palygintos su medicininio lygio titano lydinio savybėmis.

1.1 Struktūrinės mėginių su biokeraminėmis Al_2O_3 dangomis savybės

Al 6028 lydiniu pasirinktas dėl jo santykinai didelio stiprumo ir atsparumo korozijai [208]. Lydinio grynumas siekia 96.52wt %, o likusią dalį sudaro legiruojantys elementai: Mg (2.28 wt %), Si (0,53wt %), Fe (0.36wt %) ir Mn (0.31wt %). Viso tyrimo metu gauti duomenys buvo lyginami su neanoduotu Al lydiniu bei medicininės paskirties Ti lydiniu BT1, kurio grynumas siekia 96.32wt%, o likusią dalį sudaro legiruojantys elementai Mn (1.76 wt %), Al (1.75wt %); Fe (0.11 wt %), Si (0.06 wt%). Palyginimas su Ti lydiniu, laikomu biomedicininio etalonu, leido objektyviai įvertinti anoduotų mėginių tinkamumą biomedicininiam taikymams. Tuo tarpu palyginimas su neanoduotu Al lydiniu buvo atliktas siekiant nustatyti, įvertinimui, kaip anodavimo procesas pakeitė medžiagos savybės.



1 pav. Mėginių SEM topografija (kairėje) esant mažam ir dideliam padidimui bei vandens lašo ant mėginių paviršiaus nuotraukos ir kampai (dešinėje).

Al 6028 lydinys (tekste nurodomas kaip Al lydinys) buvo anoduotas dviem skirtingais elektrolotais: sieros rūgštimi bei fosforo rūgštimi. Gautųjų mėginiai paviršiaus morfologija ir poringumo charakteristikos buvo analizuoti naudojant SEM nanotopografiją (**1 pav.**) ir pateikti **1 lentelėje**. Anodavimas sieros rūgštimi (tekste nurodomi kaip $\text{Al}_2\text{O}_3^{\text{S}}$) suformavo storesnes anodines dangas ($\sim 60 \mu\text{m}$) su siauromis nanoporomis ($< 20 \text{nm}$), o anodavimas fosforo rūgštimi (tekste žymimi $\text{Al}_2\text{O}_3^{\text{P}}$) - plonesnes dangas ($\sim 10 \mu\text{m}$) su didesnėmis mikroporomis (200nm). Paviršiaus šiurkštumas padidėjo lyginant su neanoduotu lydiniu, tuo tarpu $\text{Al}_2\text{O}_3^{\text{S}}$ mechaninis kietumas prilygo Ti lydinio savybėms (**1 lentelėje**).

1 lentelė. Biokeraminių aliuminio oksido dangų, gautų anodavus Al 6082 lydinį skirtinguose elektrolituose, charakteristikos.

Mėginiai	Dangos storis, μm	Porų diametras, nm	Pore tankis, poros/ μm^2	Atstumas tarp porų, nm	Poringumas, %
$\text{Al}_2\text{O}_3^{\text{S}}$	58.4 \pm 2.3	13.7 \pm 0.1	912.0 \pm 83.8	30.9 \pm 4.4	13.5 \pm 1.4
$\text{Al}_2\text{O}_3^{\text{P}}$	8.7 \pm 1.1	177.2 \pm 15.5	19.7 \pm 4.0	284.3 \pm 29	47.6 \pm 2.4
Mechaninis kietumas					
	Paviršiaus šiurkštumas, μm	Mechaninis kietumas			
		įspaudai, GPa	Vickers, HV		
$\text{Al}_2\text{O}_3^{\text{S}}$	1.5 \pm 0.2	4.6 \pm 0.5	279 \pm 39		
$\text{Al}_2\text{O}_3^{\text{P}}$	1.5 \pm 0.1	1.0 \pm 0.5	115 \pm 12		
Al lydinys	1.3 \pm 0.1	1.5 \pm 0.2	139 \pm 10		
Ti lydinys	1.2 \pm 0.1	nd	245 \pm 20		

1.2 Jonų išsiskyrimas ir atsparumas korozijai

Implantuotos biomedžiagos organizme yra veikiamos nepalankios korozinės aplinkos, kuri gali sukelti jonų išsiskyrimą, biomedžiagos irimą ir koroziją [211]. Labai porėti ir šiurkštūs paviršiai gali turėti įtakos metalų jonų išsiskyrimui, ypač tais atvejais, kai medžiagose nėra chemiškai gryna. Šiam poveikiui įvertinti atliekami standartizuoti pagreitintos korozijos eksperimentai, kuomet mėginiai inkubuojami naudojamas SBF buferyje. Šio buferio sudėtis yra tokia, kad kuo labiau atitiktų žmogaus kraujo plazmos joninę sudėtį [47]. Siekiant įvertinti mėginių cheminę stabilumą ir koroziją, buvo atlikti 1-28 dienų imersijos eksperimentai SBF tirpale. Rezultatai atskleidė, kad toksinių jonų (Fe, Al) išsiskyrimas buvo veiksmingai slopinamas tiek anoduotuose mėginiuose dangose. Tuo tarpu neurotoksiško Mn jonų išsiskyrimas buvo nustatytas kiek didesnis: 0,04 mg/l $\text{Al}_2\text{O}_3^{\text{S}}$ ir 0,06 mg/l $\text{Al}_2\text{O}_3^{\text{P}}$, tačiau koncentracijos išliko saugiose ribose (neviršijo 0,1 mg/l) [215]. Svarbių jonų (Mg, Si) išsiskyrimas

buvo saugus, o Si jonų išsiskyrimas $\text{Al}_2\text{O}_3^{\text{S}}$ mėginyje buvo padidėjęs, kas kaip tik gali palengvinti biologinius procesus, pvz., osteogenezę ir ląstelių proliferaciją [219], [220]. Sulfatų ir fosfatų išsiskyrimas skirtingose mėginiuose skyrėsi: $\text{Al}_2\text{O}_3^{\text{S}}$ išskyrė daugiau sulfato jonų, kurie gali įtakoti lokalų vietinio rūgštingumo padidėjimą. $\text{Al}_2\text{O}_3^{\text{P}}$ mėginyje fosfato išsiskyrimas siejamas su hidroksiapatito susidarymo, kas taip pat skatina osteoblastų aktyvumą.

Al lydinio ir Al_2O_3 dangų korozinės savybės buvo tirtos naudojant elektrocheminę impedanso spektroskopiją (EIS) ir potentiodynaminės poliarizacijos testus. Rezultatai atskleidė reikšmingus skirtumus tarp skirtingų mėginių dangų atsparumo korozijai:

1) Neanoduoto Al lydinio korozijos greitis pradžioje didėjo dėl sąveikos su SBF esančiais jonais. Vis dėlto po 28 dienų imersijos korozijos greitis sumažėjo iki 6.8×10^{-6} mm/metus.

2) $\text{Al}_2\text{O}_3^{\text{P}}$ dangos viso imersijos laikotarpiu pasižymėjo didžiausiu korozijos greičiu - iki $24,6 \times 10^{-3}$ mm/metai.

3) $\text{Al}_2\text{O}_3^{\text{S}}$ dangos užtikrino geriausią apsaugą – po 21 dienų imersijos korozijos greitis buvo tik $1,4 \times 10^{-6}$ mm/metai.

4) Palyginimui, publikuoti medicininiai Ti lydinio korozijos duomenys apie rodo gerokai prastesnį atsparumą korozijai: komerciškai švaraus titano (CP-Ti) korozijos greitis varijuoja nuo 3.54×10^{-2} mm/metus iki 7×10^{-4} mm/metus esdintam CP-Ti [224], [225].

Iš gautų rezultatų gaunama išvada, kad $\text{Al}_2\text{O}_3^{\text{S}}$ danga pasižymi išskirtiniu atsparumu korozijai, pranokstančią ne tik Al lydinį bei $\text{Al}_2\text{O}_3^{\text{P}}$, bet ir plačiai naudojamą CP-Ti. Todėl $\text{Al}_2\text{O}_3^{\text{S}}$ dangos šiuo aspektu būtų tinkamos biomedicininį implantų panaudojimui.

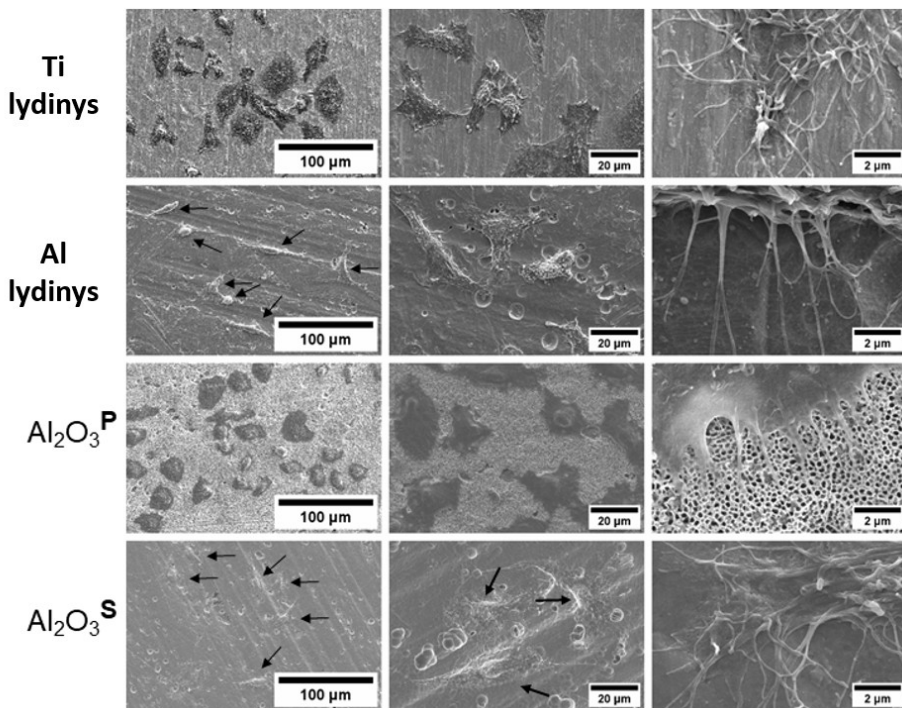
1.3 Biosuderinamumo tyrimai

Biologinis suderinamumas yra esminis reikalavimas, kurį turi atitikti bet kuri medžiaga, norint ją klasifikuoti kaip biomedžiagą. Jis apibrėžia medžiagos gebėjimą sąveikauti su biologine aplinka nepadarydamas žalos, užtikrinant funkcinį ir ilgalaikį saugumą. Biologinis suderinamumas nustatomas pagal ląstelių sąveiką su paviršiumi bei gyvybingumą. Šie tyrimai leidžia spręsti apie biomedžiagos biologines savybes ir jos potencialą integravimui į priimančiąjį audinį. Biosuderinamumo tyrimams standartiškai naudojami fibroblastai, dažniausiai L929 ląstelių linija, dėl savo svarbaus vaidmens ląstelių adhezijoje, žaizdų gijime ir tarpląstelinio užpildo (ECM) gamyboje.

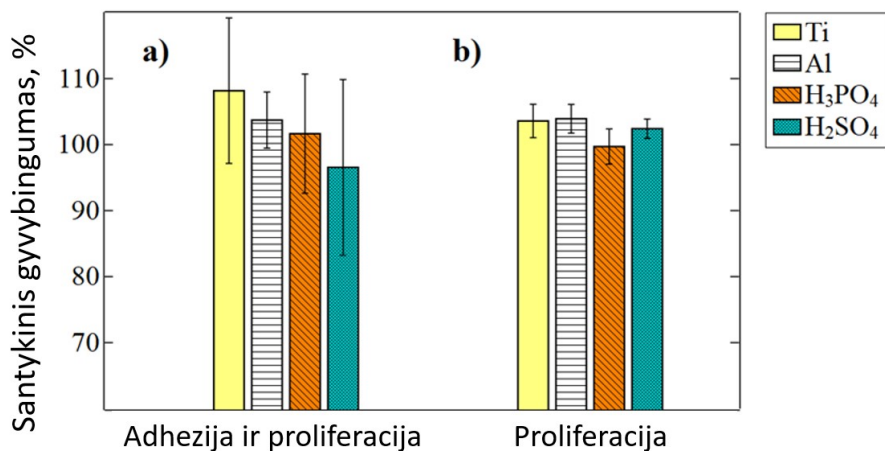
Ląstelių sąveika su mėginiais analizuota auginant L929 ląsteles tiesiogiai ant mėginių paviršiaus. Po 24 val. inkubacijos ląstelės fiksuotos ir vizualizuotos SEM (2 pav.). Buvo vertinama, ar ląstelės vykdė adheziją bei analizuojama jų

morfologija. Normalios fiziologijos ląstelės turi pasižymėti trimis požymiais: pailgair plokščia formomis bei turėti išreikštas filopodijas. Jei kurio nors požymio trūksta, reiškia ląstelių fiziologiniai procesai yra sutrikę [229].

SEM analizė parodė, kad Ti ir $\text{Al}_2\text{O}_3^{\text{P}}$ mėginiai turi didelį ląstelių kiekį ant mėginių paviršiaus, tuo tarpu Al lydinio ir $\text{Al}_2\text{O}_3^{\text{S}}$ mėginių kiekybinis įvertinimas nebuvo įmanomas dėl mažo ląstelių ir mėginių kontrasto. Ląstelės, augintos ant Ti lydinio, Al lydinio ir $\text{Al}_2\text{O}_3^{\text{S}}$, išlaikė vienodą morfologiją: dalis ląstelės buvo pailgos, dalis – plokščios; taip pat visur buvo stebimi filopodijų išsišakojimai. Tuo tarpu ant $\text{Al}_2\text{O}_3^{\text{P}}$ paviršiaus augančios ląstelės buvo išskirtinai tik plokščios formos, o filopodijų išaugos buvo mažiau ryškios – jos buvo arba įterptos į paviršiaus poras arba pasklidusios jų paviršiuje, todėl SEM vaizduose jas sunku vizualizuoti. Tokia ląstelių, augančių ant $\text{Al}_2\text{O}_3^{\text{P}}$, morfologija rodo sutrikusius gyvybinius procesus, kas gali neigiamai paveikti biomedžiagos integraciją su audiniu ir jos ilgalaikį funkcionalumą [229]. Tikėtina, kad tokia suplokštėjusi morfologija buvo nulemta paviršiaus topografijos ir porų dydžio.



2 pav. SEM vaizdai, rodantys L929 ląstelių adheziją ant Ti lydinio, Al lydinio, $\text{Al}_2\text{O}_3^{\text{P}}$, ir $\text{Al}_2\text{O}_3^{\text{S}}$. Rodyklėmis pažymėtos ląstelės mažo kontrasto nuotraukose.



3 pav. Tiriamųjų mėginių poveikis L929 ląstelių santykiniam gyvybingumui: (a) bendram ląstelių augimui, įskaitant ir adheziją ir proliferaciją; (b) proliferacijai. Vienkryptė ANOVA analizė neparodė statistiškai reikšmingų skirtumų: a) $p=0,61$ ir b) $p=0,66$.

Mėginių citotoksiškumas buvo vertintas pagal L929 ląstelių mitochondrinę aktyvumą po 24 val. inkubacijos su mėginių ekstraktais. Ekstraktai gauti po tiriamųjų mėginių inkubacijos 4 dienas augimo terpėje. Analizuoti du aspektai: ekstraktų įtaka bendram gyvybingumui, įskaitant ląstelių adheziją bei proliferaciją, bei įtaka konkrečiai ląstelių proliferacijai. Rezultatai parodė, kad visų tirtų mėginių poveikis ląstelių gyvybingumas siekė 96-105%, tačiau reikšmingų skirtumų tarp mėginių nenustatyta ($p>0,05$) (**3 pav.**). Gauti rezultatai leidžia teigti, kad tirti mėginiai nepasižymi citotoksiškumu trumpalaikiam 24 val. eksperimente.

1.4 Biokeraminių dangų biosuderinamumo apibendrinimas

Biologinis suderinamumas labai priklauso nuo biomedicininų medžiagų paviršiaus ir metalų jonų išsiskyrimo, korozijos, kurie atlieka svarbų vaidmenį ląstelių adhezijoje, gyvybingume ir integracijoje. Buvo tirti du mėginiai, gauti anoduojant Al 6028 lydinį su sieros ir fosforo rūgšties elektrolitais, įvertinant jų potencialą panaudojimui biomedicinoje. Apibendrinti rezultatai kartu Ti lydinio charakteristikomis pateikti **2 lentelėje**. Duomenys parodė, kad nanoporėtas $Al_2O_3^S$ pasižymi geromis biosuderinamumo savybėmis: $Al_2O_3^S$ mėginys efektyviai slopina toksiškų jonų išsiskyrimą, pasižymi puikiu atsparumu korozijai, ir palankiomis sąlygomis ląstelių adhezijos bei gyvybingumo savybėmis. Tuo tarpu mikroporėta $Al_2O_3^P$ danga, nors ir slopina jonų išsiskyrimą, tačiau pasižymi didesniu korozijos greičiu bei demonstruoja sutrikusias ląstelių

gyvybines funkcijas sprendžiant pagal ląstelių morfologiją. Šie rezultatai tiesiogiai pagrindžia ginamąjį teiginį, kad Al 6082 lydinys, anoduotas naudojant sieros rūgšties elektrolitą, gali būti priskirtas biomedžiagoms.

2 lentelė. Biomedžiagoms reikšmingos $\text{Al}_2\text{SO}_3^{\text{S}}$, $\text{Al}_2\text{SO}_3^{\text{P}}$, and Ti lydinio savybės

Savybė	$\text{Al}_2\text{SO}_3^{\text{S}}$ (anoduota sieros rūgštimi)	$\text{Al}_2\text{SO}_3^{\text{P}}$ (anoduota fosforo rūgštimi)	Ti lydinys (medicininis)
Paviršiaus struktūra	Nanoporos (palaiko adheziją)	Mikroporos	Tankus
Kietumas/ patvarumas	Aukštas	Žemas	Aukštas
Jonų išsiskyrimas: Fe ir Al	Nėra	Nėra	Nėra
Jonų išsiskyrimas: Mn	0.04 mg/L (saugus)	0.06 mg/L (aukščiausias; dar saugus)	Žemiausias
Jonų išsiskyrimas: Si ir Mg	Žemas (biologiškai palankus)	Žemas	Nėra
Hydroksiapatito formavimasis	Minimalus	Išreikštas	Nėra
Atsparumas korozijai	Puikus	Žemas	Puikus
Ląstelių morfologija	Plokščios ir pailgos	Plokščios	Plokščios ir pailgos
Ląstelių gyvybingumas (trumpalaikis)	Aukštas	Aukštas	Aukštas
Biomedicininis tinkamumas	Perspektyvus kandidatas implantams	Nerekomenduoja mas implantams	Standartinė klinikinė medžiaga

2. POLIKARBONATO OPTIMIZAVIMAS LĄSTELIŲ ADHEZIJAI

Polikarbonatas (PC) yra antroji šioje disertacijoje tyrinėjama biomedžiaga, pasirinkta dėl jo potencialaus panaudojimo mikroskysčių sistemose, skirtose

ląstelių auginimui. Porėtą PC membrana integruota į disertacijos metu gamintą mikrolustą (žr. 3. skyrių). Mikroluste PC membrana atlieka dvejopą funkciją: yra paviršius ląstelių adhezijai, tuo pačiu yra du lygiagrečius mikrokanalus atskirianti pertvara. Porėta membrana leidžia molekulinis mainus tarp mikrokanalų, tuo pačiu išlaikydama erdvinius ląstelių populiacijų atskyrimus. Todėl membrana yra esminis mikrolusto komponentas.

PC yra plačiai pripažįstamas dėl savo palankių fizikinių ir cheminių savybių, įskaitant skaidrumą, mechaninį stiprumą, mažą svorį, elektrinę izoliaciją ir atsparumą karščiui, ir yra klasifikuojamas kaip biomedžiaga. Tarp įvairių PC formų mikrorenginiams ypač tinka porėtos PC membranos. Tačiau PC turi svarbų trūkumą: jo paviršius yra hidrofobinis, chemiškai inertiškas, neturi funkcinių grupių, reikalingų efektyviam ląstelių prisijungimui [236], [237]. Tai kelia iššūkius ląstelių auginimo tiesiogiai ant PC. Be papildomo paviršiaus modifikavimo, PC membrana nesukuria biologinės palankios aplinkos ląstelių prisijungimui ir auginimui.

2.1 PC membranai būdingos adhezinės savybės

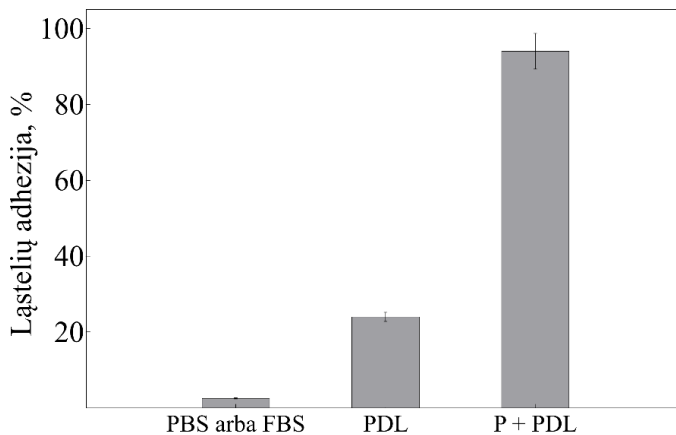
Siekiant išsiaiškinti PC membranos adhezinės savybes, atlikti trys ląstelių adhezijos eksperimentai naudojant:

1) nemodifikuotas membranas su PBS arba FBS - gauta itin menka ląstelių adhezija, - prie membranos paviršiaus prisitvirtino mažiau nei 3% CHO-K1 ląstelių.

2) membranas padengtas PDL - adhezija padidėjo iki 24%.

3) deguonies plazma modifikuotas membranas, po kurio padengtos PDL – užtikrino itin aukštą adhezijos lygį - iki 94% prisikabinusių ląstelių (**4 pav.**).

Gauti duomenys rodo, kad PC membranų paviršiaus oksidacija reikšmingai gerina jų tinkamumą ląstelių adhezijai, pabrėždami šio modifikavimo svarbą taikant PC membranas biologinėse sistemose.



4 pav. Prisikabinusių CHO-K1 ląstelių kiekis ant PC membranos, įvertintas esant trimis paviršiaus apdorojimo sąlygoms: PBS arba FBS – kontrolinė grupė; PDL – membrana padengta PDL; P + PDL – PC apdorota plazma, po kurios sekė PDL padengimas.

2.2 PC membranos cheminis modifikavimas

Atsižvelgiant į plazmos sukeltos oksidacijos grįžtamąjį pobūdį [129], PC modifikavimui buvo naudojami cheminiai oksidatoriai; natrio metaperjodatas (NaIO_4 , 0,117 M), sieros rūgštis (10%) ir piranijos tirpalas (10%) – visi šie reagentai yra gerai žinomi polimerų paviršiaus oksidacijai. Reagentų pasirinkimas ir jų koncentracijos buvo grindžiamos būtinybe išlaikyti suderinamumą su kitais mikrolusto komponentais, ypač OSTE ir COC, kurie yra jautrūs agresyvioms cheminėms medžiagoms.

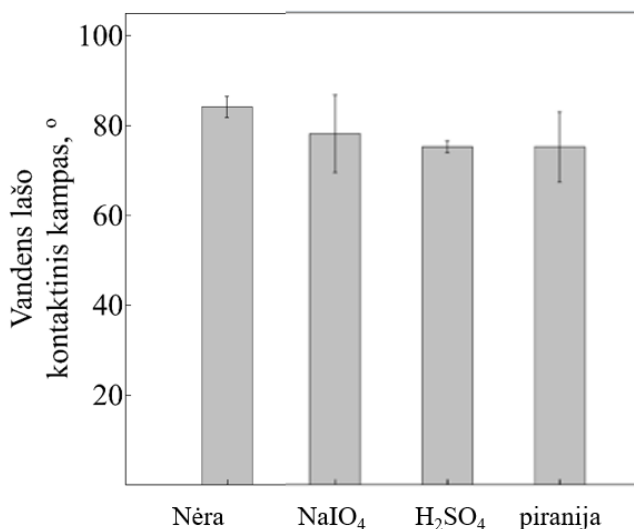
NaIO_4 yra kristalinė neorganinė druska ir stiprus oksidatorius, plačiai naudojamas organinėje ir polimerų chemijoje medžiagų funkcionalizavimui [260].

Sieros rūgštis (H_2SO_4) yra stiprus oksidavimo reagentas, kuris didelėje koncentracijoje gali sukelti visišką įvairių medžiagų, tame tarpe PC, degradaciją [241]. Šiame tyrime buvo naudojamas 10% sieros rūgšties tirpalas, nes tokia koncentracija nesukelia PC ir kitų polimerinių komponentų mikroluste skilimo. Pažymėtina, kad OSTE - polimeras, naudojamas mikrolusto gamyboje, yra atsparus sieros rūgščiai tik iki 10%. Todėl buvo daroma prielaida, kad 10% sieros rūgšties tirpalas gali būti pakankamas PC membranos paviršiaus modifikacijoms sukelti.

Piranijos tirpalas taip pat yra stiprus oksidatorius, susidarantis iš H_2SO_4 and H_2O_2 , ir yra stipresnis už sieros rūgštį. Piranijos tirpale sieros rūgšties ir vandenilio peroksido tūrio santykis paprastai svyruoja nuo 3:1 iki 5:1. Šiame tyrime buvo naudojamas 10% Piranijos tirpalas dėl tos pačios priežasties kaip ir

sieros rūgštis: sieros rūgšties koncentracija, didesnė nei 10%, sugadina kitus mikrolusto polimerinius komponentus.

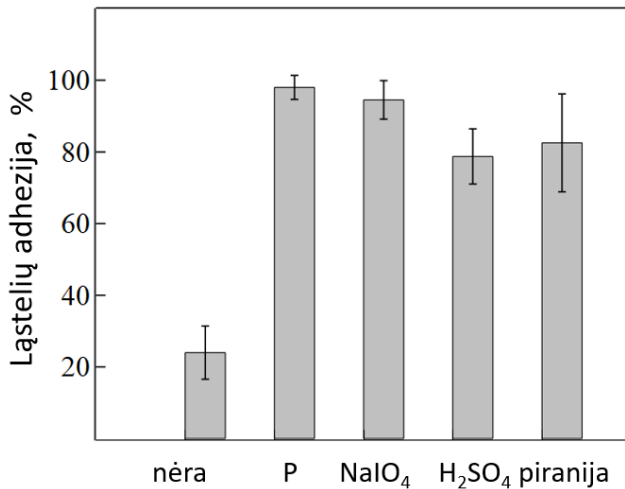
Po cheminės membranų modifikacijos išmatuoti vandens lašo kontaktiniai kampai, kad įvertinimui, ar pakito hidrofiliškumas. Pagal gautus rezultatus, modifikuotos membranos kurie reikšmingai nesiskyrė nuo nemonifikuotos (5 pav.). Išmatuoti kontaktiniai kampai buvo $78 \pm 8^\circ$ naudojant NaIO_4 , $75 \pm 1^\circ$ H_2SO_4 atveju ir $75 \pm 7^\circ$ naudojant Piranijos tirpalą (8 pav.). Nė vienas iš jų neparodė reikšmingo hidrofiliinių savybių padidėjimas palyginti su neoksiduotu PC, kurio kontaktinis kampas buvo $84 \pm 2^\circ$ (* $p > 0,05$, Tukey HSD post-hoc testas po vienkryptės ANOVA). Šie rezultatai skatina toliau svarstyti, ar cheminio oksidavimo metodai gali veiksmingai pakeisti paviršiaus savybes, svarbias biologinės funkcijoms, įskaitant ląstelių adheziją.



5 pav. Modifikuotų PC membranų hidrofiliškumas po cheminio modifikavimo.

2.3 Ląstelių adhezija ant modifikuotų PC membranų

PC membranos cheminės modifikacijos poveikis ląstelių adhezijai tirtas auginant SK-MEL-28 ląstelės ant modifikuotų bei padengtų PDL membranų. Rezultatai parodė reikšmingai didesnę ląstelių adheziją ant modifikuotų paviršių (iki 95%), lyginant su nemonifikuota kontrole (24%). Statistinė analizė patvirtino visų modifikacijų efektyvumą ($p < 0,005$) (6 pav.).



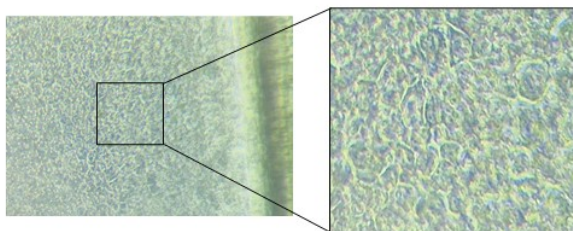
6 pav. PC membranos modifikacijų įtaka SK-MEL-28 ląstelių adhezijai. Plazma apdorotos PC membrana pažymėta P.

Siekiant nustatyti, ar cheminė PC modifikacija yra tinkama ir mikroskysčių sistemoje, atliktas eksperimentas su sukonstruotu mikrolustu (žr. žemiau). PC membrana buvo modifikuota mikrolusto viduje, bei padengta PDL. U2OS ląstelės buvo suleistos į paruoštą mikrokanalą ir paliktos prisitvirtinti be tėkmės per naktį. Sekančią dieną paleistas skysčio tekėjimas pradedant nuo 0,08 dyn/cm² šlyties įtempio.

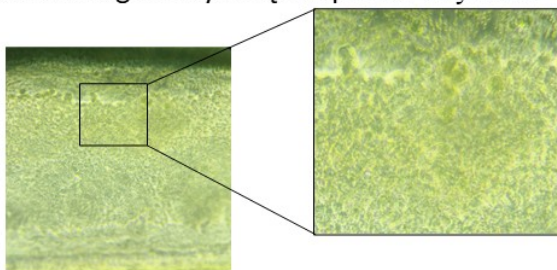
Šlyties įtempis yra pagrindinė mechaninė jėga, veikianti ląsteles tėkmės sąlygomis, ir kuri įtakoja įtaką ląstelių adheziją, morfologiją ir signalų perdavimą. Nors U2OS ląstelių linija kilusi iš kaulinio audinio vėžinių ląstelių, jos patiriama fiziologinis šlyties įtempis nėra nustatyta. Todėl orientaciniu atskaitos tašku galima laikyti fiziologinį mezenchiminių ląstelės šlyties įtempį, susidarančią dėl intersticinio srauto. Intersticinis srautas – tai lėtas skysčio judėjimą per ECM, konkrečiai per skysčiu užpildytas erdves, vadinamas intersticinėmis erdvėmis. Šis srautas sukelia mažą šlyties įtempį, paprastai $\leq 0,1$ dyn/cm² [245], [246].

Viso dviejų savaitių eksperimento metu šlyties įtempis buvo dvigubinamas kasdien iki 0,64 dyn/cm². Iki kol buvo pasiektas 6 kartus didesnis nei fiziologinis šlyties įtempis. Eksperimento metu U2OS ląstelės išliko nepakitusios, formuodamos vis tankesnę monosluoksni, bei išlaikydamos adheziją (**7 pav.**). Tai rodo, kad piranijos tirpalu modifikuota PC membrana kartu su adheziją palaikančiu PDL, užtikrina stabilią ląstelių adheziją net ir esant nuolatiniam skysčio tekėjimui.

a) Adhezija be tėkmės



b) Po 14 dienų,
6x fiziologinis šlyties įtempis 0.64 dyn/cm²



7 pav. U2OS ląstelių adhezija mikrokanale ant oksiduotos PC membranos, apdorotos piranijos tirpalu ir padengta PDL. Ląstelių adhezija parodyta (a) eksperimento pradžioje statinėmės sąlygomis ir (b) eksperimento pabaigoje esant 0,64 dyn/cm² šlyties įtempiui.

2.4 PC paviršiaus modifikacijų siekiant pagerinti ląstelių adheziją aptarimas

Gauti duomenys rodo, kad paviršiaus oksidacijos metodai yra veiksmingi gerinant PC membranos gebėjimą palaikyti ląstelių adheziją. Nors plazminis apdorojimas leidžia greitai įvesti deguonies turinčias funkcines grupes, jo poveikis yra trumpalaikis dėl paviršiaus senėjimo. Tuo tarpu cheminės modifikacijos, naudojant NaIO₄, H₂SO₄ ir piranijos tirpalą, užtikrino stabilų ir ilgalaikį paviršiaus aktyvumą bei suderinamumą su mikrolusto gamybos procesais. Cheminė PC membranos modifikacija kartu su adheziją skatinančiomis molekulėmis pagerino ląstelių adheziją 4,3 kartus NAIO₄ atveju, 3,2 kartus H₂SO₄ atveju ir 4.3 karto piranijos tirpalo atveju. Tuo tarpu mikroluste esanti PC membrana buvo modifikuota piranijos tirpalu bei padengta PDL molekulėmis – tokia modifikacija leido U2OS ląstelėmis išlaikyti adheziją net esant 6 kartus didesniam bnei fiziologinis šlyties įtempiu.

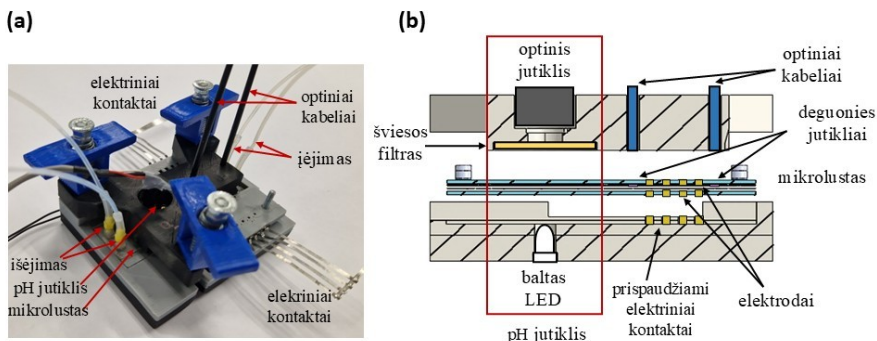
3. MIKROFIZIOLOGINĖ SISTEMA SU INTEGRUOTA PC MEMBRANA LAŠTELIŲ ATSAKO Į IMPULSINIO ELEKTRINIO LAUKĄ TYRIMAMS

3.1 MPS konstrukcija ir mikrolustas

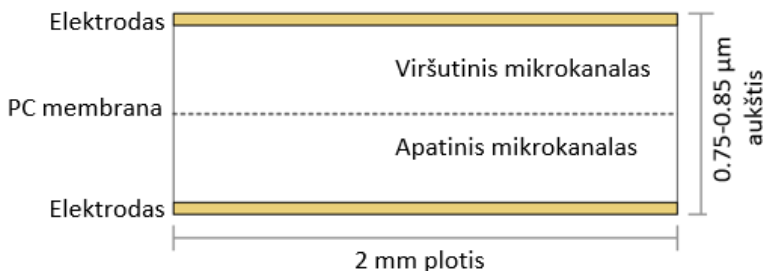
Disertacijos metu sukonstruota MPS (**8 pav.**), kurią sudaro pagrindinis komponentas mikrolustas, papildomas MPS laikiklis su įmontuotais pH jutiklių ir deguonies jutiklių komponentais. Mikrolusto kanale yra integruoti elektrodai bei deguonies sensoriai. Šis kanalas turi integruotą porėtą PC membrana, kuri padalina kanalą į du lygiagrečius mikrokanalus (**9 pav.**). Mikrolusto gamyba paremta OSTE technologija [175], turinti du pagrindinius privalumus:

1) Mikrolustas yra pagamintas naudojant minkštąją litografiją, todėl galima lengvai keisti kanalų geometriją, elektrodų skaičių ir padėti pagal konkrečius poreikius.

2) Naudojant COC, OSTE, pašalinamos neigiamos PDMS savybės, pvz., molekulinė absorbcija, dujų prasiskverbimas ir kanalų deformacija.



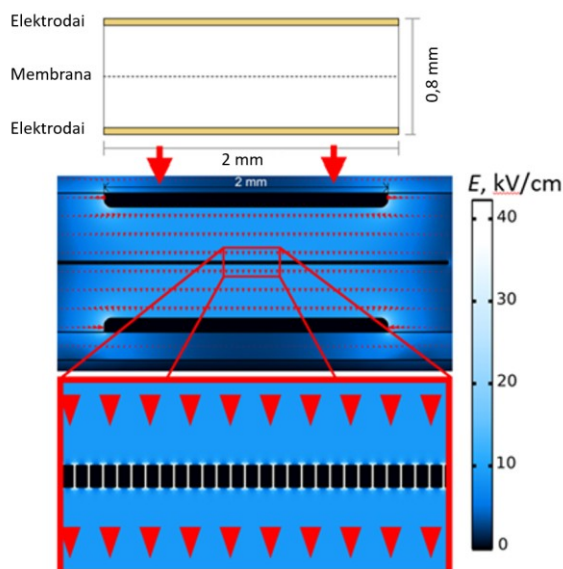
8 pav. (a) MPS prototipas ir (b) schematinis MPS skerspjūvis ir atraminio įtaiso dekompozicija.



9 pav. Mikrokanalo skerspjūvio vaizdas ties elektrodais.

3.2 Elektrinio lauko mikroluste modeliavimas

Sukonstruotos MPS paskirtis – IEL lauko tyrimai su žinduolių ląstelėmis. Norėdami įvertinti, kokią įtaką daro integruota porėta membrana elektrinio lauko pasiskirstymui, atliktas matematinis modeliavimas. Paaiškėjo, kad elektrinis laukas mikrokanaluose pasiskirstęs beveik tolygiai ir siekia maždaug 9 kV/cm, kai kanale be membranos elektrinis laukas siekė 10 kV/cm. Tuo tarpu tiesmembrana elektrinis laukas buvo sustiprintas maždaug 2 kartus, o membranos porose – 4 kartus (**10 pav.**).

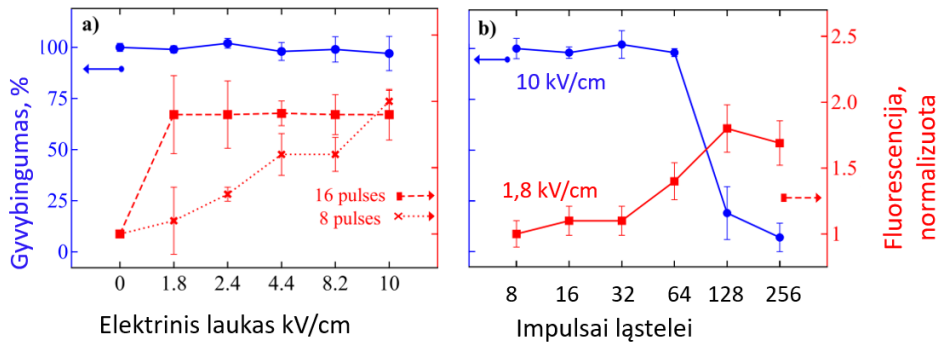


10 pav. Elektrinio lauko pasiskirstymo mikroluste vizualizacija, imituota naudojant COMSOL Multiphysics, su membrana, kurios porų dydis yra 3 μm , o poringumas – 21,2 %. Pritaikius 800 V įtampą, kanale be membranos susidaro 10 kV/cm elektrinis laukas. Spalvų gradientas iliustruoja elektrinio lauko stiprumą kV/cm, o raudoni trikampiai rodo elektrinio lauko kryptį.

3.3 Ląstelių gyvybingumas ir pralaidumas po elektroporacijos

Siekiant patvirtinti MPS tinkamumą tirti IEL poveikį ląstelėms, buvo atlikti suspensinių ląstelių elektroporacijos eksperimentai. Tyrimai buvo atliekami dviem režimais: sustabdytos ir nuolatinės tėkmės. Šie eksperimentai atlikti su C6 ląstelių suspensija naudojant 0–10 kV/cm stiprumo elektriniu lauką, 100 μs trukme ir 1 Hz dažnį. Elektroporacijos efektyvumas yra vertinamas pagal ląstelių gyvybingumą bei ląstelių membranos permeabilizacija po IEL poveikio.

Rezultatai parodė, kad esant 10 kV/cm, ląstelių gyvybingumas išlieka nepakitęs sustabdytos tėkmės IEL su 8 impulsais (**11a pav.**), o nuolatinės tėkmės sąlygomis gyvybingumas mažėja naudojant 128 impulsus/ląstelei (**11b pav.**). Tuo tarpu maksimalus ląstelių permeabilumas esant 1.8 kV/cm pasiekta naudojant 16 impulsų sustabdytos ir 128 impulsus/ląstelei nuolatinės tėkmės režimu (**11a,b pav.**). Atlikti eksperimentai patvirtina, kad pagamintas MPS yra tinkamas žinduolių ląstelių elektroporacijai, leidžiantis efektyviai kontroliuoti membranos permeabilizaciją tiek sustabdytos, tiek nuolatinės tėkmės IEL sąlygomis.

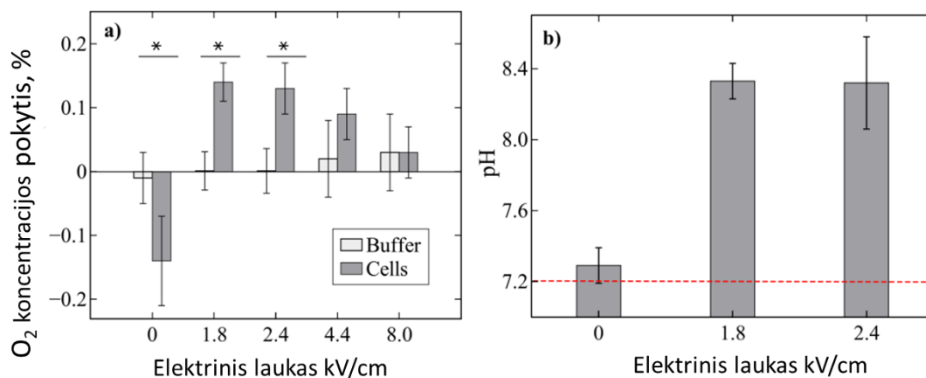


11 pav. IEL poveikis C6 ląstelėms ir pralaidumui esant (a) sustabdytai tėkmei ir (b) esant nuolatinėi tėkmei. Mėlyna spalva vaizduoja gyvybingumo duomenis, o raudona – membranos pralaidumo duomenis. (a) taikomas 0–10 kV/cm elektrinis laukas su 8 (raudoni kryželiai) arba 16 (raudoni kvadratai) impulsais. (b) gyvybingumo eksperimentams buvo naudojamas 10 kV/cm elektrinis laukas, o pralaidumo eksperimentams – 1,8 kV/cm laukas su 0–128 impulsais, tenkančiai ląstelei. Tiek (a), tiek (b) atveju IEL buvo atliekamas naudojant 100 μ s impulsų trukmę ir 1 Hz pakartojimo dažnį. Pralaidumas buvo kiekybiškai įvertintas kaip fluorescencija, normalizuota pagal neelektroporuatą kontrolę.

3.4 Deguonies koncentracijos ir pH matavimai

Kultivuojant ląsteles *in vitro*, būtina užtikrinti nuolatinį reikalingų dujų – O₂ ir CO₂ – tiekimą. Deguonis reikalingas ląstelių kvėpavimui, o CO₂ užtikrina tinkamą augimo terpės pH. Iškreiptas O₂ ir pH lygis trukdo ląstelių išlikimui ir yra susijęs su įvairių patologijų, įskaitant vėžį, vystymusi [252], [253]. Mikrolusto gamybai naudotos medžiagos OSTE ir COC yra nepralaidžios dujoms, todėl šių dujų tiekimą reikia kontroliuoti papildomai. O₂ ir pH lygių stebėjimui MPS sistemoje įmontuoti šiuos abu parametrus stebintys jutikliai. Mikroluste yra du deguonies jutikliai – vienas yra prieš elektrodus, o kitas – už jų (**8b pav.**).

Abu jutikliai yra vienodu atstumu nuo kraštinių elektrodų. Esant skysčio tėkmei, pirmas jutiklis matuoja deguonies koncentraciją šviežioje terpėje, kuri praeina pro elektrodus, o antras jutiklis matuoja koncentraciją terpėje po IEL poveikio. Siekiant įvertinti MPS veiksmingumą nustatant deguonies koncentracijos pokyčius, buvo atlikti eksperimentai su C6 ląstelių suspensija, IEL naudojant kaip stimulą deguonies koncentracijos pasikeitimui. Duomenys apie deguonies koncentraciją buvo renkami iš abiejų jutiklių prieš IEL ir iškart po jo. Nesant IEL (0 kV/cm), deguonies koncentracija ląstelių suspensijoje ties antru jutiklio sumažėjo, palyginti su pirmu jutikliu ($\Delta = -0,14\%$) (**12a pav.**). Šis sumažėjimas buvo žymus lyginant su kontroliniu mėginiu be ląstelių ($\Delta = -0,01\%$). Tačiau, kai ląstelės buvo veikiamos IEL, deguonies koncentracija pastebimai padidėjo $\Delta = 0,14\%$, $0,13\%$, $0,09\%$ ir $0,03\%$ esant 1,8 kV/cm, 2,4 kV/cm, 4,4 kV/cm ir 8,0 kV/cm elektros lauko stipriams. Pažymėti, kad esant mažesniems elektros laukams (1,8 kV/cm ir 2,4 kV/cm) deguonies koncentracijos pokyčius lėmė ląstelės, tuo tarpu esant 4,4 kV/cm ir 8,0 kV/cm – pagrindiniai pokyčiai įvyko pačiame skystyje, o ne dėl ląstelių veiklos.



12 pav. IEL poveikis (a) dviejų jutiklių deguonies koncentracijos skirtumui ir (b) pH, iškart po IEL. IEL buvo atliekamas sustabdytos tėkmės režimu, naudojant įvairius elektrinius laukus, su 16 impulsais, 100 μ s impulso trukme ir 1 Hz pakartojimo dažniu. Eksperimentų skaičius $n \geq 3$; žvaigždutės* žymi statistiškai reikšmingus skirtumus ($p \leq 0,00001$). Brūkšninė linija (b) atitinka buferio bazinę liniją.

Optinis pH matuoklis, integruotas į MPS (**8 a,b pav.**), registruoja augimo terpėje esančio fenolio raudonojo spalvos pasikeitimus, kurie vyksta priklausomai nuo pH pokyčių. Norint įvertinti pH matuoklio veikimą, buvo tirti pH svyravimai po suspensijoje esančių C6 ląstelių stimuliacijos IEL esant 0, 1,8 ir 2,4 kV/cm elektrinio lauko stipriui. Nustatytas pradinis terpės pH buvo 7,2.

Be IEL stimuliacijos, ląstelių suspensijos pH $7,29 \pm 0,06$, tuo tarpu IEL poveikis padidino pH iki $8,3 \pm 0,14$ esant $1,8 \text{ kV/cm}$ ir $8,3 \pm 0,26$ esant $2,4 \text{ kV/cm}$ elektrinio lauko stipriui (**12b pav.**).

Šie rezultatai parodo, kad pagamintas MPS geba registruoti deguonies koncentracijos bei pH pokyčius.

3.5 MPS sistemos su aptarimas

Šioje disertacijoje buvo sukonstruotas MPS, mikrolustą gamybai pasitelkiant OSTE technologiją [203]. Mikrolusto kanale buvo integruota porėta PC membrana, o IEL generavimui - elektrodai. Pirmiausia buvo atliktas išsamus membranos poveikio elektrinio lauko pasiskirstymui vertinimas naudojant matematinį modeliavimą. Tyrimai parodė, kad porėtos membranos buvimas nežymiai įtakoja elektrinio lauko stiprį mikrokanale, išskyrus ties membranos paviršiumi ir jos porose, kur elektrinio lauko stipris reikšmingai padidėja 2 ir 4 kartus, atitinkamai. Tai reikia turėti omeny elektroporuojant adhezines ląsteles, augančias ant membranos paviršiaus. IEL eksperimentai su suspensinėmis ląstelėmis parodė, kad MPS galima naudoti tiek sustabdyto, tiek nuolatinės tėkmės režimais, efektyviai sukeliant membranų permeabilizaciją ir išlaikant aukštą gyvybingumą.

Siekiant užtikrinti mikroaplinkos stebėjimą realiuoju laiku, į MPS buvo integruoti deguonies bei pH jutikliai. Jų veikimas įvertintas naudojant IEL kaip stimulus fiziologinės aplinkos pokyčiams inicijuoti. Tyrimo metu integruoti jutikliai sėkmingai fiksavo deguonies ir pH pokyčius, o TEER matavimai parodė, kad MPS jautriai reaguoja į ląstelių buvimą nepaisant to, kad buvo naudotos suspensinės ląstelės. Šie rezultatai patvirtina, kad sukonstruota MPS yra tinkama IEL taikymui ir mikroaplinkos stebėjimui realiuoju laiku.

Visi šie rezultatai kartu rodo, kad sukurta MPS su integruota porėta PC membrana yra tinkami IEL poveikio tyrimams bei realaus laiko fiziologinių sąlygų stebėjimą mikroskopių aplinkoje, patvirtindami ginamąjį teiginį.

IŠVADOS

1. Al 6082 lydinys, anoduotas sieros rūgšties elektrolite, padidino mėginio kietumą 2 kartus, nepakeitė jonų išsiskyrimo lyginant su neanoduotu lydiniu, ir pagerino atsparumą korozijai 1,5 karto palyginti su titano lydiniu.

2. Pelės fibroblastų L929 ląstelių morfologija ant Al 6082 lydinio, anoduoto sieros rūgšties elektrolite, patvirtina normalią ląstelių fiziologiją. Ląstelių gyvybingumo rezultatai patvirtina lydinio biosuderinamumą. Šios savybės, artimos medicininio titano lydinio charakteristikoms, pagrindžia anoduoto Al 6082 lydinio tinkamumą taikymui biomedicinoje.

3. Natrio metaperjodatu, sieros rūgštimi ir piranijos tirpalu modifikuotos polikarbonato membranos, padengtos poli-D-lizinu, ląstelių adheziją padidino daugiau kaip 3 kartus.

4. Piranija modifikuota membrana kartu su poli-D-lizinu statinėse sąlygose padidino ląstelių adheziją 4,3 karto. Dinaminėmis sąlygomis epitelinės U2OS ląstelės atlaikė šlyties įtempį, 6 kartus viršijantį fiziologinį intersticinį srautą.

5. Porėta polikarbonato membrana sėkmingai integruota į mikrolustą, skirtą impulsinio elektrinio lauko (IEL) poveikio tyrimams. Porėtos membranos konstrukcija elektrinio lauko stiprį padidina iki 200% ties membranos paviršiumi, lyginant su identišku kanalu be membranos, o mikrokanale elektrinio lauko stipris išlieka didesnis nei 90%.

6. Sukurta mikrofiziologinė sistema (MPS), skirta žinduolių ląstelių IEL poveikio tyrimams. Rezultatai parodė padidėjusį ląstelių membranų pralaidumą po IEL poveikio, išlaikant nepakitęs gyvybingumą. Išmatuoti deguonies koncentracijos bei pH pokyčiai po IEL poveikio patvirtina MPS tinkamumą fiziologinių parametrų stebėjimui.

ACKNOWLEDGEMENT

I am sincerely thankful to my supervisor, Dr. Arūnas Stirė, for his support, encouragement, and the opportunity to pursue my scientific goals. I am especially grateful to him for inviting me back into the scientific community after a long break. His continued encouragement and involvement were essential to the development of this work and to my academic growth. I am grateful to my institution, FTMC, for providing the research infrastructure and financial support that made this work possible. I would also like to express my sincere gratitude to prof. Dr. Nerija Źurauskienė, head of the department, for granting me the position and for her unwavering efforts in securing the opportunity to pursue these studies.

I would like to thank my colleagues from the Bioelectronics Laboratory and the Department of Functional Materials and Electronics for the friendly atmosphere and inspiring conversations over a cup of coffee. I appreciate the contributions to the realization of this work: Dr. Eivydas Andriukonis for his practical assistance in designing the microchip and manufacturing the MPS, Dr. Vilius Vertelis for the electrode deposition in microchip production, Jorūnas Dobilas for mathematical modelling and simulations, Dr. Martynas Źapurov for adapting pH sensor measurements to the MPS system, and Dr. Skirmantas Keršulis for his practical assistance and advice during PEF experiments. I would like to thank the students who contributed to the experimental work: Agnė Damarackaitė, Elinga Bražionytė, Paulina Kizinievič, and Kamilė Kasperavičiūtė.

I would like to thank all colleagues who contributed to the research project aimed at assessing the suitability of anodized specimens for biomedical applications. Special thanks go to Dr. Tadas Matijošius for inviting me to join the project and for his close collaboration in data analysis and manuscript preparation. I am also deeply grateful to Dr. Asta Grigucevičienė for her work on electrochemical investigations and for her extensive and dedicated efforts in data analysis. My sincere appreciation goes to Dr. Asta Selskienė for conducting SEM analysis, and to Dr. Aleksey Źarkov for performing ICP-OES measurements.

I sincerely thank Dr. Antanas Strakšys for his scientific insights, valuable contributions to the PC membrane modification project, thoughtful advice throughout its implementation, and for his exceptionally thorough review of my dissertation — his critique and recommendations greatly helped refine the doctoral thesis.

A special note of gratitude goes to my closest colleagues in the laboratory: Dr. Raimonda Celešiūtė-Germanienė, Dr. Antanas Strakšys, PhD students Greta Tartėnė and Kamilė Jonynaitė. I am truly thankful for your friendship,

meaningful conversations, and for fostering an environment where work felt deeply fulfilling. I would also like to thank my friend and former colleague Justina Kavaliauskaite, whose encouragement prompted me to return to science, and who suggested this particular laboratory. Her inspiration was instrumental in reviving my scientific journey.

I remain deeply appreciative of my early mentors who introduced me to the fundamentals of work in the laboratory, work, and discipline - Dr. Rimantas Šapranauškas and Dr. Milda Plečkaitytė, who guided me through my bachelor's and master's studies, respectively. I am also sincerely grateful to my supervisor, Prof. Dr. Virginijus Šikšnys, head of my former lab, as well as the consultant Dr. Mindaugas Zaremba, whose guidance played a vital role in shaping my scientific thinking and expanding my knowledge.

And last, but not least, I am very thankful to my family, my children, and my husband for their unwavering support and patience throughout this journey, especially during long hours and the intense period of writing my dissertation. I also extend my gratitude to my entire family, my parents, sisters, and friends, for their unwavering encouragement and for patiently listening to the countless stories about my experiments and projects, when the details may have sounded like a foreign language.

CURRICULUM VITAE

NERINGA BAKUTĖ

e-mails:

neringa.bakute@ftmc.lt

PROFESSIONAL EXPERIENCE

State Research Institute Center for Physical Science and Technology

- Junior Scientist 2022 – 2025
- Engineer 2017- 2022

ThermoFisher Scientific, Vilnius

- Manager 2011-2013

Institute of Biotechnology, Vilnius

- Engineer, Junior Scientist 2002-2009

EDUCATION

Vilnius UNIVERSITY

- **MSc.** in Molecular Biology and Genetics 2002-2004
- **BSc.** in Molecular Biology 1998-2002

NOTES

NOTES

Vilniaus universiteto leidykla
Saulėtekio al. 9, III rūmai, LT-10222 Vilnius
El. p. info@leidykla.vu.lt, www.leidykla.vu.lt
bookshop.vu.lt, journals.vu.lt
Tiražas 20 egz.